AFML-TR-71-100

THE REDUCTION OF RESONANT VIBRATIONS IN INTEGRALLY STIFFENED SKIN-STRINGER PANELS USING VISCO-ELASTIC MATERIALS

FERNANDO CICCI

INSTITUTE OF SOUND & VIBRATION RESEARCH
UNIVERSITY OF SOUTHAMPTON

TECHNICAL REPORT AFML-TR-71-100

JUNE 1971

AIR FORCE MATERIALS LABORATORY
AIR FORCE SYSTEMS COMMAND
WRIGHT-PATTERSON AIR FORCE BASE, OHIO

NOTICE

When Government drawings, specifications, or other data are used for any purpose other than in connection with a definitely related Government procurement operation, the United States Government thereby incurs no responsibility nor any obligation whatsoever; and the fact that the government may have formulated, furnished, or in any way supplied the said drawings, specifications, or other data, is not to be regarded by implication or otherwise as in any manner licensing the holder or any other person or corporation, or conveying any rights or permission to manufacture, use, or sell any patented invention that may in any way be related thereto.

Copies of this report should not be returned unless return is required by security considerations, contractual obligations, or notice on a specific document.

300 - July 1971 - CO305 - 45-71-777

THE REDUCTION OF RESONANT VIBRATIONS IN INTEGRALLY STIFFENED SKIN-STRINGER PANELS USING VISCO-ELASTIC MATERIALS

FERNANDO CICCI

FOREWORD

This report was prepared by the Institute of Sound and Vibration Research, University of Southampton, U.K., under USAF Contract No. F61052-68-C-0027. The contract was initiated under Project No. 7351, "Metallic Materials", Task No. 735106, "Behavior of Metals". The contract was administered by the European Office of Aerospace Research. The work was monitored by the Air Force Materials Laboratory, Air Force Systems Command, Wright-Patterson Air Force Base, under the direction of Mr. W. J. Trapp.

The work described in this work was supervised by Professor B. L. Clarkson and was undertaken in detail by Mr. F. Cicci.

This report covers work from 15 February 1968 to 14 February 1970.

This technical report has been reviewed and is approved.

W. J. TRAPP
Chief, Strength and Dynamics Branch
Metals and Ceramics Division
Air Force Materials Laboratory

ABSTRACT

The vibration characteristics of integrally stiffened skin stringer panels have been determined using the method of transfer matrices. It was found that this type of structure can behave in a manner quite unlike a conventional structure composed of a flat skin and extruded open section stringers. The integrally stiffened skin tends to have mode shapes and natural frequencies governed by the bending stiffness of the stringers. As a result the stringers deflect with the skin and the panel mode shapes resemble those of simple flat plates. The calculated mode shapes have been verified experimentally by exciting a typical panel with harmonic sound waves at approximately grazing incidence. The response was measured by mean of accelerometers and strain gauges. The response to random noise was also determined experimentally.

The damping of the resonant vibrations induced in integrally stiffened panels was investigated theoretically and experimentally. The theoretical calculations were verified by measurements of modal loss factors of a beam taken from the cross secton of an integrally stiffened skin. The most efficient method of those considered consisted of strip dampers bonded to the free edge of the stringers. The strip dampers used were of two types. The first consisted of a stiff viscoelastic material (LD400 of the Lord Manufacturing Company) and the second was a shear system made up of two skins of aluminium alloy with an interlayer of silicone rubber. The reduction of rms panel response to random acoustic excitation was typically seventy percent for a weight additon of one and one half percent.

A transient technique of excitation and analysis was used in some beam and panel measurements, and it was found to be an effective means of quickly determining natural frequencies and, in some cases, modal loss factors.

The effectiveness of the damping treatments on full scale structure was confirmed experimentally. The addition of negligible weight reduced the rms response by forty percent or more.

TABLE OF CONTENTS

LIST OF ILLUSTRATIONS

LIST OF TABLES

NOTATION

b	stringer pitch (in.)
d	beam width (in.) subscript "d" designates damping material
f	frequency (Hz)
h	skin thickness (in.)
h_s	stringer thickness (in.)
h_d	damping beam thickness (in.)
ℓ	frame pitch, or damping beam length (determined by context) (in.)
n	number of half waves along the length of a simply supported beam
E, E_d	Moduli of elasticity ($lb.in^{-2}$)
F	force (lbs)
G	shear modulus ($lb.in^{-2}$)
H	stringer height (in.)
I, I_d	moments of area (in^4)
K	extensional stiffness ($lb.in^{-1}$)
L	simply supported beam length (in.)
M	number of stringers in a panel, or moving mass in a single degree of freedom system (lbs) determined by the context)
M_ℓ, M_r	skin bending moments to the left and right of a stringer (in.lb)
$\hat{M}$	damping material bending moment (lb.in)
N	number of skin stringer spans
Q	shear force (lbs)
T_m	strain energy of a simply supported beam (lb.in)
T_{de}, T_{df}	extensional and flexural strain energies of the strip dampers (lb.in)
w	transverse displacement (in.)
x, y	linear coordinates (in.)
μ, μ_d	beam mass per unit length ($lb.in^{-1}$)
η, η_d, η_t	loss factors
ν	Poisson's ratio
ω	frequency (radian sec^{-1})

λ	beam parameter $= (\frac{\mu\omega^2}{EI})^{\frac{1}{4}}$	(in^{-1})
θ	angle of rotation (radians)	
ρ	density $(lb.in^{-3})$	
$\lvert\ \rvert$	denotes the absolute value of	

I. INTRODUCTION

Parts of the external skin of a modern high speed aircraft will spend most of their working life in a rather hostile acoustic environment. They will have to contend with such things as a turbulent boundary layer, noise from high speed jet engines, and vibrations induced by large scale air turbulence and by runway roughness, among others. If large scale fatigue problems are to be avoided careful consideration must be given to those forces generating random vibrations in the structure and the actual vibration characteristics of the structure itself.

The stresses induced in structural members by fluctuating loads are of several types. The primary ones due, for instance, to aircraft accelerations caused by atmospheric turbulence or runway roughness, will be relatively low frequency phenomena creating axial stresses in such components as stiffened skins. These are resonant phenomena, but will involve only a few of the overall bending or torsion modes of the wings, fuselage, or other primary structure.

A very important secondary form of stress is that due to localized high frequency vibration of some parts of the overall structure. These are transverse vibrations which result in bending stresses and they can be caused by high frequency short wavelength fluctuating acoustic pressures. The local behaviour of stiffened skins under these conditions will almost always be multi-modal, resulting in stresses over a range of frequencies. In some cases it will be possible at the design stage to reduce these resonant transverse vibrations within the structure to insignificant levels, but unfortunately such cases are rather rare. Usually it will be necessary to know the limits which they will reach and if these are too high some external means must be used to further reduce these vibrations or the stresses induced by them.

Fortunately, when dealing with effects in the high frequency range it is not usually necessary to study the vibration characteristics of the structure as a whole. Although it is true that the manner in

which one component vibrates does depend on all the other parts to which it is attached, on the ways in which they are joined together, and on the mean or static component of stress present, it is almost always possible to identify predominant modes of vibration in which major displacements are in either the underlying support structure or in the skin and its associated stringers. Having made this identification it is then possible to analyse the modes as though they were totally independent.

In this report this approach has been taken and it has been decided to concentrate on those frequencies in the range from about 100 to 1000 Hz. It is in this range that the noise from most modern jet engines contains a great deal of its energy, as does a turbulent boundary layer. These two forms of excitation are usually the most severe ones affecting skin stringer panels and will therefore cause the most severe fatigue damage due to transverse vibrations. This is especially true because in this range of frequencies built up structures have a great many natural frequencies (even considering the above stated simplification) and thus any reasonable, practical design must have some resonances in the frequency band of strongest excitation.

At present there is a growing trend away from what, in this report, will be called a conventional built up structure. This will be defined as a structure made up of a light alloy skin stiffened in one direction by stringers which may be open or closed in section. These stringers are generally rivetted to the skin, although other methods, such as bonding, have been used. Since they are usually rivetted, the situation can be quite serious from the point of view of fatigue both under axial and bending stress conditions. The myriad of rivet holes act as stress concentrations in themselves and also trap moisture and other corrosive substances, which create further stress raisers. Also, rivet fit is a very difficult quality control item and a loose rivet can cause fretting and further fatigue problems. Finally there is the fairly expensive process of actually assembling the whole skin-stringer, which is in itself a disadvantage.

One alternative type of skin structure which is being used to eliminate some of the problem areas is a honeycomb or laminated construction with the centre layer being shear stiff but very light. A second is

a fibre reinforced material. This type can have anisotropic stiffness and strength characteristics and can be made up in various matrix-fibre configurations ranging from the very familiar glass-fibre in plastic to the more exotic carbon or boron fibre in metal matrix.

A third alternative which is quite widely used and which is to be investigated in this report is the integrally stiffened or machined plank construction. In this type of construction the material starts as a homogeneous, thick slab of material (light alloy for the cases of interest here) and large quantities of the material are machined away either mechanically or chemically. This leaves a finished skin-stringer panel with the desired dimensions.

This type of structure has several advantages over the conventional type. The first and a very important one is that manufacturing costs can be reduced by the high degree of automatic processing possible. Secondly, the elimination of a great many rivet holes cannot help but be a step in the right direction in the alleviation of the fatigue problem. Certainly when dealing with the primary axial fluctuating stresses the integrally stiffened skin with its lack of rivet holes and superior strength and buckling characteristics is very attractive. However, this type of structure has some characteristics which tend to reduce the benefits to overall fatigue performance. In any builtup structure the majority of the damping which limits the resonant local or transverse vibrations comes about due to friction between moving components. Since the machined plank eliminates all of the stringer-skin interfaces, the total absence of the small but important energy dissipating sliding motion of one over the other is also eliminated. As a result the damping will be lower, perhaps by as much as an order of magnitude and the resonant transverse vibrations can build up to a higher level subjecting the structure to higher stresses.

It has been found that the vibration characteristics of integrally stiffened skins are significantly different from those of a conventional structure. The basic difference is that the stringers deflect with the skin rather than acting as a high degree of fixity on the skin. This means that the stringers are subjected to relatively

high bending stresses and a fatigue crack can start at the tip of the stiffener. Under axial load conditions this crack might not grow too rapidly, but under the influence of the bending stresses it will propagate readily across the stringer. Since there is no interface between the stringer and the skin the crack is then free to grow into and through the skin as well, and total failure can result quickly.

Thus, the integrally stiffened skin has some rather severe limitations because it can readily be excited to rather high stress levels, and under the influence of these, fatigue cracks can readily be propagated. However, its superior cost and static strength characteristics make it quite attractive. By a study of the dynamic behaviour of this type of structure it should be possible to minimize the effects of the shortcomings and take advantage of the superior qualities.

In this report attention has been focussed on the integrally stiffened skin-stringer construction and its local transverse vibration characteristics. Little has been reported in the open literature on these vibration characteristics and it was hoped that a little understanding could be achieved concerning the dynamic behaviour under the influence of acoustic forces similar to those to which the structure will be subjected in service.

Since it is likely that these structures will have inherently lower damping, there is a need to look at some ways of adding means of energy dissipation. Due to the geometric properties of the type of structure it is possible to use some rather efficient configurations for this purpose. It was decided to investigate the use of visco-elastic materials in various ways including tension-compression, bending and shear to dissipate the energy and this led to a third and final area of investigation.

It has already been pointed out that the frequency range of interest extends from about 100 to 1000 Hz. In a modern aircraft there is also a wide temperature variation imposed on the materials present. In a supersonic aircraft, for instance, temperatures might vary from $-50^{\circ}C$ at subsonic speeds at high altitude to perhaps $150^{\circ}C$ at supersonic cruise.

Viscoelastic materials are inherently nonlinear, frequency dependent and generally extremely temperature sensitive. It was therefore considered necessary to make at least a cursory investigation of some of the available viscoelastic materials so as to be able to make if not the optimum choice at least a sensible one.

II THE VIBRATION CHARACTERISTICS OF STIFFENED SKIN PANELS

The two major types of skin stringer configuration are shown schematically in Figures 2.1(a) and (b). In Figure 2.1(a) the conventional structure is shown to be made up of a flat skin with Z section stringers attached by rivets. The skin could be curved as in a fuselage and the stringers, of course, could have other shapes and might be closed section, but the Z shaped extruded stringer is typical. The integrally stiffened structure is shown in 2.1(b) for comparison. In this configuration the stringers are almost invariably rectangular in shape due to the necessity of machining from a solid slab.

The basic difference in stringer cross section leads to some interesting variations in behaviour. The extruded stringers tend to be very deep relative to their thickness, which means that the transverse bending rigidity will be quite high relative to the torsional rigidity. This effect is reinforced by the flange which is the full stringer depth away from the line of attachment to the skin.

The integral stiffener, on the other hand, is usually quite thick relative to its depth. This means that the bending rigidity is now considerably smaller than that of an extruded stringer when compared to the torsional rigidity. In fact for a given material weight or stringer cross sectional area for a builtup structure the ratio of bending stiffness to torsional stiffness might be of the order of 2000:1. For an integrally stiffened structure the corresponding figure would be closer to 20:1. This stiffness ratio difference in particular results in some differences in vibration characteristics.

II.1 The Vibration Characteristics of Builtup Structures

In a typical complete aircraft structure the skin-stringer panels are supported on a grid of very stiff sub structure of ribs and spars. Since these are much stiffer than the stringers themselves, they tend to divide the skin up into panels which will vibrate in transverse modes almost independently of the adjacent or other more widely separated panels. The stiff and massive substructure will itself vibrate, probably in modes which will cause motions and stresses in the skin, but in general this will occur at frequencies other than those at which the skin panels themselves respond strongly. In practice it will usually be possible to identify and separate those stresses which involve predominantly local skin vibrations from those primary stresses due to the total structure motion.

If it is assumed that the vibrations of various major sub sections of structure can be separated it becomes possible as a first step in obtaining the overall picture of the dynamic characteristics of a structure to analyse individual panels. These will be bounded by ribs or spars on all four edges and will consist of several skin-stringer spans. The individual plates (one skin-stringer span) have quite a high aspect ratio, and hence the vibration characteristics will not be seriously affected by end conditions along the edges perpendicular to the stringers.

There exists in the literature a considerable amount of information concerning the calculation of the natural frequencies and normal modes of vibration of this type of structure. Lin (1) has shown that the natural frequencies fall into groups and was able to calculate the values for the lower and upper bounding modes of the groups. Lin and his associates (2, 3) and Mercer and Seavey (4) have developed transfer matrix techniques to calculate normal modes and natural frequencies other than the lower and upper bounding modes, but the modes are still found to fall into groups or bands. Lindberg and Olson (5) have developed a finite element technique which gives results which are in agreement with the other methods.

The finite element approach is a numerical method and therefore

approximate, but it has the advantage of flexibility of edge conditions. It is possible to specify the restraints on all four edges of the panel. The transfer matrix method, however, is a normal mode approach and it is necessary to assume that the short plate edges are simply supported in order to have an exact solution. Appropriate long edge restraints can be specified using either method and the results are similar for those cases in which they can be compared. The normal modes and corresponding natural frequencies for the first band of modes of a 6 span panel with the edges parallel to the stringers simply supported are shown in Figure 2.2. This figure is taken from reference (4), and the characteristics displayed are typical of this type of structure.

The modes fall into groups and the first band contains modes with one half wave between frames (stringer ends) and one half wave in each skin-stringer span. The mode with the lowest natural frequency in the group is the one in which adjacent plates vibrate out of phase, that is, each stringer twists only and does not tend to bend. The mode with the highest natural frequency is one in which all plates vibrate in phase, with the stringers tending to bend and not twist. These two modes are called the stringer twisting and stringer bending modes respectively. Between these bounding modes there are intermediate modes in which the stringers both bend and twist. The theoretical total number of modes in a band is the same as the number of spans. In practice, however, extra modes appear with forms similar to those which are predicted. These arise from the small but not insignificant coupling of the panel with the surrounding structure.

The typical variation of the natural frequencies of the upper and lower bounding modes with skin thickness for this type of structure is shown in Figure 2.3. Also shown in the figure are the natural frequencies for a simply supported and a fully fixed plate with the same dimensions as the individual plates of the stiffened panel. The upper bounding mode has a frequency very close to that corresponding to the fully fixed edge condition. This is as expected because in the upper bounding mode the plates are all moving in phase and the stringer moves very little due to its very high bending stiffness. The plates are essentially vibrating as independent units with fixed edges.

The lower bounding mode has a frequency somewhat higher than the simply supported plate frequency. This is again as expected because the stringer torsional rigidity is not negligible compared to the skin bending rigidity. Hence it does impose some elastic torsional restraint and raise the natural frequency. This effect is somewhat reduced by stringer rotary inertia, but this quantity is usually very small.

For a given skin thickness an increase in stringer dimensions will have little effect on the upper bounding mode, but as the stringer torsional rigidity increases the lower bounding mode frequency increases. Hence the frequency bandwidth of the total group decreases and the modal density of the structure increases in the same frequency regions.

Thus far only the first group of modes has been considered. There will be other groups containing one half wave between adjacent stringers and two or three or more half waves between frames. There will also be groups containing one half wave between frames and two or three or more half waves in each skin span. The order of appearance of these groups cannot generally be predicted as this depends on the panel geometry. In fact some groups will overlap others in the frequency domain. However, the considerations which apply to the first band apply equally to the others.

The behaviour of typical builtup structures has been investigated experimentally by Clarkson and Ford (6,7,8). In reference (6) they found that the response of skin stringer panels tended to be as expected from the theory. In the fundamental mode adjacent panels vibrated out of phase, and the motions of panels separated by frames were not correlated when vibrating at frequencies of major skin resonances. Thus the assumption that it is suitable to consider only the skin stringer panel bounded by frames for model construction and theoretical calculations was justified. They also found that usually only two or three skin plates were involved in any one mode. They felt this was due to physical differences in the plates. In damping calculations they found that the damping ratio of the major peaks generally fell between 1 and 2 percent of critical.

Clarkson, in reference (8), gave filtered space correlograms of the noise pressures on aircraft components due to typical jet engines.

He pointed out the fact that noise pressures would be correlated over many skin stringer bays in the frequency range of 100 to 1000 Hz. As a result the fundamental mode of a conventional type of structure with adjacent plates vibrating out of phase with each other would not be strongly excited. The upper bounding mode, however, would be quite definitely excited as would some intermediate modes. It is then necessary at the design stage to ensure that the upper bounding mode falls well above the frequency at which the sound energy peaks.

Intermediate modes will also interact; that is, noise of one frequency will excite several modes. As a result, stresses due to intermediate modes can be quite high. Accordingly, to keep total stresses down, the lower bounding mode should fall at the same or higher frequency than the noise peak and the upper bounding mode should have as high a frequency as possible. This will result in more widely spaced intermediate modes and generally lower stresses. As described earlier open section stringers have very high bending to torsional stiffness ratios and hence well separated upper and lower bounding modes can be obtained by proper skin geometry selection.

II.2 The Vibration Characteristics of Integrally Stiffened Structures

The vibration characteristics of builtup structures are quite well documented in the literature, but there is very little available concerning the behaviour of integrally stiffened structures under conditions of acoustic or other vibratory excitation. Holehouse (9) briefly described some calculations on integrally stiffened panels. He applied Lin's technique to obtain upper and lower bounding modes for this type of structure. His results are shown in Figure 2.4. This shows the variation of frequency of the stringer torsion mode and the stringer bending mode (as described in section II.1) with increasing skin thickness for a panel with constant stringer geometry and frame pitch.

When the skin is very thin the skin plates in adjacent spans vibrate completely independently of one another because they are not stiff or massive enough to cause stringer vibration or motion. Thus, even if adjacent spans are out of phase the stringer acts as a full fixity and both bounding modes collapse on one frequency near that of the fully fixed single plate.

As the skin thickness increases it begins to influence the stringer vibration via the addition of both mass and stiffness. At some point the skin flexural rigidity approaches the stringer torsional rigidity in magnitude and the stringer twisting mode frequency drops towards that of the simply supported single plate. At the same time the stringer bending mode draws nearer to the natural frequency of the stringer as a simply supported beam.

The interaction of the stringers and skin becomes quite complex with each adding mass and stiffness to the other and influencing the overall behaviour. When this happens, however, the stringers, unlike those of a conventional structure, deflect an amount which approaches the displacement of the skin.

Lyons (10) has formulated an energy method for calculating the normal modes and natural frequencies of integrally stiffened panels and obtained values which agreed well with those obtained using a transfer matrix method. Lyons, in his experimental work, used a single panel

consisting of six spans and seven stringers. This panel was still available for use and since no tests involving acoustic excitation had been carried out on it, it was decided to use it for the panel response and damping tests. The panel calculations made by the author were by a transfer matrix method and were based on the basic geometry of this panel, which is shown schematically in Figure 2.5. This figure shows the typical features of this type of structure, i.e. rectangular and fairly thick stringers, quite close stringer spacing and relatively thick skin. Lyons, in his experiments, had clamped the panel between frames 22 inches apart (also shown in Figure 2.5) and this was adopted as frame separation for some of the calculations. However, the effect of varying this parameter and the associated aspect ratio, i.e. ratio of frame pitch to stringer pitch, was investigated. This was felt to be quite important for two reasons. In any full scale structure (or experimental apparatus) the ends of the panel perpendicular to the stringers will be supported in some way by frames. Lin and his co workers consider these to be simple supports. To obtain exact solutions the same assumption must be made in the case of the transfer matrix method.

In builtup structures the individual plate aspect ratio will always be quite high and hence this length will have little effect on the natural frequency or overall mode shape. For a typical integrally stiffened panel, however, the stringers will probably bend appreciably. Hence the important aspect ratio may be that of panel length to overall width. This is not very large and may even be less than unity in some cases. Frame pitch might, therefore, have quite a large effect on the results. Another reason for the importance of the length is the possibility, in fact certainty, of having frames which are something other than simple supports. The actual support conditions will lie somewhere between simple and fully fixed. Although there is no precise one to one correspondence or even a rigorous relationship, Szechenyi (11) has shown that a panel fixed along two opposite edges will behave very much like a similar but shorter panel simply supported along the same two edges. If the behaviour of a stiffened panel is calculated for various lengths and is not found to vary too rapidly, then a good approxi-

mation to actual full scale vibration characteristics can be made even though the true end conditions are not known.

II.2.1 Transfer Matrix Concepts

The method of transfer matrices as described in references (4) and (12) relates the displacement, slope, moment and shear at a point within a structure to the same quantities at another point. For the use of this method the analysis has to be split into two parts. One segment will deal with the individual skin plates and is referred to as the field transfer. The second part relates to the stringer influence and is called a point transfer.

II.2.1(a) The field transfer

In the case of a stiffened skin panel, either conventional or integrally stiffened, it is assumed that the skin in each span is uniform in thickness, density, modulus of elasticity, and width. Different spans need not be the same. It is also assumed that the edges perpendicular to the stringers are simply supported. A general integrally stiffened panel and the coordinate axes are shown schematically in Figure 2.6.

The equation of motion of free undamped vibration of the i^{th} span is given by

$$\nabla^4 w + \frac{h_i \rho_i}{D_i} \ddot{w} = 0 \qquad (2.1)$$

D_i is the bending rigidity of the i^{th} plate and is given by

$$D_i = \frac{E_i h_i^3}{12(1-\nu_i^2)} \qquad (2.2)$$

w is the transverse displacement of the skin and a dot denotes differentiation with respect to time.

Since each skin plate will be considered as a unit a local coordinate $\bar{y}$ is useful. This is defined by

$$\bar{y} = \frac{1}{b_i} (y - y_{\text{stringer } i}) \tag{2.3}$$

and $0 \leq \bar{y} \leq 1$

Substituting equation (2.3) into (2.1) and expanding leads to

$$\frac{\partial^4 w}{\partial x^4} + \frac{2}{b_i^2} \frac{\partial^4 w}{\partial x^2 \partial \bar{y}^2} + \frac{1}{b_i^4} \frac{\partial^4 w}{\partial \bar{y}^4} + \frac{h_i \rho_i}{D_i} \ddot{w} = 0 \tag{2.4}$$

The edges $x = 0$ and $x = \ell$ are simply supported and the harmonic solution to (2.4) is

$$w(x, \bar{y}) = Y_i(\bar{y}) \sin \frac{n\pi x}{\ell} e^{i\omega t} \tag{2.5}$$

where ω is the frequency of vibration and $Y_i(\bar{y})$ is given by

$$Y_i(\bar{y}) = A_1 \cosh k_i \bar{y} + A_2 \sinh k_1 \bar{y} + A_3 \cos k_2 \bar{y} + A_4 \sin k_2 \bar{y} \tag{2.6}$$

The four A's are unknown constants determined by boundary conditions and the k's are defined as

$$k_1 = b_i \{\omega(\frac{h\rho}{D})_i^{\frac{1}{2}} + (\frac{n\pi}{\ell})^2\}^{\frac{1}{2}} \tag{2.7a}$$

$$k_2 = b_i \{\omega(\frac{h\rho}{D})_i^{\frac{1}{2}} - (\frac{n\pi}{\ell})^2\}^{\frac{1}{2}} \tag{2.7b}$$

If the expression for Y is differentiated with respect to $\bar{y}$ three times and the result written in matrix form it can be shown that the following equation is obtained for the i^{th} span

$$\vec{Y}_i(\bar{y}) = B_i(\bar{y}) \vec{A}_i \tag{2.8}$$

where $\vec{Y}$ is the vector Y, Y', Y", Y"' (displacement and its first three

derivatives) and $\vec{A}_i$ is the vector of coefficients. B_i is a square matrix consisting of cosh $k_i\bar{y}$, sinh $k_1\bar{y}$, cos $k_2\bar{y}$ and sin $k_2\bar{y}$ and their derivatives.

Because B_i is a matrix with known elements the coefficient vector, $\vec{A}_i$, can be written explicitly. The vector $\vec{Y}_i(\bar{y})$ consisting of displacement and its three derivatives can be converted to the state vector comprising the displacement, slope, moment and shear by a simple transformation; and the final result for the field transfer is

$$\vec{Z}_i(1) = F_i\vec{Z}_i(0) \tag{2.9}$$

$\vec{Z}_i(1)$ is the state vector at the right hand side of span i and $\vec{Z}_i(0)$ is the state vector at the left side. F_i is a field transfer matrix with elements dependent on span geometry and frequency of vibration.

II.2.1(b) The point transfer

The concepts of the previous section enable the components of the state vector at one edge of a span to be related to those at the other edge. When a stringer is reached, in order to proceed to the next span it is necessary to account for the effect of that stringer. There are several assumptions made in the analysis of this effect. It is assumed that the stringer is actually attached to (or is part of) the skin only along a line and not over an area. It is further assumed that the stringer remains perpendicular to the skin and that there is no cross sectional distortion of the stringer itself. The various necessary parameters and their geometric relationship are shown schematically in Figure 2.7.

Having made these assumptions the stringer forces and moments can be calculated from the displaced shape of the skin at the stringer line plus the inertia effects due to transverse and angular velocity. The equations of continuity and equilibrium can then be applied. The former states that displacement and slope on one side of the stringer attachment line must be equal to those on the other side. The latter ensures that the sum of moments and forces applied to the stringer are

exactly balanced by inertia effects of the stringer. These effects are summed up by the expression

$$\vec{Z}(\text{Right}) = \hat{P}\vec{Z}(\text{Left}) \tag{2.10}$$

where $\hat{P}$ is a known point transfer matrix.

If the stringer cross sectional distortion were taken into account it would be necessary at each stringer to branch the system. That is, field transfers would be necessary for both attached skins and the stringer (acting as a third plate). The geometry of the integrally stiffened system, however, suggests that this will be a high frequency effect, at least higher than the frequency range of primary interest, and it has been neglected.

Some of the parameters necessary for the point transfer calculations are not completely straightforward and a resumé will be given of the methods and equations used.

Because the stringers of an integrally stiffened structure are not clearly defined entities in the region of junction with the skin some care must be taken. Some of the skin will be effective in bending, acting as part of the stringer, and this should be included in the calculations of the moment and polar moments of inertia. Holehouse (9) has suggested an effective width of skin equal to 4/3 the stringer thickness for this quantity.

The St. Venant pure tension constant for a rectangular section is not an exact quantity but for a rectangle of depth equal to or greater than about 5 times the width the constant can be approximated by 1/3 x width^3 x depth (13).

Lin (3) has defined the warping constant about the restrained shear centre as

$$c_{ws} = c_w + I_\zeta s_z^2 \tag{2.11}$$

where c_w is the warping constant about the shear centre, I_ζ is the moment of inertia of the stringer about a vertical line through the centroid and s_z is the vertical separation of the centroid and the restrained shear centre.

II.2.1(c) The total transfer and solution

Having defined the point transfer matrices it is possible to write down a chain of transfers, that is, to proceed across the entire panel. Intermediate state vectors can be eliminated by a series of vector multiplications, noting that the state vector at the right end of a span is identically equal to the state vector to the left of a stringer, leaving the required matrix equation

$$\vec{Z}_M^R = T\vec{Z}_o^L \qquad (2.12)$$

T is the total transfer matrix and is obtained by the necessary matrix and vector multiplications. All its elements are known, and its effect is to relate the vector $\vec{Z}_M^R$ at the right of the last stringer to the vector $\vec{Z}_o^L$ at the left of the first stringer. Since two of the elements of each of the $\vec{Z}$ vectors are known from panel boundary conditions, the final result is a sub-matrix from T which must have a zero determinant for the boundary conditions to be satisfied. This will occur for many frequencies, which can be found one at a time.

Seavey and Mercer (14) have developed an iteration program using Gaussian elimination to solve for these natural frequencies. When the natural frequency of a mode is known the state vector is calculated throughout the panel by back substitution into the individual transfers, and this yields the normal mode. This whole process is then repeated to find as many normal modes as required.

II.2.2 Normal Mode and Natural Frequency Calculations

The method chosen for the calculation of normal modes and natural frequencies was that of the previous section, and all computations were made using the computer program of reference 14 and the University of Southampton I.C.T. 1907 digital computer. The elastic and geometric constants for the panel of Figure 2.5 are listed in Table 2.1.

Natural frequencies, mode shapes and bending moment distributions were calculated for three cases. The edges parallel to the stringers

were considered to be (1) simply supported, (2) fully fixed, and (3) free. As was stated previously, the only condition which could be analysed using this method at present was that of simple supports along the other two edges.

The mode shapes and bending moment diagrams for the first few modes of each of these cases are shown in Figures 2.8, 2.9 and 2.10. The natural frequencies of these modes are listed in Table 2.2.

Because the existing panel had one extra skin span on each edge, the calculations for the free edge case were made assuming eight spans. This configuration is not likely to be found in practice, however, and this is the only instance in which the case was considered.

From Figures 2.8, 2.9 and 2.10 it appears that the integrally stiffened structure being considered tends to behave in a manner very similar to a flat plate. That is, the stringers deflect a great deal. This fact was expected considering the ideas of Section II.2. The one variation from pseudo-flat plate behaviour is the appearance of the first two modes in the free edge case. These modes are quite feasible, however, because the program was written to consider a stringer support at each free edge. It is not surprising, therefore, that the two outer spans tend to act as independent cantilevered plates with a large mass on the free edge.

Since these mode shapes (except for the first two of the free edge case) looked so much like flat plate modes it was felt to be advantageous to calculate the natural frequencies and mode shapes for the cases with all stringer constants identically zero. This was, in effect, the flat plate case. Only the simply supported and fixed edge configurations were considered and the values are also listed in Table 2. These calculations made it possible to have an independent check on the reliability of the transfer matrix technique, because another method was available.

Warburton (15) has used a Rayleigh-Ritz method assuming beam functions to calculate the natural frequencies of free transverse vibration of flat plates. His equations were used to calculate

the natural frequencies to compare with the transfer matrix results, and the values are listed in Table 2.2. From the comparison it appears that the method being used here is accurate and reliable.

In this context it should be pointed out that in some of the calculations some numerical difficulties did arise, resulting in spurious modes. These were always characterised by the fact that the iteration required to find them was rather slow to converge and that the mode shapes were often such that they could be discarded on appearance alone as being spurious and impossible. Since these difficulties were infrequent and the faulty values easily discarded, continued use was made of the method.

If the natural frequencies of Table 2.2 are plotted versus mode number as in Figure 2.11, an interesting observation can be made. For the lower order modes the unstiffened plate natural frequencies were much lower than those of the stiffened panel. However, as the mode number increased the natural frequency of the former increased much more rapidly than that of the latter.

This would imply that for modes involving relatively small skin curvatures the stringer stiffness effect is higher than its mass or inertia effect. However, as curvatures (and mode numbers) increase the inertia effect becomes predominant. This is a reasonable effect because the stringers are quite massive and in the higher order modes they tend to translate a great deal, rotate a great deal, or in some cases do both. It is probably the rotational effect which is making the major contribution in this respect.

Two possible problem areas related to noise excitation and acoustic fatigue became apparent in a study of Figures 2.8 to 2.11. The first is that due to the presence of stringers, the modal density or the number of the modes per unit frequency is increased and hence a band-limited noise source is capable of exciting more of the modes. Secondly, it was pointed out in Section II.1 that Clarkson has found the noise pressures to be correlated at least over several skin stringer bays. In the conventional structure this was advantageous because the fundamental and lower order modes would, therefore, not be excited strongly. In the

integrally stiffened structure under consideration, however, this is not the case. Now the fundamental mode is one in which allspans vibrate in phase, hence it can be very strongly excited. The criterion of designing the fundamental panel frequency to be near the peak in the excitation pressure spectrum could have drastic repercussions. Even if the peak is not at or near the frequency of the fundamental, this mode, being an easily excited one, can be set in motion by any significant level of excitation.

One important parameter in determining the vibration characteristics of the integrally stiffened panel is the frame spacing (for a given number of spans). The values in Table 2.2 were computed using ℓ = 22.0". The effect of varying this between 10.0 inches and 26.0 inches was investigated. In preliminary calculations it had been found that the effect of edge fixity (simply supported or clamped) parallel to the stringers had very little influence on mode shapes, natural frequencies and variation of natural frequency with mode number. The end fixity (perpendicular to the stringers), unlike in the case of a conventional structure, is likely to have a more profound effect because the bending stiffness of the stringer comes into play. Since the true end conditions are unknown, an investigation of the effect of changing distance between simple supports can also be used as a crude approximation to changing end conditions (11).

For this part of the investigation the cross-sectional geometry was kept constant as listed in Table 2.1. Only the fixed edge case was analysed due to the general similarity in behaviour which the simply supported edge case displayed. As many natural frequencies were calculated for each length as were needed to establish the general pattern of behaviour. The natural frequencies obtained are listed in Table 2.3.

The results listed in Table 2.3 can be summarised by plotting natural frequency versus mode number, with frame pitch as an independent parameter. This is shown in Figure 2.12. The shapes of all the curves in this figure are quite similar, and they tend to converge at the higher mode numbers. The higher modes involve many half waves between edges and,

therefore, the fact that the curves come together is to be expected.

The assumption that a panel with fixed ends can be approximated by a shorter one with simply supported ends is also supported by Figure 2.12. Lindberg et al have calculated some of the normal modes and natural frequencies for the same panel using their finite element method, but they assumed fixed ends. Their mode shapes agreed with those calculated by the author. The calculated natural frequencies are also shown in Figure 2.12. The natural frequencies of the high order modes should not be influenced greatly by end conditions because these contain many half waves in the width of the panel and only one in the length. This is shown to be true by the convergence of the two lines representing 22 inch frame pitch. However, the values of natural frequency for fixed ends are much higher than those for simply supported ends for the low order modes. From the change in natural frequency with mode number for the fixed end panel it would appear that a 16 inch simply supported frame pitch would adequately describe the configuration.

A closer look at the spacing of the curves of Figure 2.12 reveals that there may be some change in the behaviour pattern of the panel. As the length of the panel changes from 26 inches to 12 inches the spacing of the natural frequencies for any one mode gets larger, as it would in the case of a simple plate or of a simple beam with the inherent dependence of natural frequency on $1/\ell^2$. For lengths less than 12 inches however, the spacing then decreases again, at least for the first few modes.

The natural frequencies have been re-drawn in Figure 2.13, with frame pitch as abscissa. The mode number is now the independent variable. The first four modes definitely show the above mentioned trend. At a length of 12 inches these four are almost coincident. This effect is similar to the behaviour of a conventional builtup structure when the stringer bending and stringer torsion modes are very close together. In the builtup structure this occurs when the stringers are so rigid or the skin so flexible that each skin plate vibrates independently of all others. This cannot be the case for the integrally stiffened panel because the skin thickness has not been changed. Moreover, a further

decrease in length, which further enhances the stringer effect, allows the frequencies to diverge again.

The explanation becomes apparent if the natural frequencies of the component parts of the structure are drawn, as in Figure 2.13. The figure shows the natural frequency of the stringer as a simply supported beam. It also shows that of a single skin plate as a plate simply supported on all edges (calculated using reference 15). For completeness the natural frequencies for a plate with the same dimensions as the overall panel are shown. The single plate with fixed edges has a natural frequency above the range of the graph.

The natural frequency of the first mode tends to follow the stringer curve for the larger frame pitches. However, the stringer curve and that for the single plate simply supported on all edges intersect at $\ell \approx 12.0$ inches. At about the same length the curve giving the frequency of the panel fundamental mode begins to flatten, following more closely the curve for the simply supported single plate. This would suggest that the form of the fundamental mode might be changing at this length. If it is changing, the short frame pitch must be causing the stringer twisting mode to replace the stringer bending mode as the one with the lowest natural frequency.

If this is the case then one further difference between the two types of skin-stringer structure becomes apparent. This dissimilarity is that for a conventional structure the stringer twisting mode is always the lower bounding mode and its frequency is governed by the natural frequency of an individual plate simply supported on all edges. Because of the finite torsional restraint of the stringer the natural frequency is somewhat higher than that of the plate. Similarly, the upper bounding mode is the stringer bending mode, and its frequency is determined by the fixed single plate condition.

Thus, in a conventional structure, the order of appearance of the modes is always the same. It must be because the two bounding modes are both governed by plate relationships, and as the length between frames changes these two relationships change frequency in about the same way. Under some conditions (e.g., a very thin skin) they may come close together,

but for any length their order of appearance in the frequency domain remains unchanged. The only other factor which might change this is natural frequency of the stringer as a simply supported beam becoming very low. This cannot happen with the assumed very large (or infinite) bending stiffness.

The fundamental mode natural frequency for the integrally stiffened panel is governed by either the stringer beam frequency or skin plate frequency. The change of these two quantities with frame pitch is radically different. The stringer frequency is inversely proportional to the length squared. The natural frequency of the single plate varies much less rapidly for the very large aspect ratio involved and hence the two intersect. In fact, it is probable that for very short lengths when the stringer natural frequency would be even higher than the single fixed plate frequency the panel would then behave in exactly the same manner as a builtup panel. However, for a practical range of frame pitches, represented by figure 2.13, the stringer is of prime importance in determining natural frequencies.

In the integrally stiffened skin a major factor governing the frequency and shape of the fundamental mode is the frame pitch. For the particular panel geometry studied, for frame pitches greater than about 12 inches the first mode is expected to be the stringer bending mode. For frame pitches less than that it is expected to be the stringer twisting mode. The important thing, however, is that it is not possible to say, a priori, what the order of appearance of modes will be.

The easiest way to determine whether or not the order of appearance of the various modes is, in fact, changing is to inspect the mode shapes for various frame pitches. It has already been seen in Figure 2.9(a) that the 22 inch frames result in mode shapes similar to those of an unstiffened flat plate. In Figures 2.14, 2.15, 2.16 and 2.17 are shown the first 10 calculated mode shapes for 10 inch, 11 inch, 12 inch, and 14 inch frame pitches and there is a very definite change in behaviour. From Figure 2.12 it is apparent that the three shortest lengths could possibly be considered to have their natural frequencies divided into

groups as with a conventional structure. Figure 2.14 shows clearly that the stringer torsion mode is the fundamental mode for the panel with 10 inch frames. Similarly, the sixth and highest mode in the first band is the stringer bending mode. For this case even the next group of modes is conforming to the pattern. The first mode in the second band is the one with effectively two half waves per span. Again successive modes have one fewer half wave.

The first six mode shapes of the 11 inch panel shown in Figure 2.15 also conform to the behaviour of a builtup structure. However, beginning with the seventh mode, each successive mode has one more half wave. It is expected that this frame pitch will have natural frequencies which are not grouped beyond the first six.

Figure 2.16 shows the mode shapes of the 12 inch panel. This is, as expected, the transition length. The first four modes fall very close together in frequency and the fundamental mode is neither pure stringer torsion nor pure stringer bending. Even for this length, however, for modes higher than the second the number of half waves increases one per mode.

Figure 2.17 shows the 14 inch panel mode shapes. At this length the behaviour has settled completely into that involving very long frame pitches. The first mode has one half wave across the specimen and this is incremented one per mode.

Figures 2.14 to 2.17 inclusive show that there is, indeed, a change in the fundamental behaviour of the integrally stiffened panel with frame pitch and that some care must be taken at the design stage to ensure that the correct frequency and wavelength criteria are adopted.

Even when the stringer twisting mode precedes the stringer bending mode in an integrally stiffened structure, the behaviour is not exactly like that of the conventional structure. In a builtup stiffened skin the natural frequencies tend to be somewhat higher than those of the governing component of the lower bounding mode. That is, the stringer torsional stiffness effect is greater than its inertia effect. In the integrally stiffened skin the natural frequency tends to be lowered, indicating that the inertia effect of the stringer is greater than its

stiffness effect.

When the stringer bending mode appears first the natural frequency is somewhat lower than that of the stringer alone. The skin is now adding more inertia than stiffness to the stringer.

It has been stated that some modes will contain more than one half wave between frames. Natural frequencies and mode shapes were calculated for the panel with 22 inch frames and 2 half waves in the length. These values are listed in Table 2.3 and they can be seen to be exactly the same as those for the 11 inch panel with one half wave. The mode shapes as well as the natural frequencies were also exactly the same. Because of this there is little further to be gained from an investigation in depth of the panel with multi-half waves in its length and no further values were calculated.

III. THE VIBRATION CHARACTERISTICS OF BEAMS TAKEN FROM AN INTEGRALLY STIFFENED SKIN CROSS SECTION

Lyons (10) in a series of tests found that he could greatly reduce the response of an integrally stiffened panel to single point excitation by adding a narrow strip of damping material to the tops of the stringers across the middle of the panel. In order to be able to analyse the energy dissipation phenomenon it will be necessary to know the energies and motions involved in the whole system. The natural frequencies and mode shapes can be calculated for the panel using the method of II.2. When the mode shapes are known the kinetic and potential energies can be calculated by making use of the relationships of elasticity theory. This process, however, will be long and tedious and it will be difficult to make general conclusions because the results will be highly dependent on the interacting effects of different panel parameters.

From the results of section II it is expected that in most cases the integrally stiffened panel mode shapes will closely resemble beam functions involving the total panel width, and that the majority of the modes in the frequency range of interest will have only one half wave in the length. Therefore, the damping material across the panel centre line will effectively be in motion under the influence of a vibrating beam. Since this is the case, a beam which is a narrow slice of an integrally stiffened panel should prove useful as a model for energy dissipation estimates in the calculations of the next section. Such a model will add nothing to the understanding of the panel vibration characteristics but should prove manageable enough to be able to draw some general conclusions concerning the phenomenon taking place when damping material is added to the tops of the stringers.

One other very real advantage of using a beam model for the structure is the relative ease of obtaining controlled experimental conditions for beams. This will prove useful in the quantitative verification of the estimates made.

The beam structure itself, however, must be analysed before it can be used in energy dissipation calculations. It is expected that the beam will retain some, but not all, of the features of the machined plank. In the panel analyses the ends of the stringers were assumed to be simply supported along the skin line. As a result, these stringers were deformed in bending and in torsion along their length to conform with the skin in displacement and slope. Therefore, they contributed a great deal of stiffness. In the beam structure the stringers are only as long as the beam is wide and they are not supported in any other manner than through the skin attachment. The stringers will have no tendency to bend along their length until their natural frequency as free-free beams is approached. For a narrow beam and, hence, a short stringer, this frequency is extremely high and the effect can be ignored.

In section II it was pointed out that the stringer cross section can also distort, with the stringer effectively acting as a cantilever about the skin attachment line. As in the case of the panel, the stringer in the beam model is quite thick and the fundamental cantilever frequency is well above the frequency range of interest. The stringer is attached to an elastic member and not a rigid foundation. Hence the coupled system natural frequency involving stringer distortion will be somewhat lower than that of the stringer alone as a cantilever, but still high enough for the effect to be neglected.

As a result of the above assumptions the stringers in the beam model can be considered to be blocks of inertia with one finite dimension. This places their effect out of the plane of the beam (skin) and makes rotational effects important.

The natural frequencies for the beam model will be first calculated by an energy method assuming simple mode shapes. These will then be compared with exact mode shapes and natural frequencies calculated using a modification of the transfer matrix program of the previous section, and their suitability for use in damping estimates assessed.

III.1 Energy Method Using Simple Assumed Mode Shapes

For ease of analysis the energy method calculations will be made for a simply supported beam. It has been shown in Section II that for most practical lengths between frames an integrally stiffened skin has mode shapes which closely resemble beam functions involving the whole width. It may be possible, with reasonable accuracy, to consider the centre section of the plate with simply supported edges, and hence the simply supported beam model, to have the mode shape

$$w = w_o \sin \frac{n\pi y}{L} \sin \omega t \tag{3.1}$$

where $L = \sum_i b_i$ of Section II.

The case analysed was an N span beam having M stringers where M = N + 1 or N - 1 (with or without a stringer at each end respectively). The stringer spacing was assumed constant and it was assumed, as in the panel calculations, that the stringers remain perpendicular to the skin and that they do not distort.

Since the stringers do not bend in either plane, the total strain energy in the system is contained within the bending beam. This total strain energy is given by the expression

$$T_m = \frac{EI}{2} \int_o^L (w'')^2 dy \tag{3.2}$$

(ref. 16, for example).

For the assumed mode shape this can be shown to be

$$T_m = \frac{EIn^4\pi^4}{4L^3} w_o^2 \sin^2 \omega t \tag{3.3}$$

The total kinetic energy is made up of contributions from the beam and each of the stringers.

The kinetic energy of the beam is given by

$$V_b = \frac{\rho h d}{2} \int_o^L (\dot{w})^2 dy \tag{3.4}$$

and this is equal to

$$v_b = \frac{\rho h d L}{4} \omega^2 w_o^2 \cos^2 \omega t \tag{3.5}$$

If stringer i is at location y_i, then the transverse translational velocity of that stringer will be $\dot{w}_i$ and the translational kinetic energy will be

$$v_{t_i} = \frac{H \rho h_s d}{2} (\dot{w}_i)^2 \tag{3.6}$$

where h_s is the stringer thickness.

The total translational kinetic energy for all the stringers will be

$$v_t = \frac{H \rho h_s d}{2} \sum_{i=1}^{M} (\dot{w}_i)^2 \tag{3.7}$$

This can be shown to be

$$v_t = \frac{H \rho h_s d}{2} \omega^2 w_o^2 \cos^2 \omega t \sum_{i=1}^{M} \sin^2 \frac{n \pi y_i}{L} \tag{3.8}$$

Each stringer is also rotating about its line of attachment to the skin, and the kinetic energy associated with this is given by

$$v_{r_i} = \frac{\rho d h_s H^3}{6} (\dot{\theta}_i)^2 \tag{3.9}$$

When the value of $\dot{\theta}_i$ is substituted and the sum over all stringers taken

$$v_r = \frac{\rho d h_s H^3}{6} \frac{\omega^2 n^2 \pi^2}{L^2} w_o^2 \cos^2 \omega t \sum_{i=1}^{M} \cos^2 \frac{n \pi y_i}{L} \tag{3.10}$$

For resonance (stationary total energy) the maximum kinetic energy in one cycle equals the maximum potential energy. The kinetic energy is a maximum when $\cos \omega t = 1$ and the potential energy greatest for $\sin \omega t = 1$. w_o^2 is common to equations (3.3), (3.5), (3.8) and (3.10) and cancels. The relationship for resonance is given by

$$\frac{EIn^4\pi^4}{4L^3} = \frac{\rho L\omega^2 hd}{4} + \frac{H\rho Lh_s d\omega^2}{4}\left[\frac{2}{L}\sum_{i=1}^{M}\sin^2\frac{n\pi y_i}{L}\right.$$

$$\left. + \frac{2H^2}{3L^3}n^2\pi^2\sum_{i=1}^{M}\cos^2\frac{n\pi y_i}{L}\right] \qquad (3.11)$$

This can be rewritten

$$\frac{EIn^4\pi^4}{\rho hdL^4} = \omega^2\left[1 + \frac{2Hh_s}{Lh}\sum_{i=1}^{M}\sin^2\frac{n\pi y_i}{L} + \frac{2H^3h_s}{3L^3h}n^2\pi^2\sum_{i=1}^{M}\cos^2\frac{n\pi y_i}{L}\right] \qquad (3.12)$$

Define $\frac{h_s}{h} = \alpha$ and $(\frac{H}{L}) = \beta$, and note that $\frac{n^4\pi^4 EI}{\rho hdL^4} = \omega_{on}^2$ (3.13)

where ω_{on} is the natural frequency of the n^{th} mode for the beam without any stringers. (Reference 17, for example.) Equation (3.12), after some algebraic manipulation becomes

$$(\frac{\omega_{on}}{\omega_{Mn}})^2 = 1 + 2\alpha\beta\left[M + (\frac{\beta^2n^2\pi^2}{3} - 1)\sum_{i=1}^{M}\cos^2\frac{n\pi y_i}{L}\right] \qquad (3.14)$$

In equation (3.14) the frequency has been written as ω_{Mn}, which is the natural frequency of the n^{th} mode for the beam with M stringers.

In Appendix I it is shown that for the internal stringers

$$\sum_{i=1}^{M}\cos^2\frac{n\pi y_i}{L} = N - 1 \quad \text{for } \frac{n}{N} \text{ an integer} \qquad (3.14a)$$

and $$\sum_{i=1}^{M}\cos^2\frac{n\pi y_i}{L} = \frac{N}{2} - 1 \quad \text{for } \frac{n}{N} \text{ not an integer.} \qquad (3.14b)$$

When there are stringers at the ends of the beam, the contribution to the summation from the end stringers is $\cos^2 0 + \cos^2 n\pi = 2.0$. Therefore, whether n/N is an integer or not the summation with end stringers is 2.0 greater than the summation without. Equation (3.14) can then be rewritten for each case of interest. For $\frac{n}{N}$ equal to an

integer

$$(\frac{\omega_{on}}{\omega_{Mn}})^2 = 1 + \frac{2M\alpha\beta^3 n^2 \pi^2}{3} \tag{3.15}$$

whether there is a stringer at each end or not.

For n/N not equal to an integer and a beam without a stringer at each end (M = N - 1)

$$(\frac{\omega_{on}}{\omega_{Mn}})^2 = 1 + N\alpha\beta + \frac{\alpha\beta^3 n^2 \pi^2 (N - 2)}{3} \tag{3.16}$$

For n/N not equal to an integer and a beam with stringers at each end (M = N + 1)

$$(\frac{\omega_{on}}{\omega_{Mn}})^2 = 1 + N\alpha\beta + \frac{\alpha\beta^3 n^2 \pi^2 (N + 2)}{3} \tag{3.17}$$

Equations (3.15), (3.16) and (3.17) were used to calculate natural frequency ratios for various configurations of the beam with the parameters listed in Table 3.1. The ratio ω_{Mn}/ω_{on} is shown in Figure 3.1 for the beam with and without stringers at each end.

Equation (3.13) was used to calculate ω_{on} and these values were then substituted into (3.15), (3.16) and (3.17) to obtain the derived natural frequencies of the beam with stringers. These values of ω_{Mn} are listed in Table 3.2.

III.2 Transfer Matrix Analysis

III.2.1 Concepts and Derivation

In order to be able to use in subsequent damping analyses the mode shapes assumed for the energy method calculations, it is necessary to verify that the results of Section III.1 are a reasonable approximation to the true solution. To do this the transfer matrix method, as briefly outlined in Section II.2.1, has been applied.

The beam geometry of Section III.1 is considered and it is again assumed that the stringers remain perpendicular to the skin and do not bend or distort. The equation of each span is given by the general beam function,

$$Y_i = A_1 \cosh k_i\bar{y} + A_2 \sinh k_i\bar{y} + A_3 \cos k_i\bar{y} + A_4 \sin k_i\bar{y} \qquad (3.18)$$

where

$$k_i = b_i\left(\frac{12\omega^2\rho}{Eh_i^2}\right)^{\frac{1}{4}} \qquad (3.19)$$

and

$$\bar{y} = \frac{1}{b_i}\left(y - \sum_{g=1}^{i} b_g\right) \qquad (3.20)$$

The notation used is that of section II.2.1 with the exception that there is no x coordinate or variation in the x direction.

The various transformations described in II.2.1 are made to arrive at a matrix equation relating displacement, slope, moment and shear force at the right edge of the span to the same quantities at the left. That is, the state vector at $\bar{y} = 1.0$ is related to the state vector at $\bar{y} = 0$.

This can be written

$$\{Z(1)\} = [T_{span}]\{Z(0)\} \qquad (3.21)$$

$[T_{span}]$ is the total field transfer and involves known geometric, trigonometric and elastic constants.

The analysis at the stringers amounts to writing down the simple equations of continuity and equilibrium. The following sketch

shows the notation and sign convention.

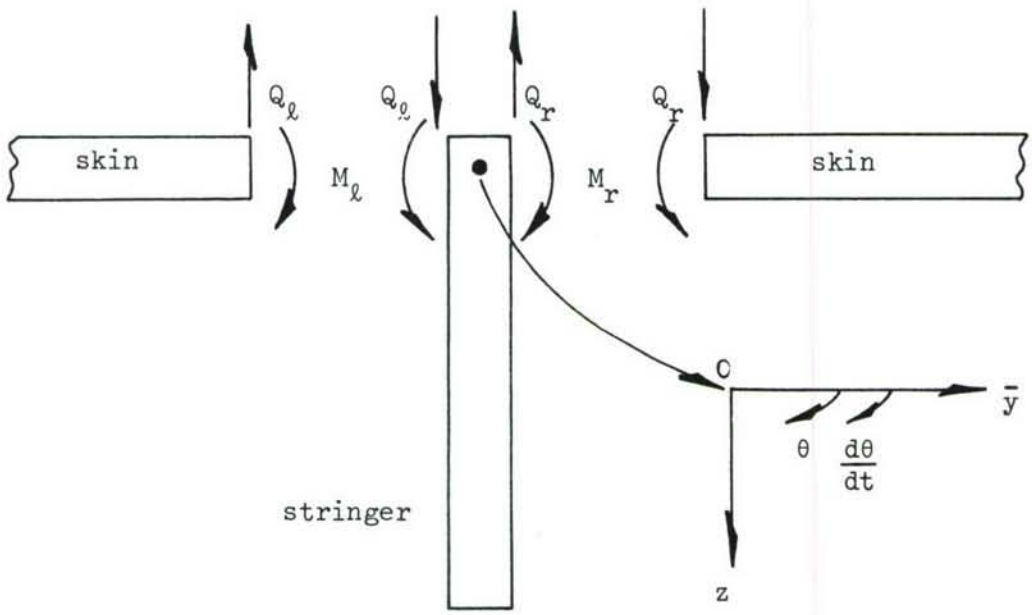

The subscript "ℓ" denotes left and "r" denotes right.

By equilibrium of forces and moments

$$Q_\ell - Q_r = \rho H h_s \ddot{w}$$

and per unit width (3.22)

$$M_\ell - M_r = -\rho I_s \ddot{\theta}$$

By continuity

$$w_\ell = w_r$$

and (3.23)

$$\theta_\ell = \theta_r$$

Combining equations (3.22) and (3.23) results in

$$\{Z_r\} = [T_{str}] \quad \{Z_\ell\} \tag{3.24}$$

where $[T_{str}]$ is a known matrix.

Equations (3.21) and (3.24) can then be used across successive stringers and skin spans to set up a chain of transfers to carry the calculations right across the total structure.

For any end conditions two of the values at each end will be known. The result is that in the total transfer matrix there is a sub-matrix which must have a zero determinant for a solution to exist. The frequency at which the determinant becomes zero is then the natural frequency, and when this is substituted back into the individual transfers the state vectors (displacements, slopes, moments and shear forces) are obtained. These are the normal modes.

The program of reference 14, using the Gaussian elimination method, was suitably modified for use in the beam analysis. It was written such that there was always considered to be a stringer at each end of the beam. This allowed the general solution to be obtained, and if the solution for the case with no end stringers is desired the suitable parameters can be set to zero.

Because of the assumptions made, the program is written with each stringer considered to be only a mass with finite dimensions. However, in the point transfer or stringer effect analysis it would be a relatively easy task to include linear and rotary spring forces. This would, in effect, give the solution to the beam on many elastic supports with added inertia at the supports. Letting the inertia terms go to zero would give the case of a simple beam on many elastic supports. Similarly, a beam on elastic supports with added inertia between supports could be treated by considering each support or mass to be a stringer with the suitable parameters.

III.2.2 Transfer Matrix Calculations and Comparison with the Energy Method

The method and computer program were first tested by letting all stringer parameters go to zero. This, in effect, should yield the solution to the simple beam problem. The calculated natural frequencies are listed in Table 3.3 together with the natural frequencies calculated by reference

18 for the same beams. The agreement between the two is close enough to inspire confidence in both the technique and the computer program used to make the iterations and calculations.

The program was then used to calculate the natural frequencies and normal modes for the beam with stringers. The values were computed for the simply supported and fully fixed beams with 5 and 7 stringers. As expected, the presence or absence of stringers at the ends made no difference to the frequencies or mode shapes of the fixed end beam. The calculated natural frequencies are shown in Table 3.2. The transfer matrix calculations are also summarised in Figure 3.2.

Figure 3.2 can be compared with Figure 2.11, which shows the same quantities for the stiffened panel. In the region where the natural frequency of the panel was raised above that of the unstiffened one, the effect of the stringers on the beam natural frequency is relatively small. In the panel the stiffening effect of the stringers predominated and this is absent in the beam. When the stringers began acting to depress the panel natural frequency they were beginning to have a greater mass effect and were also beginning to influence the mode shapes. This also occurs in the beam, and this is the point at which the simple sinusoidal modes begin to be less useful and accurate as an approximation to the true mode shapes.

From Table 3.2 it appears that the simple energy method approach of Section III.1 gives reasonable results for about the first 5 modes. The mode shapes obtained by using the computer for these modes are shown in Figure 3.3(a) and the bending moments in 3.3(b). The mode shapes are virtually indistinguishable from simple sinusoids, but the bending moments give a good indication of when the two methods begin to disagree appreciably. The bending moment for the assumed sinusoidal mode shape of a simply supported beam is also sinusoidal. Thus, when the true bending moment begins to vary appreciably from a sinusoid the approximation will be seriously in error.

From Figure 3.3(b) it can be seen that the bending moment for the first four modes has approximately the right form for good agreement. Mode 5 shows some deviation, but is probably still useful. Mode 6 is

already different enough to make the use of the simple mode shapes very doubtful.

The natural frequencies and mode shapes were also calculated for beams with different skin thickness. These results are plotted in Figure 3.4. The thickness was not taken to be less than 0.05 inches because the stringer geometry was kept constant and it was felt that any thickness less than this would not be practical with a stiffener of the given size. The stringers, of course, affect the thin beams more than they do the thicker ones, as shown by the dependence of equations (3.15), (3.16) and (3.17) on α, but even in the thinnest considered the first four modes had bending moment distributions which would enable the sinusoidal mode shape assumption to be used with reasonable accuracy.

Figure 3.5 shows the same information as 3.4, but the independent variable is now the mode number. Figures 3.4 and 3.5 by their smooth and continuous change show that there is no effect taking place in the beam similar to the fundamental mode shape change which took place in the panel and became evident in Figure 2.13. This was expected because of the absence of the stringer stiffness terms.

If the thickness were allowed to decrease still further, the stringers would undoubtedly have so much effect as to change even the low order mode shapes, but this was felt to occur at such a low value of h that it was not investigated further.

IV. DAMPING TREATMENT AND ANALYSIS

It was shown in Section II that in most cases of interest an integrally stiffened panel will have mode shapes which resemble beam functions over the whole width. In Section III an analysis was carried out for a beam with the integral stiffeners acting as added inertia, and it was found that for the first few modes of the simply supported beam the simple sinusoidal mode shapes are a good approximation to the exact functions. It is now necessary to investigate some damping treatments and their behaviour when applied to the beam vibrating in the assumed modes.

Lyons (ref. 10) mounted the panel of Figure 2.5 in a steel framework and excited it harmonically at a single point (indicated in the Figure) by an electrodynamic vibrator. This was carried out with no added damping and also after the application of each of the three treatments shown in Figure 4.1. The frequency response was determined in each case and the damping of the major peaks was measured. The width of damping material added across the tops of the stringers (Figure 4.1(b)) was also varied. The damping material used for these tests was LD400 (Lord Manufacturing Company). The density of this material is about 0.0577 lbs per cubic inch. The elastic properties are not accurately known and they vary rapidly with temperature and somewhat with frequency, but at room temperature and over the range of frequencies of interest, values of E_d of 7×10^5 lbs per square inch and η_d of 0.6 are reasonable. The thickness used was 0.060 inches in these experiments.

The frequency response curves obtained are shown in Figure 4.2, together with the measured damping of the peaks. The reduction of the peaks shown by this figure is quite remarkable in the light of the small mass addition which has been made in some of the cases. There is no curve shown for the damping treatment illustrated in Figure 4.1(c) because there was no significant difference between this treatment and that of 4.1(b).

A summary of the results of these single point excitation tests is given in Table 4.1. The RMS values were obtained by summing over the whole of the frequency response curve in the frequency range of interest.

It is interesting to note from Figure 4.2 that a strip of the damping material only 1 inch wide bonded to the tops of the stringers was somewhat more effective in reducing the response than a strip some 20 times wider bonded to the inner skin surface between stringers, and this phenomenon warrants further investigation.

IV.1 Analysis of the Damping System

The damping treatment of Figure 4.1(a) has been well documented in the literature. This is an unconstrained damping layer and has been analysed in references 20, 21, 22 for example, for beams and plates. In this configuration the energy loss depends upon the ratios of flexural stiffness of the structural material and the damping material and also on the location of the neutral axis of the composite system. Since the integrally stiffened skin will normally vibrate in modes resembling flat plate modes the neutral axis will be somewhere in the skin. As a result the unconstrained damping layer will be close to the neutral axis and relatively inefficient. This is borne out by Figure 4.2 and Table 4.1.

The treatments shown in Figures 4.1(b) and (c) will be a combination of the viscoelastic link effect as discussed by Jones (23, 24) and the tuned damper effect discussed and analysed by Henderson (25) and by Jones and his associates (26 to 29). The treatment of 4.1(c) might be fairly closely related in behaviour to the systems of references 25 to 29, but the masses would then have to be quite large in order that the damping beam will tend to act only as a viscoelastic suspension for the masses. The treatment of 4.1(b) most closely resembles that of reference 29, but there is a distinct difference. In reference 29 Nashif and Jones considered the energy dissipated by the motion of the ends of an elastic beam. In the case being considered here the energy is being dissipated throughout the whole of a beam of viscoelastic material.

The damping material bridging the stringers, whether or not there are added masses, will behave as a continuous system in its own right forced to vibrate by the ends of the stringers to which it is attached. The transverse vibration of the damping beam will certainly be influenced by the extensional excitation also exerted by the stringers as they rotate about the skin line. However, the solution of the problem of the simultaneous transverse and longitudinal vibrations of a heavily damped beam excited by known motions of the ends was considered to be far too complex and rather unnecessary at this stage.

The energy dissipated in a viscoelastic material is proportional to the elastic energy contained in the material. When the damping material is added to the stringers, it will add both mass and stiffness to the original structure. The former lowers the natural frequency and the latter raises it, but only in proportion to the amount by which they change the kinetic and strain energies respectively. If the addition of the damping material influences the total kinetic or strain energy of the system to a great extent then it is no longer the same system with a small addition but rather it is an entirely new system, and the basic structural analysis of Section III no longer applies. Therefore, in order to calculate the strain energy in the damping material it is assumed that the addition of the viscoelastic damper to the tops of the stringers affects only the amplitude of vibration and not the natural frequencies or mode shapes of the integrally stiffened structure.

The fact that the peaks in the response curves of Figure 4.2 for the damped and undamped panel fall at approximately the same frequency tends to justify this assumption. It is not conclusive proof because the mass and stiffness effects could be just balancing, but it would be fortuitous for this to be the case for all the frequencies and modes involved.

A further assumption made in the damping treatment analysis is that the extensional and flexural effects can be treated separately. The energy dissipated by each effect will be calculated and this will be added to the base structure energy loss to evaluate a total dissipation and overall loss factor.

IV.2 Extensional or Link Analysis

The extensional effect is quite straightforward to analyse if some further assumptions are made. It is assumed that the frequencies involved are low enough that longitudinal wave effects can be ignored. That is, the whole of the damping material between adjacent stringers is considered to be in a state of uniform axial stress or strain.

For viscoelastic materials subjected to steady state harmonic strain a good representation of the stress strain curve is given by an ellipse. It can be shown that a material whose modulus of elasticity is complex, i.e., has a real and imaginary part, conforms with this behaviour. The method of analysis used in the literature, therefore, is the same as that for purely elastic materials with a complex modulus substituted for the real quantity.

Let the extensional stiffness of the damping material between adjacent stringers be represented by $K^* = K(1 + i\eta_d)$ and the elongation by δ. Then the extensional force required is $K(1 + i\eta_d)\delta$. This "complex" force applied at the stringer tip parallel to the skin applies to the skin a moment which is added to the stringer inertia term. The force is designated "complex" because it is not in phase with the displacement, and the out of phase component contributes the energy dissipation capability. The magnitude of the moment due to this force will depend on H, the stringer depth. The magnitude of δ will be proportional to H and to the change in skin slope between adjacent stringers.

For a material in extension or compression

$$K = \frac{E_d b_d h_d}{\ell} \tag{4.1}$$

It will later be convenient to have all force and energy quantities in terms of the damping beam flexural rigidity, $E_d I_d$, where

$$E_d I_d = \frac{1}{12} E_d b_d h_d^3 \tag{4.2}$$

Therefore, write

$$E_d b_d h_d = \frac{12 E_d I_d}{h_d^2} \tag{4.2(a)}$$

and

$$K = \frac{12E_dI_d}{h_d^2\ell} \tag{4.3}$$

The energy dissipation in a system with damping characterised by a complex modulus can be calculated from the expression (ref. 30)

$$\frac{\text{Energy dissipated per cycle}}{\text{Maximum energy stored during the cycle}} = 2\pi\eta \tag{4.4}$$

Ungar (ref. 31) gives the relationship between strain and strain energy for a system in extension as

$$\Delta T_{de} = \tfrac{1}{2}\, k|\varepsilon|^2 \tag{4.5}$$

where ΔT_{de} is the extensional strain energy per unit length, $|\varepsilon|$ is the modulus of the strain phasor and k is the extensional stiffness (real part) per unit length. Since it has been assumed that the strain is uniform throughout, and the material cross section is uniform, the total extensional strain energy is

$$T_{de} = \tfrac{1}{2}\, K\, |\delta|^2 \tag{4.6}$$

Substituting for K (eq. (4.3)) gives

$$T_{de} = \frac{6E_dI_d}{h_d^2\ell}\, |\delta|^2 \tag{4.7}$$

This strain energy must be summed with the flexural strain energy in the damping material to give a total from which the energy dissipation can be calculated.

IV.3 Flexural Analysis

To determine the flexural behaviour of the damping material analytically, the equations of motion must be solved. The beam is considered to be undergoing steady state forced harmonic transverse vibration. However, the forcing functions are applied at the ends in the form of known translations and rotations and will enter the solution as end conditions.

The Euler-Bernoulli equation with the force equated to zero describes the motion of an element of a beam undergoing transverse vibrations with no external force applied to that element. This is exactly the case of the beam excited at the ends only (all forces and moments are applied at the ends only and not on internal elements) and the end translations and rotations will be used as some of the boundary conditions necessary to solve for the unknown coefficients in the solution.

The standard procedure of replacing the real flexural rigidity by the corresponding complex one $E_d I_d(1 + \eta_d)$ is also adopted and the equation of motion is

$$E_d I_d(1 + i\eta_d) \frac{d^4 w}{dy^4} = - \mu_d \frac{d^2 w}{dt^2} \qquad (4.8)$$

The usual assumption that $w = Ye^{i\omega t}$ leads to the solution

$$Y = B_1 \cos \phi y + B_2 \sin \phi y + B_3 \cosh \phi y + B_4 \sinh \phi y \qquad (4.9)$$

where $$\phi = \lambda(1 + i\eta_d)^{-\frac{1}{4}}. \qquad (4.10)$$

The values of the coefficients are determined by substituting the end or boundary conditions.

The damping material could be attached to and excited by a stringer at one end only or at both ends. These will give different coefficients and must be treated separately.

IV.3(a) Cantilivered treatment

When the damping material is bonded to only one stringer it is acting as a cantilever. Consider the stringer to be at $y = 0$, (damping beam coordinates). Then

$$\frac{d^2w}{dy^2} = \frac{d^2Y}{dy^2} = 0 \quad \text{at} \quad y = \ell \tag{4.11}$$

and

$$\frac{d^3w}{dy^3} = \frac{d^3Y}{dy^3} = 0 \text{ at } y = \ell \tag{4.12}$$

At $y = 0$ we have

$$\begin{aligned} w &= w(0) \\ \text{and} \quad \frac{dw}{dy} &= \theta = \theta(0) \end{aligned} \tag{4.13}$$

These are known quantities from the structural beam mode shape, which is assumed unchanged. Substituting (4.11), (4.12) and (4.13) into (4.9) and its derivatives, leads to the following solution for the coefficients:

$$B_4 = \frac{1}{2\phi[1 + \cos \phi\ell \cosh \phi\ell]}\{[\theta(0)\cos \phi\ell - \phi w(0)\sin \phi\ell][\cosh \phi\ell + \cos \phi\ell]$$

$$- [\phi w(0)\cos \phi\ell + \theta(0)\sin \phi\ell][\sinh \phi\ell - \sin \phi\ell]\} \tag{4.14}$$

$$B_3 = \frac{1}{\phi[\cosh \phi\ell + \cos \phi\ell]} [\phi w(0)\cos \phi\ell + \theta(0)\sin\phi\ell - B_4\phi(\sinh \phi\ell + \sin \phi\ell)] \tag{4.15}$$

$$B_2 = \frac{\theta(0)}{\phi} - B_4 \tag{4.16}$$

$$B_1 = w(0) - B_3 \tag{4.17}$$

This method of solution is similar to the inverse method described by Jones in reference 22, and the end force and moment required to sustain the motion can be calculated. The system is linear, and for ease of

calculation $E_d I_d \frac{d^2w}{dy^2}$ and $E_d I_d \frac{d^3w}{dy^2}$, which are the moment and force exerted (by the stringer on the damping beam and vice-versa) were computed for $w(0) = 1.0$ and $\theta(0) = 0$ and then for $w(0) = 0$ and $\theta(0) = 1.0$ as separate cases. These can then be added in any ratio by the theory of superposition. In order to have values for a range of frequencies (λ) and loss factors, the equations were programmed for a digital computer. Curves of the modulus of the force required to maintain unit translation and unit rotation are shown in Figure 4.3. Similar curves for the moment are in Figure 4.4. The phase angle of the moment for the cantilever excited by translation only is shown in Figure 4.5. Similar curves exist for the other three sets of curves of Figures 4.3 and 4.4 but are not shown.

An examination of Figures 4.3, 4.4 and 4.5 begins to show why this form of damping treatment is effective. For all but the very low frequencies (small λ) the forces and moments exerted on the stringers are quite large. Also, the phase angle is not zero and hence energy dissipation takes place. Unlike tuned dampers, however, the effect spreads over a wide frequency bandwidth because of the multi-modal behaviour of the damping materials. This last fact also begins to explain why the treatment of figure 4.1(c) was no more effective than that of 4.1(b). At the frequencies involved, the value of λ is well above the point in the curves at which the forces and moments have become quite large and the damping beam undergoes considerable transverse flexural motion. An added mass would slightly displace the peaks and troughs in the curves along the frequency axis, but the total effect must be quite small for any reasonable mass addition.

The effect of increasing the loss factor is that of reducing the variations of the force and moment curves. Effectively the modal overlap is increased. Even for the fairly low value of 0.2, however, the excursions are not too severe and the method is useful.

A form of reciprocity behaviour can be seen in Figures 4.3 and 4.4. The moment required to maintain unit displacement is the same as the force required to maintain unit rotation. The phase angles too,

have the same form but differ by 180 degrees.

In Figures 4.6 and 4.7 are shown typical displaced shapes of the damping material beam for a loss factor of 0.6 and for various values of λ. These further reinforce the conclusion concerning the multi-modal behaviour of the damping beam.

IV.3(b) Beam Excited at Both Ends

If each end of the damping material beam is bonded to a stringer the coefficients of equation (4.9) will be determined by known displacements and rotations at $y = 0$ and $y = \ell$.

$$\text{At } y = 0, \quad w = w(0) \text{ and } \theta = \theta(0) \tag{4.18}$$

$$\text{At } y = \ell, \quad w = w(\ell) \text{ and } \theta = \theta(\ell) \tag{4.19}$$

Following the same procedure as in Section IV.3(a) leads to the coefficients:

$$B_4 = \frac{1}{2\phi[1 - \cos\phi\ell \cosh\phi\ell]} \{[\theta(\ell) + \phi w(0)\sin\phi\ell - \theta(0)\cos\phi\ell] \times [\cosh\phi\ell - \cos\phi\ell] - [\sinh\phi\ell + \sin\phi\ell][\phi w(\ell) - \phi w(0)\cos\phi\ell - \theta(0)\sin\phi\ell]\} \tag{4.20}$$

$$B_3 = \frac{1}{\phi[\cosh\phi\ell - \cos\phi\ell]} [\phi w(\ell) - \phi w(0)\cos\phi\ell - \theta(0)\sin\phi\ell - \phi B_4(\sinh\phi\ell - \sin\phi\ell)] \tag{4.21}$$

$$B_2 = \frac{\theta(0)}{\phi} - B_4 \tag{4.22}$$

$$B_1 = w(0) - B_3 \tag{4.23}$$

The values of moment and shear were calculated taking one end condition at a time to be non zero. In this case it is necessary to compute the force and moment at each end due to the excitation at each end.

In Figures 4.8 to 4.11 inclusive are shown these quantities considering excitation at one end only. As in the cantilevered beam

the phase angle is, in general, non zero. This again implies forces and moments which are not in phase with the displacement and hence energy dissipation capability. Two of the calculated sets of phase angle curves are shown in Figures 4.12 and 4.13. These are typical of all the others of the same type.

A comparison of Figures 4.3 and 4.8 and of 4.4 and 4.9 reveals that for a given excitation the force and moment at the excited end are very similar despite the different conditions at the other end of the beam. The phase angle curves of Figures 4.5 and 4.12 are also very similar. This implies that most of the energy which is fed into the ends of the beam is, in fact, dissipated and that very little of it is reflected back from the opposite end. This is highly desirable and points to good structural vibration damping capabilities.

The fact that the forces and moments at the forced end are similar whether the other end is fixed or free does not imply that the two systems will have the same flexural effect in practice. It must be remembered that when the beam is attached to stringers at both ends these will both undergo translations and rotations. From Figures 4.10 and 4.11 it can be seen that the opposite end to that excited does have a force and a moment exerted on it and this will modify the overall effect. The total vibration of the beam will be determined by the sum of effects of the two ends and may be different from the cantilevered case.

From Figures 4.10 and 4.11 it can also be seen that the more lightly damped beams exert more force and moment at a given distance from the excitation. This is to be expected because the flexural waves are not attenuated as much as they travel from one stringer to the next.

In Figures 4.14 and 4.15 are shown some displaced shapes of the beam attached at both ends but moving at one end only, for comparison with 4.6 and 4.7. From these it can be seen that despite the fact that the forces and moments are similar the shapes are quite different. They would differ even more if the other end were moving.

With the capability of calculating the deflected shape of the

damping beam it is now possible to compute the maximum flexural strain energy, T_{df}, and this is done in the next section.

Before carrying on with the flexural strain energy calculations, however, it is of interest to look at the limit of the expressions for w as the parameter ϕ goes to zero. This is, in effect, the same as λ going to zero and hence ω becoming very small. An attempt was made to do this using the computer program, but since the coefficients are calculated first and these were all singular, the technique failed. Therefore, a limit analysis has been carried out in Appendix II, to prove that the results do, indeed, have the static beam solution as a limit.

IV.4 Total Strain Energy and System Loss Factor

Ungar, in reference 31, gives an expression for flexure similar to equation (4.5) for extension, and the total flexural strain energy in the damping beam is then given by

$$T_{df} = \frac{E_d I_d}{2} \int_0^{\ell} \left|\frac{d^2 w}{dy^2}\right|^2 dy \tag{4.24}$$

Equation (4.9) with the values of equations (4.14) to (4.17) or (4.20) to (4.23) for the coefficients becomes far too unwieldy to differentiate twice, take the modulus and square in closed form. The digital computer was again programmed to calculate the shapes and integrate numerically using the trapezoidal rule.

The total strain energy in the damping beam is then

$$T_d = T_{de} + T_{df} = \frac{E_d I_d}{2}\left[\frac{12|\delta|^2}{\ell h_d^2} + \int_0^{\ell} \left|\frac{d^2 w}{dy^2}\right|^2 dy \right] \tag{4.25}$$

and the energy dissipated per cycle, ψ_d, is given by

$$\psi_d = 2\pi\eta_d T_d \tag{4.26}$$

Since there will be more than one beam of damping material in a multi span structure, ψ_d in fact, will be a summation over all spans.

It was shown in Section III that simple sinusoidal mode shapes adequately describe the first few modes of a simply supported beam. To avoid confusion with damping beam displacement notation, write

$$v = v_o \sin \frac{n\pi x}{L} \tag{4.27}$$

for the base material mode shapes, where x is the linear coordinate in the beam length. Then the displacement and slope can be written explicitly for each stringer and hence $w(0)$, $\theta(0)$, $w(\ell)$ and $\theta(\ell)$, are known for each damping beam. To keep the solution more flexible the end fixity of each damping beam could be chosen during computation and two cases were evaluated.

The first case considered the six span beam of Table 3.1 with double cantilevers of LD400 bonded to stringers 2, 4 and 6 (stringer notation of Figure 2.6). These damping beams considered were 3 inches long (on each side of the stringer), 0.5 inches wide and 0.08 inch thick. The values of T_{df} were calculated for the first seven structural beam modes for three values of loss factor and a range of λ. The curves are shown in Figure 4.16 for a damping beam loss factor of 0.6. Calculating each mode over a range of frequencies enables the graph to be used for any frequency as long as the mode shape is approximately right. For example, the simply supported beam has a fundamental frequency of about 40 Hz and the simply supported panel with 22 inch frames about 250 Hz. The structural mode shapes are about the same, however, and the same curve can be used by choosing the appropriate λ.

The cantilever mode shapes calculated in this way for two values of λ for the fundamental and second modes of the structural beam are shown in Figure 4.17. This figure shows quite clearly that the same basic mode can excite quite different damper response for different values of frequency.

The second case was that of a strip of damping material 1 inch wide and 0.060 inch thick joined to all the stringers. The values of T_{df} were calculated and are shown in Figure 4.18 for the first seven modes. The mode shapes for the damping beams were also calculated and these displayed typical multi-modal behaviour and are not shown.

To be able to use the flexural strain energy calculations to evaluate the system total loss factor it is necessary to relate the energies stored and dissipated by the various components. Although the metal base structure will have a relatively small loss factor, it may not be negligible and should be included in the calculations. Assume this loss factor is η_m and the maximum strain energy is T_m. Then ψ_m, the energy dissipated per cycle in the metal beam, is

$$\psi_m = 2\pi\eta_m T_m \tag{4.28}$$

But the total energy dissipated in the system is $\psi_m + \psi_d$ and the total strain energy is $T_m + T_d$. Therefore, the total loss factor η_t

can be found from equations (4.26) and (4.28) to be

$$2\pi\eta_t\left[T_m + T_d\right] = 2\pi\eta_m T_m + 2\pi\eta_d T_d \tag{4.29}$$

or

$$\frac{\eta_t}{\eta_d} = \frac{1}{\frac{T_m}{T_d} + 1} + \frac{\eta_m}{\eta_d}\left[\frac{1}{\frac{T_d}{T_m} + 1}\right] \tag{4.30}$$

For the simple sine modes assumed,

$$T_m = \frac{n^4\pi^4}{4L^3} EIv_o^2 \tag{4.31}$$

From equations (4.14) to (4.17) and (4.20) to (4.23) it can be seen that each of the damping beam coefficients will be linear in v_o. Similarly δ will be linear in v_o. Therefore, both T_{de} and T_{df} will contain v_o^2 and in the ratio T_d/T_m the v_o^2 terms will cancel. Thus, v_o can be set to unity without loss of generality.

Only the system with the damping beams attached to all stringers can have an extensional effect. This was considered first. T_{de} can be calculated for each mode by calculating the slopes at adjacent stringers and using the difference to calculate δ, which is then used in equation (4.7). The individual strain energies calculated in this way are listed in Table 4.2. The values were only calculated for the first five modes because of the conclusion drawn in Section III concerning the suitability of sine modes for more than that number.

The frequencies used to determine λ for use in conjunction with Figure 4.18 to obtain T_{df} were the relevant ones from Table 3.2. (For mode 1 the experimentally observed natural frequency was used.)

The values of η_t were not calculated for the beam with the damping material attached to each stringer because the very high extensional strain energies listed in Table 4.2 show that this system invalidates some of the original assumptions. Here $T_{df} << T_{de}$ and

$$\frac{T_d}{T_m} \simeq \frac{E_d I_d}{EI} \times 10^4.$$

Unless T_d/T_m is considerably less than 1 there is so much energy contained in the damping material that the mode shapes and natural frequencies are certain to be affected. In the present system, $EI \simeq 70E_dI_d$ and therefore the assumptions of unaffected mode shapes and natural frequencies are invalid. This in fact, was verified experimentally. A much smaller strip of damping material than that used in the calculations (about 0.06 inch by 0.06 inch by 18 inches) was bonded to the test specimen and this reduced the response to the extent that it was almost impossible to find any peaks. Those that were found were not at the same frequencies as those of the undamped beam.

This does, however, explain why the system is so effective in the case of the panel. Experimentally it had been verified (Figure 4.2) that the fully fixed treatment did not seriously affect the natural frequencies. The calculations were not made for the panel, but T_m for the stiffened skin is several orders of magnitude higher than for the beam. The assumptions are then valid and large amounts of energy can be dissipated, leaving the system otherwise undisturbed.

The fact that the extensional effect is so much greater than the flexural also explains fully why treatment 4.1(c) was no more effective than 4.1(b). Even if the masses seriously affected the flexural behaviour, they do not affect the major contributor, the extensional effect.

The system with three double cantilevers does not have any extensional effect. The values of T_m in Table 4.2 will still apply and the values of T_{df} were taken from Figure 4.16, again for the first five modes. In order to be able to calculate η_t it is necessary to know η_m. This cannot be determined theoretically and the values were measured experimentally (see a later section) and were assumed not to change when the damping was added. These were then used in equation (4.30) to give η_t. These results are listed in Table 4.3 for various cantilever configurations. The expected values of η_t are much higher than the measured values of η_m in all cases and thus even the vastly less effective cantilever system is extremely beneficial in adding damping. The values are still of such a magnitude, however, that it is

expected that the original assumptions are valid, and this will be shown experimentally.

In table 4.3 the added weight expressed as a percentage of the structural beam weight is also shown. The values indicate that the damping is increased far more than the weight.

IV.5 Shear System and Adaptation of Analysis

The material used in the bulk of the experimental work and whose properties were used in the analysis has extremely good damping and elastic properties, but only at room temperature. In practice, a supersonic aircraft, for instance, might require the use of a material with substantial damping and strength up to 150°C. Similarly, cold climate take-offs and high altitude subsonic flight demand a temperature capability down to -40°C or lower. Moreover, aircraft applications demand a resistance to hydrocarbon fluids of various sorts.

One material which meets these conditions is silicone rubber. However, it is a low modulus material and will have to be utilized in shear in either a sandwich or otherwise constrained configuration.

A technique was devised to manufacture a sandwich type of beam damper and attach it to the integrally stiffened structure as shown in Figure 4.19. The segmented inner sandwich skin was bonded to the stringer tips.

This system is amenable to the foregoing analyses with only minor modifications. The transverse vibration characteristics of sandwich beams is quite well documented in the literature (references 32, 33, 34, 35), and it is possible to compute an equivalent E_dI_d and η_d for the laminated beam. These can then be used directly in the equations of transverse vibration of the homogeneous beams.

Similarly, an extensional stiffness can be calculated by using δ to determine the shear strain and hence the shear force. This value can then be used to calculate T_{de}. In this respect, however, one problem arises. The upper sandwich skin is not anchored and so the shear strain will depend on the relative motion between the lower segments and the upper skin. In Appendix III it is shown that for the sinusoidal beam modes and a beam with equal stringer spacing the upper skin is effectively anchored in space (in a longitudinal direction). Thus the calculation of the shear strain is quite straightforward.

The extensional stiffness of the shear system (shear layer of thickness, t, shear modulus G, length $\ell/2$) is

$$K = \frac{Gb_d\ell}{2t} \tag{4.32}$$

and the elastic shear strain energy is

$$T_{ds} = \frac{Gb_d \ell}{4t} |\delta|^2 \qquad (4.33)$$

Recall equation (4.1) and compare it with (4.32). For the material in tension K was proportional to the thickness. For the shear system the stiffness is inversely proportional to the shear layer thickness. In the shear system, for a given δ, a thinner layer will result in more energy dissipation, and the shear system makes more efficient use of the damping material. This, however, must be used with caution, because the shear strain is also inversely proportional to the thickness for a given total extension, and excessive strains will result if the material is made too thin.

No attempt was made to optimise the shear damping configuration, although it is probably possible to do so.

V. METHOD OF DETERMINING DAMPING MATERIAL PROPERTIES

It was stated in the previous section that the bulk of the experimental work for this report was carried out using the damping material LD400 of the Lord Manufacturing Company. This material has a value of E_d equal to approximately 7×10^5 lbs per square inch, ρ_d of 0.05777 lbs per cubic inch and η_d of about 0.6. These properties are of the right magnitude to make the material very useful, but they apply only in a very narrow temperature bandwidth centred at room temperature. For aircraft applications it would be preferable to have a material with better temperature characteristics, even if the loss factor is lower.

One such material which might be useful is silicone rubber or one of its derivatives. The fluorinated silicone rubbers have extremely good resistance to typical fluids to which they might be exposed in aircraft service, have reasonably good temperature characteristics and appear to be quite "lossy". An embrittlement temperature of minus 60 or 70 degrees centigrade and useful strength to 200 degrees centigrade for short periods are typical properties.

There is, however, very little in the literature concerning the dynamic properties of these materials and their variation with temperature, frequency, material composition, strain magnitude, cure times and the other variables which influence their behaviour (Ref. 36, for example). Moreover, these materials tend to have very low moduli and hence they will almost certainly have to be used in shear. It is, therefore, preferable to measure the shear properties for a range of parameters.

There are many techniques in the literature for measuring the damping properties of materials and each has its advantages and disadvantages. Some recent methods are given in References 37 to 41. Nashif (38) describes a variation on the coated cantilever method first suggested

by Oberst. This method measures the tensile properties and is better suited to relatively stiff materials.

Cannon and Nashif (40) have developed a method for soft materials, but again the properties in extension-compression are measured. This method is also a resonance technique and hence involves a mass change to measure the properties over a range of frequencies.

The method of Adkins (37) and the shear method of Grootenhuis (ref. 39) appear to be suitable for use with silicone rubbers. However, the method of McConnell in reference 41 appears most attractive. Some of the derivation is repeated here because there appears to be an error in the reference.

The method is based on an electronic "mass change" and has the advantage that the only phase angle which must be measured is the relatively easily measured one of $\frac{\pi}{2}$. It is a resonance technique which does not require a physical mass change. Fig. 5.1 is taken from reference 41 and shows the block diagram of the electronic system. This applies to use with a single degree of freedom system with mass, M, force P, displacement x, and stiffness, $K(1 + i\eta)$. The equation of motion for the system is

$$M\ddot{x} + K(1 + i\eta)x = P(t) \tag{5.1}$$

If there is no feedback, the steady state solution when

$$P(t) = P_o e^{i\omega t}$$

is given by

$$x = X_o e^{i\omega t}$$

where

$$X_o = \frac{\frac{P_o}{K}\left[(1 - \Omega^2) - i\eta\right]}{\left[(1 - \Omega^2)^2 + \eta^2\right]} \tag{5.2}$$

where $$\Omega = \frac{\omega}{\omega_n} = \omega\sqrt{\frac{M}{K}} \tag{5.3}$$

at resonance $\Omega = 1$, and the loss factor is

$$\frac{P_o}{\text{acceleration amplitude x } M} \tag{5.4}$$

The stiffness can be calculated easily from

$$K = \omega^2 M \tag{5.5}$$

Thus, any system which enables "resonant" measurements to be taken at any frequency will be very useful.

In Figure 5.1, $G(s)$, G_f, G_x are amplifier transfer functions which operate on the excitation voltage, the force signal and the acceleration signals, respectively. S_x and S_f are acceleration and force transducer sensitivites.

The excitation voltage (from an oscillator for example) is

$$E(t) = E_o e^{i\omega t} \tag{5.6}$$

Subtracted from this is the feedback voltage due to the force and acceleration. The net excitation voltage is then

$$E_e = E(t) - E_f \tag{5.7}$$

But

$$E_f = e_f + e_x = S_f G_f F + S_x G_x \ddot{x} \tag{5.8}$$

Therefore

$$E_e = E(t) - S_f G_f F - S_x G_x \ddot{x} \tag{5.9}$$

and

$$F = E_e G(s) \tag{5.10}$$

is the force generated.

Substitute (5.9) into (5.10) and rearrange to obtain

$$F = \frac{G(s)}{\left[1 + G(s) S_f G_f\right]} \left[E(t) - S_x G_x \ddot{x} \right] \tag{5.11}$$

This force, F, is now complex and is the actual force measured by the

force transducer. It is, in fact, $P(t)$ of equation (5.1), for the case with feedback. Therefore,

$$M\ddot{x} + K(1 + i\eta)x = \frac{G(s)\left[E(t) - S_x G_x \ddot{x}\right]}{\left[1 + G(s)S_f G_f\right]} \tag{5.12}$$

Gather terms in $\ddot{x}$ and

$$\ddot{x}\left[M + \frac{G(s)S_x G_x}{1 + G(s)S_f G_f}\right] + K(1 + i\eta)x = \frac{G(s)\,E(t)}{\left[1 + G(s)S_f G_f\right]} \tag{5.13}$$

Equation (5.13) has exactly the same form as equation (5.1) and therefore has the same solution. All the resonance conditions previously described apply and the properties can be obtained. It can be seen from equation (5.7) that the feedback signal is out of phase with the excitation voltage. This results in a "mass" increase and natural frequency decrease. If the polarity is reversed, the "mass" is decreased and natural frequency increased.

This technique is a resonance technique, but the fact remains that the mechanical system is being driven to resonance amplitudes off true resonance. This means that large forces will be required, and these should be calculated. For these calculations it was decided to let $G_f = 0$, that is, there was no force feedback loop. With this assumption equation (5.11) becomes

$$F = E(t) - S_x G_x \ddot{x} \tag{5.14}$$

and equation (5.13) becomes

$$\ddot{x}\left[M + G(s)S_x G_x\right] + K(1 + i\eta)x = E(t)G(s) \tag{5.15}$$

It is assumed that the transducer and the amplifiers have constant electronic characteristics, and therefore we can write

$$G(s)S_x G_x = M' \tag{5.16}$$

and

$$E(t)\,G(s) = P_o e^{i\omega t} \tag{5.17}$$

Then

$$\ddot{x}\,[M + M']\, + K(1 + i\eta)x \;=\; P_o e^{i\omega t} \tag{5.18}$$

and

$$F = P_o e^{i\omega t} - M'\ddot{x} \tag{5.19}$$

Equation (5.18) has equation (5.2) as a solution (with the use of the proper mass parameter). Therefore

$$x \;=\; \frac{P_o}{K}\,\frac{[(1 - \Omega^2) - i\eta]}{[(1 - \Omega^2)^2 + \eta^2]}\, e^{i\omega t} \tag{5.20}$$

It is a harmonic quantity and, therefore,

$$\ddot{x} \;=\; -\,\omega^2 x \tag{5.21}$$

Substituting (5.21) and (5.20) into (5.19) gives

$$F \;=\; P_o e^{i\omega t}\,\{1 + \frac{\omega^2 M'}{K}\;\frac{[(1 - \Omega^2) - i\eta]}{[(1 - \Omega^2)^2 + \eta^2]}\,\} \tag{5.22}$$

At "resonance" $\Omega = 1$ and

$$F = P_o e^{i\omega t}\,\left[1 - \frac{i\omega^2 M'}{K\eta}\right] \tag{5.23}$$

But

$$\omega \;=\; \omega_{new} \;=\; \sqrt{\frac{K}{M + M'}} \tag{5.24}$$

Therefore

$$\frac{F}{P_o e^{i\omega t}} \;=\; \left[1 - \frac{iM'}{\eta(M + M')}\right] \tag{5.25}$$

From equation (5.25) the two limiting cases can be easily deduced. When $M' = 0$ (no feedback or mass change) the force ratio is 1.0. When $M' \to \infty$ the force ratio approaches $\left[1 - \frac{i}{\eta}\right]$. This has a magnitude given by

$$\left|\frac{F}{P_o e^{i\omega t}}\right| \;=\; \left[\frac{\eta^2 + 1}{\eta^2}\right]^{\frac{1}{2}} \tag{5.26}$$

which can be quite large for small values of η.

If the mass is to be decreased, equation (5.25) becomes

$$\frac{F}{P_o e^{i\omega t}} = \left[1 + \frac{iM'}{\eta(M - M')}\right] \tag{5.27}$$

When $M' = 0$ again the ratio is 1. However, as $M' \rightarrow M$ the ratio approaches infinity and the natural frequency also approaches infinity, because the apparent mass approaches zero.

In general, the "resonant" force required can be written

$$\frac{F}{P_o e^{i\omega t}} = \left[1 - \frac{i}{\eta}\left(\frac{m}{1 + m}\right)\right] \tag{5.28}$$

where $m = \frac{M'}{M}$ and can vary between -1 and $+\infty$.

The real part of this force ratio is fixed and hence the variation of the overall ratio can be seen by looking at the variation of the modulus of the imaginary part. This is shown, normalized by η, in Figure 5.2.

The other quantity of interest is the change of the "resonant" frequency. The new resonant frequency is given by

$$(\omega_{new})^2 = \frac{K}{M + M'} \tag{5.29}$$

Therefore

$$\left(\frac{\omega_{new}}{\omega_n}\right) = \left(\frac{M}{M + M'}\right)^{\frac{1}{2}} = \left(\frac{1}{1 + m}\right)^{\frac{1}{2}} \tag{5.30}$$

This ratio is also shown in Figure 5.2.

From Figure 5.2 it can be seen that for a "mass" decrease the required force goes up very rapidly and for a "mass" increase, the amount of increase needed is very large to obtain an appreciable frequency shift.

Such a system was constructed and tested, with only limited success for very small changes in natural frequency. There are several possible reasons for this. The analysis assumes that all amplifiers have constant characteristics with frequency. This is not necessarily true to the degree of accuracy required. Since it is so important to maintain the correct phase information in the signals it was probably this failing in the equipment which led to failure and abandonment of the method. It

does, however, appear workable and it is possible that a working system could be set up taking great care in the design and construction of the electronic system.

McConnell's method, however, gives no force advantage. The force required to obtain a given response is the same as that required to drive the single degree of freedom system without feedback to the same amplitude by "brute force". For this reason, and because the implementation of the method presented the problems already described, it was decided to investigate an off resonant technique similar to that used by Grootenhuis (39). The major difficulty likely to be encountered in the use of such a technique will be the necessity of accurately measuring a phase angle which may be quite small (Fig. 5.4). electronic equipment is available for this task, however.

The single degree of freedom shear system shown schematically in Figure 5.3 is the one to be considered. Equation (5.2) is a valid solution for this system and it is only necessary to convert K into shear parameters to obtain the desired properties.

For a system with hysteretic damping the phase relationships between force and displacement, velocity or acceleration are all the same and any one of the three can be used experimentally. Curves of the phase angle Φ defined by

$$\tan \Phi = \frac{-\eta}{1 - \Omega^2} \tag{5.31}$$

are shown in Figure (5.4) for various values of η. For frequencies well below the natural frequency the phase angles do not change rapidly with frequency, but they are well separated for different values of loss factor. Thus the value of Ω cannot be accurately determined, but this is not necessary to determine the properties. The only things which are required are measures of force and response amplitude and phase angle between them. These are all finite quantities which can be determined quite accurately. In the region of $\Omega > 2$ or 2.5, the curves begin to converge rather rapidly and so, if possible, the measurements should be made for $\Omega \lesssim$ approximately 2.0.

The experimental technique to be adopted is to drive the system to a constant amplitude over a range of frequencies and to measure the amplitude of the force required and the phase angle between the two. Following the analysis of Grootenhuis (39) the displacement is taken to be

$$x = X_o e^{i\omega\hat{t}} \tag{5.32}$$

The acceleration is

$$\ddot{x} = -\omega^2 X_o e^{i\omega\hat{t}} \tag{5.33}$$

and the force is equal to $P_o e^{i\omega\hat{t}}$. The shear force acting on the viscoelastic material will be the applied force minus the inertia force of the moving mass. The moving mass will, in fact, be the moving central block plus the effective mass of the force transducer plus approximately $\frac{1}{2}$ the mass of the viscoelastic material. The inertia force is then

$$M\ddot{x} = -M\omega^2 X_o e^{i\omega\hat{t}} \tag{5.34}$$

Since phase angles will be measured relative to the force, it is assumed that P_o is real. Figure 5.5 shows the system forces in the phase plane. The sum of components in the two principal directions must be zero. Hence,

$$P_o + M\omega^2|X_o|\cos\Phi + \eta K|X_o|\sin\Phi - K|X_o|\cos\Phi = 0 \tag{5.35}$$

and

$$M\omega^2|X_o|\sin\Phi - \eta K|X_o|\cos\Phi - K|X_o|\sin\Phi = 0 \tag{5.36}$$

(5.35) and (5.36) can be used to simultaneously solve for η and K.

$$\eta = \frac{-P_o \sin\Phi}{P_o\cos\Phi + |X_o| M\omega^2} \tag{5.37}$$

and

$$K = \frac{P_o\cos\Phi + |X_o|M\omega^2}{|X_o|} \tag{5.38}$$

If the surface area of one face of the block, M, of Figure 5.3 is A_r then

$$K = \frac{2GA_r}{t} \tag{5.39}$$

from simple stress strain relationships. Substituting (5.39) into (5.38) gives

$$G = \left[\frac{P_o \cos \Phi + |X_o| M\omega^2}{2A_r |X_o|} \right] t \qquad (5.40)$$

Equations (5.37) and (5.40) can then be used at any frequency within the capability of the equipment to maintain $|X_o|$ at the required value and measure Φ accurately.

One danger of using a technique such as this is the possibility of the error in the derived quantity being intolerably large. The values of $|X_o|$, M, ω, A_r and t can be measured quite accurately, leaving Φ as a possible major source of error. From equation (5.40) it is easily seen that

$$\frac{\partial G}{\partial \Phi} = \frac{- P_o t \sin \Phi}{2 A_r |X_o|} \qquad (5.41)$$

Using equations (5.2) and (5.39)

$$\frac{\partial G}{\partial \Phi} = G \sin \Phi \left[(1 - \Omega^2)^2 + \eta^2 \right]^{\frac{1}{2}} \qquad (5.42)$$

Therefore,

$$\frac{\partial G}{G} = \left[(1 - \Omega^2)^2 + \eta^2 \right]^{\frac{1}{2}} \sin \Phi \; \partial \Phi \qquad (5.43)$$

It can be easily shown that

$$\sin \Phi = \frac{\eta}{\left[(1 - \Omega^2)^2 + \eta^2 \right]^{\frac{1}{2}}} \qquad (5.44)$$

Therefore

$$\frac{\partial G}{G} = \eta \partial \Phi \qquad (5.45)$$

This means that the percentage error in G is η times the error in Φ in radians. This can be maintained at an acceptable level over a wide range of values of Φ.

Similarly,

$$\frac{\partial \eta}{\partial \Phi} = \frac{-(P_o \cos \Phi + |X_o| M\omega^2) P_o \cos \Phi - P_o^2 \sin^2 \Phi}{[P_o \cos \Phi + |X_o| M\omega^2]^2} \qquad (5.46)$$

It can be shown by simple substitutions that

$$\frac{\partial \eta}{\eta} = \left[\frac{(1 - \Omega^2) + \eta^2}{\eta}\right] \partial \Phi \qquad (5.47)$$

This percentage error in η can also be kept small as long as Ω^2 does not become too large and η is non zero. As predicted earlier, therefore, the technique should be applicable up to values of Ω of at least 2.

An outline of some experimental results and the apparatus used are given in Section VIII.

VI. SIMPLY SUPPORTED BEAM EXPERIMENTAL RESULTS

In section III it was shown that a simply supported beam with sinusoidal mode shapes would be a reasonable model for the middle portion of the panel with simply supported edges for the purpose of damping predictions using strip dampers. In section IV the energy dissipation theory was developed using this assumption. The experimental part of the beam response and damping phase of the work are presented in this section.

A beam specimen of the configuration analysed in section III was constructed for use in the experimentation. This specimen and the small electrodynamic vibrator used to excite it are shown in Figure 6.1. The beam in the photograph has applied to it the damping cantilevers of section IV.3(a).

The simple supports for the beam consisted of small diameter steel pins inserted into and cemented to the beam as close to the extreme ends of the skin centre line as possible. These pins were held down on the edges of razor blades by four extension springs. The vibrator was mounted horizontally to exert a moment at the junction of the skin and the end stringer. The end stringer rotates about the simple support for all modes and hence this one vibrator location is sufficient to excite any mode. There was a distinct possibility that the beam would tend to move longitudinally in a rigid body mode, but it was felt that the inertia of the beam plus the small but finite restraining force of the pins on the razor blades would be sufficient to keep this from happening to any appreciable extent.

The response of the beam was measured by means of strain gauges bonded at mid span to the outside surface of the skin. The axis of the gauges was aligned with the beam axis. The first gauges tried were the foil type but it was found that the whole system became non linear if the beam were forced enough to obtain a measurable signal. Therefore, semiconductor gauges were bonded to the skins of spans 3 and 5 (numbered from the vibrator end). These, even taking into account their lower current

carrying capacity, have an equivalent sensitivity about 30 times greater than that of a typical foil gauge.

The strain gauge signal was amplified and either measured with a voltmeter or recorded on magnetic tape for subsequent analysis. The mode shapes were deduced by looking at the phase and amplitude relationships of the two gauges and by manually probing for nodes. Accelerometers were not used because the beam is a low stiffness structure and the accelerometer mass added to the skin might influence the modes.

The force applied by the vibrator was monitored by measuring the current into it. In general, back emf effects will be present, as will inertia effects due to the moving components of the vibrator. These will be quite small if the amplitudes are kept small and a reasonable approximation will be that a constant current produces a constant exciting force.

A block diagram of the electronic system is shown in Figure 6.2.

VI.1 Steady State Measurements

The first series of tests consisted of measurements taken on the beam without any added damping. These were to confirm the natural frequency and mode shape calculations and to determine the transfer function or frequency response curve and the damping of the individual modes of the system.

The natural frequencies calculated by the simple energy method and those calculated using the transfer matrix method (listed in Table 3.2) are repeated in Table 6.1, together with the experimentally determined natural frequencies. These measured natural frequencies for the beam with no added damping are shown in Figure 3.2 for comparison with theory. The agreement is quite good for all but the fundamental mode. It was shown by changing and finally removing the springs altogether that the action of these pulling the pins down onto the razor blades was causing this shift in the fundamental frequency. However, it was felt to be necessary to restrain the beam, and since the effect was repeatable it was decided to keep the springs in place. The primary purpose of the experimental work was to compare response with and without added damping and, hence, this frequency discrepancy was considered to be unimportant. For the damping calculations, however, the measured fundamental natural frequency was used for this mode.

Figure 6.3 shows the frequency response of the beam. This was measured by keeping the vibrator current constant and measuring the amplified strain gauge signals as the frequency was changed. The curve of 6.3 was taken from the signal from strain gauge 3.

The normalized response of the two strain gauges is shown in Figure 6.4. This was used to aid in the verification of the theoretical mode shapes. The bending moment diagrams calculated by the transfer matrix method are effectively the ratio of the bending stress at any point along the length to the maximum in the beam. Thus, the maximum bending stress in the beam can be calculated by dividing the measured stress at a point by this ratio. This, of course, is only true if the assumed mode shape and bending moment are correct.

The measured strain response of gauges 3 and 5 were normalized

in this way for use in Figure 4. The agreement between the two for modes 1, 2, 3 and 6 is a good indication that the theoretical bending moment distributions for these modes are quite accurate. The results for modes 4 and 5 are not as good, but this was expected. In mode 4 strain gauge 5 is at a location with almost zero curvature (Fig 3.3(b)) and hence is almost unstrained. Similarly, in mode 5 gauge 3 is at a location where the strain is quite low. The strain gauges, however, give a signal proportional to the average strain over their length, which is finite. This effect, together with the probable error in the actual location of the gauges could easily result in a small difference in the absolute value but a large percentage error in measured strain. This discrepancy is then passed on to the normalized values and the agreement between the two is not as good as in the other four modes.

These calculations together with the manual node location plus the close agreement of natural frequencies confirmed that the transfer matrix method gives reliable results and hence that the simple sine modes can be used in damping calculations for the first few modes.

The damping of the individual modes was first measured using the vector response plot as described by Kennedy and Pancu in reference 42. In this method the response is measured as a component in phase with the force and a component 90 degrees out of phase. When the imaginary part of the response of a system with light hysteretic damping is plotted versus the real part the result is a circular diagram as the frequency passes through resonance. If a structure has two or more modes which are well separated in frequency, distinct circles are obtained as the frequency is varied through each mode. As the natural frequencies come closer together the circles begin to coalesce and finally lose their usefulness in determining the modal loss factor or natural frequency. This happens in structures with high modal densities, but the peaks of Figure 6.3 are well separated and the method is quite useful.

The two strain gauges gave similar results, and since strain gauge 3 was in a position which enabled it to give a reasonable signal for all of the first six modes, at least, most of the damping measurements were made with this gauge.

Figures 6.5 and 6.6 are typical vector plots for modes 3 and 5

respectively. Also shown in Figure 6.6 is the notation for determining the loss factor from the vector plot. This is based on the method used by Ford in reference 7. The resonant vector is drawn and two vectors are drawn from the origin (the point where this cuts the diameter) to points on either side of, but close to, the resonant vector. The angle between these two vectors is ε (radians) and the frequencies above and below the resonant frequency, ω_n, are ω_2 and ω_1, respectively.

Then

$$\eta = \frac{\omega_2 - \omega_1}{\omega_n} \times \frac{1}{\varepsilon} \qquad (6.1)$$

These measured values of η are η_m of section IV.4 and are listed in Tables 4.3 and 6.2 for the modes considered. These are of the correct order of magnitude for this type of structure in all cases but mode 1. That vector plot, however, was decidedly flattened, even with very low excitation, indicating that there was some non linearity present and the measured damping may well be higher than it should be.

The readings were then repeated after adding three double cantilevers of LD400 to the structure as shown in Figure 6.1. The material used in this case was 0.080 inch thick by 0.5 inch wide.

The frequency response curve for this configuration is shown in Figure 6.3 for comparison with the undamped beam. It had been concluded in section IV that even the cantilever method should be quite effective in reducing the response. Figure 6.3 shows this to be the case.

The peaks in Figure 6.3 for the beam with the cantilever dampers are displaced slightly to a lower frequency. In this configuration the damping material is adding mass to the stringer tips and little stiffness. Hence it is expected to depress the natural frequencies somewhat and the measured values are listed in Table 6.1. Since,in the damping beam calculations, λ is proportional to the square root of the frequency, a change of a few percent in the natural frequencies will make little difference in the values of λ and hence in the total loss factor calculations. Therefore, this effect has been neglected.

Figures 6.7 and 6.8 show the vector response plots for the beam with added damping for the same modes as in Figures 6.5 and 6.6. The much

greater frequency change for a given increment in phase angle indicates a much higher value of loss factor in each case. The values of η determined from these plots are η_t of section IV.4 and can be compared with those calculated from the theory of that section.

The theoretical and measured values of η_t are listed in Table 6.2 with the values of η_m. The worst disagreement between predicted and measured values of η_t occurs in modes 2 and 5, but even these are within a factor of two. The error in the value in mode 2 can be partly attributed to experimental error. In the vector plot for this mode the values in the region of resonance were rather erratic. The best fit circle was determined by trial and error, but it is possible that the true circle should have been of much smaller diameter and hence given a higher value for the damping.

In section IV it was indicated that mode 5 was beginning to be marginal for the use of the sine mode. The effect of the stringers is, in fact, to reduce rotation and translation at the stringer location, reducing the excitation on the damping beams and hence reducing the amount of damping added in this mode. This effect is shown by the measured loss factor for mode 5 and is also indicated by mode 4, where the measured value was lower than the predicted.

Despite these shortcomings, the prediction technique appears to be valid and the predicted and measured values agree closely enough to be useful.

The steady state vector response method of measuring damping, however, has some very great disadvantages. Firstly, it is extremely time consuming, and in a system which is temperature sensitive a long test can lead to errors due to a temperature change. Secondly, if the damping is light, the control over, stability of, and accuracy of the electronic equipment used is absolutely critical. In Figures 6.5 and 6.6, for example, it can be seen that a very small frequency change causes a large change in the response vector. The oscillator and other electronic equipment used must be very stable to maintain the frequency long enough to obtain a reliable reading.

There is an alternative transient method available, and this should eliminate some of the problems. The amenability of the transient

technique to this system was tested and the remainder of the beam response data obtained using it.

VI.2 Transient Excitation Tests

One transient technique of obtaining the natural frequencies and damping of a structure is to excite the system and then suddenly remove the excitation. The decaying response contains the required information. This method, however, will be most effective if the excitation is at or near a natural frequency. An even better method is to excite the structure with an impulse. If the impulse is sufficiently short, it will have a spectrum containing all frequencies up to a lower limiting value, which is determined by the pulse duration (Ref. 43, p.7, for example). Then the Fourier transform of the response will peak at the natural frequencies of the system. An impulse, however, is extremely difficult to produce reliably and its characteristics even more difficult to determine experimentally. A more suitable technique is one in which the frequency is swept rapidly over the range of interest.

White (44) has recently developed an oscillator in which the excitation frequency is swept linearly over a chosen period of time between chosen frequency limits. When this equipment is used to drive a vibrator which in turn excites the structure, as in the case of the beam, the frequency content of the force generated should be virtually constant over the range of frequencies being swept. If the starting and finishing frequencies are chosen such that they are slightly below and slightly above the frequency range of interest, all the required modes can be excited.

The use of this technique means that the problems associated with steady state tests are avoided and the total time required to perform the experiments is greatly reduced.

In general, the frequency response function $f(i\omega)$ of a linear system excited by a transient force is given by (44)

$$f(i\omega) = \frac{Y(i\omega)}{F(i\omega)} \qquad (6.2)$$

where $Y(i\omega)$ is the Fourier transform of the response and $F(i\omega)$ is the Fourier transform of the excitation. The beam structure excited by the swept sine oscillator is non-stationary, but because the excitation and

response decay quickly, the necessary Fourier transforms can be evaluated numerically and the transfer function derived.

With the use of this sweep equipment to drive the system being considered here, the Fourier transform of the forcing function is almost a constant value over the frequency range of interest. This means that a good approximation to the transfer function can be obtained simply by Fourier transforming the response.

Figure 6.9 shows typical traces of the response and excitation of the beam with the frequency swept between 10 Hz and 600 Hz in 5 seconds. 6.9(a) shows the traces for the beam with no added damping and 6.9(b) for the beam with three double cantilevers of LD400, 0.5 inch wide by 0.060 inch thick added. In both cases the response is the amplified output of strain gauge 3.

Qualitatively these traces begin to show the pertinent facts. Firstly, the magnitude of the force (vibrator current) is virtually constant. Secondly, in 6.9(a), the individual mode responses increase more rapidly, rise higher and decay more slowly than those in 6.9(b). This shows that the damping is lower in 6.9(a). Thirdly, the slight decrease in natural frequency is shown by the fact that the modes occur earlier in the sweep cycle for the case with damped cantilevers attached. However, for quantitative results, the Fourier transforms must be evaluated.

The Institute of Sound and Vibration Research Data Analysis Facility (45) was used to digitize the magnetic tape records of the signals and calculate the Fourier transforms numerically. The complex division of the Fourier transforms was then carried out to obtain the transfer function. To obtain the damping for individual modes the frequency resolution is increased and the division carried out over a frequency bandwidth containing only one peak in the response function. The results can be used to plot the transfer function or the vector response.

Fourier transforms as plotted directly by the computer are shown in Figures 6.10(a) and (b). The transform of the response shown in Figure 6.9(a) is shown in 6.10(a) and in 6.10(b) is that of the excitation of 6.9(a). From 6.10(b) it can be seen that the excitation does have a

very flat transform, and therefore 6.10(a) is a very good approximation to the magnitude of the system transfer function. The heights of the peaks will be changed a little by the irregularities in the excitation spectrum, but not significantly. The peaks should also be very close to the natural frequencies.

The vector diagram for mode 3 of the undamped beam was obtained by the transient method by investigating only the frequency region of that peak and is shown in Figure 6.11. This is the transient method vector plot for the same mode of the beam in the same configuration as that of Figure 6.5, and the two are directly comparable. The two are almost identical, with the plot from the transient test yielding a slightly higher loss factor.

The natural frequencies and individual mode loss factors were determined in this way for the beam with no added damping and are listed in Table 6.3. The natural frequencies can be compared with those in Table 6.1 and the loss factors with the steady state value of η_m of Table 6.2. All the natural frequencies determined by the two methods agree to within less than 1/5 of 1% except mode 1, which is within 1%. The loss factors do not agree nearly as well (on a percentage basis) but the actual values are quite small and the general agreement is excellent. There is no certainty, in fact, that repeating the steady state tests would give any closer agreement with the first series of tests than do the values measured by the transient technique. The loss factor measured for the fundamental mode is different by the greatest amount from the steady state test. Since, in the transient test, the amplitudes do not have time to grow to the same level as in the steady state test, it is again possible that the suspected nonlinearity is the explanation for the disagreement. The fact that the transient value is lower supports this. It is usual in a transient test to measure the damping to be slightly higher than in the steady state case because in the interest of time saving the number of samples digitized is kept to a minimum and some truncation errors can occur. These errors cause the measured loss factor to be slightly higher than the true value. The measured values for mode 1 are opposite to this trend.

The transient method of test and analysis was also applied to the beam with double cantilevers of LD400. Three variations were tested. In the first, the material was 0.5 inch wide by 0.080 inch thick. In the second it was 1 inch wide and 0.06 inch thick. The third was the same thickness as the second but 0.5 inch wide. The vector response plot for mode 5 damped by the 0.5 inch x 0.080 inch cantilevers is shown in Figure 6.12, for comparison with the steady state plot of Figure 6.8. The natural frequencies and modal loss factors measured in this way are also listed in Table 6.3.

In general, the natural frequencies listed in Table 6.3 show the expected trend for any mode. The undamped beam has the highest natural frequency and the greater the mass addition due to damping material, the lower the natural frequency becomes. This change of natural frequency in the cases considered is of the order of ten percent, in the worst cases, and less in general. This is again an indication that the assumptions made in the damping analysis are reasonable.

The loss factors for configurations b and c in Table 6.3 are the experimental values of η_t for these cases and they can be compared with the theoretical values listed in Table 4.3. The agreement is generally quite good, with the measured data showing the correct trends.

The loss factors in column d of Table 6.3 can be compared with both the theoretical and steady state values in Table 6.2. In this case the agreement between steady state and transient methods is not as close as it was in the measurements taken on the undamped beam. It is interesting to note, however, that in the values for mode 2, which shows quite a large difference between transient and steady state, the loss factor obtained by the transient method falls much nearer to the theoretical.

Loss factor and other damping measurements are at best very difficult to make, even in simple systems. The addition of a hysteretic material in the manner described here to a system which is relatively complex to begin with is certain to make the measurements more difficult. Add to this the fact that a change of temperature of a few degrees can change drastically the properties of the particular damping material being used

and the degree of certainty decreases still further. The silicone rubbers with their more stable temperature characteristics may alleviate the latter problem somewhat, at least for small changes in ambient conditions, but it is present with the LD400. Therefore, the agreement which has been reached between theoretical natural frequencies and total loss factors and the experimental quantities measured in two totally different ways is conclusive evidence that the assumptions made are valid and the techniques and models adequate.

Since the damping treatment effect has been placed on a reasonable theoretical basis it is now possible to investigate experimentally its effect on the more complex panel structure excited acoustically.

VII. PANEL EXPERIMENTAL WORK

The purpose of the beam tests of the previous section was primarily to test the transfer matrix program calculations and the damping theory accuracy using a system with reasonably well defined experimental parameters. The panel, however, is a different and more complex dyanmic system which must be tested to simulate more closely the service conditions of integrally stiffened structures.

The experimental panel, shown schematically in Figure 2.5, is the one used for the tests described in this section. The conditions under which this type of structure must operate are not those of single point excitation as used in reference 10 or in the beam tests of the preceding section. The structure will be subjected to fluctuating pressure forces due to the acoustic environment. These will be distributed over the whole of the structure and effects such as wavelength matching metnioned in section II will be important. To test this panel under these conditions it was suspended in the side of the random siren facility described in reference 46. With this facility it is possible to subject the panel to harmonic or random plane waves at approximately grazing incidence over a range of frequencies between 100 and 1000 Hz. The test section noise level can be as high as 150 dB re 2 x 10^{-4} μbar.

The specimen could not be mounted in a rigid framework because of space limitations. Therefore, the edges were stiffened as shown schematically in Figure 7.1 and the panel was suspended on metal flexures in a wooden framework, which could be placed in the side of the tunnel. The stringers were vertical, and thus the pressure in a vertical plane perpendicular to the specimen skin and parallel to the stringers was constant at any time. This means that modes with two half waves between the specimen ends will be virtually impossible to excite. This is acceptable, however, because the first such mode is almost at the upper frequency limit of the tunnel and of the frequency range of interest. The experimental effort was concentrated, therefore, on the modes with one half wave

between ends.

All the tests carried out on the panel were made with an unconstrained layer of LD400 covering the whole of the inner skin surface (between stringers). This layer was 0.060 inch thick. The reason for this was that the panel alone was expected to have extremely light damping. Lyons (10) had excited the same specimen by means of an electrodynamic vibrator with the panel bolted to a steel framework. Both of these factors can contribute damping, but in the present acoustic tests both are missing. If the initial damping is then extremely light, as it is expected to be, the effect of the added damping due to the various treatments may appear over-optimistically large. It was felt that with the unconstrained layer on the panel the initial damping would be high enough to be representative of service conditions. Then, any increase due to added treatments would be more realistic.

VII.1 Steady State Harmonic Tests

As in the beam experiments the first tests carried out were those with steady state harmonic excitation. Strain gauges 1 to 11 of Figure 2.5 were foil gauges and again found to lack sensitivity. Strain gauges 13, 14 and 15 were semi-conductor gauges and were used for all response measurements. Very early in the testing the signals from the three gauges were compared and found to agree with each other, within experimental limits as well as did the two gauges in the beam tests. The frequency content, except when a gauge was on or near a nodal point, was always the same in all three and the magnitudes could be related by assumed mode shapes and gauge location. Therefore, when results from one gauge only are presented they apply to all three.

The frequency response function was measured by monitoring a microphone placed at the centre of the tunnel cross section opposite the middle of the specimen. The sound pressure level was kept constant for various frequencies and the strain gauge readings taken. The curve for strain gauge 13 is shown in Figure 7.2 for comparison with the single point tests shown in Figure 4.2.

Two points become immediately apparent. The natural frequencies obtained in the acoustic test appear to be somewhat lower, and the damping appears to be about the same for the highest peaks in both cases. The latter justifies the assumption that the damping without the unconstrained layer would have been very much lighter in the acoustic tests than in Lyons' single point tests.

An attempt was made to measure the damping of individual modes, but this was not very successful if reasonable accuracy was desired. The vector plots were generally quite badly distorted and often contained more than one loop, as shown in Figure 7.3 for example. There are two possible reasons for this. The microphone signal is not an exact measure of the force on the specimen, but only of the pressure fluctuations at one point. Even if the noise level at one point is constant the generalized force on the specimen might change fairly rapidly with frequency. It is possible

that the acoustic properties of the tunnel are such that the pressures at various points on the specimen change more than would be indicated by a small change in the frequency of the travelling wave.

The probable cause of the secondary loops in the vector plots is the vibration of the support structure. This was by no means rigid and will thus be coupled with the plate to give additional natural frequencies. These would affect the panel vector plots to some extent. The motion of the massive supports would also explain the decrease in natural frequency.

It would have been useful to know the loss factors of the individual modes, but with the difficulties associated with their measurement it was decided to continue without them for reasons explained later. It is not likely that the transient technique would have been any more successful because the structure secondary modes would still show up and the problem of the changing pressure field would still exist.

Neither Lyon's measured natural frequencies nor those of the peaks in Figure 7.2 agree with the predicted values of Section II as well as did the beam experimental results. This was to be expected because of the difficulty of obtaining accurate boundary conditions. The mode shapes, however, are expected to be quite accurate, and Lyons found that his major peaks corresponded to theoretical modes 1 to 4.

In order to determine the overall mode shape to compare with theory the acoustic excitation was applied at the frequencies of the major peaks of Figure 7.2. The surface of the specimen, including the support structure, was probed with a 2 gram accelerometer. A preliminary phase comparison between the three semi-conductor strain gauges had indicated that the four major peaks in the acoustic excitation frequency response curve were, in fact, modes 1, 2, 4 and 5. The normalized acceleration response curves across the specimen centre line at the frequencies of these four major peaks confirm this, and are shown in Figure 7.4. These centre line mode shapes conform quite well with the theoretical values, also shown in Figure 7.4, for comparison. However, the suspected motion of the side supports is present. Figure 7.5 shows the acceleration responses for two of the modes at 5 locations along the specimen length.

These confirm that the end and side supports were definitely moving, and hence affecting the response.

This motion of the massive side supports involves a considerable amount of kinetic energy and is a possible explanation for the low values of the natural frequencies which were measured. Prior to modifying the support structure to attempt to reduce the effect, however, some preliminary measurements with added damping were taken.

The damping material was added across the stringers at the specimen centre line in the configuration of Figure 4.1(b). The LD400 strip was 2 inches wide and 0.060 inch thick. The frequency response curve was determined and one half of the damping material width was removed. The measurements were then repeated. These frequency response curves are shown in Figure 7.2. Although the modal loss factors were not measured, as explained earlier, some measure of the effectiveness of applied damping treatments can be obtained simply by evaluating the reduction of the peaks in the response curve for a given excitation noise level, and this was carried out. In this way the large effect of the very small amount of material added can be seen. The percentage reduction of the individual peaks and the percentage of weight added are listed in Table 7.1. As expected from the analysis of Section IV the treatment is seen to be very effective for a very small mass addition.

Some random excitation tests were carried out on the panel in the above stiffened condition with and without damping and these results are given in the next section. Extra support was then added to the panel in the following way. The ends were clamped between the existing lengths of angle iron and 2 inch by 1.5 inch light alloy bars with slots machined to fit over the stringers. The sides were further reinforced by clamping the skin between the existing steel bars and 1.5 inch by 1.5 inch light alloy bars. The specimen in this configuration mounted in the acoustic tunnel to be tested is shown in Figure 7.6. The figure also shows the damping treatment across the stringers.

The steady state frequency response was measured without the damping treatment on the stringers, and is shown in Figure 7.7. The peaks now occur at approximately the same frequencies as in Lyons' tests (Figure 4.2) and the general shape of the curve is quite similar.

The measured peak response values of 7.7 are lower than those of 7.2, but this is due to a reduction in excitation intensity. . The sound pressure level for Figure 7.2 was maintained at 145 dB and for 7.7 it was 140 dB. This implies a reduction by almost a factor of two in the pressure fluctuations and therefore a reduction of about two in the stress levels.

It was believed that the extra stiffeners had eliminated most of the motion of the supports and this was found to be the case at the frequencies of all the peaks but one. The acceleration responses were again measured with the 2 gram accelerometer. These are shown in Figure 7.8 for the specimen centre line at the frequencies of the major peaks except the one at 670 Hz. In each of the modes shown the support structure accelerations were negligible and those on either side of the centre line indicated that these were very pure modes with one half wave between ends. The mode shapes were those predicted in Section II.

The peak at 670 was the only one which involved major support structure motion, and it was probably a combination of support bending and panel mode 5.

From the results of this section it is concluded that the mode shapes calculated by the transfer matrix method reliably approximate the manner in which an integrally stiffened panel vibrates when excited acoustically. The natural frequencies predicted did not agree closely with experimental values but this can be explained by support structure deviations from those assumed in the theory. The variation with mode number, however, conforms with the trends shown in Figure 2.12.

VII.2 Stationary Random Acoustic Excitation Tests

In the previous section it was stated that the modal loss factors were not calculated for the panel under the influence of acoustic excitation. In service, panels will be excited by random acoustic pressure fluctuations, and under these conditions the important parameters from the point of view of fatigue damage accumulation and fatigue crack propagation are the root mean square of the stress and the number of stress reversals or zero crossings. The root mean square stress (or strain) is an easily measured experimental quantity, and the stress reversals can be determined from the spectral density of the strain signal. Since this is the case, the overall effect of the various damping treatments can be assessed from panel tests without actually measuring the loss factors of the individual modes. The beam experiments have confirmed the damping theory and the tests under conditions of random acoustic excitation will demonstrate the benefits to be gained in a pseudo-service environment.

The specimen of Figure 7.6 was excited with random noise in the acoustic tunnel both before the additional boundary stiffening and after. The excitation again consisted of plane waves at grazing incidence, but now the amplitude and frequency of the pressure fluctuations were random. As in the previous section, the sound pressure level was monitored by means of a microphone, and the response measured by means of the semiconductor strain gauges. Both signals were recorded simultaneously on magnetic tape for subsequent analysis.

VII.2(a) Data analysis techniques

In the case of random excitation the analysis of the data becomes somewhat more difficult. Since all frequencies and all amplitudes are present in both the excitation and the response some method must be used to determine the statistical properties and frequency content of the signals. Such methods are available in the literature.

Robson (47) describes the application of harmonic analysis to a system undergoing random motion and gives the relationship between the

autocorrelation function and the spectral density of a signal.

If the response of a system (the panel for instance) is given by $\xi(t)$ where ξ can be strain, displacement, etc., the autocorrelation function

$R_\xi(\tau)$ is defined by

$$R_\xi(\tau) = \overline{\xi(t)\xi(t+\tau)} \qquad (7.1)$$

In this equation τ is a time delay, t is time, and the bar over the expression on the right hand side designates an average over all samples being considered. Robson shows that the Fourier transform of the autocorrelation function is the spectral density $S(f)$. (In fact, the two are a Fourier transform pair.) The spectral density describes the frequency content of the signal being analysed and the autocorrelation function the temporal properties.

A useful property of the autocorrelation function and spectral density is that the autocorrelation function for zero time delay ($\tau = 0$) is equal to the mean square of the signal which is equal to the area under the spectral density curve.

Robson also shows that if a linear single degree of freedom system is excited by a stationary randomly varying force, the spectral density of the response is equal to the spectral density of the excitation multiplied by the square of the modulus of the transfer function (frequency response curve). All of these properties will be useful in the data analysis in this section because they can be used in the numerical analysis utilizing a digital computer.

Two further useful facts are pointed out by Robson. The first is that in a multi-degree of freedom system the response spectral density is approximately equal to the square of the modulus of the transfer function multiplied by the spectral density of the excitation, provided that the damping is small and the peaks in the response curve well separated. The second is that the root mean square response under the above conditions is inversely proportional to the square root of the damping. This means that the damping treatments are not expected to show as great an effect on the

root mean square response as they do on the reduction of the peaks in steady state harmonic tests.

VII.2(b) Stationary Random Excitation Experimental Results

To measure the random response characteristics of the panel in the configuration used to obtain the frequency response curve of Figure 7.2, it was excited by broadband noise. The signal from the random noise generator used to drive the siren was passed through a band pass filter to utilize the full frequency capability of the tunnel. The data analysis facility (45) was used to obtain the spectral density of the microphone signal, and this is shown in Figure 7.9. The ordinate in this figure is linear and therefore corresponds to the spectral density of the sound pressure fluctuations.

The decibel scale is based on the logarithm of the sound pressure and hence the decibel or sound pressure level variation over the frequency range of interest is very small. The noise signal can be considered to almost "white" and the spectral density of the response signal is proportional to the square of the modulus of the transfer function.

For the tests on the panel in this configuration the noise level was maintained at 150 dB (overall) re 2 x 10^{-4} μbar. The spectral density of the response (strain gauge 13) is shown in Figure 7.10* for the panel with no damping material on the stringers. The spectral density of the response of the panel to the same excitation after the addition of a strip of LD400 2 inches wide by .060 inch thick to the stringer tips is shown in Figure 7.11. The RMS strain has been reduced by about 75 percent as shown by the measured reductions listed in Table 7.2.

Keeping in mind that the spectra of 7.10 and 7.11 are essentially the square of the curves in 7.2 a comparison can be made between them. For the panel with no added damping the peaks in the spectra correspond exactly with those which are present in the frequency response curve. There is, however, an extra peak at about 480 Hz. This is probably the third mode,

---

*The ordinates in Figures 7.10 to 7.14 have been given numerical values, but these have been normalized during the computation. Therefore, to make comparisons between figures the RMS of the signal is needed, and the values are given on each figure.

which did not appear in the harmonic tests and which may have been hidden in the hump in the very large peak at 550 Hz. The heights of the peaks in the spectra are also of the proper relative magnitudes except for the mode at 720 Hz which appears to be less strongly excited by the random noise. This is partly due to the start of the fall-off of the excitation spectral density as seen in Figure 7.9.

The addition of the damping material reduces all but two of the peaks to the point where they do not appear within the resolution of the computer produced graph. Mode 2, though drastically reduced, is still predominant and mode 4 is barely in evidence.

As in Figure 7.2, the frequencies of the peaks are raised slightly by the damping material, but only by a few percent, indicating a fairly small net effect on ratio of system stiffness to mass.

When the additional edge support had been added to the panel the response to random noise was again measured with no added damping and with various widths and thicknesses of the damping material across the stringers. The microphone signal was analysed on several occasions to check that the noise field did not change appreciably, and in each case was found to agree with the spectrum in Figure 7.9. For the tests in this configuration, the noise level was reduced to 140 dB, since this was found to give adequate strain signals without unduly taxing the equipment.

The variations tested and the results obtained are listed in Table 7.3. The strain spectral densities were calculated for each variation for a comparison of frequency contents. In general, all the damped configurations yielded similar spectra with some differences in peak ratios.

The waveform and spectral density of the signal from strain gauge 13 are shown in Figure 7.12 for the case with no added damping across the stringers. The waveform display in this figure is shown for illustration only, and yields no quantitative information. The spectrum is shown for direct comparison with Figure 7.7, and the two agree quite well. The peaks at the higher frequencies in the spectrum

are again lower than expected due to noise level fall-off.

A typical waveform and spectrum are shown in Figure 7.13 for the panel with damping across the stringer tips. Unlike the case of the panel before the additional stiffening was added, most of the modes are still in evidence, but all have been reduced. One possible reason for this difference is that in the previous case the large support motion made the damping treatment relatively less effective for the affected modes due to the large mass of the moving components. In both instances, however, the RMS reductions are very large.

The final configuration of the panel which was tested was that with the shear dampers of Figure 4.19. The material selected was material 3 of the next section and the damper was made up in three combinations of skin and shear layer thicknesses. The shear dampers were all 1.0 inch wide. The excitation was maintained as in the previous random acoustic tests and the percentage reduction in root mean square response was determined. The shear beam parameters and strain reductions are listed in Table 7.4. It had been stated in Section IV that the thinnest shear layer configuration was expected to be most efficient and this is the case. This fact implies that it should be possible to optimise the thicknesses of shear layer and skins. In the present configuration the skin strain is low enough to be ignored, but as the shear layer becomes thinner, higher stresses are imposed on the skin and it will strain to a significant extent. This means that there should exist an optimum ratio, but this was not investigated.

From a comparison of Tables 7.3 and 7.4 it also appears that the shear system is somewhat more effective than an equal width of LD400, but the difference is small and the main advantage of laminated beam construction lies in the chemical properties of the silicone rubber and relative insensitivity of its stiffness and loss factor to temperature changes.

The spectra of the strain signals of the panel damped by the shear systems were also calculated and found to have frequency contents similar to the panel with no damping and with LD400 strip dampers. A typical waveform and spectrum are shown in Figure 7.14 for comparison with the others.

From the results of this section it can be concluded that the addition of either a homogeneous or a shear damping system across the stringers is an extremely efficient method of reducing the response of an integrally stiffened panel to harmonic or random acoustic excitation. This was predicted in Section IV and has been verified experimentally.

VII.3 Swept Sinewave Tests

It was stated at the beginning of this section that modal loss factors were not essential to the determination of damping treatment effectiveness and that the transient technique would probably not help to obtain very accurate values. However, this technique can be a very effective tool to obtain quickly the natural frequencies of a multi mode structure. Even a simple frequency response curve similar to Figure 7.7 can be relatively tedious to measure using a steady state method. If the structure can be excited by a measurable random force with a flat spectrum then the spectral techniques described point out the natural frequencies. However, fairly high power requirements must be met in steady state random tests because all frequencies and modes must be generated simultaneously. The transient technique is a useful alternative.

Extensive tests were not carried out using the method, but an example of its use will be given. The panel with added edge support but without strip dampers was excited in the acoustic tunnel with the input to the siren swept from 100 to 1000 Hz in 1 second. All electronic amplitude controls were unaltered during the sweep, but because of the siren and tunnel characteristics the exciting pressure (microphone signal) is not expected to have as flat a spectrum as did the vibrator current in the beam tests. This is shown to be the case by the moduli of the Fourier transforms of the response and excitation shown in Figure 7.15(a) and (b). The required complex division of Fourier transforms was carried out and the derived transfer function is shown in 7.15(c). This shows the same natural frequencies as Figure 7.12 and demonstrates the usefulness of the technique in this application.

VIII. THE MEASURED DYNAMIC PROPERTIES OF SOME SILICONE RUBBERS

VIII.1 Specimen and Apparatus Design

In the theoretical aspects of this part of the work outlined in Section V it was pointed out that it is preferable to measure the shear properties of soft materials. Therefore, a specimen was designed to subject two equal thickness layers of material to a state of stress approaching pure shear. The specimen is shown in Figure 8.1. Read (48) has shown that there is an error associated with the measured value of the stiffness of a body in shear due to the stress free ends because the absence of stress on the ends results in the surface becoming curved instead of remaining plane. Read shows a curve of the approximate error introduced by this effect, and for an incompressible solid the lower bound on the ratio of measured stiffness to stiffness in pure shear is given by

$$\text{Ratio} = \frac{\frac{\ell_{s\ell}}{t} - 0.27}{\frac{\ell_{s\ell}}{t}} \qquad (8.1)$$

where $\ell_{s\ell}$ is the shear layer length and t the thickness. For the specimen shown in Figure 8.1

$$\frac{\ell_{s\ell}}{t} = \frac{2.0 \text{ inches}}{0.063 \text{ inch}} = 32$$

and hence Ratio is greater than 0.99. The thickness of the shear layers can be changed by changing the thickness of the central moving block, but even if it is doubled to .125 inch the error is still less than 2 percent. It has therefore been assumed that measured values need not be corrected for the stress free edge effect and that the error due to this is negligible.

A more serious problem is that of the bond between the two layers of rubber and the four metal surfaces. It is relatively easy to manufacture silicone rubber sheets, but if these are then bonded to the specimen holder

it is almost certain that the properties measured will be some composite value for the rubber and the adhesive rather than those of the rubber alone. It is, therefore, desirable to vulcanize the rubber in situ to avoid the problem.

A fixture was designed to press cure the rubber in the specimen holder, which had been suitably cleaned and primed. This was carried out in the Rubber Laboratory of The Royal Aircraft Establishment (Farnborough) and the technique was successful. The shear layers shown in Figure 8.1 are, therefore, bonded directly to the metal without any additional adhesive layers. The properties measured will be those of the specimen alone.

The dynamic properties are required over a range of frequencies from about 100 to 1000 Hz. With this type of test a major problem is the spurious resonances introduced by the support structure. The specimen mounted in its steel support framework is shown in Figure 8.2. This figure also shows the accelerometer, which was used to measure response, mounted on the central block. The vibrator and connecting link, and the force transducer are also shown. To determine whether extraneous support resonances did exist the central block acceleration was maintained at 1.0g from 100 to 1000 Hz and the accelerations of various parts of the structure were measured with another accelerometer, and these quantities are shown in Figure 8.3.

The support structure, including the legs of the specimen holder, showed a very small response with some small peaks at about 600 and 800 Hz. These peaks, however, did not exceed $2\frac{1}{2}$ percent of the moving mass acceleration, and it was assumed that they could be considered negligible. The accelerations measured at the shaker spindle differed by as much as 20% from those of the moving mass at low frequencies. This was probably due to an accumulation of effects through the various threaded connections. In order to keep the accelerometer out of the changing environment (described later) the possibility of measuring response at the shaker had been considered. The above results made this a rather doubtful procedure and all response measurements were taken at the moving central mass.

The primary variations with temperature are likely to occur as the temperature rises above ambient. To provide heat a drum was designed

to fit around the specimen but not in direct contact with it. A one kilowatt heating tape was applied to the drum and this was lagged with glass fibre insulation and asbestos tape. The ends of the drum were blanked off with asbestos discs with openings for the shaker connector, the accelerometer lead and the thermometer port. With the existing large area of metal to rubber surface contact it was felt that a measure of the air temperature within the drum would be an adequate measure of the rubber temperature. Embedding thermocouples in such a thin specimen would probably change the stress field considerably and would not be likely to give much greater accuracy in the measured temperature.

An overall view of the apparatus showing the driving and measuring equipment as well as the heating drum and thermometer is shown in Figure 8.4.

In the calibration of the system it was found that having a small fan blowing on the force transducer easily kept the temperature of that component close to room temperature because the connecting link provided only a small path for heat conduction. The accelerometer had to be in the heated chamber as explained earlier, but this was a B and K type 4335 used in conjunction with a charge amplifier. At temperatures up to 150^{o}C this equipment has a negligible total change in sensitivity and can be used with confidence.

A final quantity which required verification before the properties could be measured was the temperature control and stability of the whole system. It was found that for a fixed current into the heating tape the temperature attained varied somewhat with ambient conditions, but that a steady temperature was quickly reached and was thereafter maintained to within about 0.5^{o}C for as long as required to take the measurements. The temperature rise above ambient versus heating current is shown in Figure 8.5, with the expected temperatures shown as a shaded area. During the testing the temperature in the drum was monitored and recorded.

VIII.2 Experimental Results

Since the tests of this section were of a preliminary nature, only three material variations were tested. These have been designated materials 1, 2 and 3 and their specifications are given in Appendix IV. For each of these three materials the moving block acceleration, the force, and the phase angle between the two were measured. From these the loss factor and storage modulus were calculated using the theory of Section V. These measurements and calculations were made at various temperatures between ambient and 150°C and for frequencies ranging from 200 Hz to 1000 Hz.

For the whole of the investigation the shear strain was maintained at a level of 0.001 rms. The dynamic properties are almost certain to be strain dependent and to obtain consistent values the force was adjusted to obtain the correct acceleration at every frequency. This level is low enough to preclude dynamic heating but high enough to be useful in dissipating structural energy.

The three materials tested were all silicone rubbers and in general their shear properties are not expected to vary rapidly with temperature or frequency. The tests showed that the properties of material 3 varied less rapidly than the other two and that its loss factor was somewhat higher. Curves of the measured loss factor and shear modulus for material 3 are shown in Figures 8.6 and 8.7 respectively.

From Figure 8.6 it can be seen that the loss factor is well maintained to 150°C and this property should render the material very useful in the shear damping application. From the curves for different values of frequency it can also be seen that the loss factor is increasing with frequency, as expected.

Figure 8.7 shows that the shear modulus has a local maximum at about 400 Hz, but the variation with frequency is quite small. The curves for different temperatures also show that the shear modulus is decreasing slowly with increasing temperature.

The very useful loss factor maintained to 150°C together with a shear modulus which does not vary rapidly with temperature or frequency indicate that material 3 is a suitable one to use in constructing the shear

damper of Figure 4.19. This material is also best suited to aircraft use because of its fluorinated chemistry, making it highly resistant to damage by hydrocarbon fluids.

Several shear dampers in the configuration of Figure 4.19 were manufactured in the Rubber Laboratory of the Royal Aircraft Establishment. The various combinations of skin and rubber thickness and the results using them on the single panel have been described in Section VII.

IX FULL SCALE TESTS

In Section VI tests on a beam were described and these confirmed the vibration theory and damping predictions for the model. A more complex panel structure was tested under more realistic conditions as described in Section VII. These tests verified the more general panel vibration theory and went on to show the great effectiveness of the damping treatment being considered.

The next logical step in the chain of increasing complexity and realism is the use of a full scale structure. Figure 9.1 shows the full scale test specimen mounted in the acoustic tunnel. This box specimen consists of a 3 by 3 array of bays of integrally stiffened skin mounted on spars at a 20 inch pitch and on ribs at a 14 inch pitch. Each bay contains five clear skin spans with one outer span on each end rivetted to the spars, which are parallel to the stringers. The specimen is a box section with identical and parallel skins.

The specimen was mounted in the acoustic tunnel such that the random noise impinged on almost the entire centre bay of one side at approximately grazing incidence. The reason for this restricted excitation is that in preliminary tests using a bank of loudspeakers it was found that the response was almost completely dominated by overall modes of the specimen. Some skin modes did appear but it was very difficult to separate them from the overall modes.

The first few mode shapes and natural frequencies for a single skin panel were calculated by the transfer matrix method of Section II. The mode shapes were of the type involving a great deal of stringer deflection, in effect overall panel modes as shown in Figure 2.8(a), and are therefore not shown. The variation in calculated natural frequency with mode number is shown in Figure 9.2. This curve has the same form as those shown in Figure 2.11. Thus, the skin panels on the full scale test specimen are expected to behave in a manner very similar to the panel of section VII.

The response of the panel was measured by means of strain gauges, which were bonded to the inner and outer skin surfaces and to the ribs and spars at various locations. One semi conductor strain gauge was bonded to the outer surface of the skin at the centre of the middle span on the side of the specimen facing the tunnel. The signal from this gauge was used to obtain the spectra shown in Figures 9.3, 9.4 and 9.5. As in the case of Section VII the ordinates in these figures are scaled and the measured overall rms voltage is also shown.

The excitation noise level for the tests on the box specimen was maintained at 140 dB overall and its spectrum was evaluated. This was the same as that shown in Figure 7.9, and is not repeated.

The root mean square strain gauge response was measured for the specimen with no added damping, with various quantities of LD400 across the stringers and finally with one shear damper across the stringers. The experimental results are listed in Table 9.1. The magnitudes of the strain reduction are very encouraging. The damping treatment was added only to one middle panel of the 18 skin panels in the structure. Although the excitation also acted on only one panel the structural and acoustic coupling present ensured that all the panels were vibrating to some extent. In fact a check on this point revealed that the panel facing the one which was excited responded to approximately the same level. Therefore, one strip of damping material was acting to reduce the stress in the whole structure to some extent.

The spectra were calculated for various strain gauges with and without the damping treatments applied. Figures 9.3 to 9.5 show typical spectra of the semi-conductor gauge signals under the conditions given in the figures. Other skin gauges had spectra similar to those for the same conditions. Waveform displays are also shown in these three figures and are again given for illustration.

The multi modal behaviour of the panel is clearly shown by Figure 9.3. The peak at 200 Hz corresponds to the fundamental overall specimen mode which had swamped the response in preliminary loudspeaker tests. It is still in evidence but is reduced to an acceptable level. The spectra of Figures 9.4 and 9.5 are typical of those obtained for the damped configuration, and the shapes of these are similar to that of 9.3. This

shows that the damping treatments are effective in all modes throughout the frequency bandwidth being considered. As in the single panel tests the effect of the LD400 damping treatments was greater for greater mass addition, but not directly proportional. The weight addition was not calculated, but it was certainly a negligible portion of the very large test specimen weight.

From the strain reductions measured in this section it appears that the technique of bonding damping material across the tops of the stringers is very effective, even in full scale structure. The reductions were not as great as in the case of the single panel, but were large enough to be significant in alleviating fatigue problems.

X. CONCLUDING REMARKS AND RECOMMENDATIONS FOR FUTURE WORK

The theoretical mode shape and natural frequency calculations have shown that the vibration characteristics of integrally stiffened panels may be quite different from those of a conventional or builtup structure. These characteristics are, to a large extent, governed by the transverse bending behaviour of the stringers. In the typical geometries studied the stiffener deflections are approximately as great as those of the skin, with the whole panel vibrating in modes which closely resemble those of an unstiffened plate of the same dimensions. This means that in considering the response of the panels to acoustic excitation the possibility of exciting low order modes by fluctuating pressure forces which are in phase over a large portion of the structure must be taken into account.

It has also been shown that as the panel length becomes shorter for a given stringer and skin geometry the integrally stiffened structure tends to behave more like a conventional one. Thus, in evaluating at the design stage any vibration problems which might be suspected it is necessary to first ascertain the behaviour pattern which is to be expected.

The mode shapes of a typical panel were measured experimentally under conditions of acoustic excitation and found to agree very well with the predictions. Experimental mode shapes and natural frequencies for a simply supported beam taken from a panel cross section were also found to agree with theory. From these results it was concluded that the method of analysis was suitable and that the mathematical models used were adequate.

It was found both theoretically and experimentally that the addition of a damping treatment across the tops of the stringers can effectively reduce the response of this type of structure to harmonic and random acoustic excitation. At the moment this appears to be the only reported relatively efficient means of damping integrally stiffened structures, and as such it can be very useful as a solution to existing problems. It can also be included at the design stage if the acoustic environment

forms a severe design case.

The experimental work to determine the dynamic properties of some silicone rubbers was of a very preliminary nature, but it did enable the fluorinated silicone rubber to be chosen as the most suitable of the three investigated for the construction of a laminated damping treatment. This is a more practical method of using the soft silicone rubbers, which meet the chemical and temperature requirements of aircraft applications.

Full scale tests confirmed that the addition of a strip of damping treatment to the stringers of one panel resulted in a significant reduction in the root mean square response with negligible weight penalty.

The swept sine method of transient testing was used in several cases and found to be an accurate and reliable means of establishing natural frequencies and, in some instances, modal loss factors. It is especially useful in applications with light damping and many modes.

Integrally stiffened skin stringer panels are being used increasingly in aircraft applications and the work reported here has given some insight into the behaviour of flat panels of this type. The author is aware of work being carried out in the analysis of curved stiffened skins and feels that it is essential to develop these analyses to apply to curved integrally stiffened skins. It would also be desirable in future to extend the experimental work to conditions of service excitation of flat panels and to take curved panel response measurements both in the field and in the laboratory. When the vibration characteristics of curved panels have been established damping treatment applications should be investigated.

The effect of in plane stresses is important and should be taken into account. A pressurized fuselage under bending loads, for instance, will impose biaxial in plane stresses on the stiffened skin and the vibration characteristics under these conditions are unknown. These effects should be introduced into the analysis and experimental work. In addition to this, the interaction of stiffened skins and underlying support structure should be closely investigated.

An environmental factor which is important and should be investigated is the effect of temperature change, especially as it influences the damping treatments. The materials to be used for damping treatments should

also be investigated further. The effect of varying material composition variables including catalyst and filler type and quantity should be determined and optimized if possible. The damping treatment itself, especially the shear system, may be amenable to optimization of construction and it would be worthwhile to calculate the effect of changing parameters such as damping material and skin thicknesses and shear layer stiffness and loss factor.

The damping material property measurements should be extended to include the low temperature effects. The author also feels that because the preliminary measurements of this report yielded a somewhat unexpected behaviour an independent check of these properties by another method would be very useful. One suggested method is a three point suspension of a mass on discs of the material. This can then be driven by base excitation and the properties in tension compression measured (as in ref. 40). The trends should be the same as those exhibited by the shear properties.

Some further work will be necessary on the actual method of attachment of the shear damping system. In conjunction with this a series of fatigue tests would be very useful. Some fatigue data should be accumulated for integrally stiffened panels (possibly random S-N curves) without added damping and after the addition of the shear system. These results would give some idea of the order of improvement in the fatigue life of the panel itself and would also give an indication of the fatigue resistance of the shear damper and its bond with the panel. These are of great importance and will have to be determined to evaluate the full usefulness of the suggested method of reducing the resonant vibrations in integrally stiffened skins.

APPENDIX I

The Summation over all Internal Stringers of the Cosine^2 Term in Equation (3.14)

In equation (3.14) it is required to find

$$S = \sum_{i=1}^{M} \cos^2 \frac{n\pi y_i}{L} \tag{A1.1}$$

For the internal stringers

$$M = N - 1 \tag{A1.2a}$$

and

$$y_i = \frac{iL}{N} \tag{A1.2b}$$

Substituting equation (A1.2b) into (A1.1) leads to

$$S = \sum_{i=1}^{M} \cos^2 \frac{n\pi i}{N} \tag{A1.3}$$

This summation depends on the relationship between n and N, which are both integers. If $\frac{n}{N}$ is also an integer, then each term of equation (A1.3) is equal to 1.0 and the sum is equal to M = N-1.

For $\frac{n}{N}$ not equal to an integer, rewrite (A1.3) using trigonometric identities (reference 19)

$$S = \sum_{i=1}^{M} \cos^2 \frac{n\pi i}{N} = \sum_{i=1}^{M} \left[\tfrac{1}{2}(1 + \cos \frac{2n\pi i}{N})\right] \tag{A1.4}$$

or

$$2S = M + \sum_{i=1}^{M} \cos i\zeta \tag{A1.5}$$

where

$$\zeta = \frac{2n\pi}{N} \tag{A1.6}$$

and let

$$\sum_{i=1}^{M} \cos i\zeta = S_1 \tag{A1.7}$$

$$S_1 = \cos\zeta + \cos 2\zeta \ \ldots \ + \cos M\zeta \tag{A1.8}$$

Rewrite each cosine term as a sum of exponentials to obtain

$$S_1 = \frac{e^{i\zeta} + e^{-i\zeta}}{2} + \frac{e^{2i\zeta} + e^{-2i\zeta}}{2} \ldots + \frac{e^{iM\zeta} + e^{-iM\zeta}}{2} \tag{A1.9}$$

(i is equal to $\sqrt{-1}$ in equations (A1.9) and (A1.10)

$$2S_1 = (e^{i} + e^{2i\zeta} \ldots + e^{Mi\zeta}) + (e^{-i\zeta} + e^{-2i\zeta} \ldots + e^{-Mi\zeta}) \tag{A1.9b}$$

This is the sum of two geometric series with M terms each and the sum of each series is an explicit quantity.

$$2S_1 = \frac{e^{i\zeta} - e^{i\zeta}e^{Mi\zeta}}{1 - e^{i\zeta}} + \frac{e^{-i\zeta} - e^{-i\zeta}e^{-Mi\zeta}}{1 - e^{-i\zeta}} \tag{A1.10}$$

$$= \frac{e^{i\zeta} + e^{-i\zeta} + e^{Mi\zeta} + e^{-Mi\zeta} - e^{i\zeta(M+1)} - e^{-i\zeta(M+1)} - 2}{2 - e^{i\zeta} - e^{-i\zeta}} \tag{A1.11}$$

$$= \frac{2\cos\zeta + 2\cos M\zeta - 2\cos\zeta(M+1) - 2}{2 - 2\cos\zeta} \tag{A1.12}$$

$$= -1 + \frac{\cos M\zeta - \cos\zeta(M+1)}{1 - \cos\zeta} \tag{A1.13}$$

But $(M + 1) = N$ from equation (A1.2a) and $\zeta(M + 1) = \zeta N = 2n\pi$ from equation (A1.6).

Therefore, $\cos\zeta(M + 1) = \cos 2n\pi = +1$ for all n,

and

$$2S_1 = -(1 + \frac{1 - \cos M\zeta}{1 - \cos\zeta}) \tag{A1.14}$$

But $\cos M\zeta = \cos(N - 1)\zeta$

$$= \cos\{\frac{2n\pi}{N}(N - 1)\}$$

$$= \cos(2n\pi - \zeta)$$

$$= \cos 2n\pi \cos(-\zeta) + \sin 2n\pi \sin(-\zeta)$$

$$= \cos \zeta \qquad \text{(A1.15)}$$

Substitute (A1.15) into (A1.14)

$$2S_1 = -(1 + \frac{1 - \cos \zeta}{1 - \cos \zeta}) = -2$$

$$S_1 = -1 \qquad \text{(A1.16)}$$

From equations (A1.7) and (A1.5)

$2S = M + S_1$ and, substituting (A1.16),

$$S = \frac{M-1}{2} = \frac{N}{2} - 1 \qquad \text{(A1.17)}$$

APPENDIX II

Limit Analysis of the Damping Beam Function as the Frequency approaches Zero

In the solution of the damping beam transverse vibrations the coefficients are obtained as functions of frequency and geometry. Since this is the solution for a translation and rotation of the ends it should apply down to zero frequency and yield the static solution. A limit analysis must be carried out, however, because the coefficients are singular at zero frequency.

The case of an undamped beam is relatively straightforward and will not be treated. In fact, it can be considered to be a special case of a damped beam.

Equation (4.10) gives ϕ as a function of λ and η. This can be rewritten

$$\phi\ell = \lambda\ell(1 + i\eta_d)^{-\frac{1}{4}} = (\alpha - i\beta) \qquad \text{(A2.1)}$$

α and β are both real positive numbers for all non zero η. For $\eta_d = 0$, $\beta = 0$ and this is the special case of $\phi\ell$ real.

It is now necessary to expand each of the terms in equations (4.9), (4.14) to (4.17) and (4.20) to (4.23) in exponential form.

$$\cos \phi\ell = \cos(\alpha - i\beta)$$

$$= \frac{e^{i(\alpha-i\beta)} + e^{-i(\alpha-i\beta)}}{2} = \frac{e^{\beta}e^{i\alpha} + e^{-\beta}e^{-i\alpha}}{2}$$

$$= \frac{e^{\beta}(\cos\alpha + i\sin\alpha) + e^{-\beta}(\cos\alpha - i\sin\alpha)}{2}$$

$$= \cos\alpha\left(\frac{e^{\beta} + e^{-\beta}}{2}\right) + i\sin\alpha\left(\frac{e^{\beta} - e^{-\beta}}{2}\right)$$

$$= \cos\alpha\cosh\beta + i\sin\alpha\sinh\beta \qquad \text{(A2.2)}$$

By a similar expansion and rearrangement of terms it can be shown that the following relationships apply:

$$\sin \phi\ell = \sin \alpha \cosh \beta - i \cos \alpha \sinh \beta \qquad \text{(A2.3)}$$

$$\cosh \phi\ell = \cos \beta \cosh \alpha - i \sin \beta \sinh \alpha \qquad \text{(A2.4)}$$

$$\sinh \phi\ell = \cos \beta \sinh \alpha - i \sin \beta \cosh \alpha \qquad \text{(A2.5)}$$

As $\phi \to 0$ $\lambda \to 0$ and hence $\alpha \to 0$ and $\beta \to 0$.

Since all the arguments in equations (A2.2) to (A2.5) are real the terms can be expanded as follows for arguments approaching zero:

$$\cos \phi\ell = \left(1 - \frac{\alpha^2}{2!} + \frac{\alpha^4}{4!} \ldots\right)\left(1 + \frac{\beta^2}{2!} + \frac{\beta^4}{4!}\ldots\right)$$

$$+ i\left(\alpha - \frac{\alpha^3}{3!} + \frac{\alpha^5}{5!}\ldots\right)\left(\beta + \frac{\beta^3}{3!} + \frac{\beta^5}{5!}\ldots\right) \qquad \text{(A2.6)}$$

$$\sin \phi\ell = \left(\alpha - \frac{\alpha^3}{3!} + \frac{\alpha^5}{5!}\ldots\right)\left(1 + \frac{\beta^2}{2!} + \frac{\beta^4}{4!} \ldots\right)$$

$$- i\left(1 - \frac{\alpha^2}{2!} + \frac{\alpha^4}{4!} \ldots\right)\left(\beta + \frac{\beta^3}{3!} + \frac{\beta^5}{5!}\right) \qquad \text{(A2.7)}$$

$$\cosh \phi\ell = \left(1 + \frac{\alpha^2}{2!} + \frac{\alpha^4}{4!} \ldots\right)\left(1 - \frac{\beta^2}{2!} + \frac{\beta^4}{4!} \ldots\right)$$

$$- i\left(\alpha + \frac{\alpha^3}{3!} + \frac{\alpha^5}{5!} \ldots\right)\left(\beta - \frac{\beta^3}{3!} + \frac{\beta^5}{5!} \ldots\right) \qquad \text{(A2.8)}$$

$$\sinh \phi\ell = \left(\alpha + \frac{\alpha^3}{3!} + \frac{\alpha^5}{5!} \ldots\right)\left(1 - \frac{\beta^2}{2!} + \frac{\beta^4}{4!}\ldots\right)$$

$$- i\left(1 + \frac{\alpha^2}{2!} + \frac{\alpha^4}{4!} \ldots\right)\left(\beta - \frac{\beta^3}{3!} + \frac{\beta^5}{5!} \ldots\right) \qquad \text{(A2.9)}$$

The cantilever and doubly attached cases must now be considered separately.

From equation (4.14) it can be seen that in the cantilever coefficients the singularity arises from the term $\dfrac{1}{2\phi\left[1 + \cos \phi\ell \cosh \phi\ell\right]}$

From (A2.6) and (A2.8) $\cos \phi\ell$ and $\cosh \phi\ell$ both approach 1.0 as α and β approach 0 (to the first order). Therefore

$$\frac{1}{2\phi\left[1 + \cos\phi\ell \ \cosh \phi\ell\right]} \rightarrow \frac{1}{4\phi} \tag{A2.10}$$

Similarly, $\sin \phi\ell \rightarrow \alpha - i\beta = \phi\ell$ (A2.11)

and $\sinh\phi\ell \rightarrow \alpha - i\beta = \phi\ell$ (A2.12)

Substituting (A2.10) to (A2.12) into equation (4.14) and retaining terms which do not go to zero leads to

$$\lim_{\phi \rightarrow 0} (B_4) = \frac{\theta(0)}{2\phi} \tag{A2.13}$$

similarly

$$\lim_{\phi \rightarrow 0} (B_3) = \frac{w(0)}{2} \tag{A2.14}$$

$$\lim_{\phi \rightarrow 0} (B_2) = \frac{\theta(0)}{2\phi} \tag{A2.15}$$

$$\lim_{\phi \rightarrow 0} (B_1) = \frac{w(0)}{2} \tag{A2.16}$$

These values must then be substituted into equation (4.9) to obtain

$$Y = \frac{w(0)}{2} \cos \phi y + \frac{\theta(0)}{2\phi} \sin \phi y + \frac{w(0)}{2} \cosh \phi y + \frac{\theta(0)}{2\phi} \sinh \phi y \tag{A2.17}$$

$$\phi y = \frac{y}{\ell} (\alpha - i\beta) \tag{A2.18}$$

Whenever ϕy appears as an argument y can be substituted for ℓ in the limit expressions.

Therefore, $\lim_{\phi \rightarrow 0} (\cos \phi y, \cosh \phi y) = 1.0$ (A2.19)

and

$$\lim_{\phi \rightarrow 0} (\sin \phi y, \sinh \phi y) = \phi y \tag{A2.20}$$

Substituting (A2.19) and (A2.20) into (A2.17) results in

$$Y = w(0) + \theta(0)y \tag{A2.21}$$

which is exactly the rigid body behaviour of a cantilever.

The doubly attached beam is not as straightforward because the singularities are of higher order than the first. Equation (4.20) contains the denominator $\frac{1}{2\phi[1 - \cos \phi\ell \cosh \phi\ell]}$. Use equations (A2.6) to (A2.9) to obtain

$$\lim_{\phi \to 0} (\cos \phi\ell \cosh \phi\ell) =$$

$$\lim_{\alpha, \beta \to 0} \left[\left(1 - \frac{\alpha^2}{2!} + \frac{\alpha^4}{4!} \ldots\right)\left(1 - \frac{\beta^2}{2!} + \frac{\beta^4}{4!} \ldots\right)\left(1 + \frac{\alpha^2}{2!} + \frac{\alpha^4}{4!} \ldots\right)\left(1 + \frac{\beta^2}{2!} + \frac{\beta^4}{4!} \ldots\right)\right.$$

$$\left. + \left(\alpha - \frac{\alpha^3}{3!} \ldots\right)\left(\beta + \frac{\beta^3}{3!} \ldots\right)\left(\alpha + \frac{\alpha^3}{3!} \ldots\right)\left(\beta - \frac{\beta^3}{3!}\right)\right]$$

$$+ i\left[\left(1 - \frac{\beta^2}{2!} + \frac{\beta^4}{4!} \ldots\right)\left(1 + \frac{\alpha^2}{2!} + \frac{\alpha^4}{4!} \ldots\right)\left(\alpha - \frac{\alpha^3}{3!} \ldots\right)\left(\beta + \frac{\beta^3}{3!} \ldots\right)\right.$$

$$\left. - \left(1 - \frac{\alpha^2}{2!} + \frac{\alpha^4}{4!} \ldots\right)\left(1 + \frac{\beta^2}{2!} + \frac{\beta^4}{4!} \ldots\right)\left(\beta - \frac{\beta^3}{3!} \ldots\right)\left(\alpha + \frac{\alpha^3}{3!} \ldots\right)\right] \quad \text{(A2.22)}$$

Multiplying out and neglecting terms of order 8 and higher leads to

$$\lim_{\phi \to 0} (\cos \phi\ell \cosh \phi\ell) = \left(1 + \alpha^2\beta^2 - \frac{\alpha^4}{6} - \frac{\beta^4}{6} + \frac{2i\alpha\beta}{3}(\alpha^2 - \beta^2)\right) \quad \text{(A2.23)}$$

Therefore,

$$\lim_{\phi \to 0}(1 - \cos\phi\ell \cosh \phi\ell) = \left(\frac{\alpha^4}{6} + \frac{\beta^4}{6} - \alpha^2\beta^2\right) - \frac{2i\alpha\beta}{3}(\alpha^2 - \beta^2) \quad \text{(2.24)}$$

But $\frac{(\phi\ell)^4}{6} = \frac{(\alpha - i\beta)^4}{6}$ is identically equal to equation (A2.24),

and $$\lim_{\phi \to 0} (1 - \cos \phi\ell \cosh \phi\ell) = \frac{(\phi\ell)^4}{6} \quad \text{(A2.25)}$$

By a similar process of expansion and multiplication it can be shown that

$$\lim_{\phi \to 0} (\cosh \phi\ell - \cos \phi\ell) = (\phi\ell)^2 \quad \text{(A2.26)}$$

that

$$\lim_{\phi \to 0}(\sinh \phi\ell - \sin \phi\ell) = \frac{(\phi\ell)^3}{3} \quad \text{(A2.27)}$$

and that

$$\lim_{\phi \to 0}(\sinh \phi\ell + \sin \phi\ell) = 2\phi\ell \quad \text{(A2.28)}$$

The expressions (A2.25) to (A2.28) can be used in (4.20) to (4.23) to determine the limits of the coefficients. These are

$$\lim_{\phi \to 0}(B_4) = \frac{3}{(\phi \ell)^2} \left[2w(0) - 2w(\ell) + \ell\theta(0) + \ell\theta(\ell)\right] \qquad \text{(A.29)}$$

$$\lim_{\phi \to 0}(B_3) = \frac{1}{(\phi \ell)^2} \left[3w(\ell) - 3w(0) - 2\ell\theta(0) - \ell\theta(\ell)\right] \qquad \text{(A2.30)}$$

$$(B_2) = \frac{\theta(0)}{\phi} - B_4 \qquad \text{(A2.31)}$$

$$(B_1) = w(0) - B_3 \qquad \text{(A2.32)}$$

Substituting (A2.29) to (A2.32) into (4.9) and y for ℓ in the limit expressions for those terms with ϕy as argument and rearranging, yields the relationship

$$Y = w(0)\left[1 - 3\left(\frac{y}{\ell}\right)^2 + 2\left(\frac{y}{\ell}\right)^3\right] + \ell\theta(0)\left[\left(\frac{y}{\ell}\right) - 2\left(\frac{y}{\ell}\right)^2 + \left(\frac{y}{\ell}\right)^3\right]$$

$$+ w(\ell)\left[3\left(\frac{y}{\ell}\right)^2 - 2\left(\frac{y}{\ell}\right)^3\right] - \ell\theta(\ell)\left[\left(\frac{y}{\ell}\right)^2 - \left(\frac{y}{\ell}\right)^3\right] \qquad \text{(A2.33)}$$

It can be shown using the standard equations for a statically deflected beam that (A2.33) is, in fact, the static deflection equation for the beam with the given end conditions.

APPENDIX III

Motion of the Upper Damping Beam Skin in the Shear System

Because the forces and hence the damping of the shear system depend on the relative motion between the upper and lower sandwich skins, it is necessary to know the motion of the upper. (That of the lower is already known because it is anchored to the stringer.)

It is assumed that the skins do not elongate. They strictly deform the interlayer in shear. The following sketch shows the general configuration.

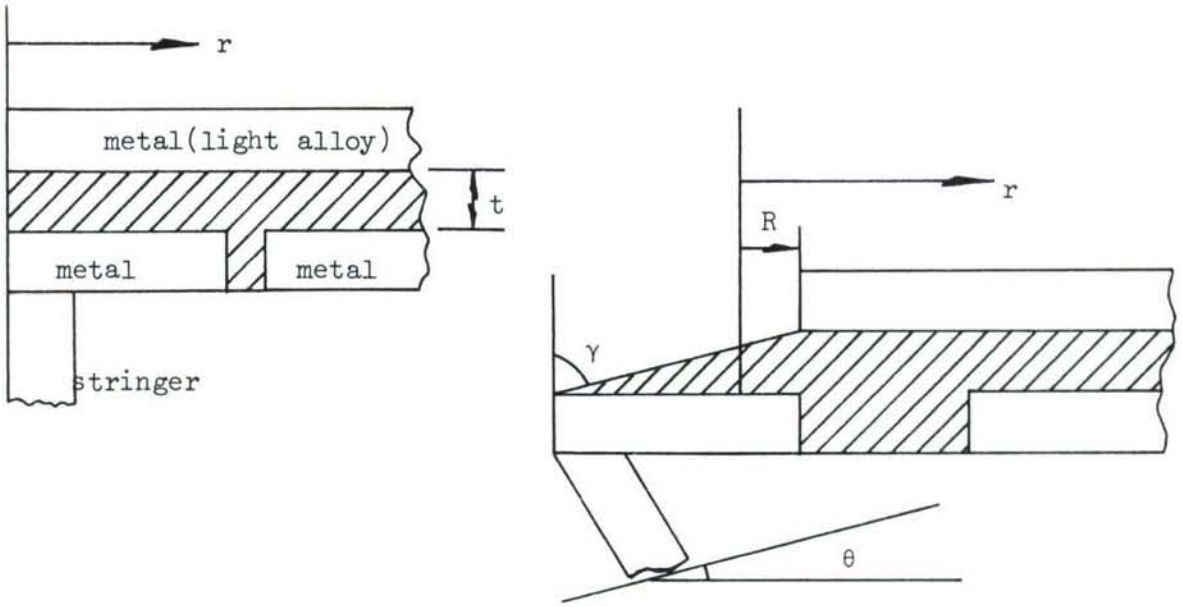

undeformed deformed

Assume the net motion of the upper skin is R in the positive r direction. This motion is due to all the segments of the lower skin acting on the upper through the shear layer.

The net motion of the tip of stringer i is $-H\theta(i)$. Therefore the relative motion between the stringer and the upper layer is $H\theta(i) + R$.

Each end stringer is attached to an inner skin of length $\ell/2$. Each internal stringer has a segment of length ℓ attached to it.

The shear strain γ is $\frac{H\theta(i) + R}{t}$ and the shear stress τ is $G^*\gamma$. Therefore,

$$\tau = G^*\left(\frac{H\,\theta(i) + R}{t}\right) \tag{A3.1}$$

The shear force is τ times the shear area.

For the internal stringers this area is $b_d\ell$ and for the end ones it is $b_d\ell/2$. The net force acting on the upper skin is a summation over all stringers. For equilibrium this must be equal to zero, expressed by

$$\frac{G^*b_d\ell}{2t}\left[\sum_{i=1}^{N+1}(H\theta(i) + R) + \sum_{i=2}^{N}(H\theta(i) + R)\right] = 0 \tag{A3.2}$$

or

$$(N + 1)R + (N - 1)R + \sum_{i=1}^{N+1} H\theta(i) + \sum_{i=2}^{N} H\,\theta(i) = 0 \tag{A3.3}$$

$$R = -\frac{H}{N}\left[\sum_{i=1}^{M}\theta(i) + \sum_{i=2}^{N}\theta(i)\right] \tag{A3.4}$$

$$= -\frac{H}{N}\left[2\sum_{i=1}^{M}\theta(i) - \theta(0) - \theta(\ell)\right] \tag{A3.5}$$

When n is odd

$$\theta(0) = -\theta(\ell) \tag{A3.6}$$

Therefore,

$$R = \frac{-2H}{N}\sum_{i=1}^{M}\theta(i) \tag{A3.7}$$

But for n odd, and equal stringer spacing

$$\theta(i) = -\theta(N + 2 - i)$$

Hence $$\sum_{i=1}^{M} \theta(i) = 0 \qquad \text{(A3.8)}$$

and $R = 0.$

When n is even

$$\theta(0) = \theta(\ell) \qquad \text{(A3.9)}$$

Therefore,

$$R = \frac{-2H}{N} \left[\sum_{i=1}^{M} \theta(i) - \theta(0) \right] \qquad \text{(A3.10)}$$

or

$$= \frac{-2H}{N} \left[\sum_{i=2}^{N} \theta(i) + \theta(0) \right] \qquad \text{(A3.11)}$$

$$\theta(i) = \frac{n\pi}{L} \cos \frac{n\pi y_i}{L} \qquad \text{(A3.12)}$$

Equation (A3.11) can be rewritten, noting that $\theta(0) = \frac{n\pi}{L}$, as

$$R = - \frac{2Hn\pi}{NL} \left[\sum_{i=2}^{N} \cos \frac{n\pi y_i}{L} + 1 \right] \qquad \text{(A3.13)}$$

But n is even. Let it be 2g.

Then

$$R = - \frac{4Hg\pi}{NL} \left[\sum_{i=2}^{N} \cos \frac{2g\pi y_i}{L} + 1 \right] \qquad \text{(A3.14)}$$

and $$y_i = \left(\frac{i-1}{N}\right)L \qquad \text{(A3.15)}$$

Therefore, $$R = - \frac{4Hg\pi}{NL} \left[\sum_{i=2}^{N} \cos \frac{2g\pi(i-1)}{N} + 1 \right] \qquad \text{(A3.16)}$$

or $$R = - \frac{4Hg\pi}{NL} \left[\sum_{i=1}^{N-1} \cos \frac{2g\pi i}{N} + 1 \right] \qquad \text{(A3.17)}$$

In appendix I it was shown that

$$\sum_{i=1}^{N-1} \cos \frac{2n\pi i}{N} = -1 \qquad \text{(A1.16)}$$

Therefore,

$$\sum_{i=1}^{N-1} \cos \frac{2g\pi i}{N} = -1 \qquad \text{(A3.18)}$$

and

$$R = 0. \qquad \text{(A3.19)}$$

Thus, $R = 0$ for n odd or even and the upper skin is effectively anchored in space for the beam with equally spaced stringers.

APPENDIX IV

Silicone Rubber Description

The materials used in the preliminary investigation of Section VIII were designated Materials 1, 2 and 3.

Material 1 was a Polymethylvinylsilicone (ICI polymer E302) with a vinyl constituent of about 0.15 mol. %. The filler used was Aerosil 380, which has a particle size of 3-15 millimicrons. The quantity of filler was approximately 20% by weight. The curing agent used was Varox, which is 50% 25 dimethyl hexane in a mineral filler. The quantity used was 3% by weight. The mill rolled rubber was press cured for 1 hour at 160°C. The post cure cycle consisted of raising the temperature in an oven from ambient to 200°C over a period of 2 hours, followed by an 8 hour soak at that temperature. The specimens were then oven cooled to ambient. The specific gravity of the resulting rubber is about 1.14.

Material 2 was a Polymethyl phenyl vinyl silicone (Midland Silicones polymer S3160/5). This material contains a considerable number of MePhSiO side chains and hence will probably have better low temperature properties than material 1. The filler and catalyst type and quantity were the same as for Material 1, as were the cure and post cure cycles. The specific gravity is again 1.14.

Material 3 was a Polytrifluoropropyl methyl vinyl silicone (Midland Silicones or Dow Corning LS63). This polymer also has many side chains, and in addition its fluorinated chemistry makes it extremely resistant to softening in a hydrocarbon environment. The filler was already in the rubber as purchased, and the exact quantity is not known. The curing agent was 1.3% by weight Perkadox PDS50, which consisted of equal portions of dichlorobenzoyl peroxide and silicone oil. The press cure was 20 minutes at 130°C. The post cure cycle was the same as for materials 1 and 2. The specific gravity of material 3 is about 1.46.

REFERENCES

1. Lin, Y.K., "Free Vibrations of Continuous Skin-Stringer Panels", Journal of Applied Mechanics, Trans ASME, Dec. 1960.

2. Lin, Y.K., Brown, I.D. and Deutschle, P.C., "Free Vibrations of a Finite Row of Continuous Skin-Stringer Panels," Journal of Sound and Vibration (I), January, 1964.

3. Lin, Y.K., et al. Free Vibration of Continuous Skin-Stringer Panels with Non-Uniform Stringer Spacing and Panel Thickness. AFML-TR-64-347, Part 1, February 1965.

4. Mercer, C.A. and Seavey, C.A., "Prediction of Natural Frequencies and Normal Modes of Skin-Stringer Panel Rows", Journal of Sound and Vibration, 6(I), 1967.

5. Lindberg, G.M. and Olson, M.D. Vibration Modes and Random Response of a Multi-Bay Panel System Using Finite Elements. National Research Council of Canada, Aeronautical Report LR-492, Dec. 1967.

6. Clarkson, B.L. and Ford, R.D., "The Response of a Typical Aircraft Structure to Jet Noise", Journal of the Royal Aeronautical Society, Vol. 66, January 1962.

7. Ford, R.D., The Response of Structures to Jet Noise. Ph.D. dissertation, I.S.V.R., The University of Southampton, March 1962.

8. Clarkson, B.L. "The Design of Structures to Resist Jet Noise Fatigue", Journal of the Royal Aeronautical Society, Vol. 66, October 1962.

9. Holehouse, I. Random Response of Builtup Structures. M.Sc. Thesis, University of Southampton, Institute of Sound and Vibration Research, 1967.

10. Lyons, S. The Vibration of Integrally Stiffened Panels and Possible Methods of Reducing the Stresses Induced in Them. M.Sc. Thesis, University of Southampton, Institute of Sound and Vibration Research, February 1968.

11. Szechenyi, E. An Approximate Method for the Determination of the Natural Frequencies of Single and Stiffened Panel Structures. I.S.V.R. Technical Report 23, March 1970.

12. Lin, Y.K. Probabilistic Theory of Structural Dynamics. McGraw-Hill, 1967.

13. Den Hartog, J.P. Advanced Strength of Materials. McGraw-Hill, 1952.

14. Seavey, C.A. and Mercer, C.A., Program for the Calculation of Natural Frequencies and Normal Modes of Skin-Stringer Panel Arrays. Institute of Sound and Vibration Research Technical Report No. 6, July 1968.

15. Warburton, G.B. "The Vibration of Rectangular Plates", Proceedings of the Inst. of Mech. Eng., 168(1954).

16. Timoshenko, S. Strength of Materials, Part 1. Van Nostrand Reinhold Company, 1969.

17. Den Hartog, J.P. Mechanical Vibrations. McGraw-Hill Book Co., 1956.

18. Bishop, R.E.D. and Johnson, D.C. Vibration Analysis Tables. Cambridge University Press, 1956.

19. Handbook of tables for Mathematics, 3rd edition. The Chemical Rubber Company, 1967.

20. Oberst, H., Über die Dämpfung der Biegeschwingungen dünner Bleche durch fest haftende Beläge", Acustica, Vol. 2, Akustische Beihefte, No. 4 (1952).

21. Ungar, E.E., "A guide to Designing Highly Damped Structures using Layers of Viscoelastic Materials", Machine Design, February 14, 1963.

22. Jones, D.I.G., Some Aspects of the Analysis of Damping and Vibrations in Simple Structures. AFML-TR-65-151, December, 1965.

23. Jones, D.I.G., Nashif, A.D. "Damping of Structures by Viscoelastic Links". Shock and Vibration Bulletin, Bulletin 36, Part 4, Jan. 1967.

24. Jones, D.I.G. "Damping of Multi-span Structures by Means of Viscoelastic Links". Shock and Vibration Bulletin, Bulletin 38, Part 3, November 1968.

25. Henderson, J.P. "Energy Dissipation in a Vibration Damper Utilising A Viscoelastic Suspension". Shock and Vibration Bulletin, Bulletin 35, Part 7, April 1966.

26. Jones, D.I.G., Nashif, A.D., Adkins, R.L. "Effect of Tuned Dampers on Vibrations of Simple Structures". AIAA Journal, Vol. 5 No. 2, February 1967.

27. Jones, D.I.G. "Response and Damping of a Simple Beam with Tuned Dampers". Journal of the Acoustical Society of America, Vol. 42, No. 1, July 1967.

28. Jones, D.I.G. "Effect of Isolated Tuned Dampers on Response of Multispan Structures". J. Aircraft, Vol. 4, No. 4, July-Aug 1967.

29. Nashif, A.D. and Jones, D.I.G. "A Resonant Beam Tuned Damping Device" Paper presented at the Winter Annual Meeting of the ASME, New York, N.Y., December 1968.

30. Mead, D.J. "The Damping of Stiffened Plate Structures", Acoustical Fatigue in Aerospace Structures, Syracuse University Press, 1965.

31. Ungar, E.E. "Loss Factors of Viscoelastically Damped Beam Structures", Journal of the Acoustical Society of America, Vol. 34, No. 8, August, 1962.

32. Oberst, H., Schommer, A. "Laminated systems with Optimumily Adjusted Vibration Damping Polymers as Intermediate Layers". Reprint from KUNSTSTOFFE combined with German Plastics. Vol. 55, (1965), No. 8.

33. Bert, C.W., Wilkins, D.J. and Crisman, W.C. "Damping in Sandwich Beams with Shear Flexible Cores". Transactions of the ASME, Journal of Engineering for Industry, November 1967.

34. Mead, D.J. and Markus, S. "The Forced Vibration of a Three Layer, Damped Sandwich Beam with Arbitrary Boundary Conditions". Journal of Sound and Vibration (1969) 10(2).

35. Di Taranto, R.A. and McGraw, J.R. "The Free Vibratory Bending of Damped Laminated Plates". Transactions of the ASME, Journal of Engineering for Industry, Vol. 91, Series B, No. 4, November 1969.

36. Lee, L.T. A Graphical Compilation of Damping Properties of Both Metallic and Non-Metallic Materials. AFML-TR-66-169. May, 1966.

37. Adkins, R.L. "Design considerations and analysis of a complex modulus apparatus". Experimental Mechanics, July 1966.

38. Nashif, A.D. "New Method for Determining Damping Properties of Viscoelastic Materials". Shock and Vibration Bulletin, Bulletin 36, January 1967.

39. Grootenhuis, P. "Measurement of Dynamic Properties of Damping Materials". Proceedings of the International Symposium on the Damping of Vibrations of Plates by Means of a Layer. Leuven, Belgium, 14-16 September, 1967.

40. Cannon, C.M., Nashif, A.D. and Jones, D.I.G. "Damping Measurements on Soft Viscoelastic Materials Using a Tuned Damper Technique". Paper presented at the 38th Shock and Vibration Symposium, St. Louis, Mo., May 1968.

41. McConnell, K.G. "A Proposed Experimental Method for Accurate Measurements of the Dynamic Properties of Viscoelastic Materials". Shock and Vibration Bulletin, Bulletin 39, April 1969.

42. Kennedy, C.C. and Pancu, C.D.P. "Use of Vectors in Vibration Measurement and Analysis". Journal of the Aeronautical Sciences, Volume 14, No. 11, November 1947.

43. Bendat, J.S., and Piersol, A.G. Measurement and Analysis of Random Data. John Wiley and Sons, 1967.

44. White, R.G. Measurement of Structural Frequency Response by Transient Excitation. I.S.V.R. Technical Report 12, January 1969.

45. Mercer, C.A. Introduction to the I.S.V.R. Random Data Analysis Centre. I.S.A.V. Memorandum No. 209, November 1967.

46. Clarkson, B.L. and Pietrusewicz, S.A. The University of Southampton Random Siren Facility. ASD-TDR-62-680, 1962.

47. Robson, J.D. An Introduction to Random Vibration. Edinburgh University Press, 1963.

48. Read, W.T. "Effect of Stress-Free Edges in Plane Shear of a Flat Body". Journal of Applied Mechanics, December 1950.

TABLE 2.1

TEST PANEL CONSTANTS

E	1.05×10^7 lbs/in^2
G	4.04×10^6 lbs/in^2
ν	0.30
ρ	0.101 lbs/in^3
h	0.090 in.
I_s	0.260 in^4
C	0.00484 in^4
C_{ws}	0.00071 in^6
I_η	0.0814 in^4
Hh_s	0.324 in^2
$I_{\eta\zeta}$	0 in^4
S_z	-0.773 inch
c_y	0 inch
ℓ	22.0 inches

TABLE 2.2

Natural Frequencies for the Integrally Stiffened Panel of Figure 2.5 (Simply Supported Ends) Calculated by the Transfer Matrix Method or by Reference 15.

Mode	Case 1	Case 2	Case 3	Case 4		Case 5		Case 6
	Transfer Matrix	Transfer Matrix	Transfer Matrix	Trans. Mat. (a)	Ref. 15 (b)	Trans. Mat. (a)	Ref. 15 (b)	Ref. 15
1	243.63	247.86	180.9162	44.2	44.2	71.2	71.5	17.8
2	259.67	276.80	180.9322	123.6	123.8	179.0	178.6	27.7
3	303.43	337.79	243.26	-	256	338.8	338.5	59.0
4	382.68	429.96	254.86	441.1	441	551.2	551.0	118.0
5	491.95	540.09	283.47	679.3	680		815	206
6		683.88	333.39					324
7		804.46	402.26					
8		914.32	484.39					
9		999.95	568.16					
10		1053.64	679.93					
11			770.90					
12			856.82					

Case 1 - 6 spans, simply supported edges

Case 2 - 6 spans, fixed edges

Case 3 - 8 spans, free edges

Case 4 - 6 spans, simply supported edges with all stringer constants 0 (flat plate)

Case 5 - 6 spans, fixed edges with all stringer constants 0 (flate plate)

Case 6 - 24 inch by 22 inch flat plate with the 22 inch sides free

TABLE 2.3

Calculated Natural Frequencies for the Panel with Fixed Edges and Simply Supported Ends for Different Values of Frame Pitch.

Mode	one half wave in the length									2 halfwaves in the length
	10 in. frames	11 in. frames	12 in. frames	14 in. frames	16 in. frames	18 in. frames	20 in. frames	22 in. frames	26 in. frames	22 in. frames
1	933.33	867.72	787.47	590.73	456.93	364.02	297.86	247.86	181.35	867.72
2	967.48	881.18	789.16	602.46	474.58	385.84	322.75	276.80	216.81	881.18
3	1017.99	902.29	793.33	632.02	515.06	434.12	377.74	337.79	287.81	902.29
4	1074.81	923.54	806.96	685.44	584.18	512.74	463.79	429.96	389.03	923.54
5	1183.04	1056.69	954.95	797.72	688.42	617.23	570.87	540.09	504.58	1056.69
6	1187.54	1056.71	956.79	832.86	769.72	730.68	703.65	683.88	657.32	1056.71
7	1342.13	1234.98	1099.44	955.27	888.62			804.46		1234.98
8	1380.27	1249.95	1149.63	1044.43	989.48			914.32		1249.95
9	1412.34	1262.40	1193.04	1113.84	1067.69			999.95		1262.40
10	1432.20	1267.98	1220.07	1156.99	1116.54			1053.64		1267.98

TABLE 3.1

BEAM PARAMETERS

E	10.5×10^6 lbs/in.^{2}
ρ	0.101 lbs/in.^{3}
h	0.108 inch
d	1.01 inches
H	1.693 inches
h_s	0.213 inches
b	3.0 inches
L	18.0 inches
M	5 or 7
N	6

TABLE 3.2

Calculated Natural Frequencies for a 6 span Beam

Mode	5 stringers, simply supported ends		7 stringers, simply supported ends		5 or 7 stringers and fully fixed ends
	Energy Method (Eq.3.16) Hz.	Transfer Matrix Method Hz.	Energy Method (Eq.317) Hz.	Transfer Matrix Method Hz.	Transfer Matrix Method only Hz.
1	20.8	20.7	20.7	20.6	46.81
2	81.6	81.8	80.0	80.1	125.79
3	178	179	172	172	237.32
4	309	307	290	286	373.31
5	465	458	424	411	532.59
6	*635	593	*565	526	658.21
7	833	767	722	670	807.06
8	1035	903	880	770	928.06
9	1245	1006	1035	867	1017.46
10	1455	1068	1195	957	1071.29

*Equation (3.15)

TABLE 3.3

Calculated Natural Frequencies for a Simple Beam
(no stringers)

Mode	Simply Supported Ends		Fixed Ends	
	Ref. 18 Hz	Transfer Matrix Method Hz	Ref. 18 Hz	Transfer Matrix Method Hz
1	30.29	30.29	68.67	68.67
2	121.17	121.18	189.29	189.30
3	272.63	272.65	371.09	371.11
4	484.68	484.71	613.43	613.46
5	757.32	757.36	916.37	916.40
6	1090.54	1090.59	1279.89	1279.93
7	1484.34	1484.42	1703.99	1704.05
8	1938.83	1938.83	2188.68	2188.76
9	2453.71	2453.84	2733.96	2734.06
10	3029.27	3029.43	3339.83	3339.94

TABLE 4.1

Panel Response (to Single Point Excitation) reduction produced by Various Damping Treatments (Reference 10)

Mode at (Hz)	Percentage Strain Reduction					
	Treatment A (centre surface)	Treatment B (widths)				
		1 in.	2 in.	3 in.	6 in.	22 in.
320	28	49	54	62	65	72
420	61	84	85	87	87	88
470	79	91	92	92	92	93
520	81	78	78	82	87	90
RMS Strain	39	43	44	45	46	51

TABLE 4.2

Calculated Strain Energies - 6 Dampers Fixed at Each End

Mode	$\frac{T_{de}}{E_d I_d}$ (Eq. 4.7)	$\frac{T_{df}}{E_d I_d}$ (Eq. 4.24) (Fig. 4.18)	$\frac{T_m}{EI}$ (Eq. 4.31)
1	39.0	5.9×10^{-3}	4.18×10^{-3}
2	5.82×10^{2}	1.8×10^{-2}	6.68×10^{-2}
3	2.62×10^{3}	6.8×10^{-1}	3.38×10^{-1}
4	6.96×10^{3}	4.0	1.07
5	1.36×10^{4}	22.0	2.61

TABLE 4.3

Total Loss Factors Calculated for the System of Three Double Cantilevers of Damping Material

Mode	η_m (experimental)	$\frac{T_m}{E_m I_m}$	$\frac{T_{df}}{E_d I_d}$ (Fig. 4.16)		η_t (Eq. 4.30)		
					.060" thick		.080" thick
			.06" Cant.	.08" Cant.	1" wide	½" wide	½" wide
1	.014	4.18×10^{-3}	4.5×10^{-2}	9.6×10^{-3}	.079	.048	.032
2	.0012	6.68×10^{-2}	.73	.30	.068	.037	.036
3	.0012	.338	1.57	2.08	.031	.017	.047
4	.0034	1.07	3.00	2.30	.022	.013	.020
5	.0016	2.61	13.30	4.70	.035	.019	.016
Percentage weight added					13.8	6.9	9.2

TABLE 6.1

Natural Frequencies of a 6 Span Simply Supported Beam with 7 Stringers

Mode	Theoretical		Experimental (steady state)	
	Energy Method (Eq. 3.7) (Hz)	Transfer Matrix Method (Hz)	No Added Damping	.5" x .080" Cantilevers
1	20.7	20.6	40.7	34.5
2	80.0	80.1	84.3	78.5
3	172	172	178.5	177.9
4	290	286	293.1	276.6
5	424	411	418.1	380.8
6	*565	526	504.2	439.6
7	722	670	676	575

* equation (3.15)

TABLE 6.2

6 Span Simply Supported Beam Loss Factors (steady state measurements)

Mode		η_t for the beam with .5 in x .080 in. cantilever dampers	
	η_m Experimental	theoretical (eq. 4.30)	experimental
1	.014	.032	.034
2	.0012	.036	.019
3	.0012	.047	.051
4	.0034	.020	.012
5	.0016	.016	.009
6	.0017	-	.007

TABLE 6.3

Characteristics of a 6 Span Simply Supported Beam with 7 Stringers
(Measured by a Transient Technique)

Mode	Natural Frequency(Hz)				Loss Factor				Added Weight (%)			
	a	b	c	d	a	b	c	d	a	b	c	d
1	41.2	37.0	37.5	34.5	.0065	.024	.030	.050	0	6.9	13.8	9.2
2	84.2	79.4	76.0	78.5	.0017	.038	.061	.032				
3	178.5	176.6	175	175	.0016	.027	.043	.013				
4	293	279	268	275	.0030	.015	.026	.0083				
5	418	386	-	380	.0019	.011	-	.011				
6	504	450	404	437	.0015	.012	.017	.009				

a - beam with no added damping

b - beam with 0.5 inch by 0.06 inch double cantilever damping

c - beam with 1.0 inch by 0.06 inch double cantilever damping

d - beam with 0.5 inch by 0.08 inch double cantilever damping

TABLE 7.1

Reduction in the Peaks of the Frequency Response Curve for a Six Span Panel by the Addition of LD400 Damping Material Across the Stringer Tips (Acoustic Excitation).

Mode at (Hz)	Percentage reduction	
	1 in by 0.060 in (.85% weight added)	2 inch by 0.060 inch (1.7% weight added)
230	80	88
350	73	71
550	90	91
720	69	80

TABLE 7.2

Measured Root Mean Square Panel Response to Random Acoustic Excitation

Strain Gauge	Response (amplified strain gauge signal) volts		Percentage strain
	No additional damping	2 inch by .060 inch LD 400	reduction
13	11.5	3.4	70
14	10.5	1.9	82
15	13.0	3.5	73

TABLE 7.3

Reduction in Panel Root Mean Square Response to Random Excitation by Two Widths and Two Thicknesses of LD 400.

Damping Material Width (in.)	Damping Material Thickness (in.)	Percentage Weight Added	Percentage Reduction in R.M.S. response*
3.0	0.125	5.25	75
1.0	0.125	1.75	66
3.0	0.035	1.5	75
1.0	0.035	0.5	63

* each value is the mean of the three gauges.

TABLE 7.4

Reduction in Panel Root Mean Square Response to Random Excitation by the Shear Damper System.

Shear Beam Skin Thickness * (in.)	Shear Layer Thickness (in.)	Percentage Reduction in Strain Response +
.018	.020	71
.036	.036	69
.018	.075	65

* Top and bottom skins equal.
+ Mean of three gauges.

TABLE 9.1

Percentage Reduction in Full Scale Specimen Response to Random Noise by the Addition of Strip Dampers.

Damping Treatment	Percentage Strain Reduction
3 in x .125 in. x 15 in LD400	42
1 in x .125 in. x 15 in LD400	32
3 in x .035 in. x 15 in LD400	38
1 in x .035 in. x 15 in LD400	27
1 in x .056 in x 15 in shear damper (.018 skins, .020 fluorinated silicone rubber layer)	35

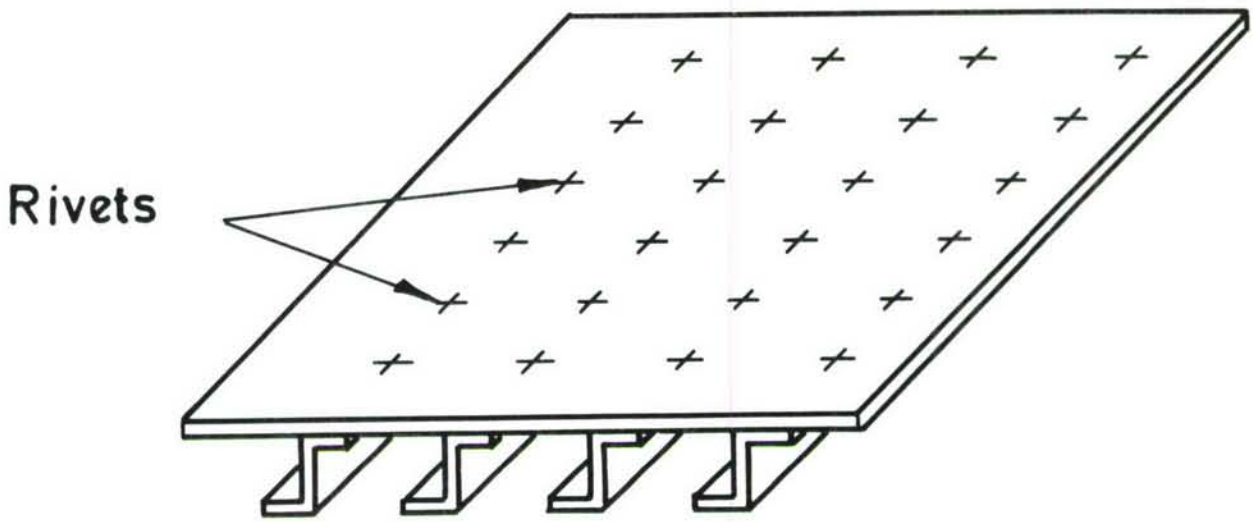

(a) Conventional skin stringer structure.

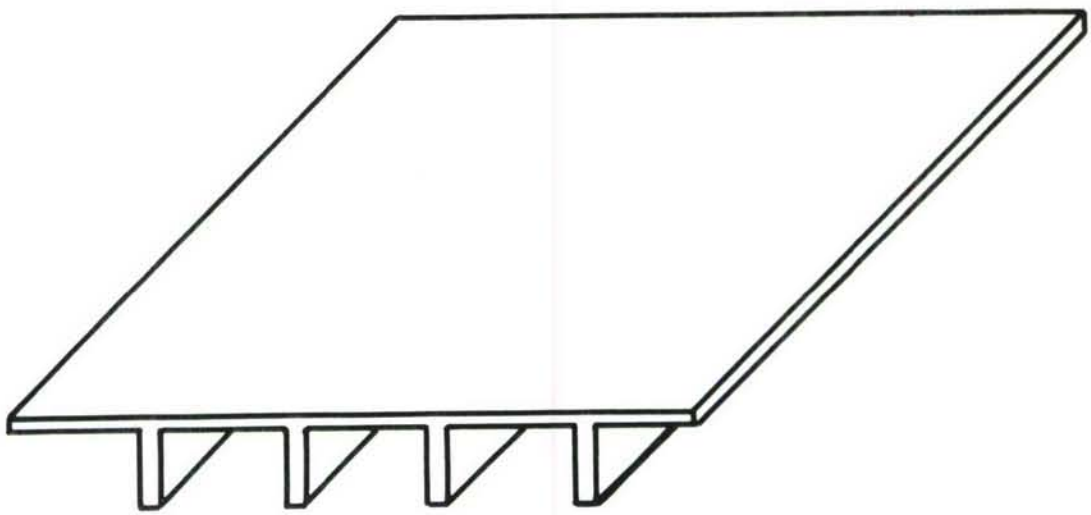

(b) Integrally stiffened structure machined from a solid slab.

Fig. 2·1 Skin stringer configurations.

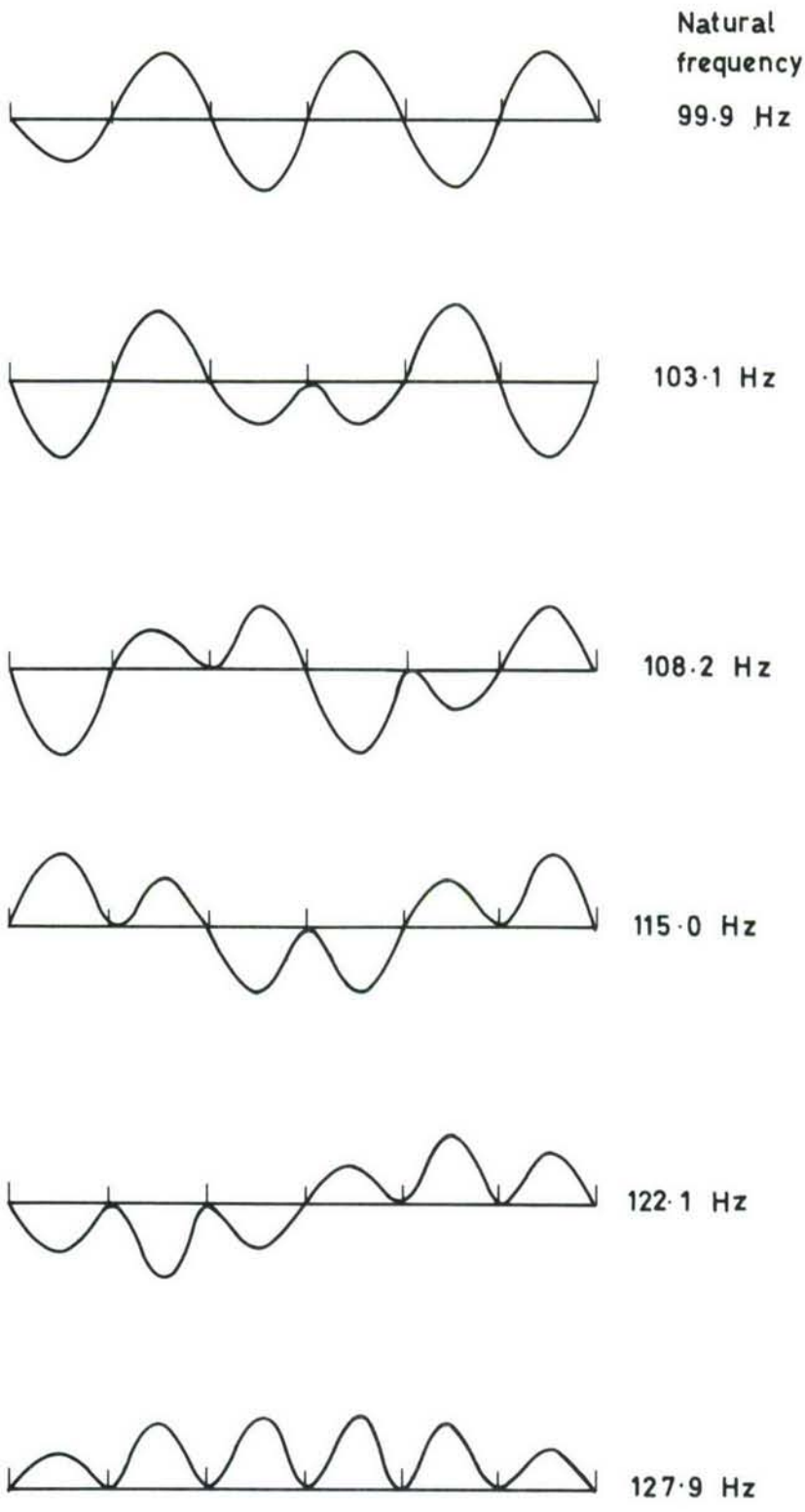

Fig. 2·2 Normal modes for six spans with equal stringer spacing. (Ref. 4).

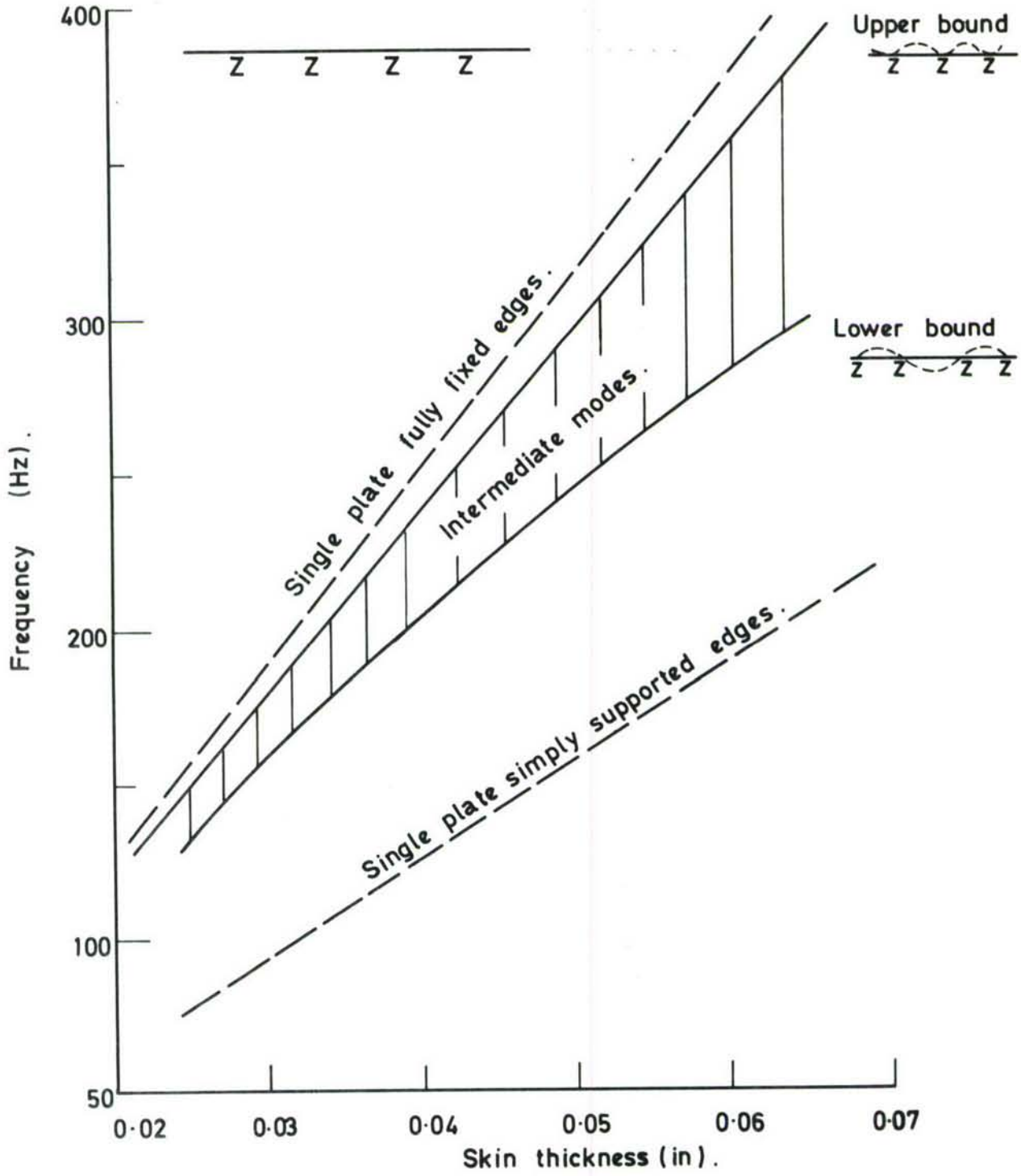

Fig.2.3 Frequencies of coupled flat plates.

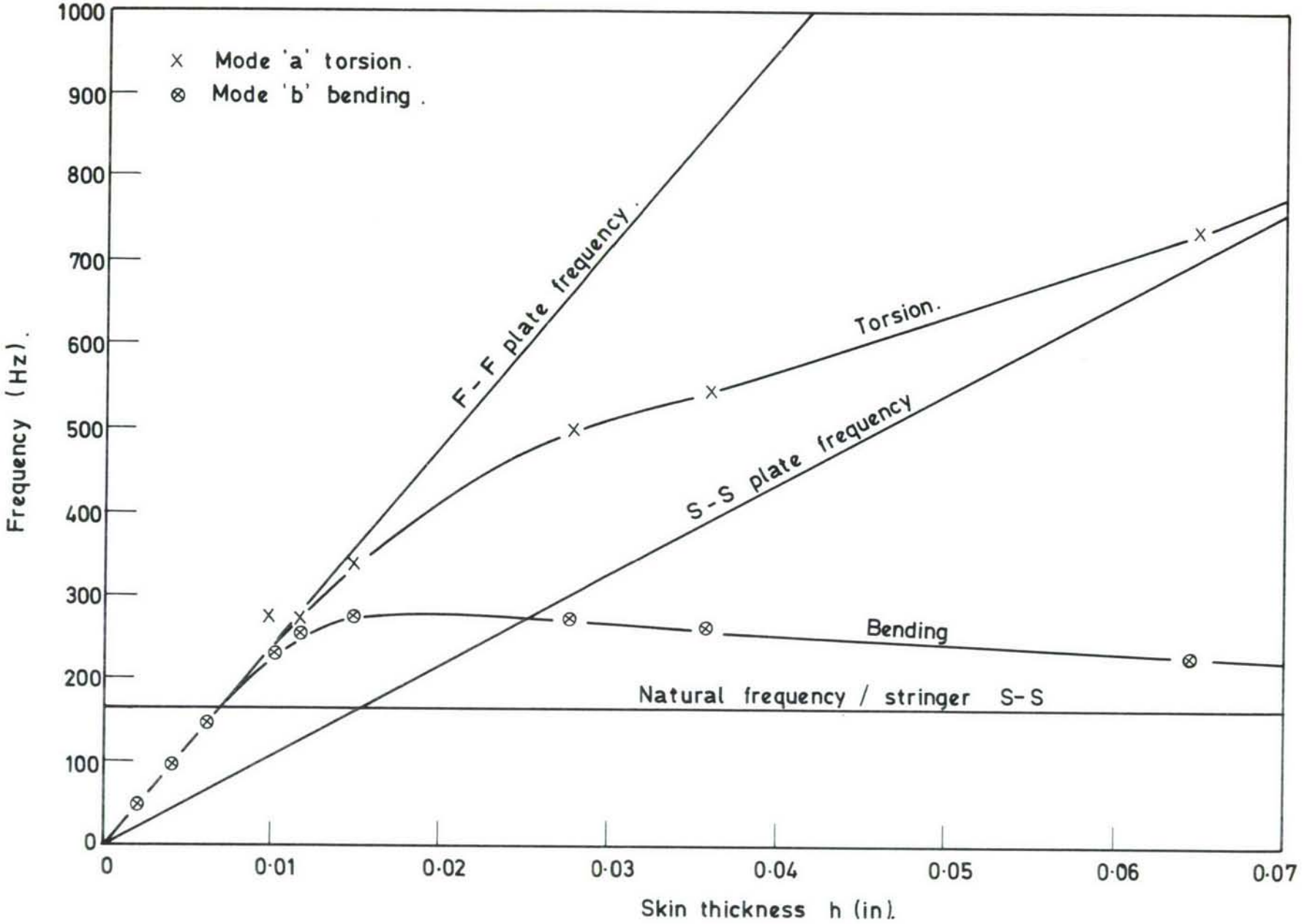

Fig.2.4 Integrally stiffened panel Variation of natural frequencies with skin thickness. $b = 3"$ $\ell = 14"$

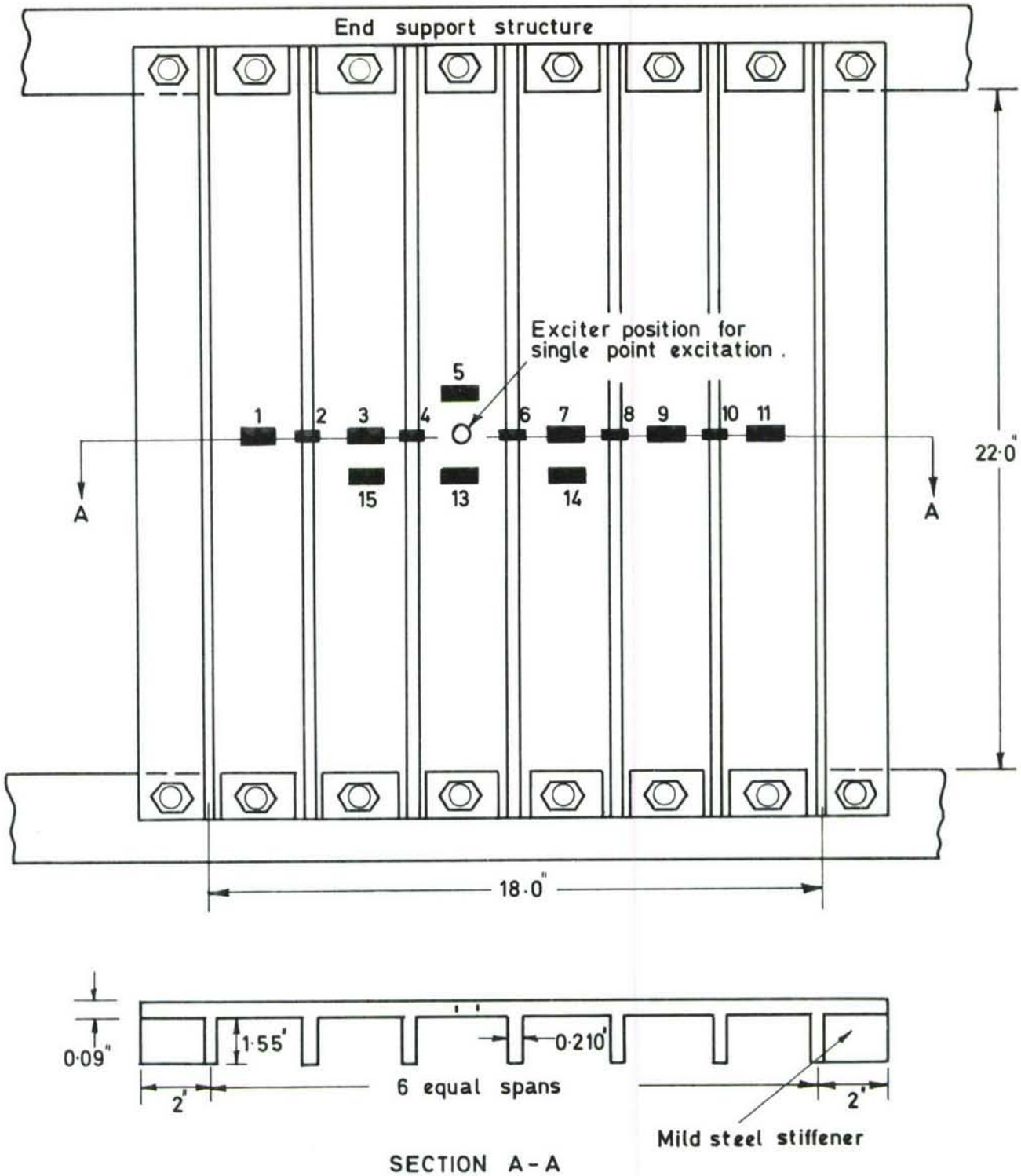

SECTION A-A

NOTE : Numbers on panel denote strain gauges bonded to outside skin surface .

Fig. 2·5 Test panel details

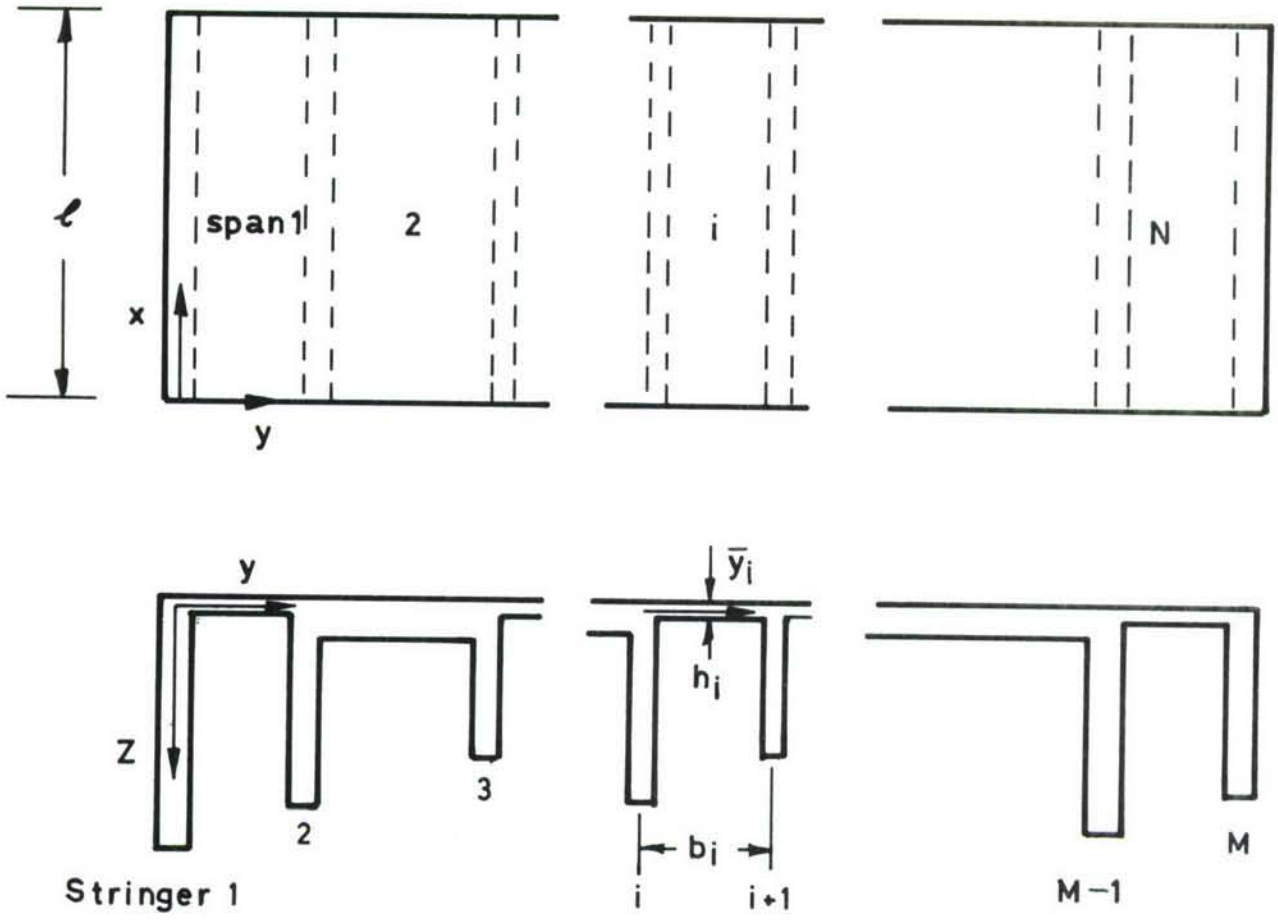

Fig 2.6 Schematic of a general integrally stiffened N span panel showing stringer and span designation.

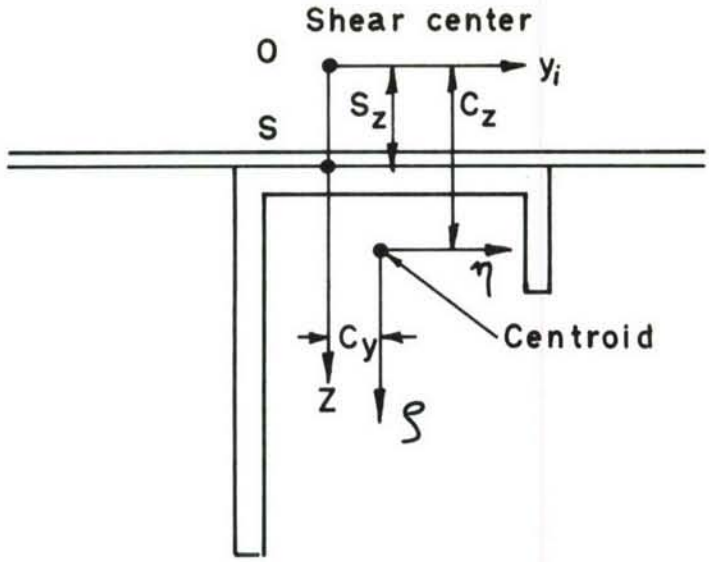

(From Ref 3) for a conventional structure

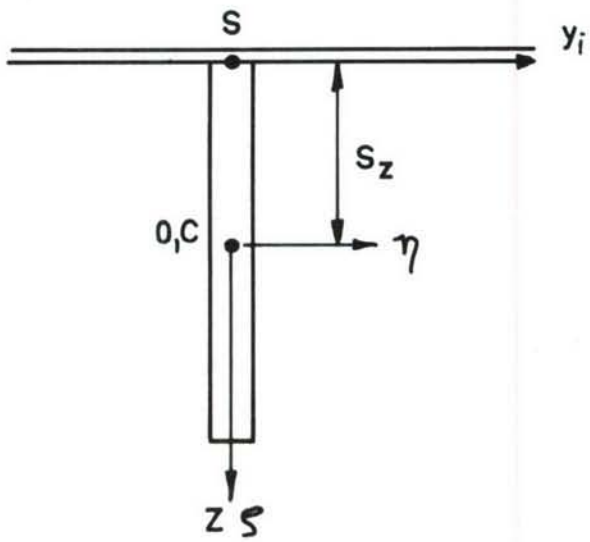

Integrally stiffened structure

Fig 2.7 Schematic of stringer geometry for parameter calculations.

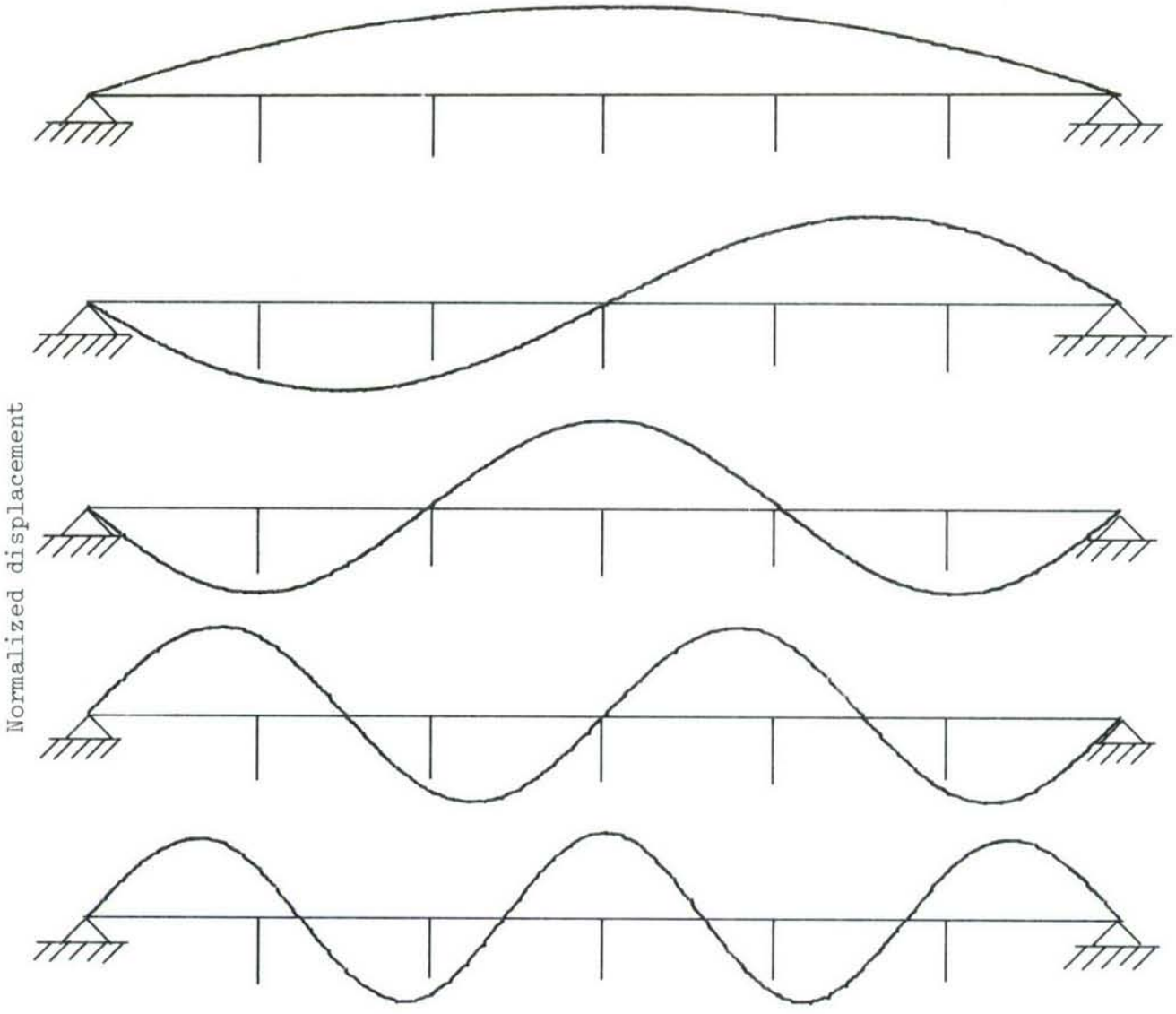

Fig. 2.8(a) Calculated mode shapes for an integrally stiffened panel with edges parallel to stringers simply supported

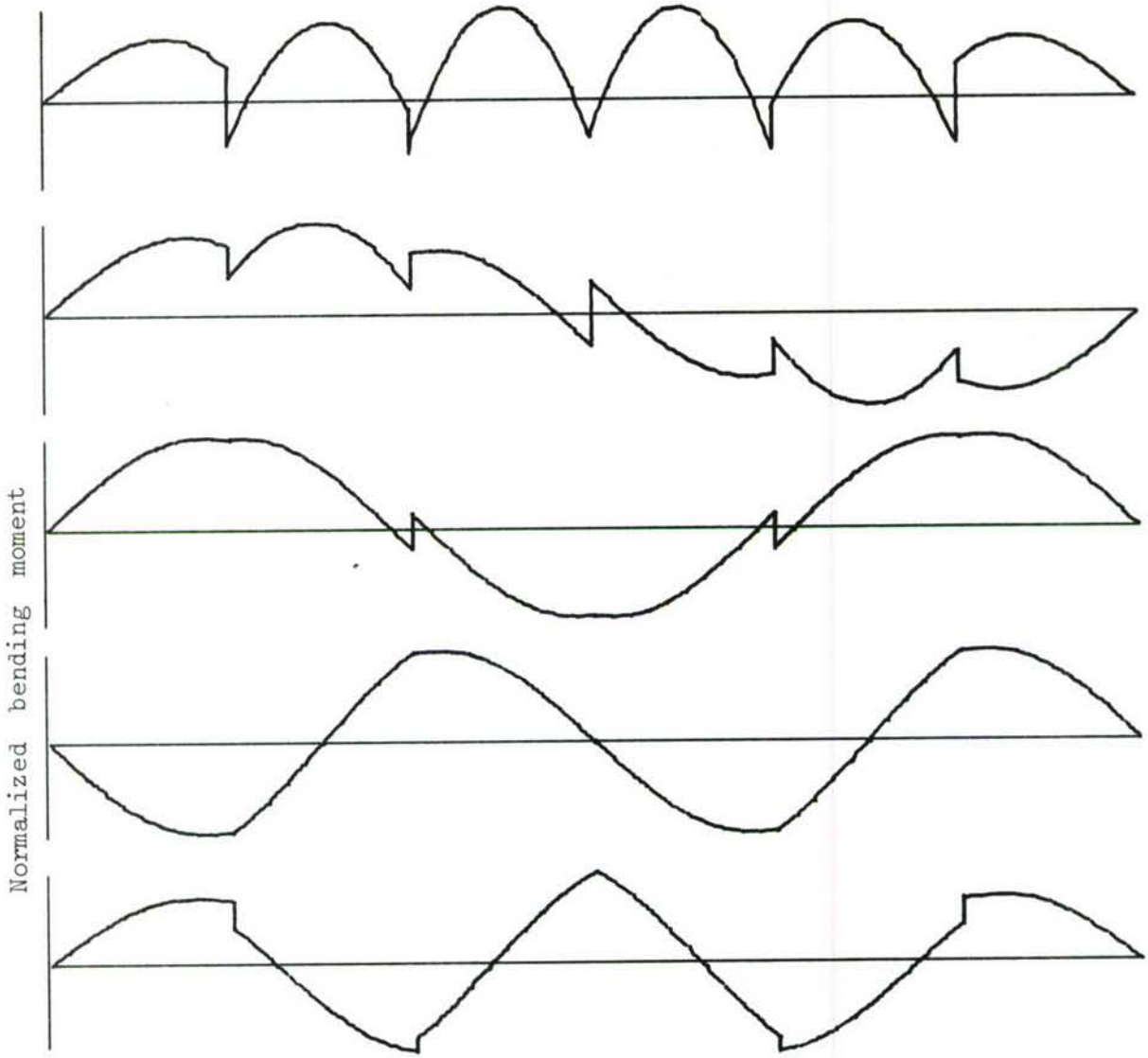

Fig. 2.8(b) Calculated bending moments for an integrally stiffened panel with edges parallel to stringers simply supported

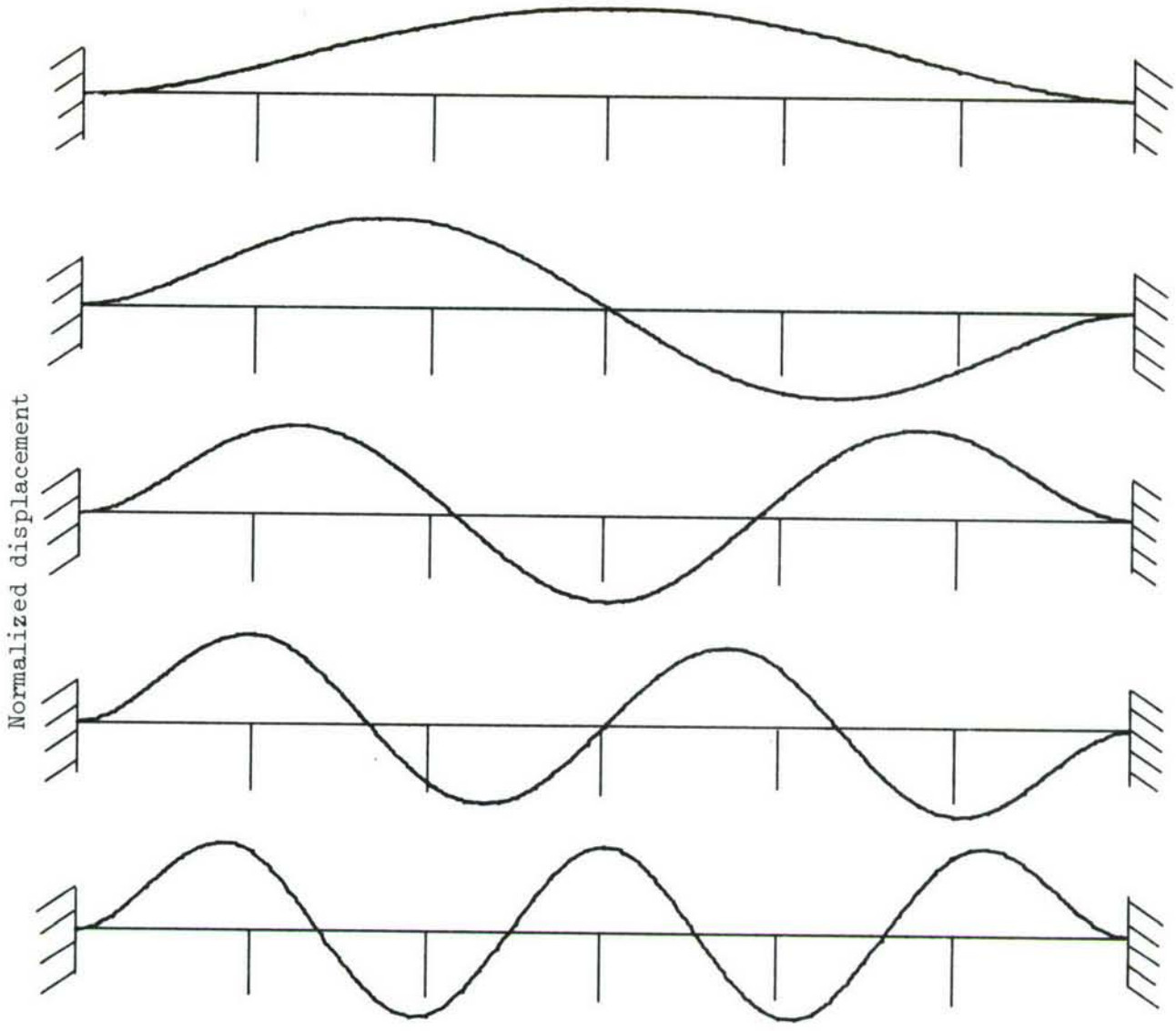

Fig. 2.9(a) Calculated mode shapes for an integrally stiffened panel with edges parallel to stringers clamped

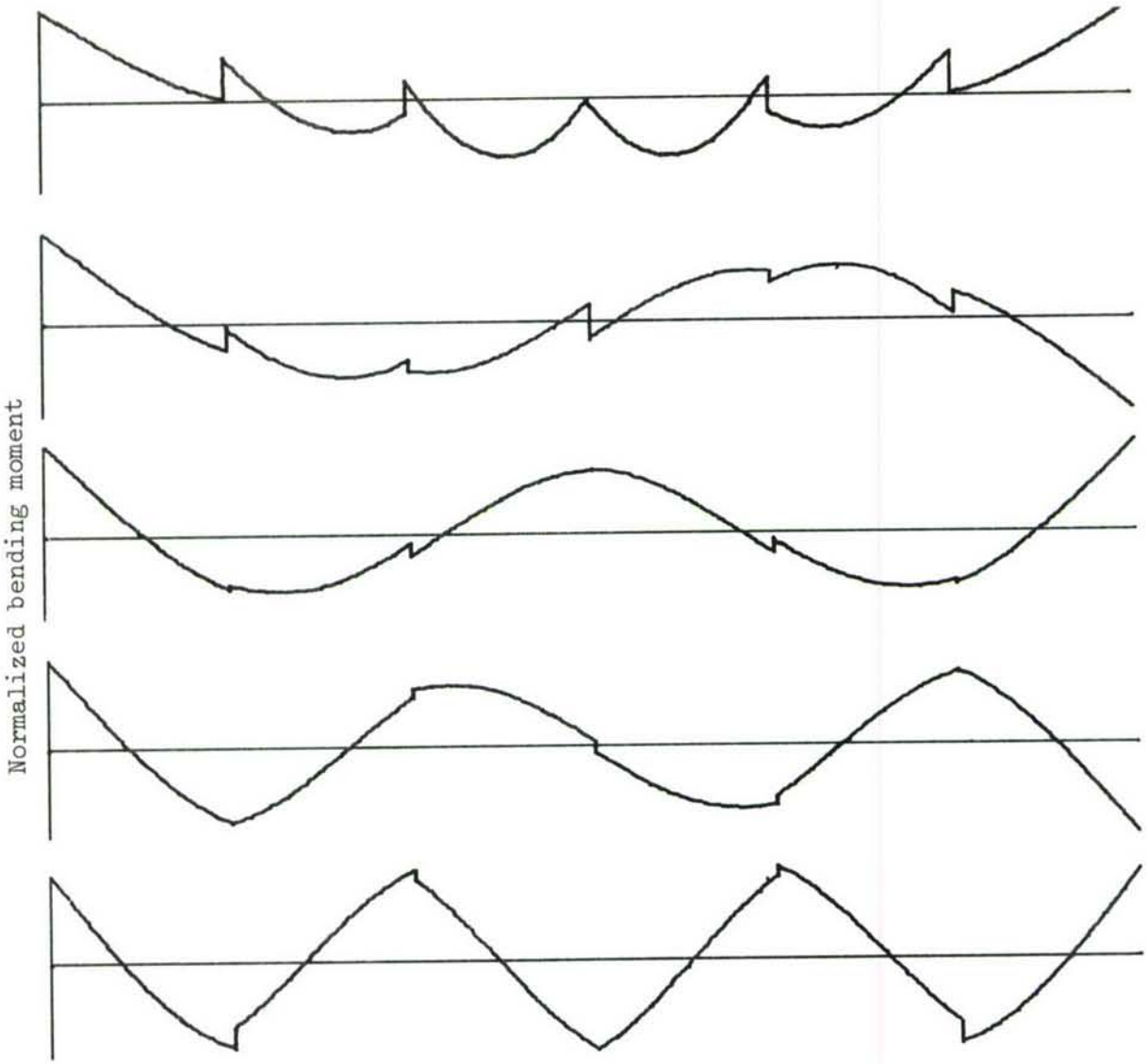

Fig. 2.9(b) Calculated bending moments for an integrally stiffened panel with edges parallel to stringers clamped

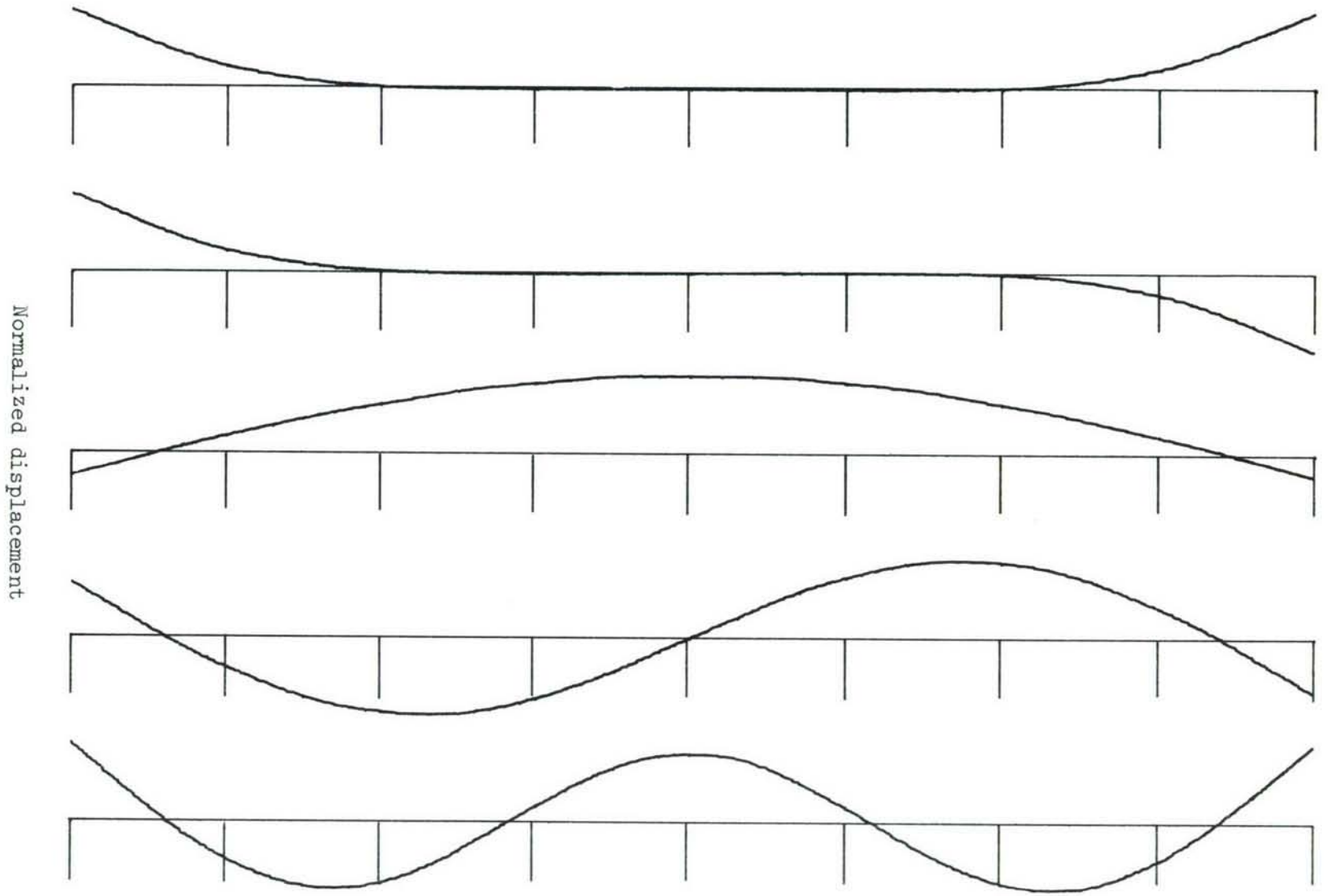

Fig. 2.10(a) Calculated mode shapes for an integrally stiffened panel with edges parallel to stringers free

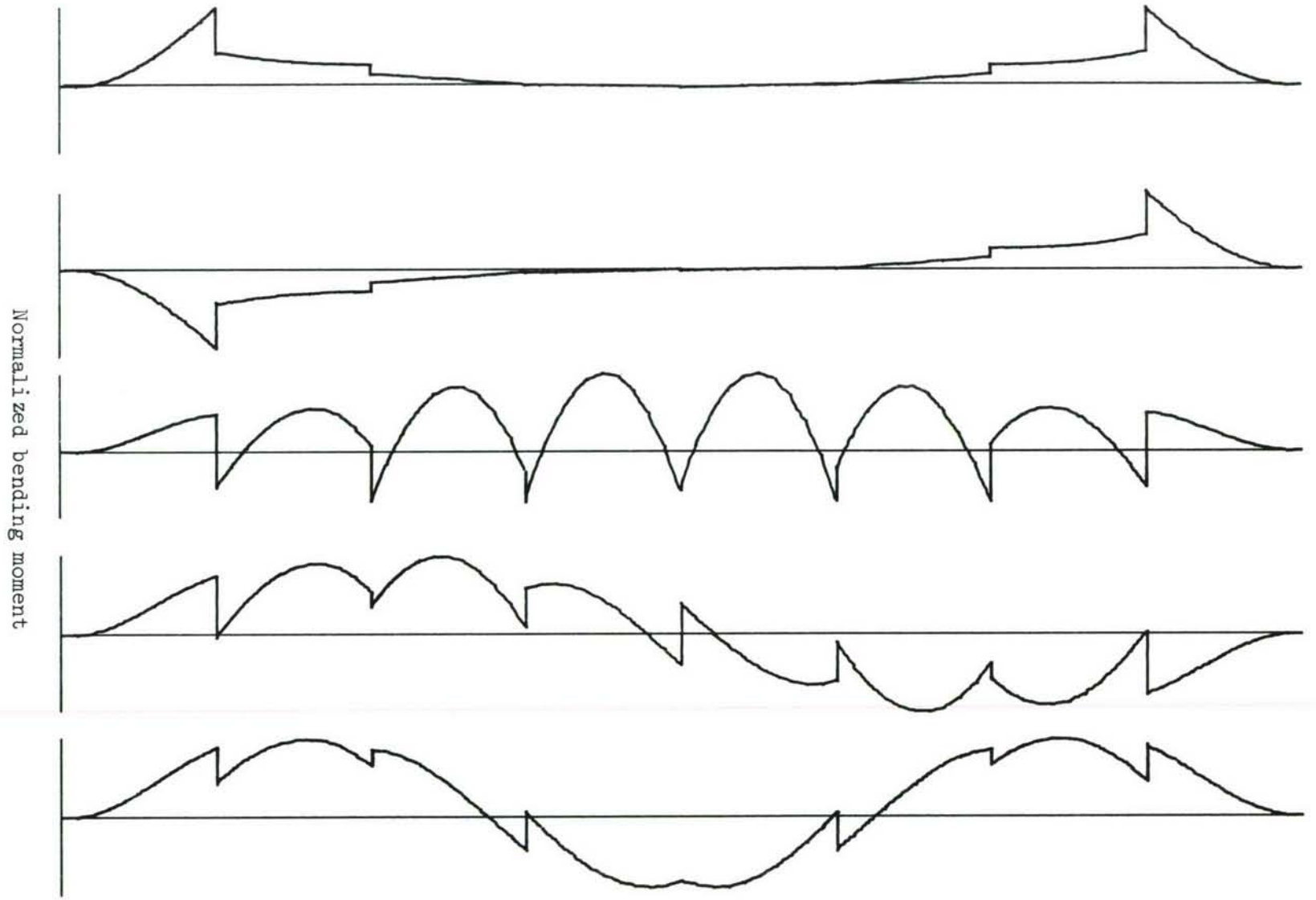

Fig. 2.10(b) Calculated bending moments for an integrally stiffened panel with edges parallel to stringers free

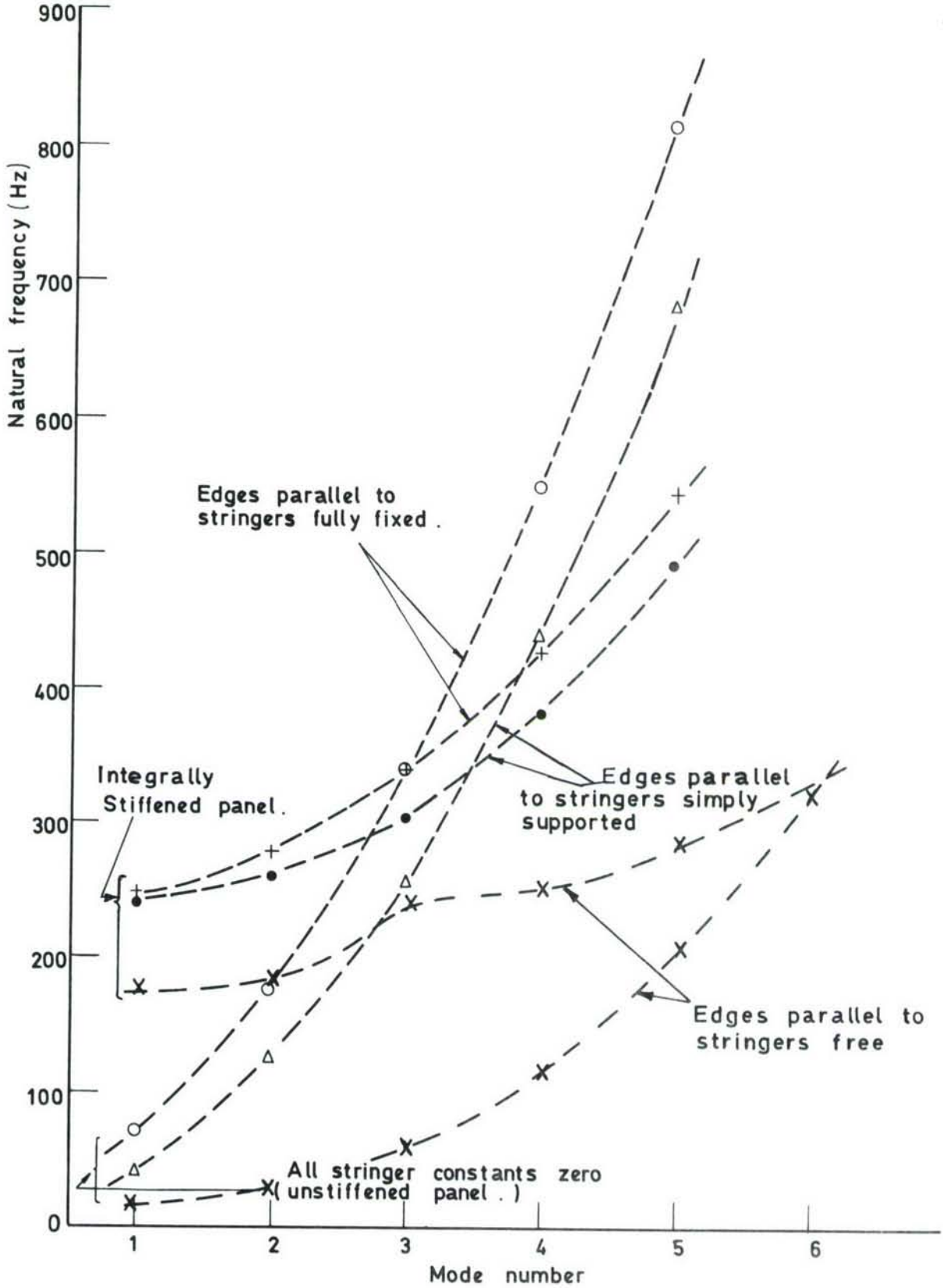

Fig.2·11 Variation in calculated panel natural frequency with mode number for various configurations.

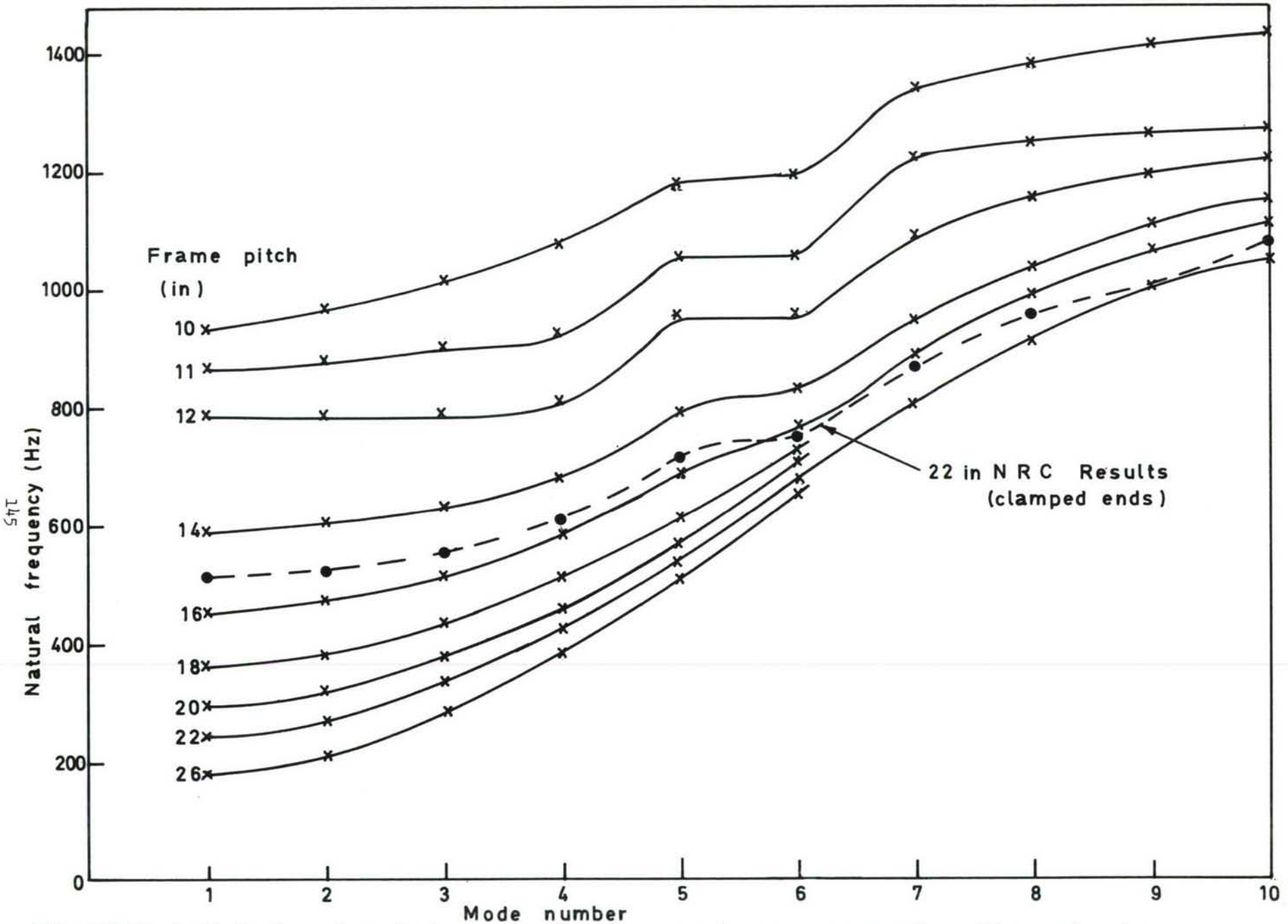

Fig 2·12 Calculated natural frequencies for a six span panel with simply supported ends and fixed edges

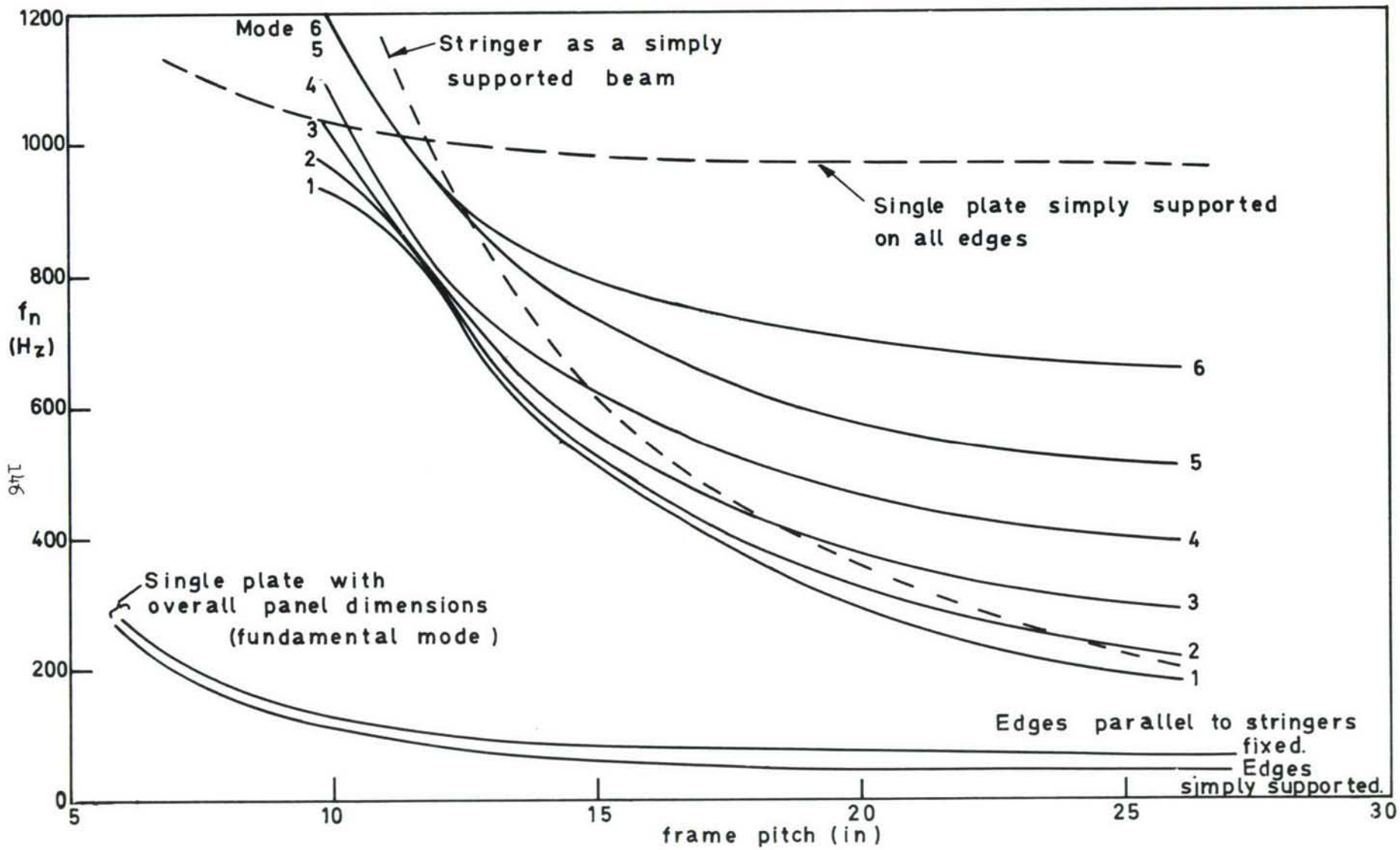

Fig 2.13 Variation of natural frequency with frame pitch for a six span panel with simply supported ends and fixed edges.

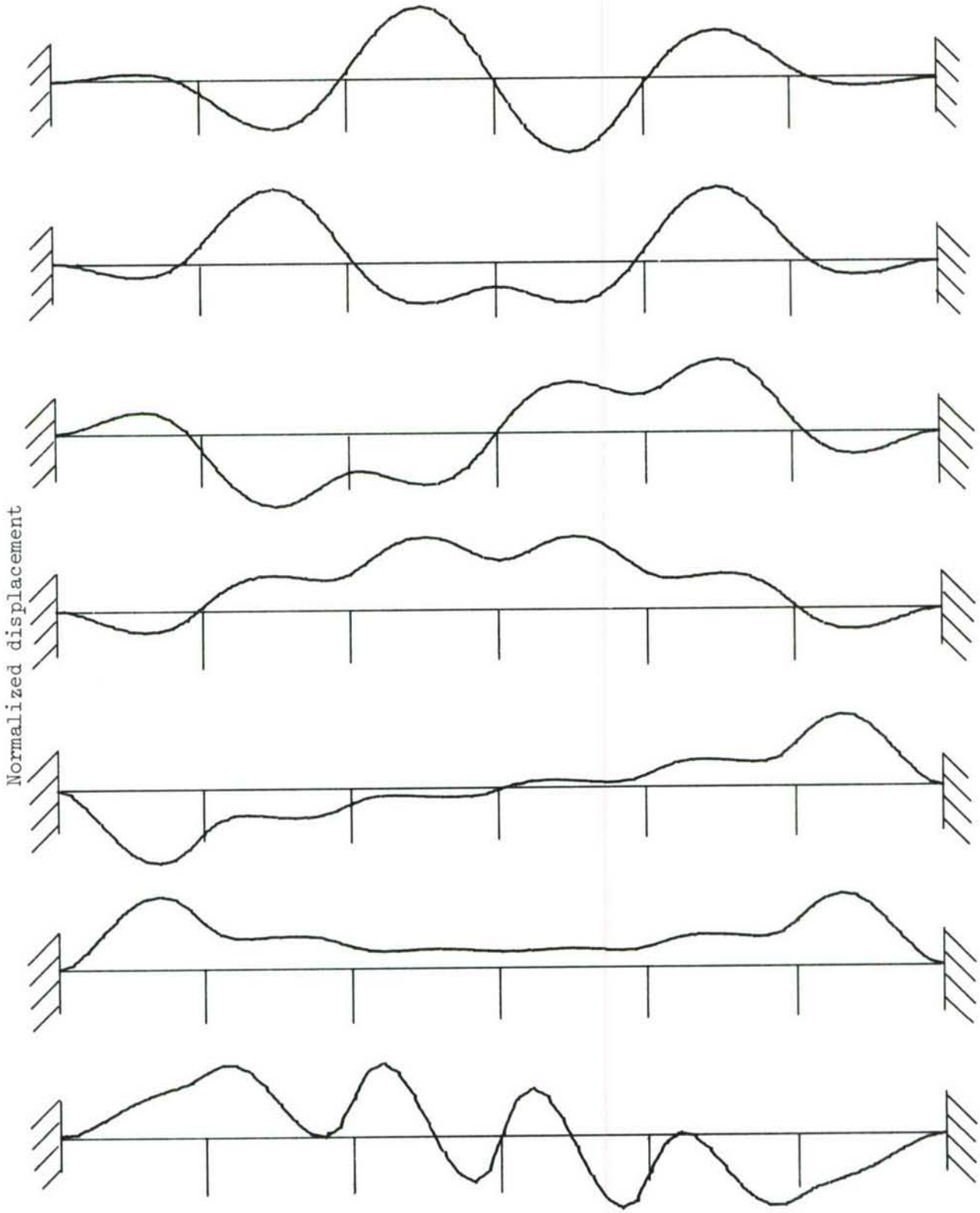

Fig. 2.14 Calculated integrally stiffened panel mode shapes for 6 spans and fixed edges. Frame pitch = 10.0 inches.

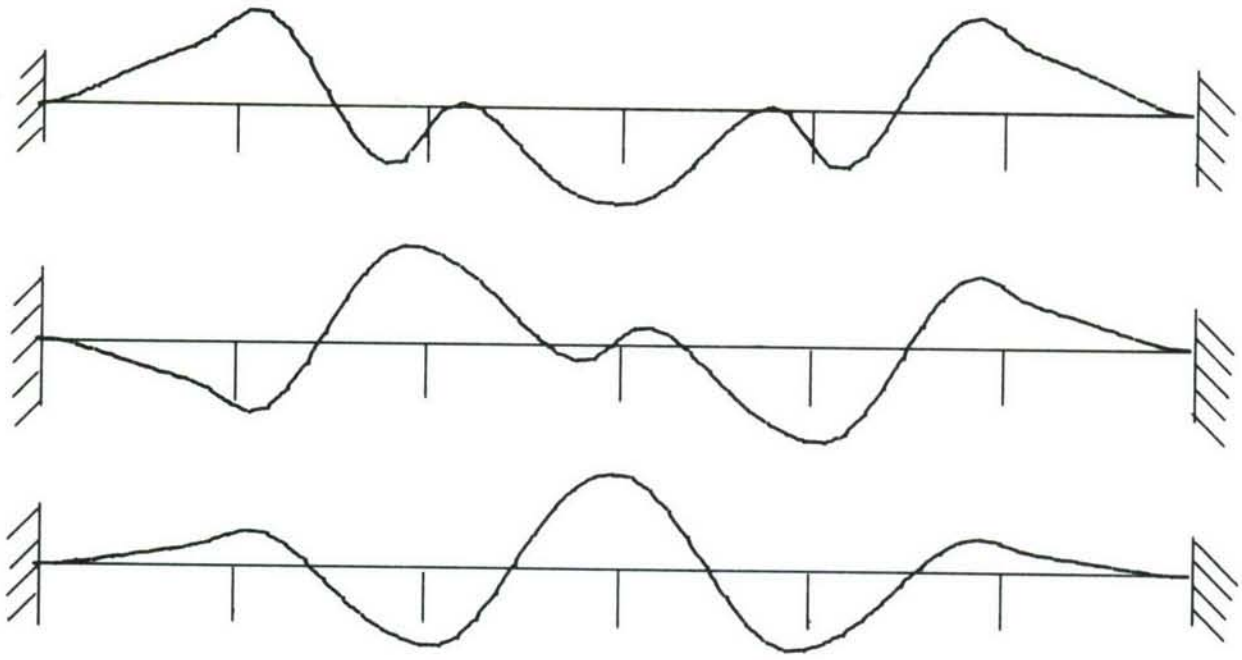

Fig. 2.14 concluded

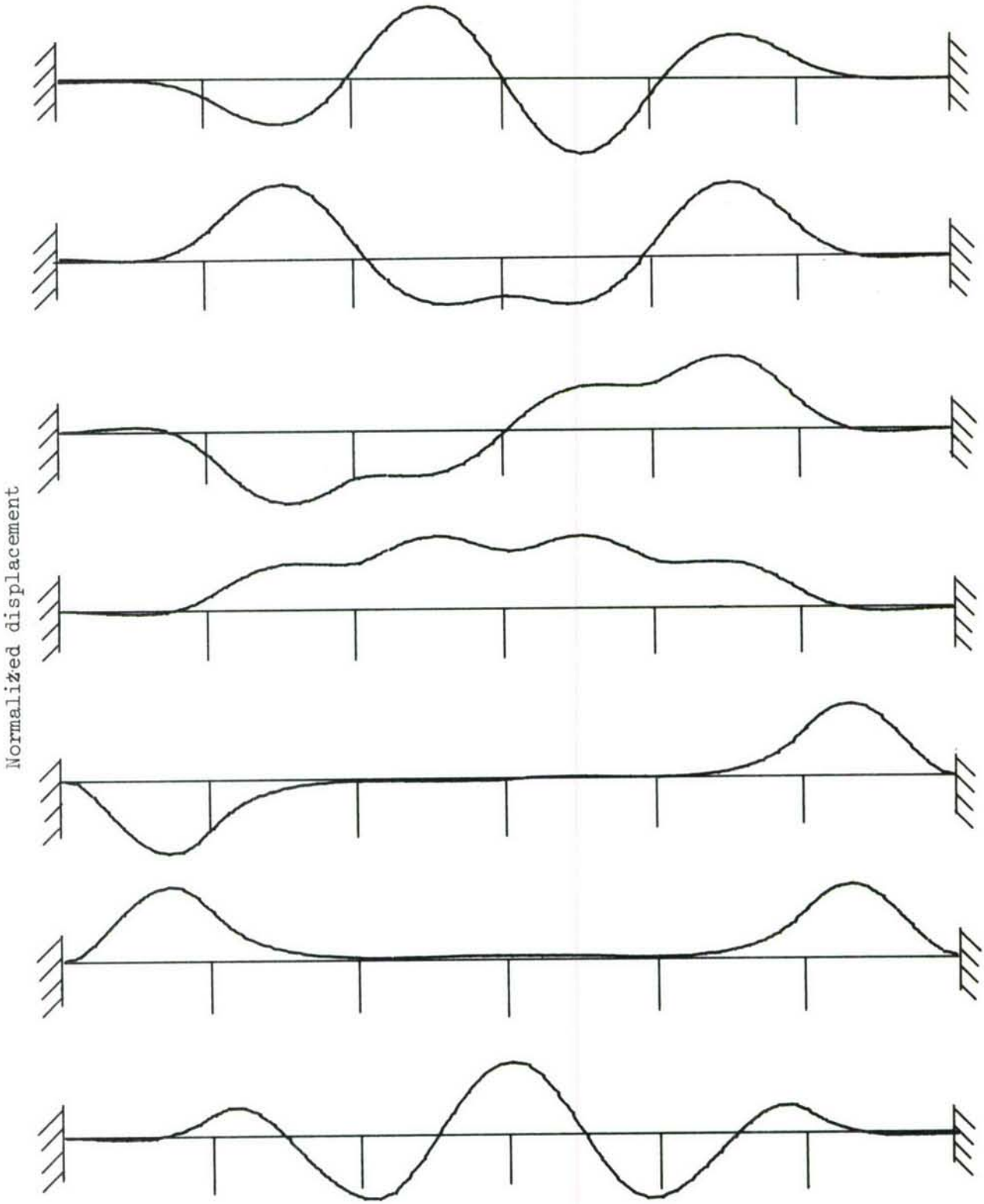

Fig. 2.15 Calculated integrally stiffened panel mode shapes for 6 spans and fixed edges. Frame pitch = 11.0 inches

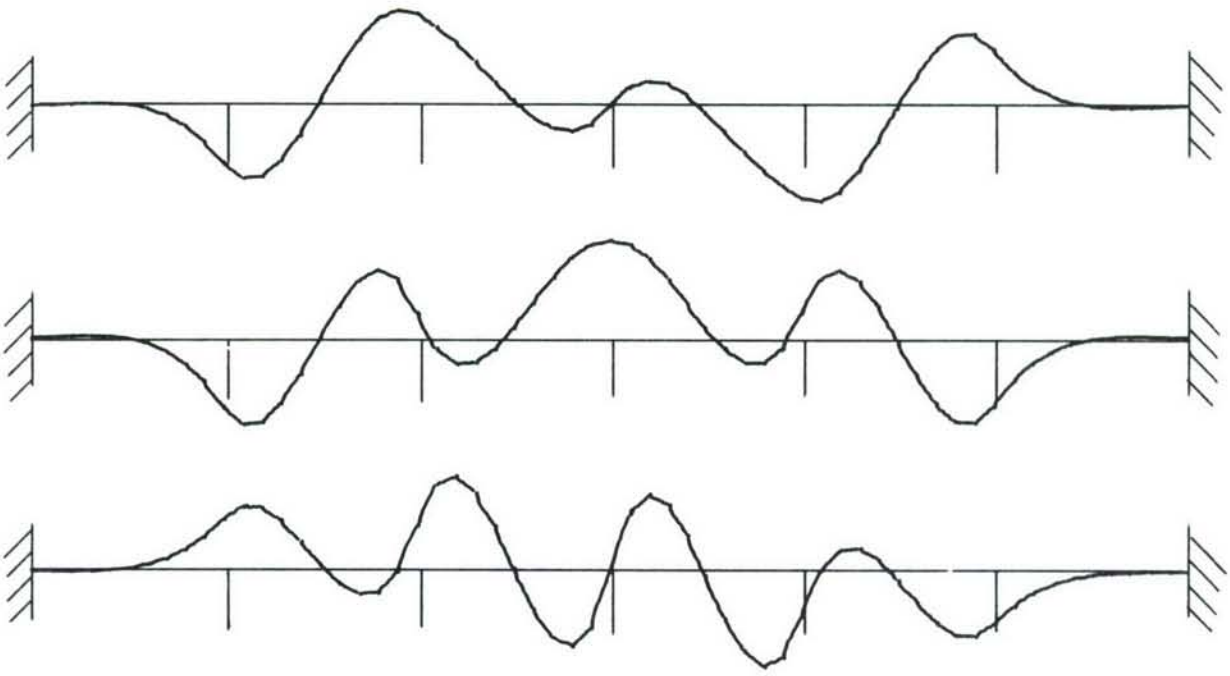

Fig. 2.15 concluded

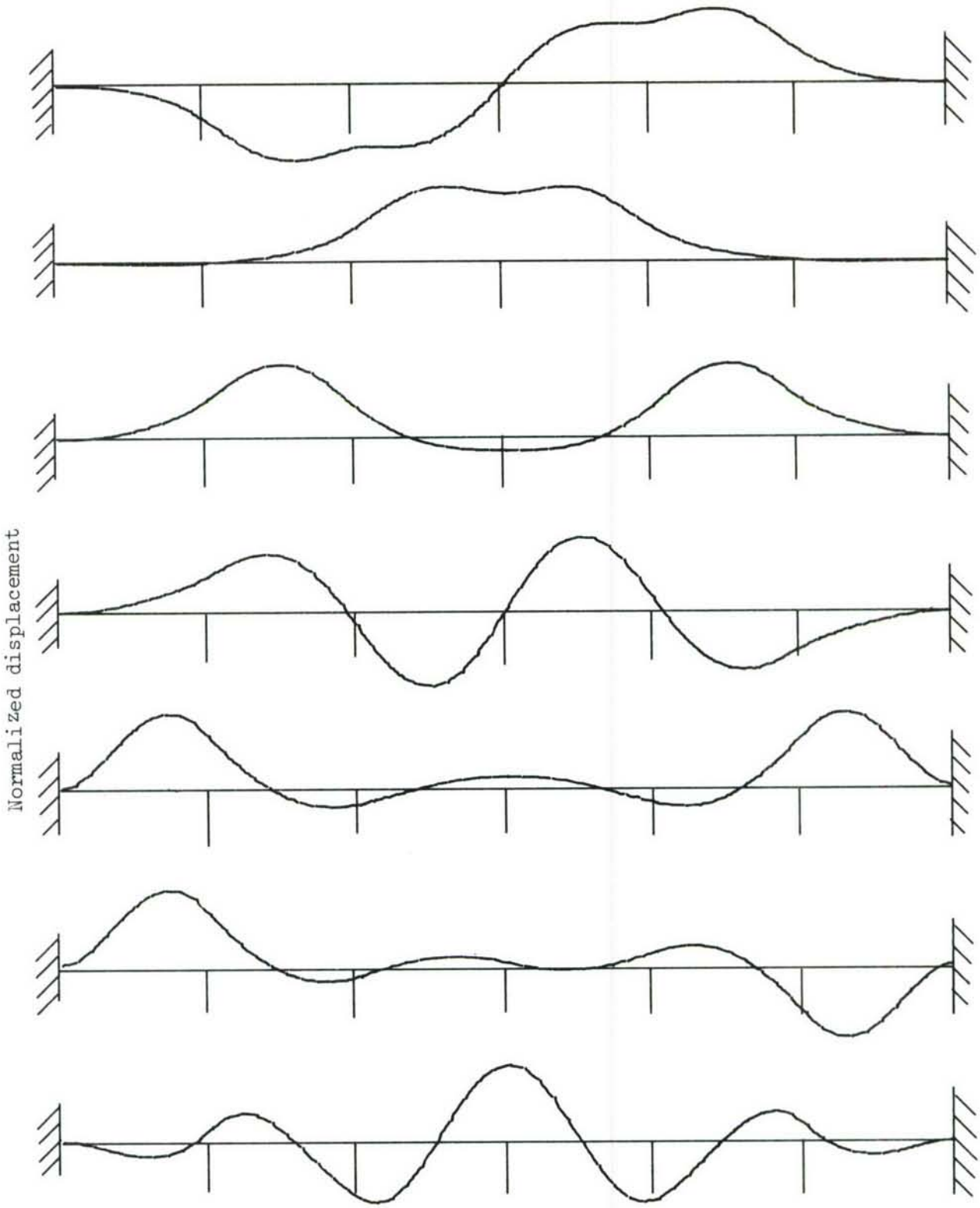

Fig. 2.16 Calculated integrally stiffened panel mode shapes for 6 spans and fixed edges. Frame pitch = 12.0 inches

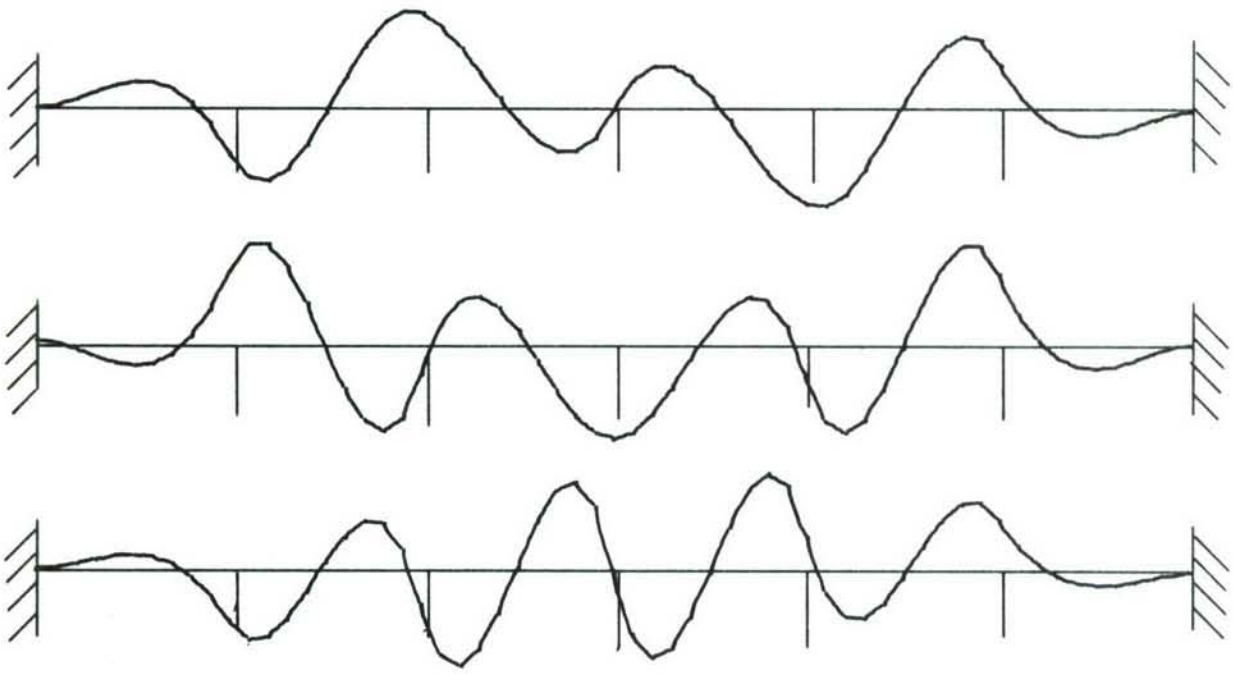

Fig. 2.16 concluded

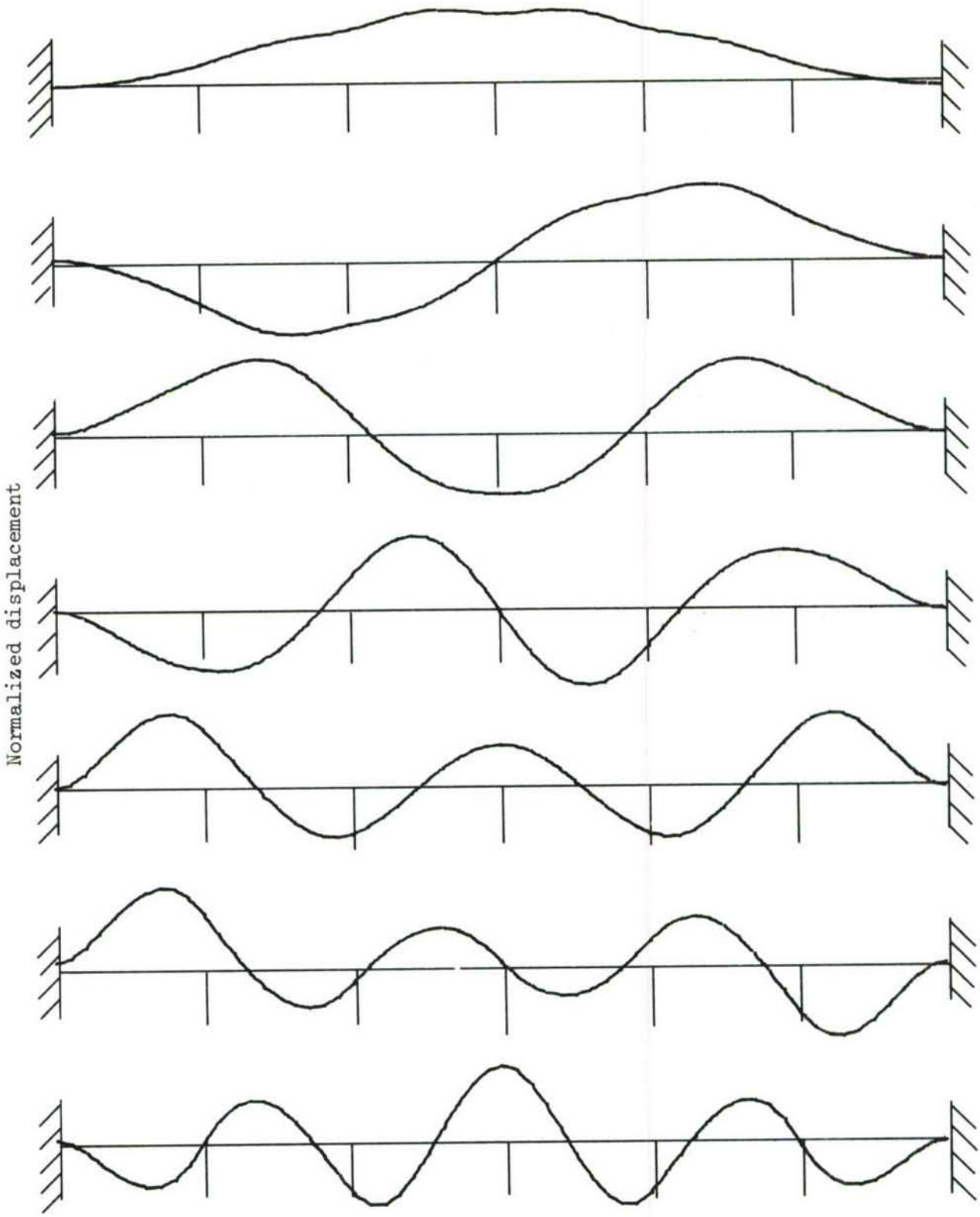

Fig. 2.17 Calculated integrally stiffened panel mode shapes for 6 spans and fixed edges. Frame pitch = 14.0 inches

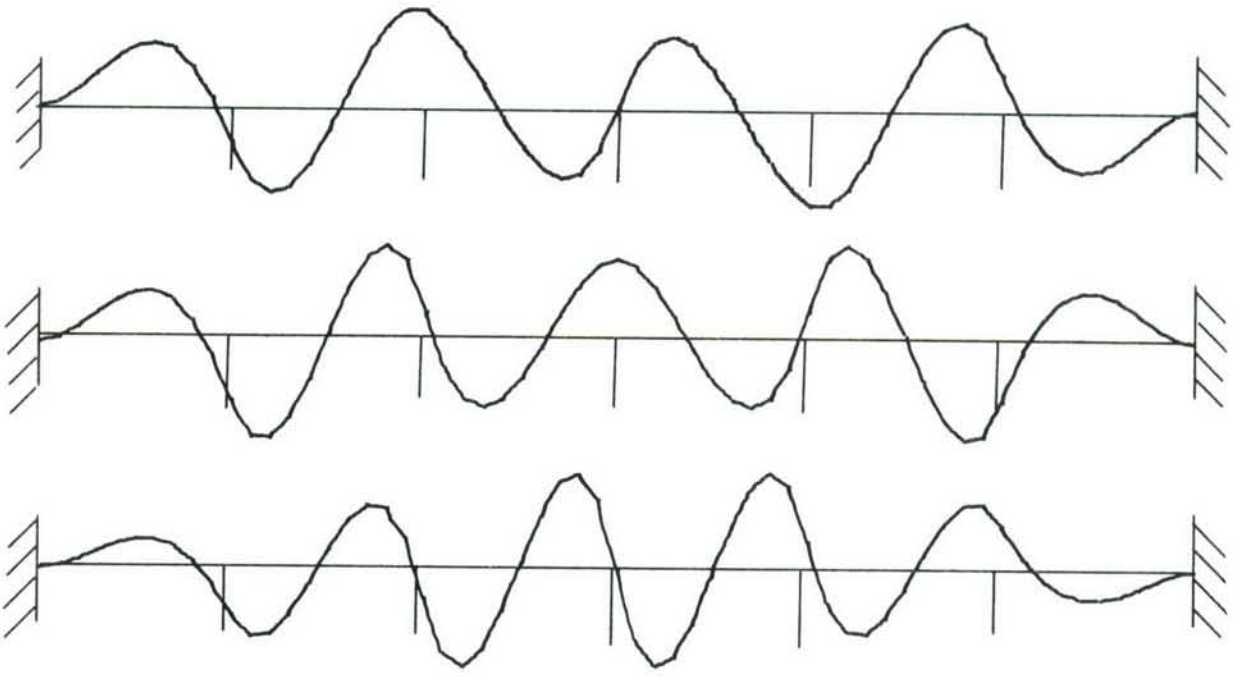

Fig. 2.17 concluded

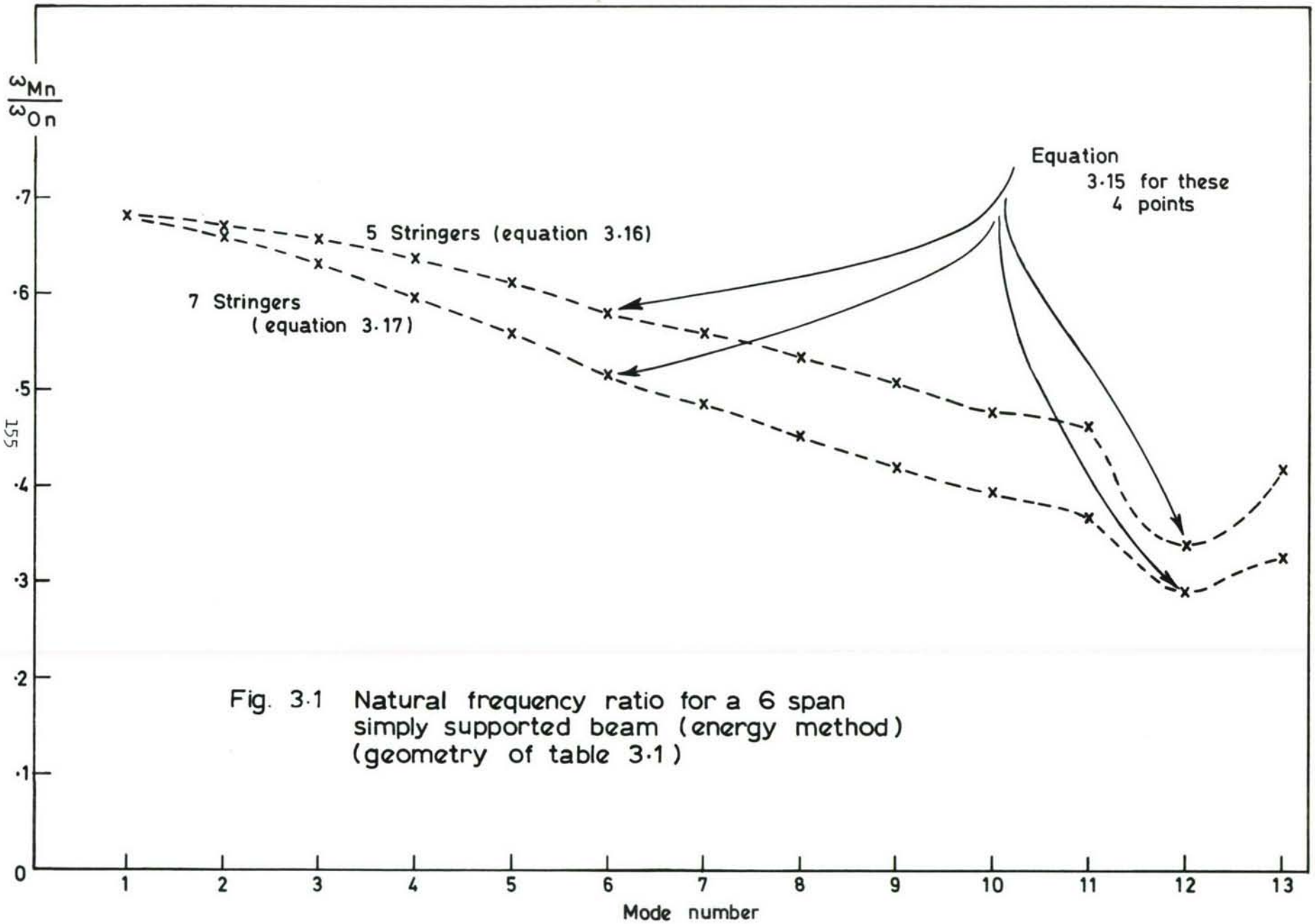

Fig. 3·1 Natural frequency ratio for a 6 span simply supported beam (energy method) (geometry of table 3·1)

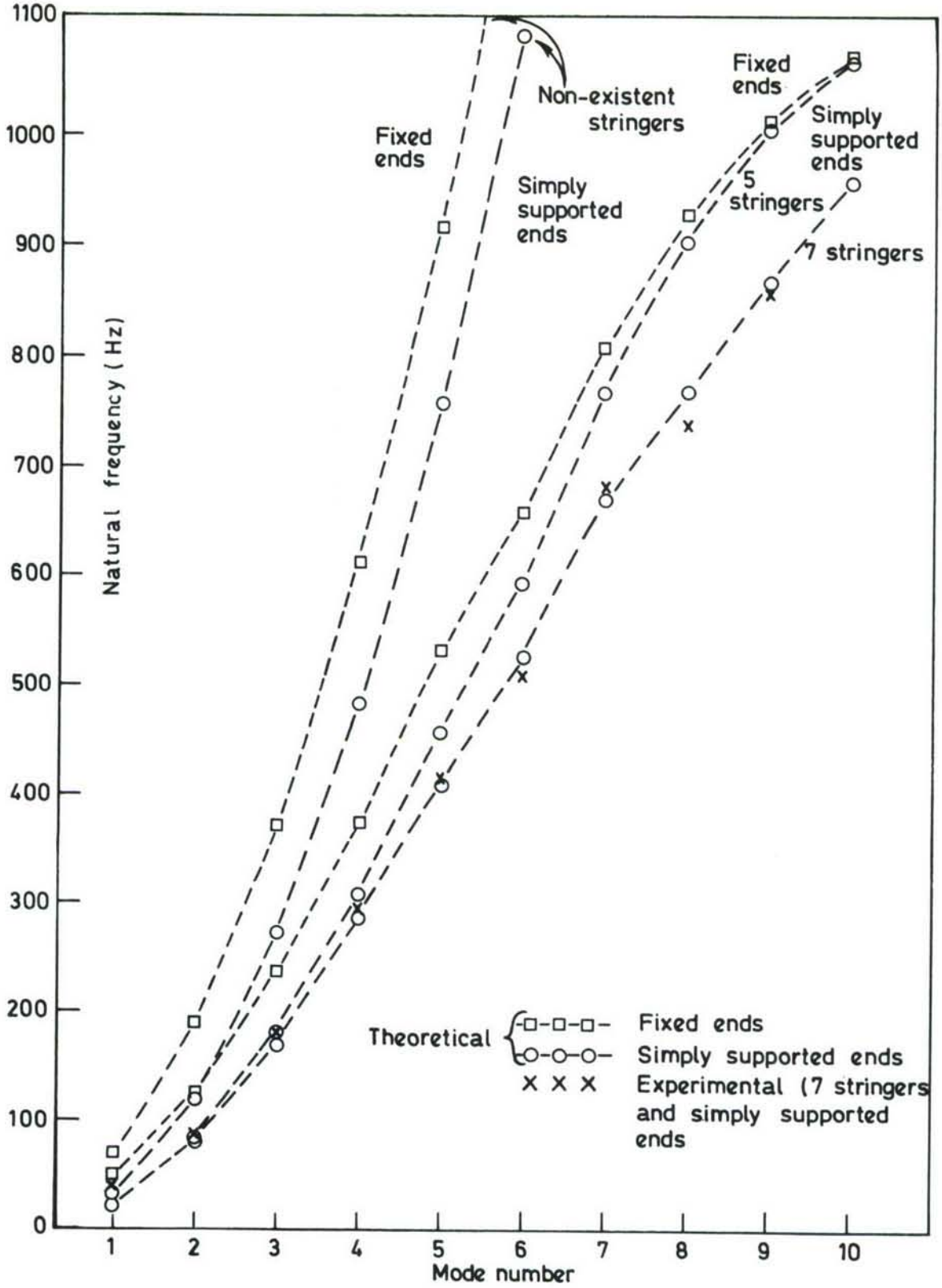

Fig. 3.2 Natural frequencies for a 6 span beam (Transfer Matrix method) (Geometry of table 3.1)

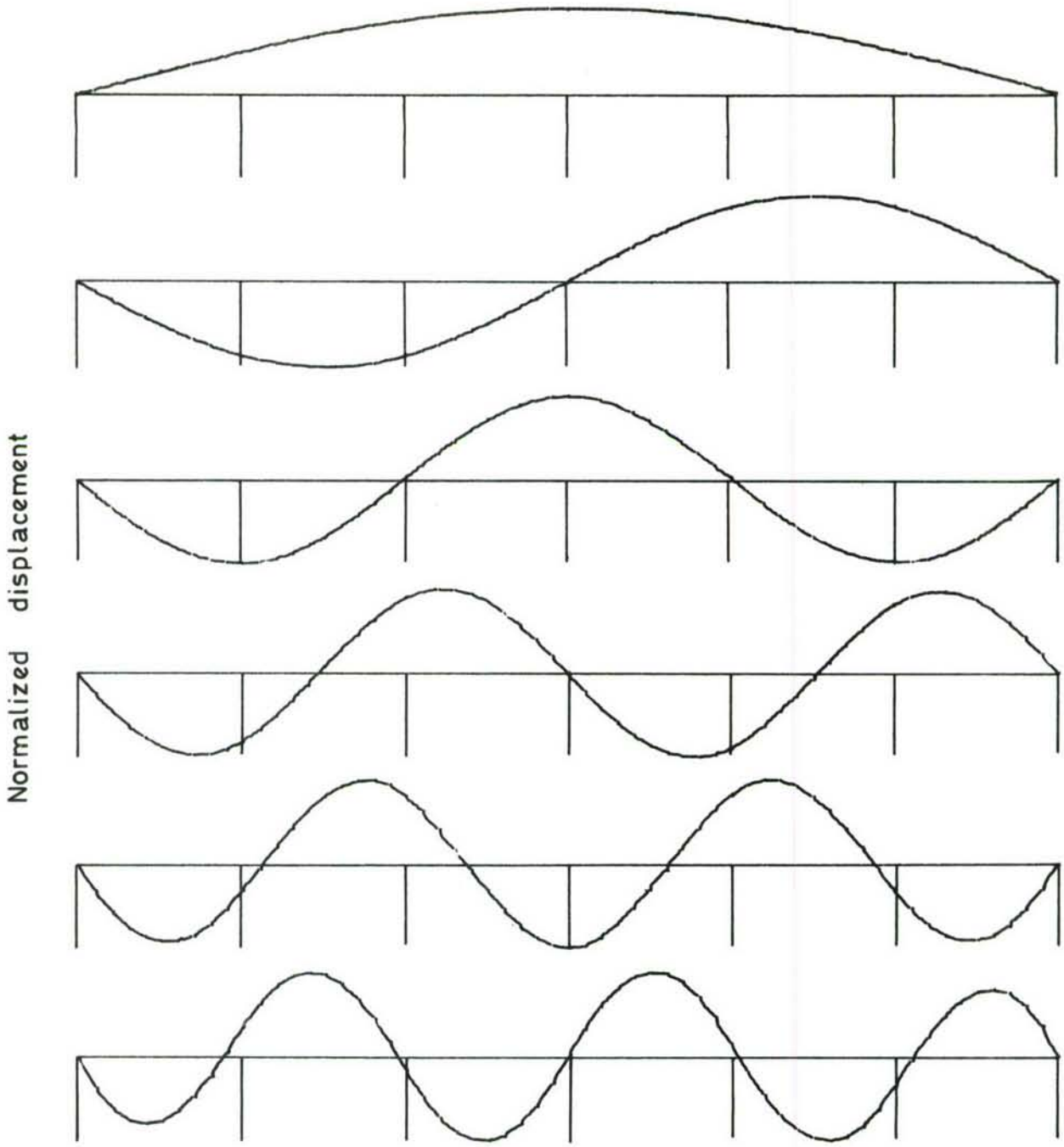

Fig. 3.3(a) Calculated mode shapes for a 6 span simply supported beam with 7 stringers

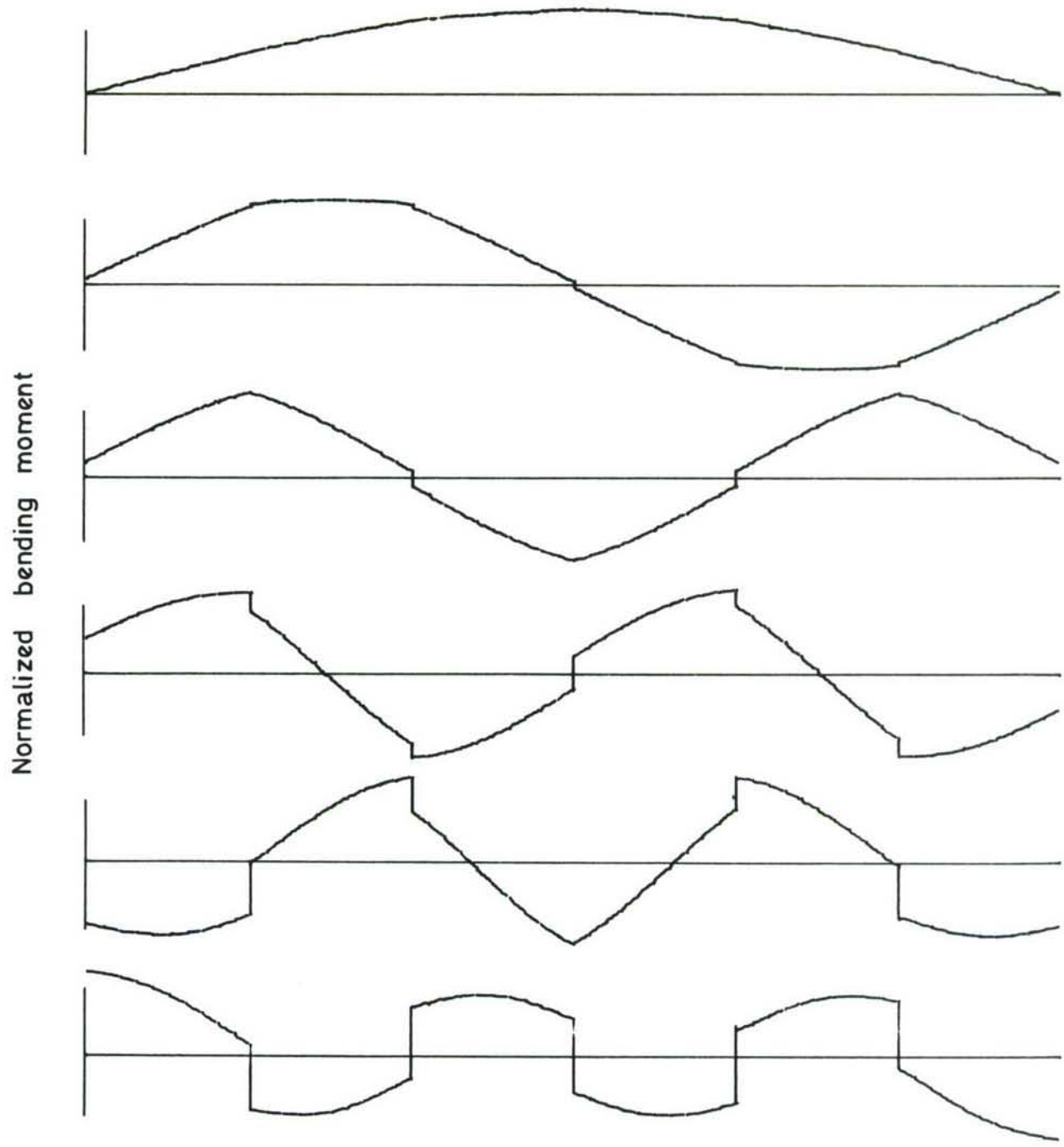

Fig. 3.3(b) Calculated bending moments for a 6 span simply supported beam with 7 stringers

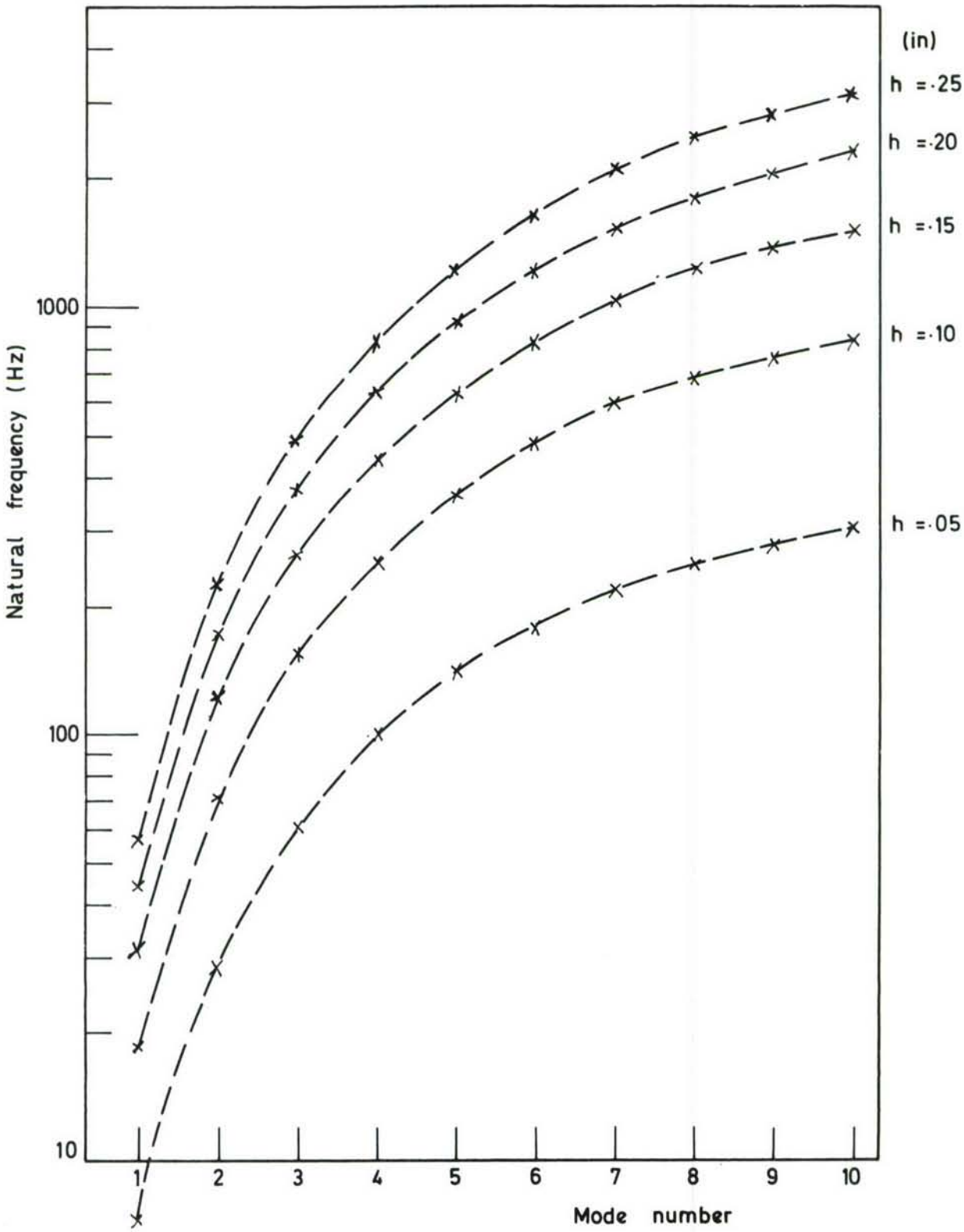

Fig. 3.4 Variation of natural frequencies of a six span simply supported beam with mode number. (7 stringers of constant geometry).

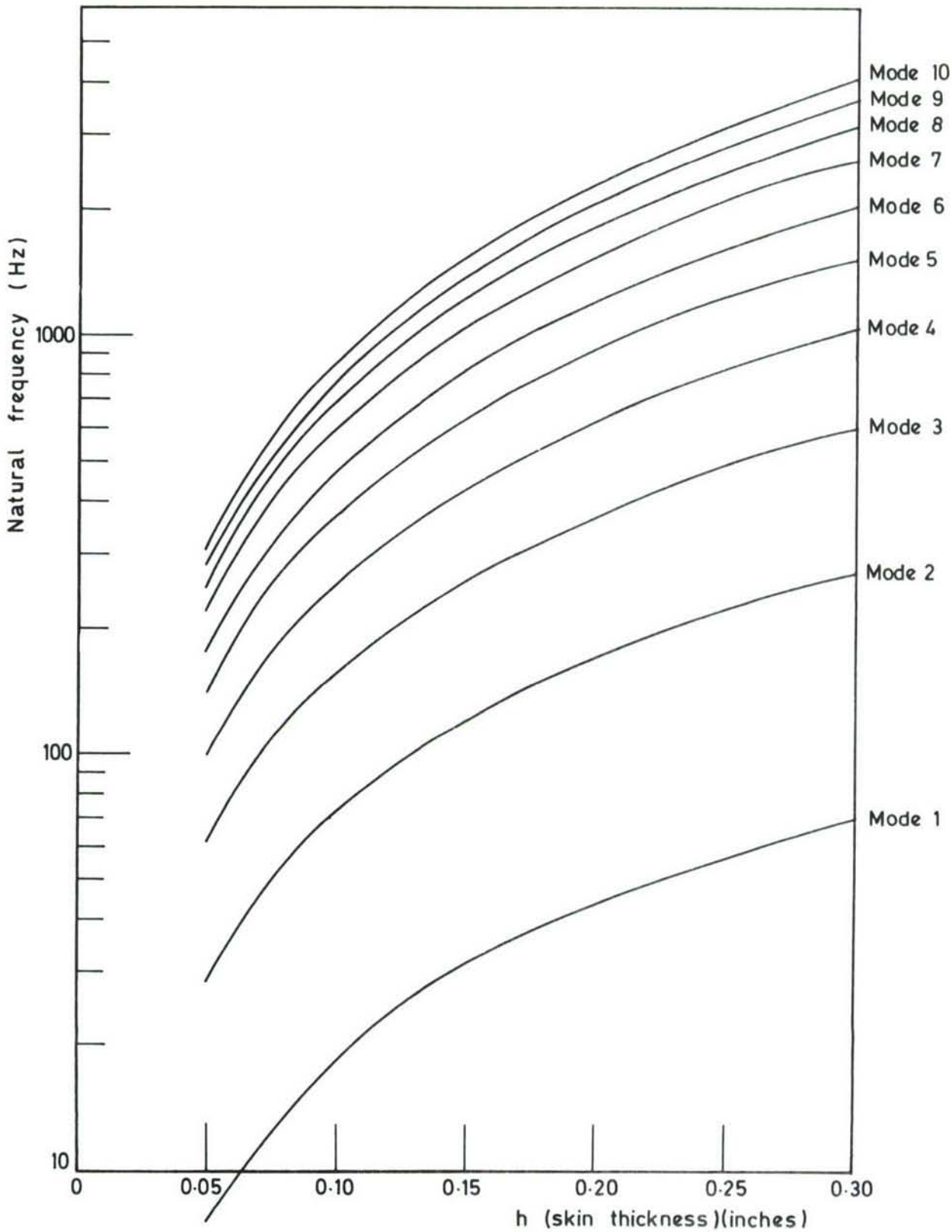

Fig. 3.5 Variation of natural frequencies of a six span simply supported beam with skin thickness (7 stringers of constant geometry).

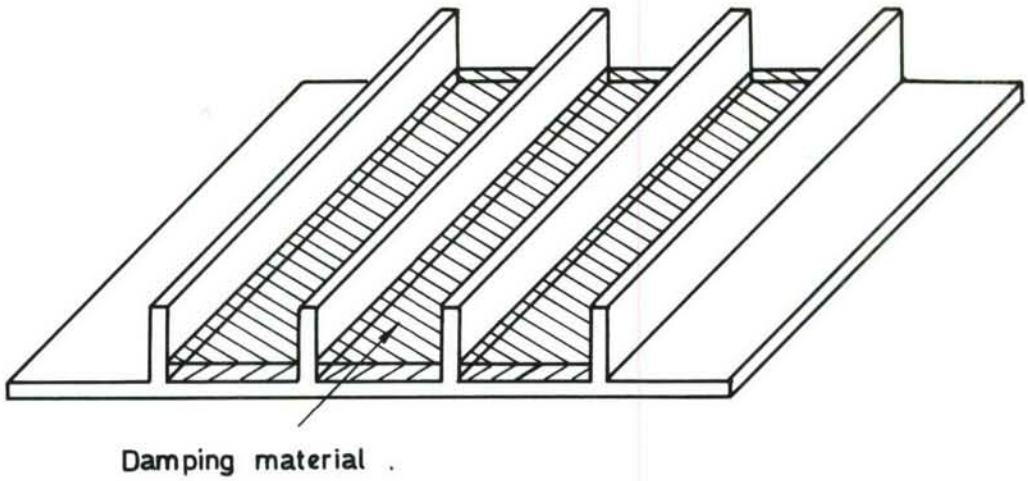

(a) TREATMENT A - Damping material bonded to skin between stringers.

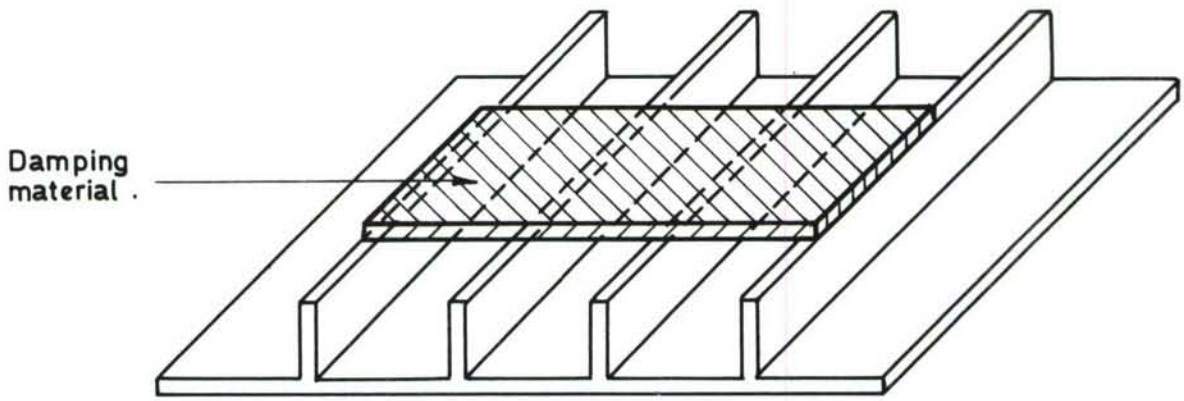

(b) TREATMENT B - Damping material bonded across the tops of the stringers.

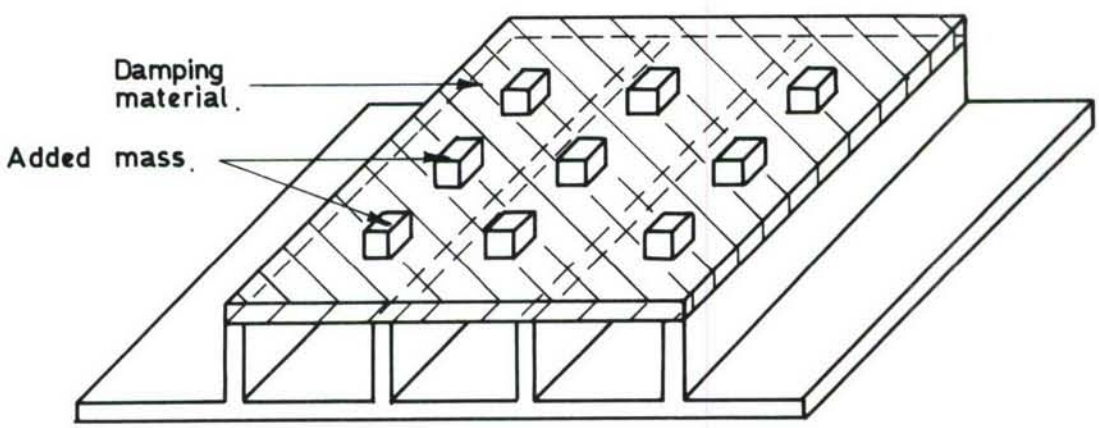

(c) TREATMENT C - Damping material bonded across the tops of the stringers and masses added to the damping material

Fig.4.1 . Damping treatments

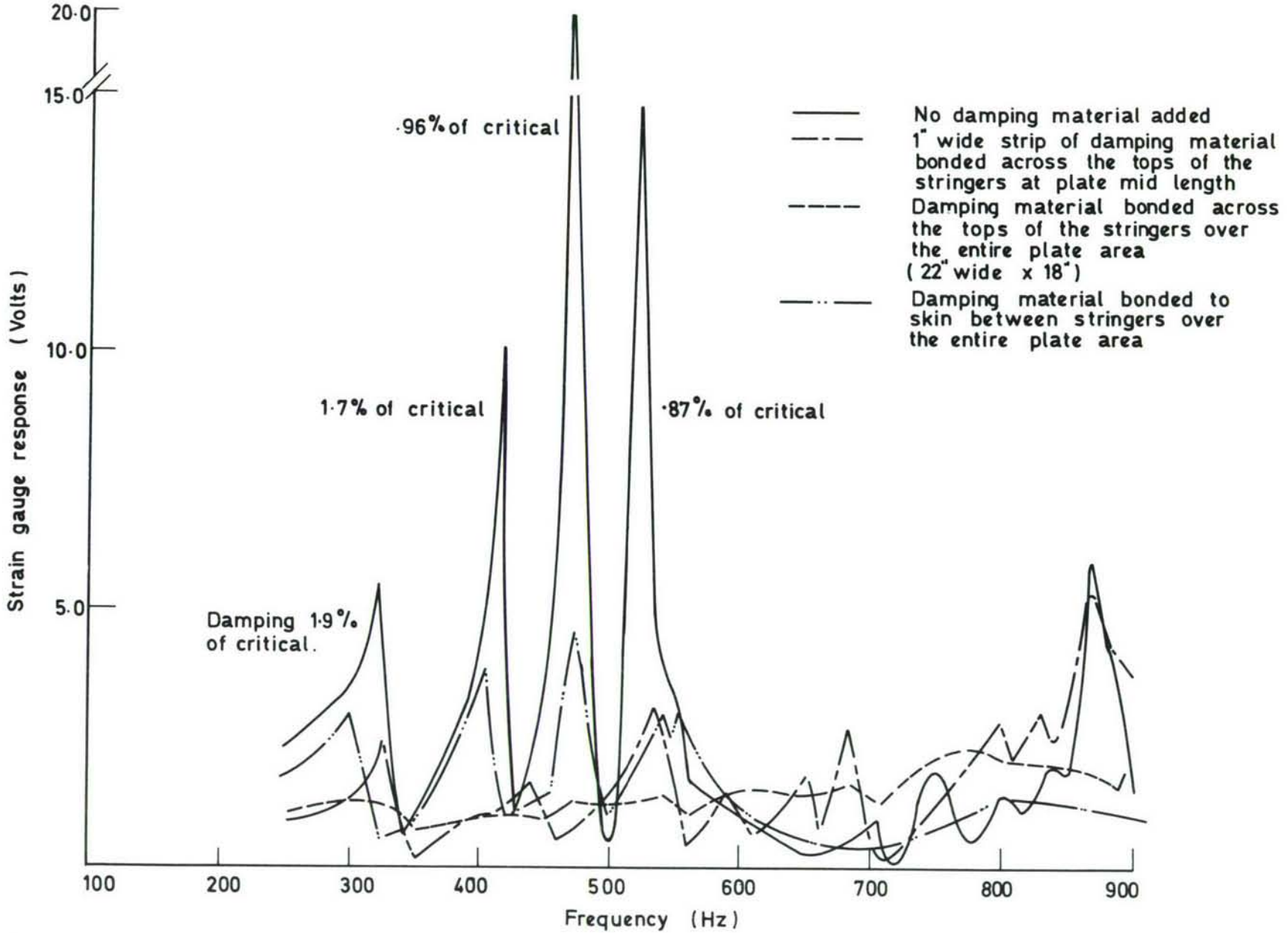

Fig.4.2. Variation in response of the test panel to single point excitation with the addition of damping material. (Ref. 10)

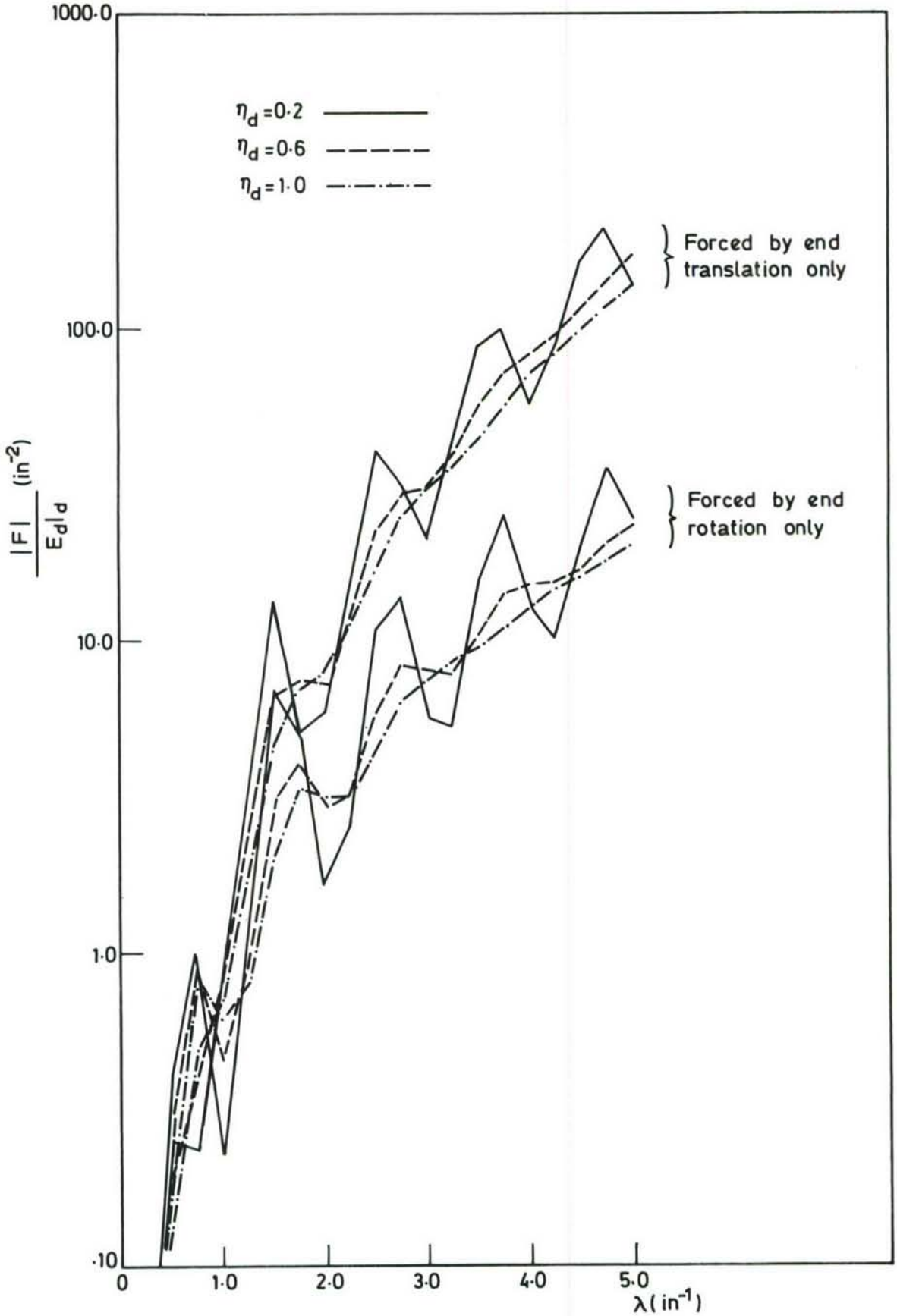

Fig. 4.3 Force at forced end of damped cantilever beam.

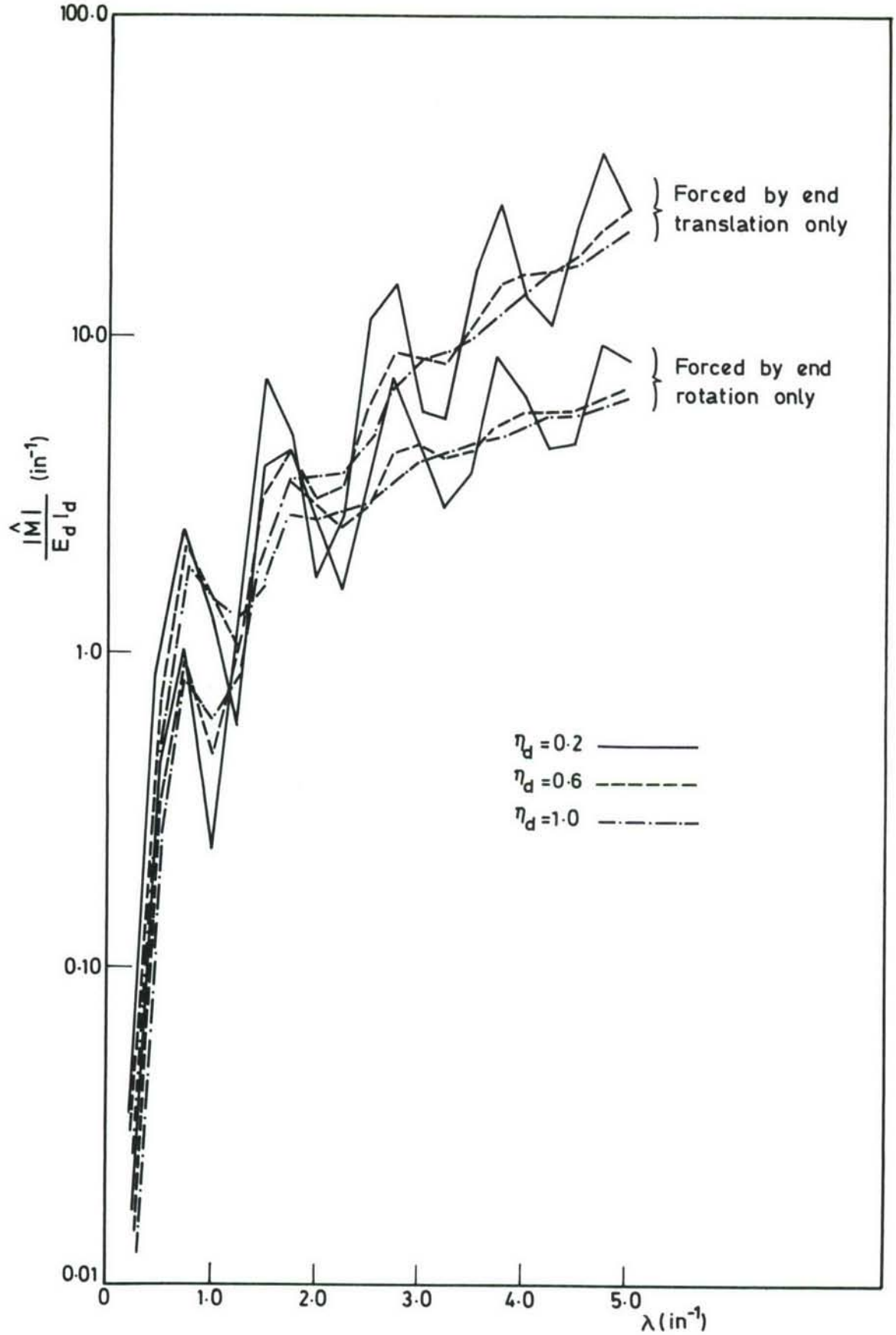

Fig. 4.4 Moment at forced end of damped cantilever beam.

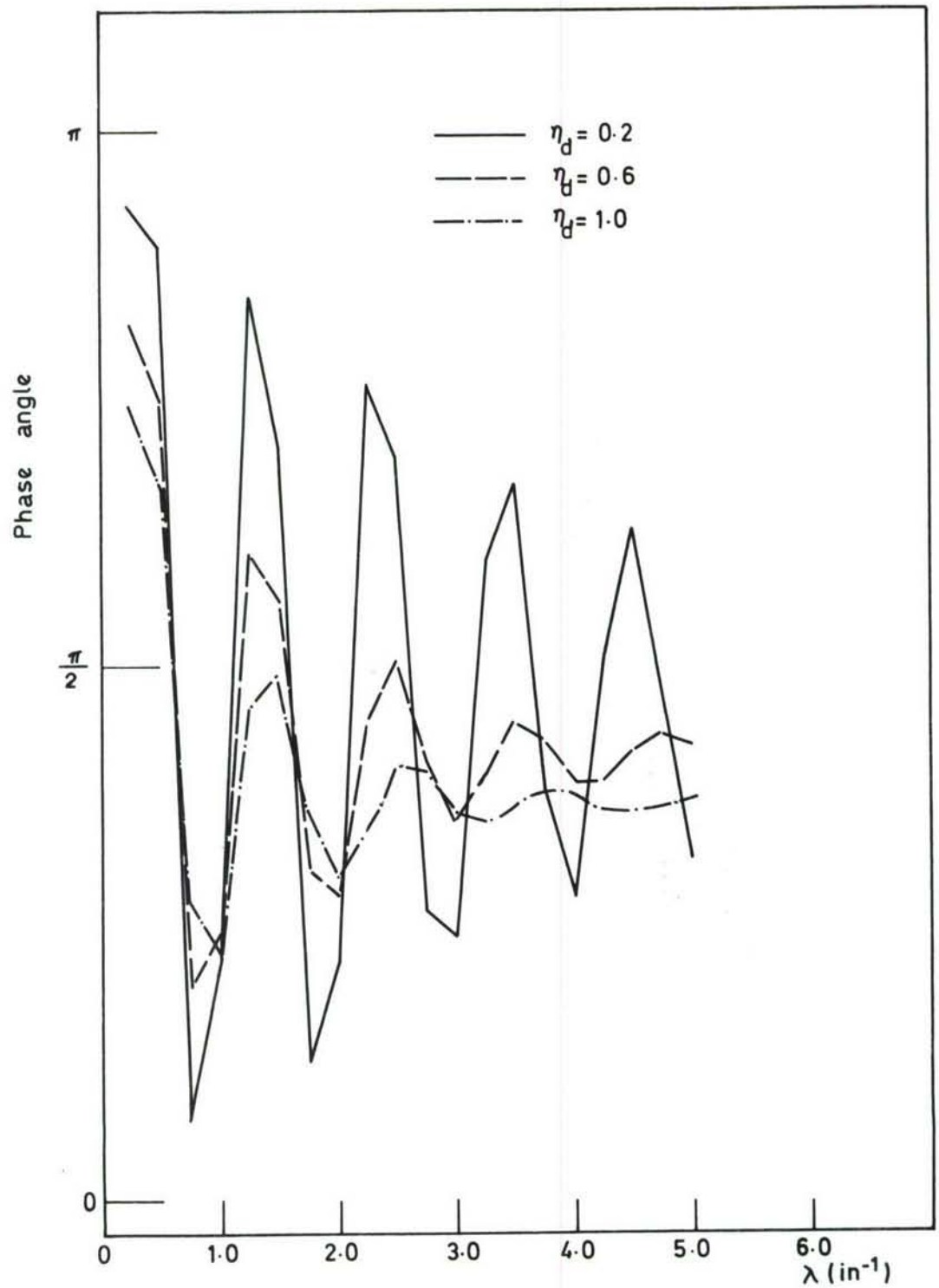

Fig. 4.5 Phase of $\frac{|\hat{M}|}{E_d I_d}$ for a damped cantilever forced by unit amplitude end translation.

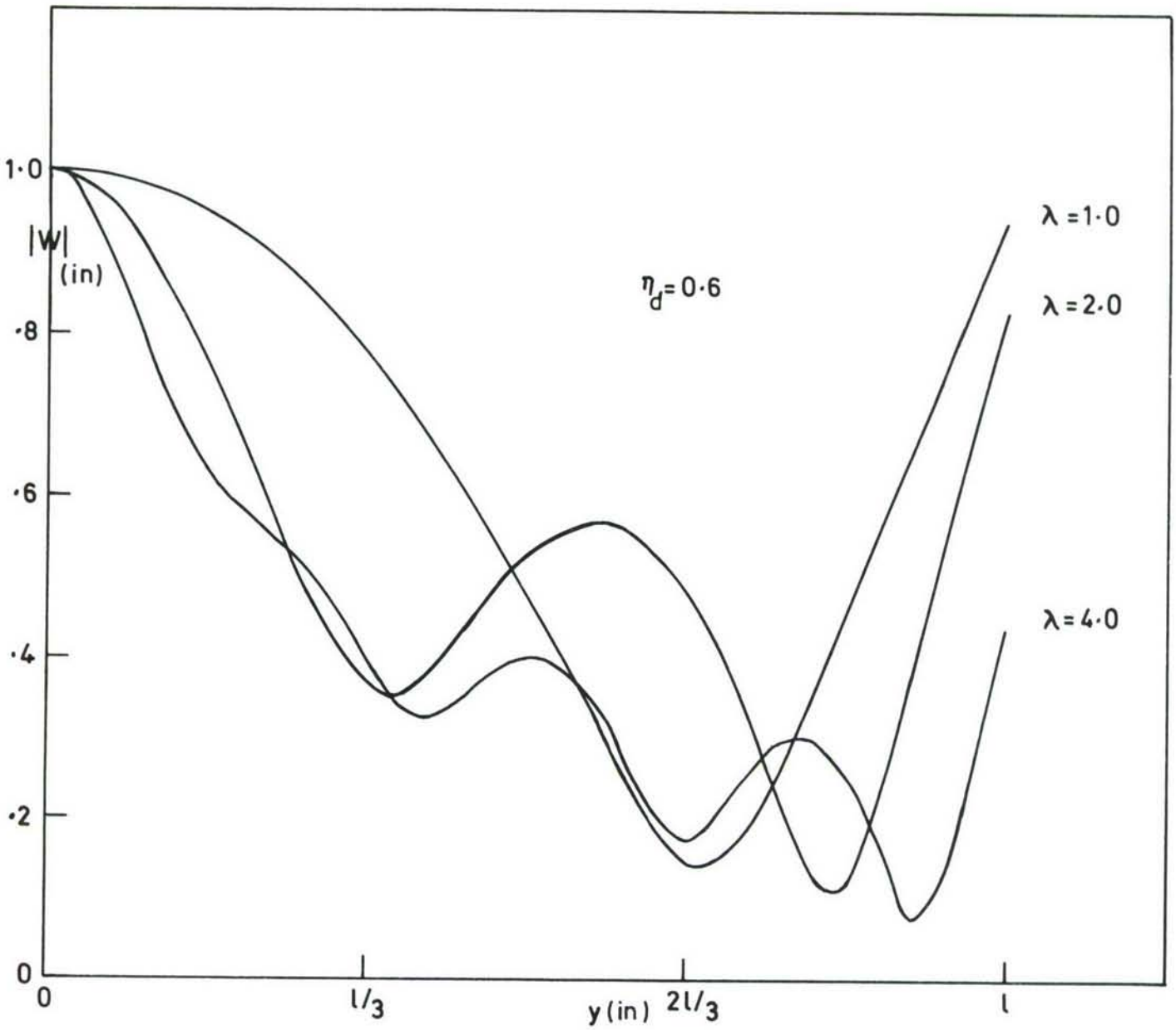

Fig. 4.6 Displaced shape of damped cantilever beam excited by end translation

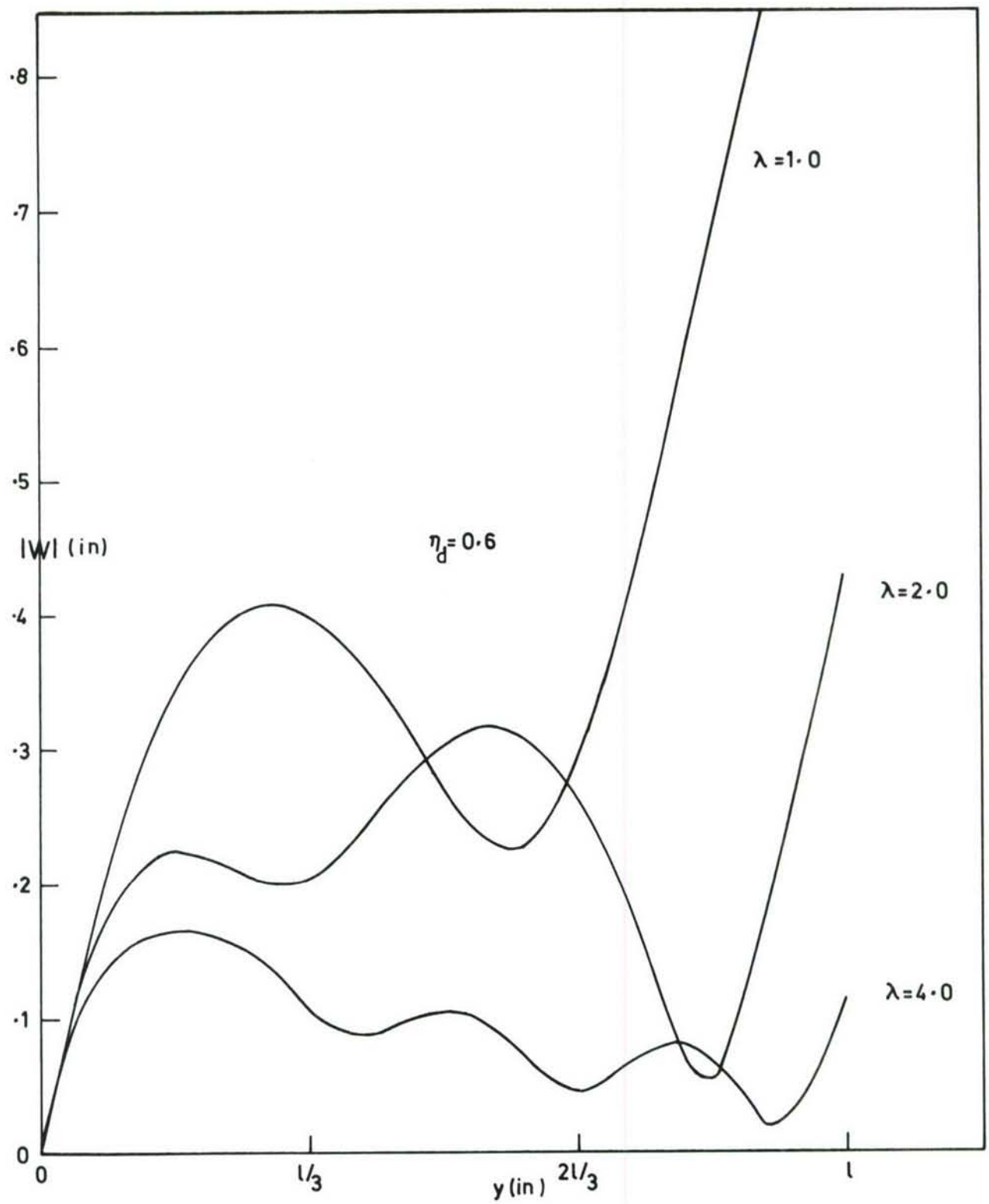

Fig 4.7 Displaced shape of damped cantilever beam excited by unit amplitude end rotation

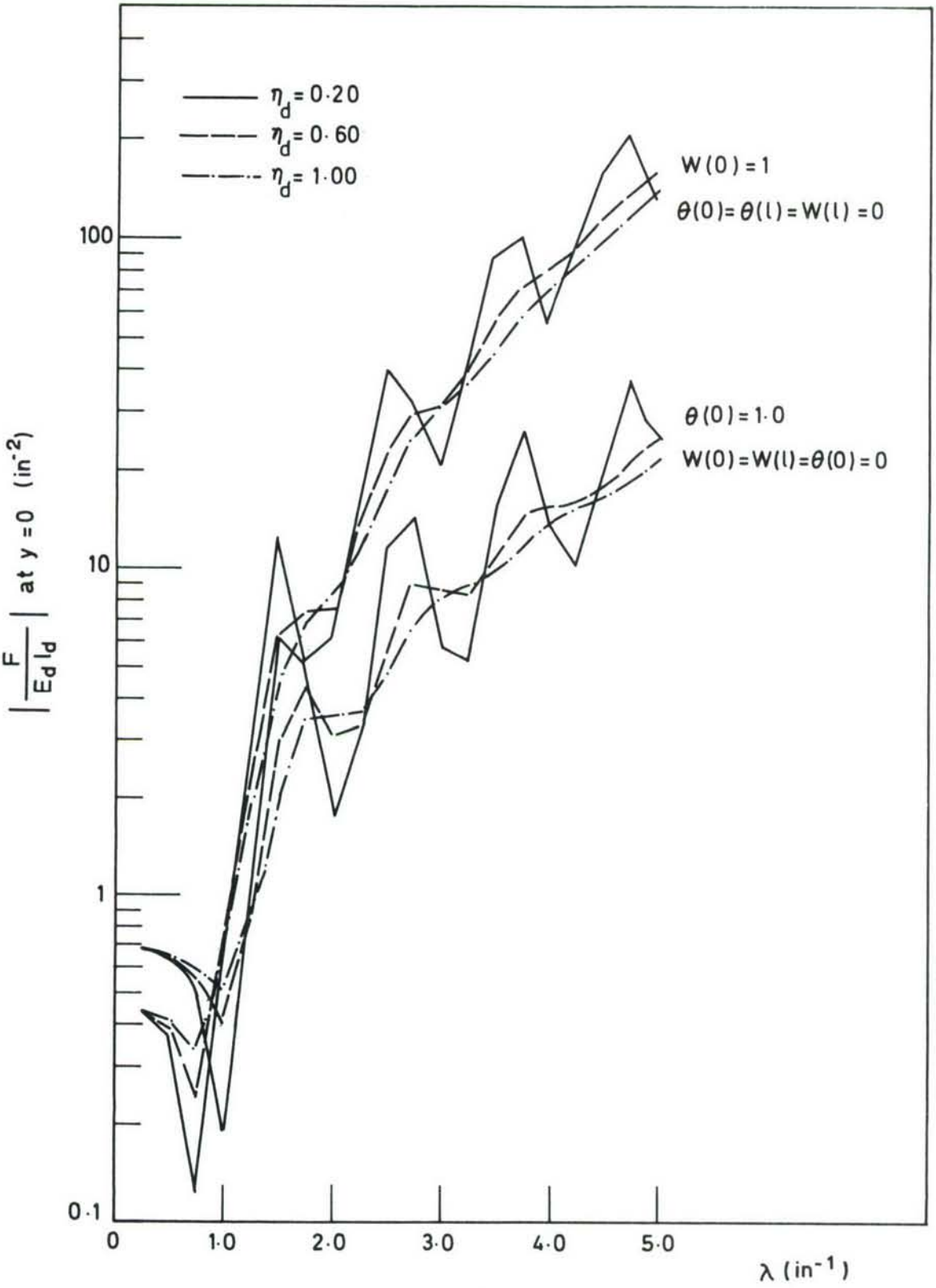

Fig. 4.8 Force at the forced end of a doubly attached damped beam.

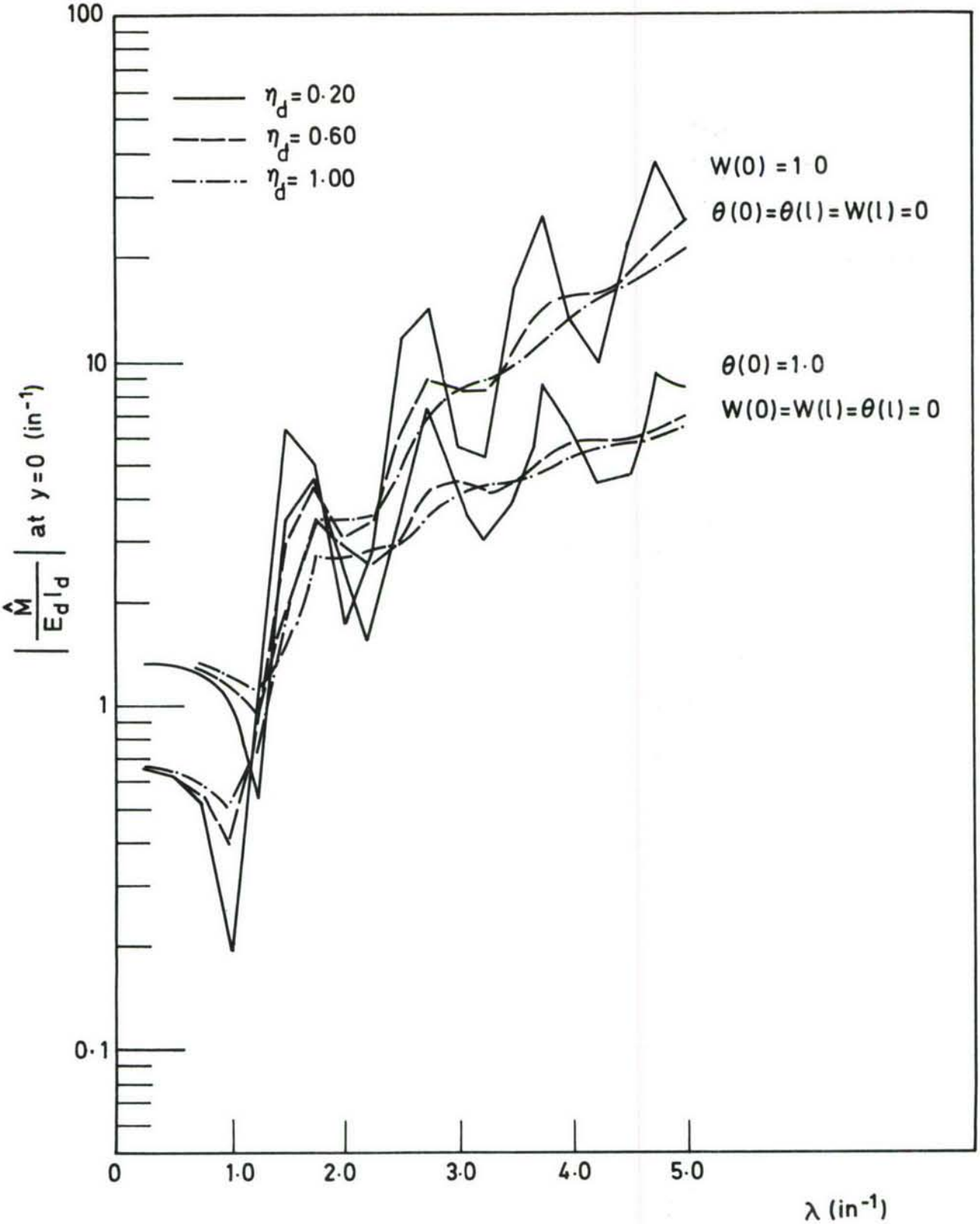

Fig. 4·9 Moment at the forced end of a doubly attached damped beam.

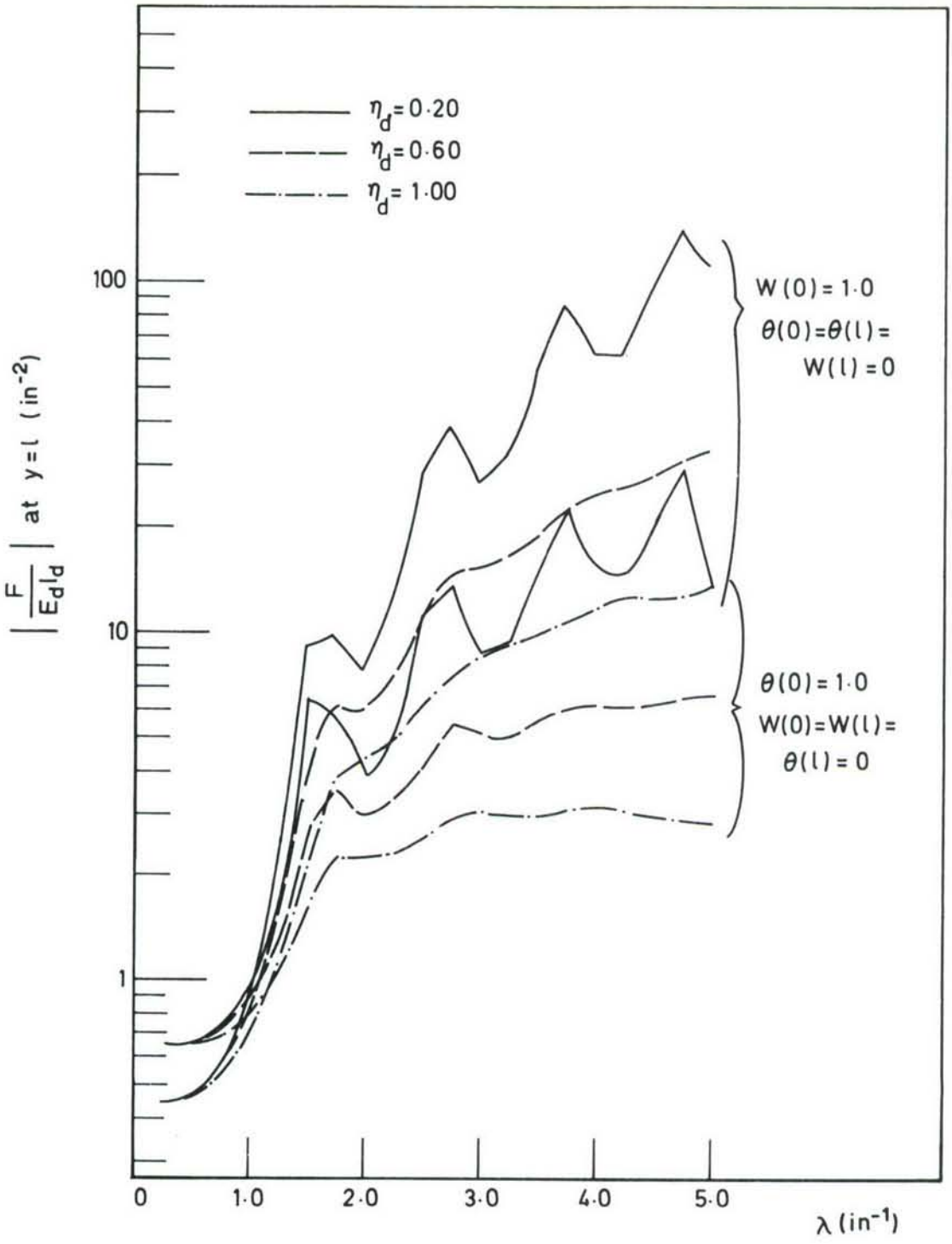

Fig. 4·10 Force at the fixed end of a doubly attached damped beam.

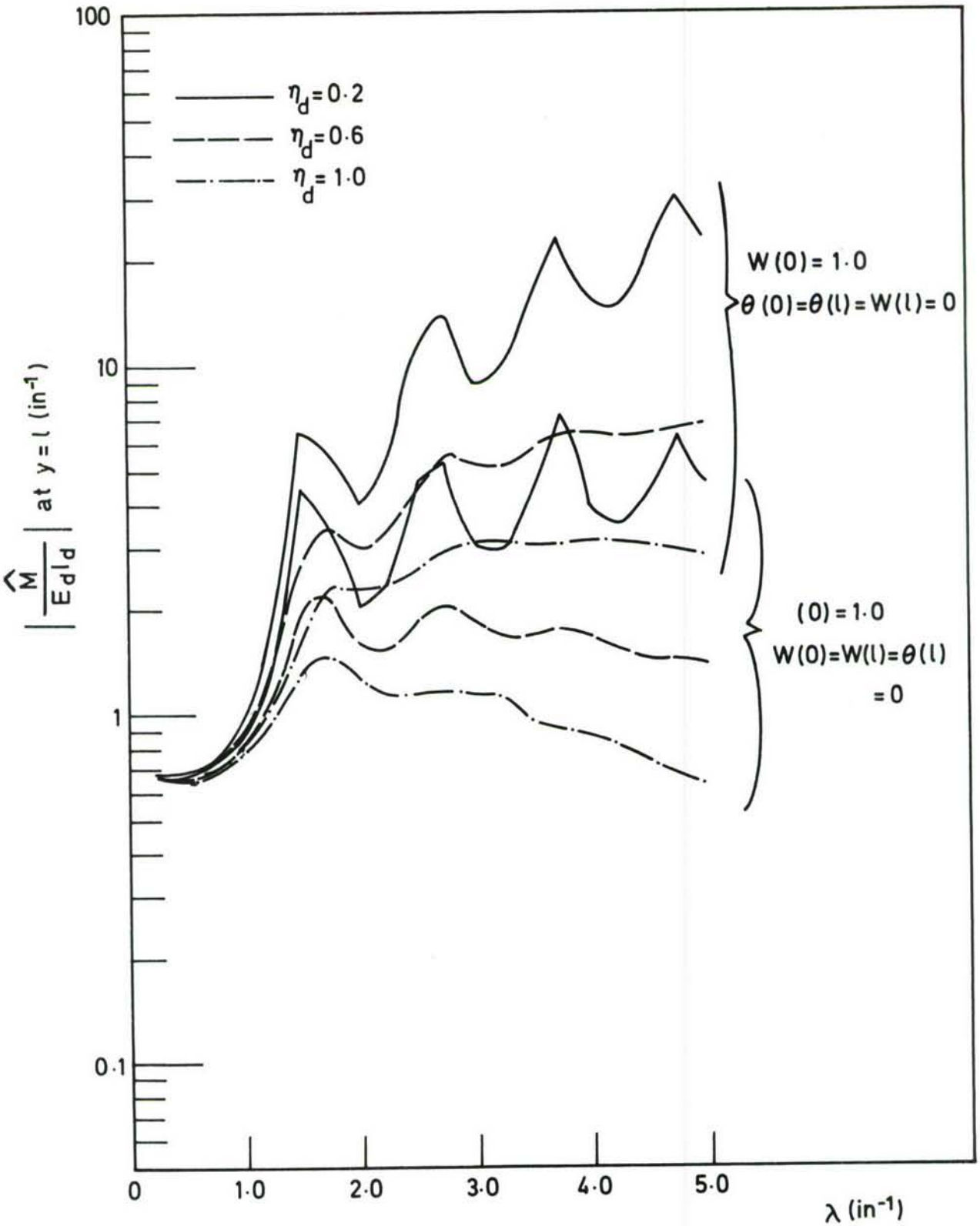

Fig. 4·11 Moment at the fixed end of a doubly attached damped beam.

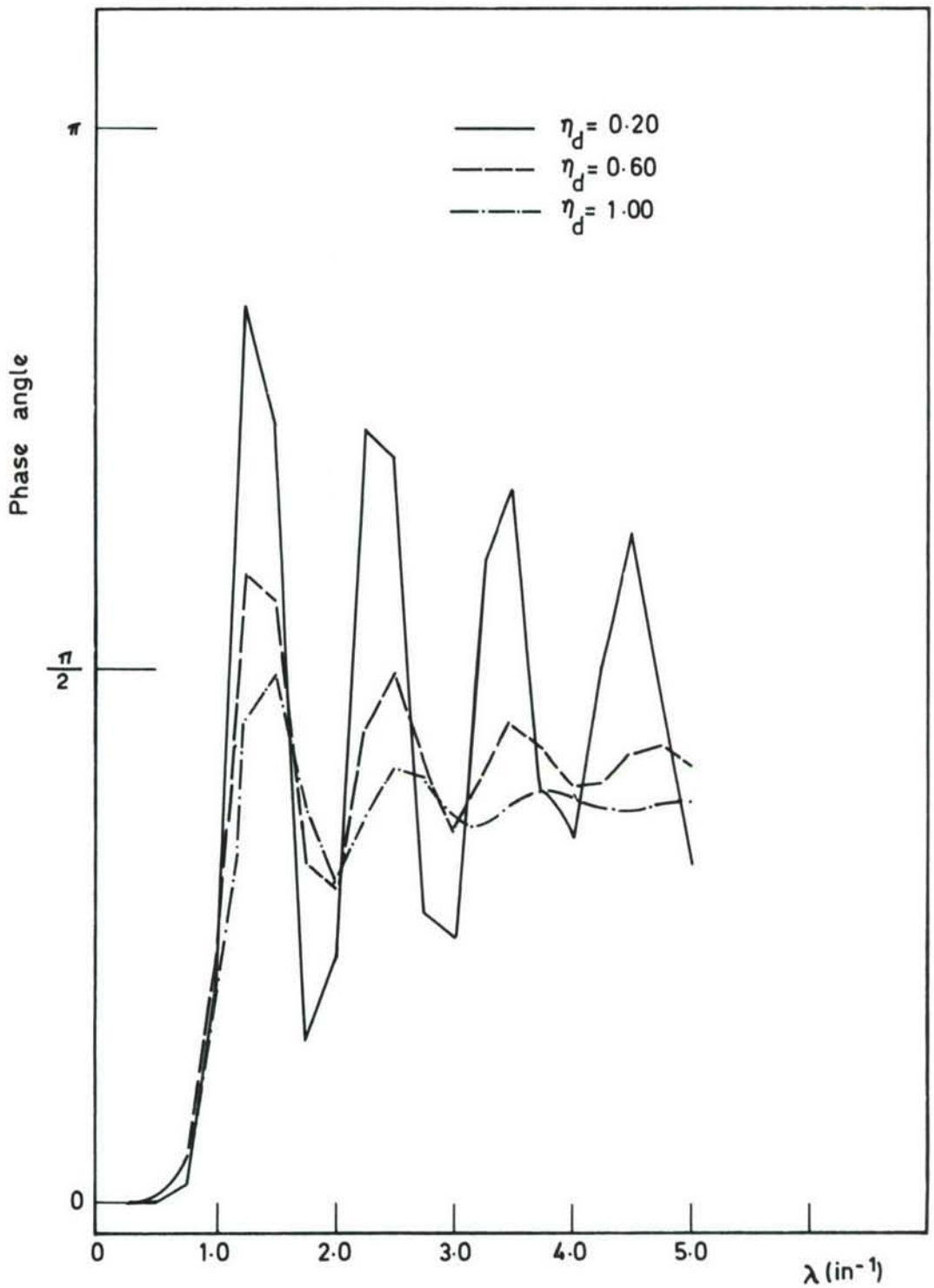

Fig. 4·12 Phase of $\frac{|\hat{M}|}{E_d I_d}$ at y=0 for a doubly attached beam excited only by W(0) = 1·0

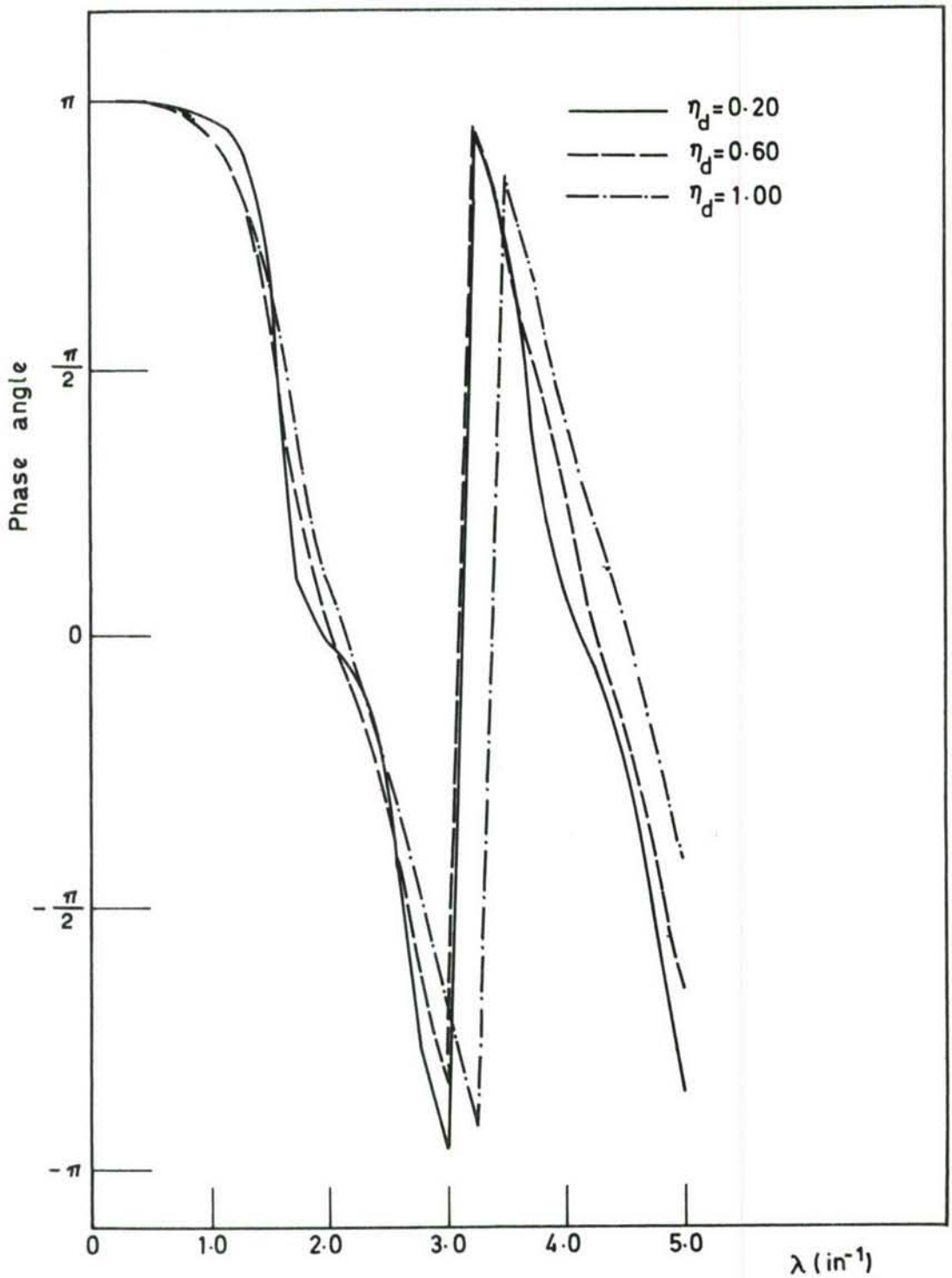

Fig. 4.13 Phase of $\frac{|\hat{M}|}{E_d I_d}$ at y=l for a doubly attached damped beam excited only by W(O) = 1 .

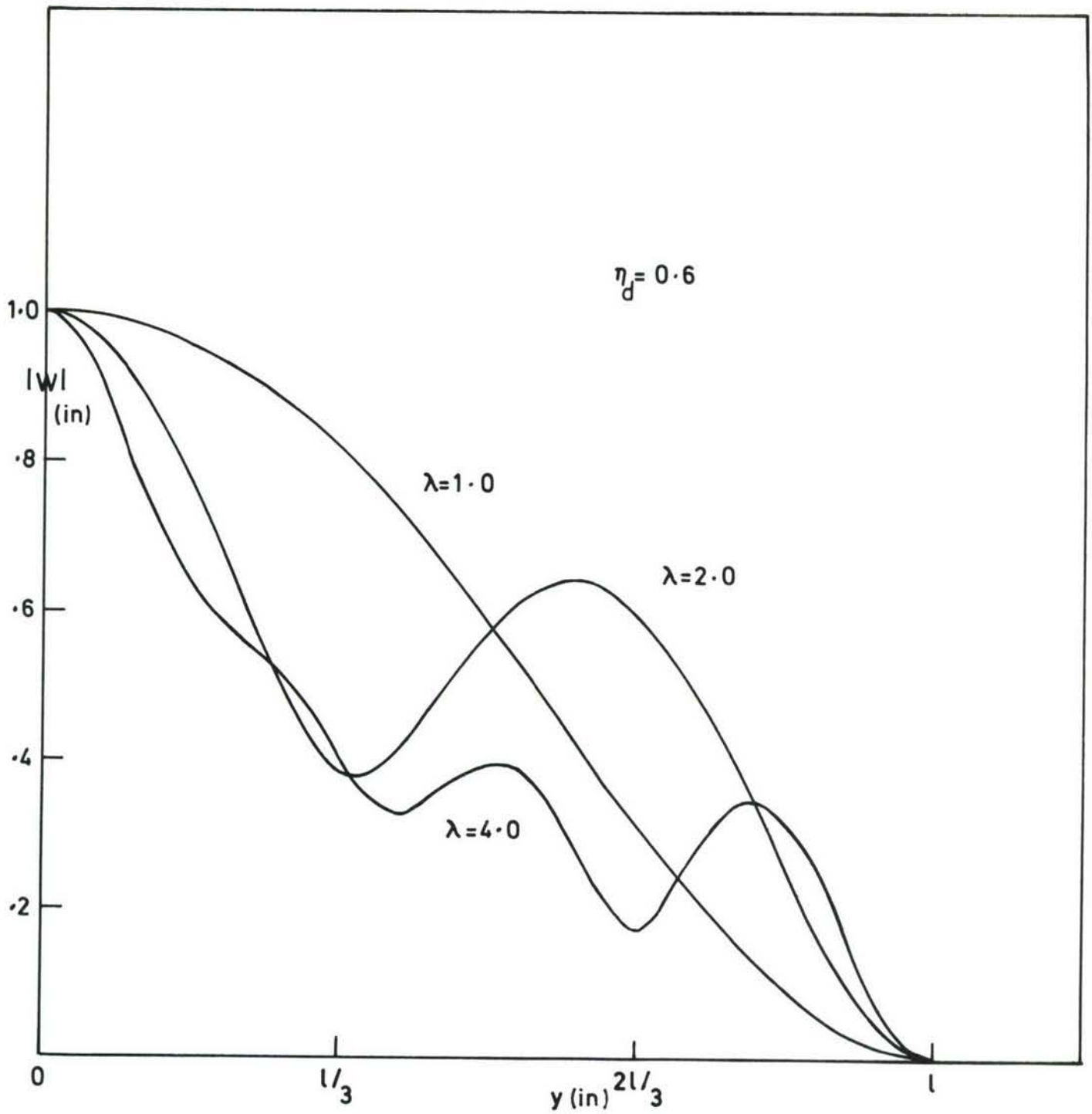

Fig 4.14 Displaced shape of a doubly attached damped beam excited only by W(O) = 1·0

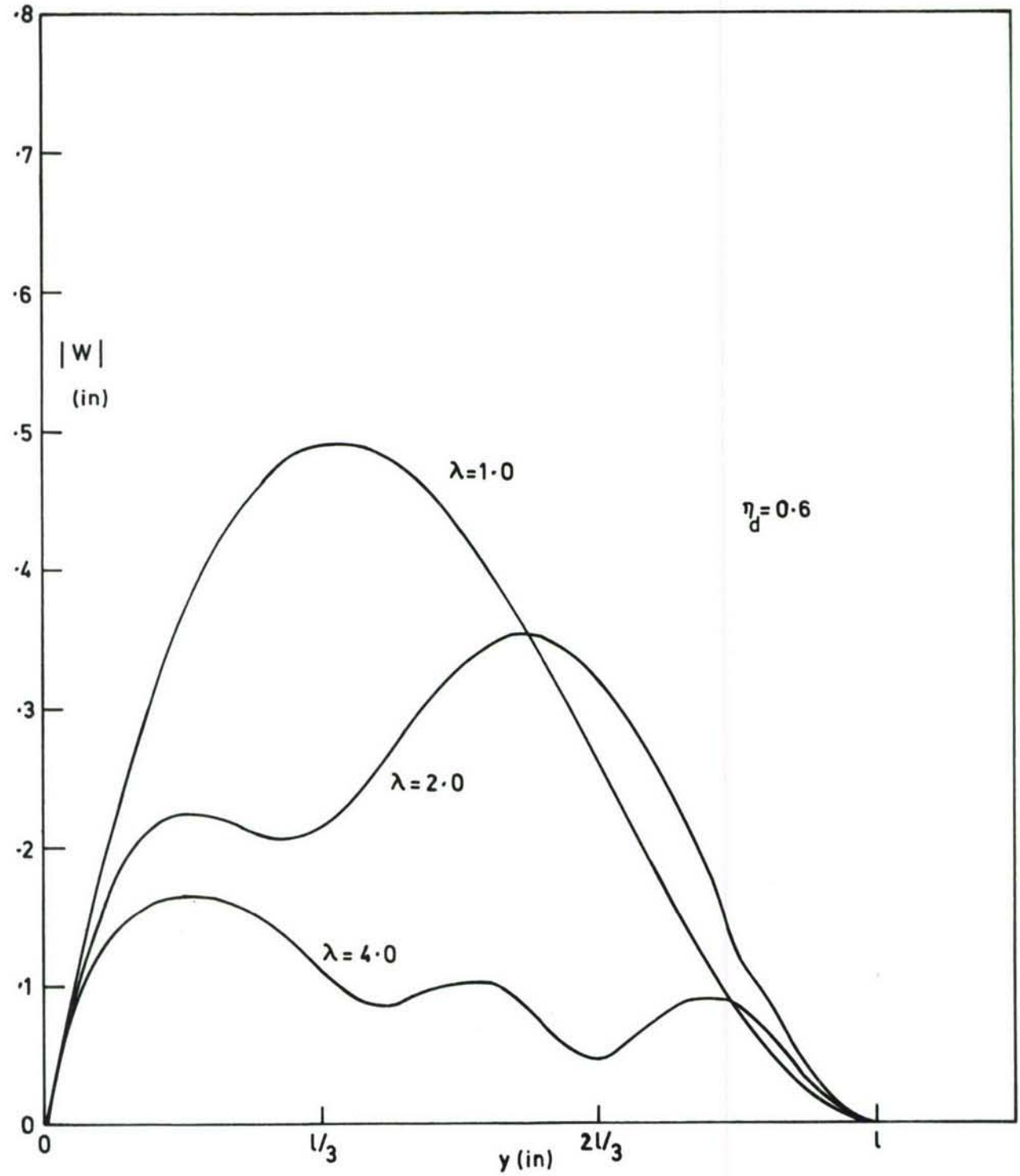

Fig. 4·15 Displaced shape of doubly attached damped beam excited only by $\theta(0) = 1 \cdot 0$

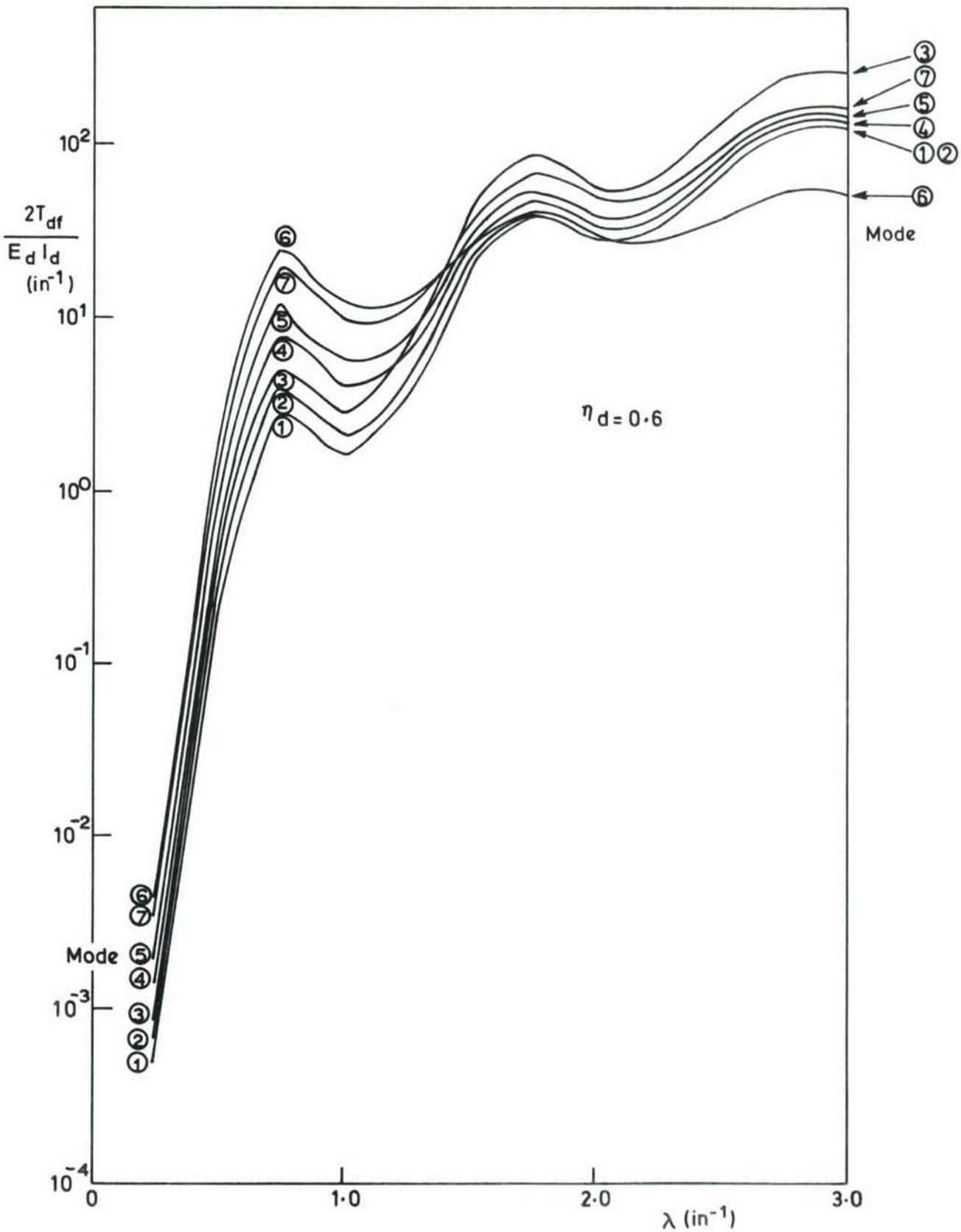

Fig 4·16 Flexural strain energy for three damped double cantilevers

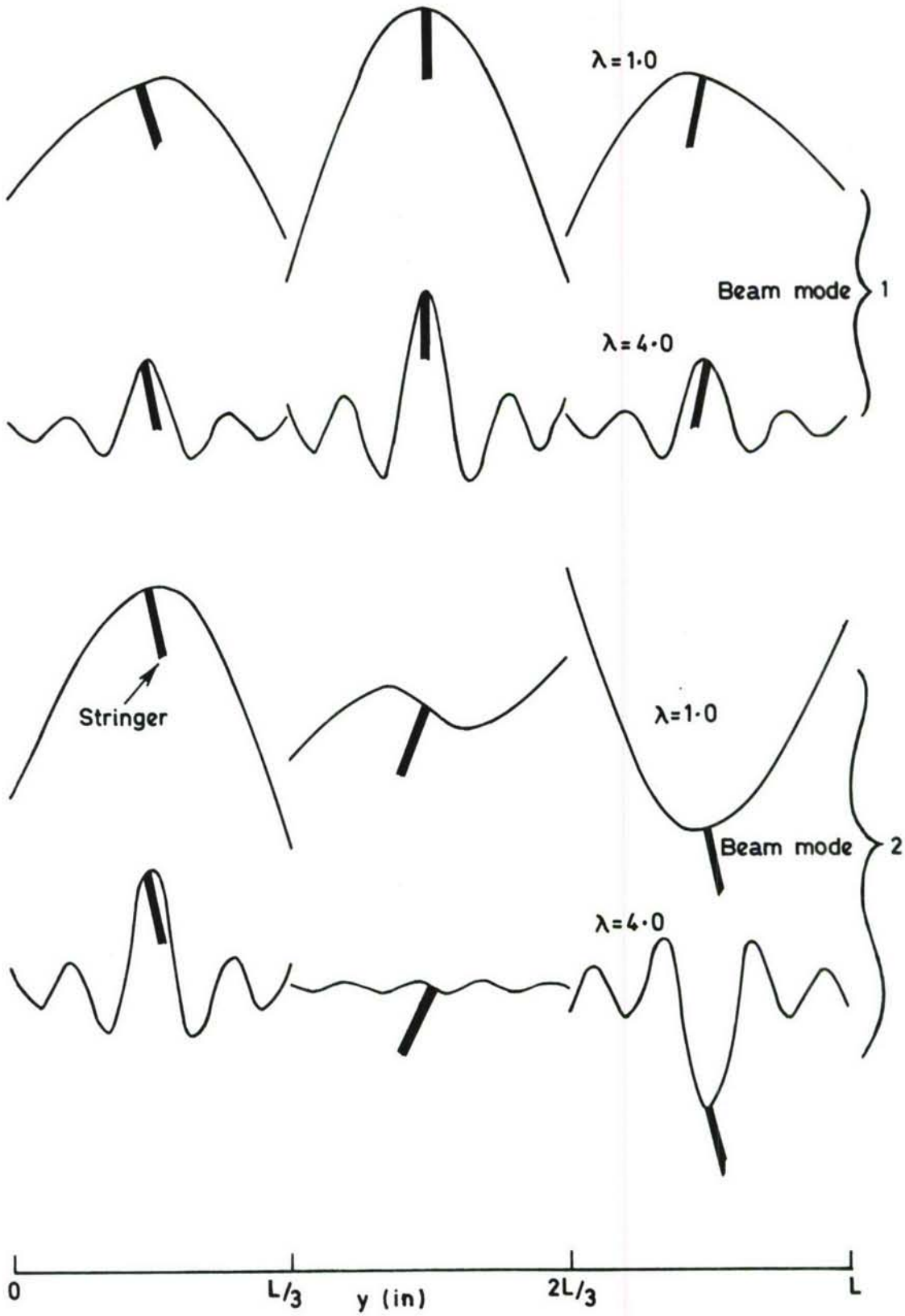

Fig. 4·17 Cantilever damper displacement when excited by a six span beam

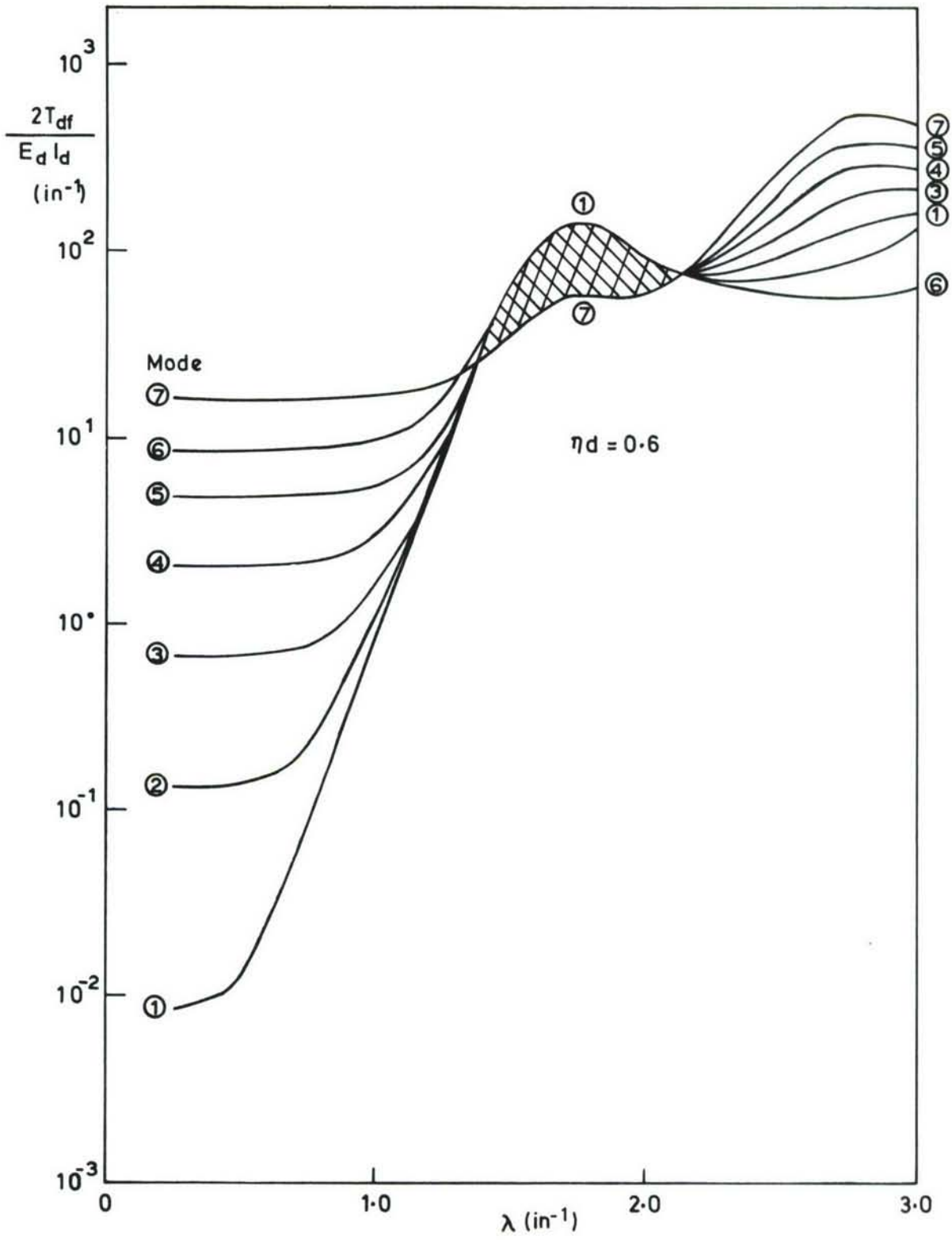

Fig 4·18 Flexural strain energy for 6 damping beams fixed to 7 stringers

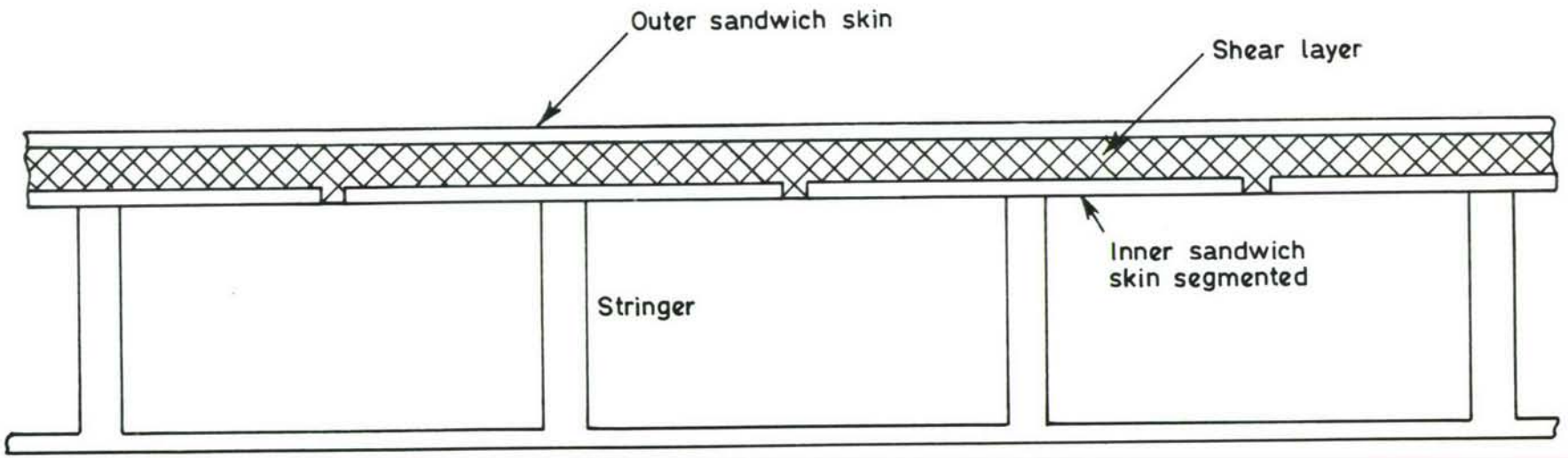

Fig. 4.19 Schematic of sandwich beam damper and method of application

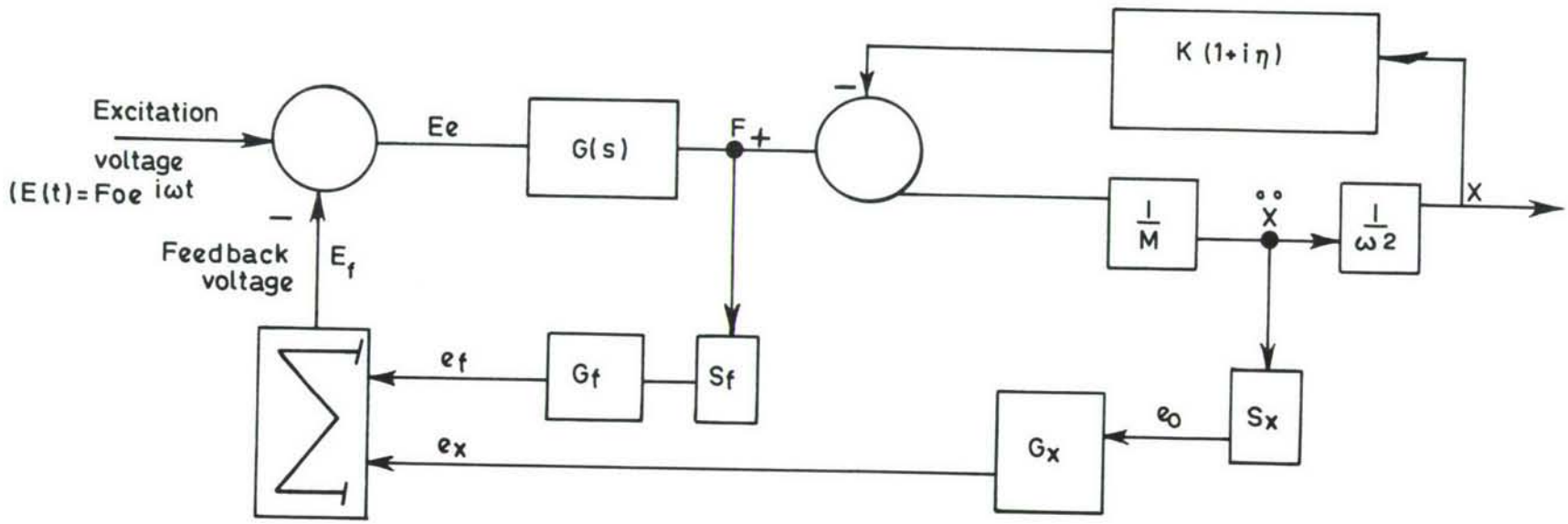

Fig 5.1 Block diagram of servo controlled test system (Ref 41)

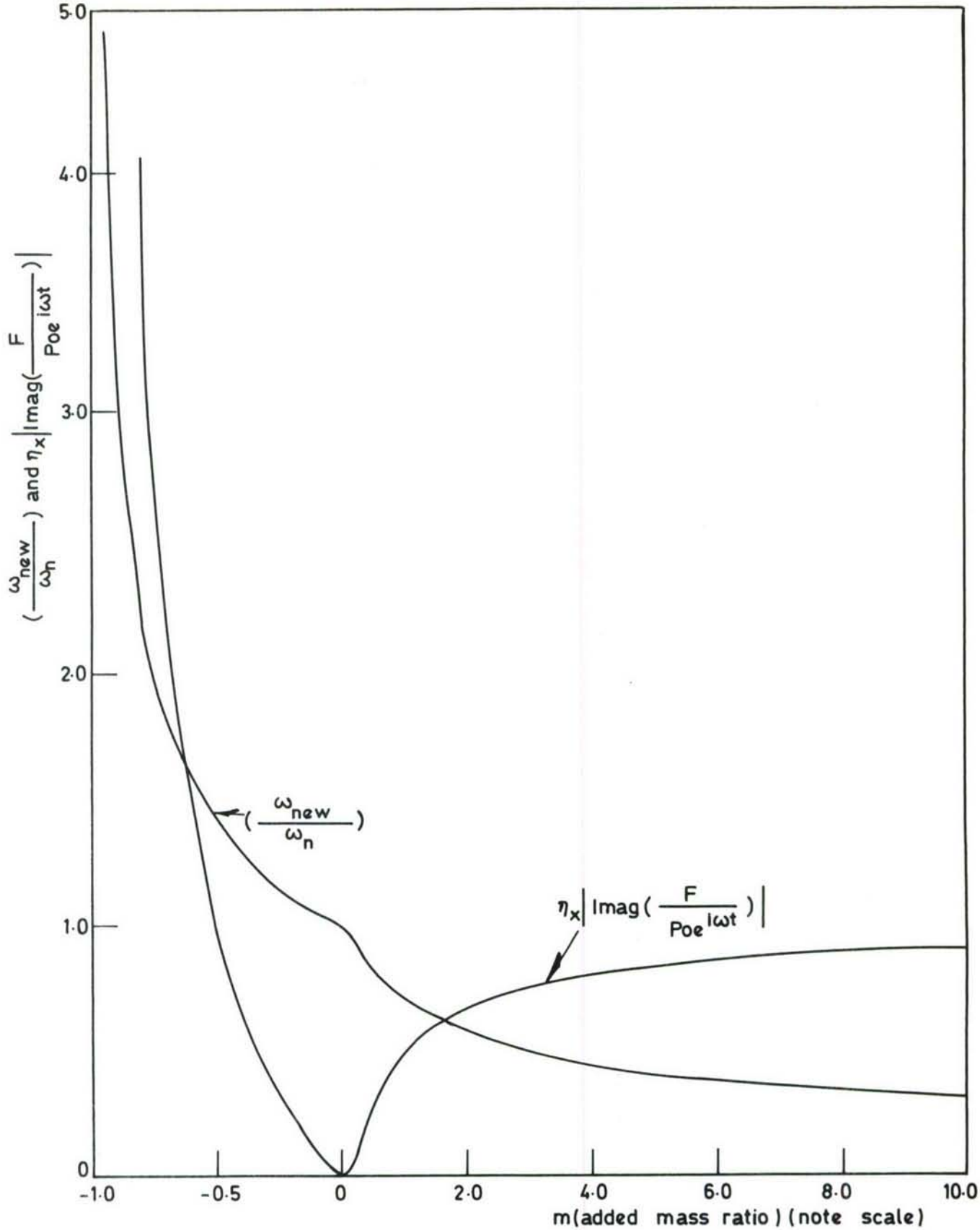

Fig. 5.2 Force (imaginary part) and natural frequency ratio as a function of "mass change" due to electronic feedback.

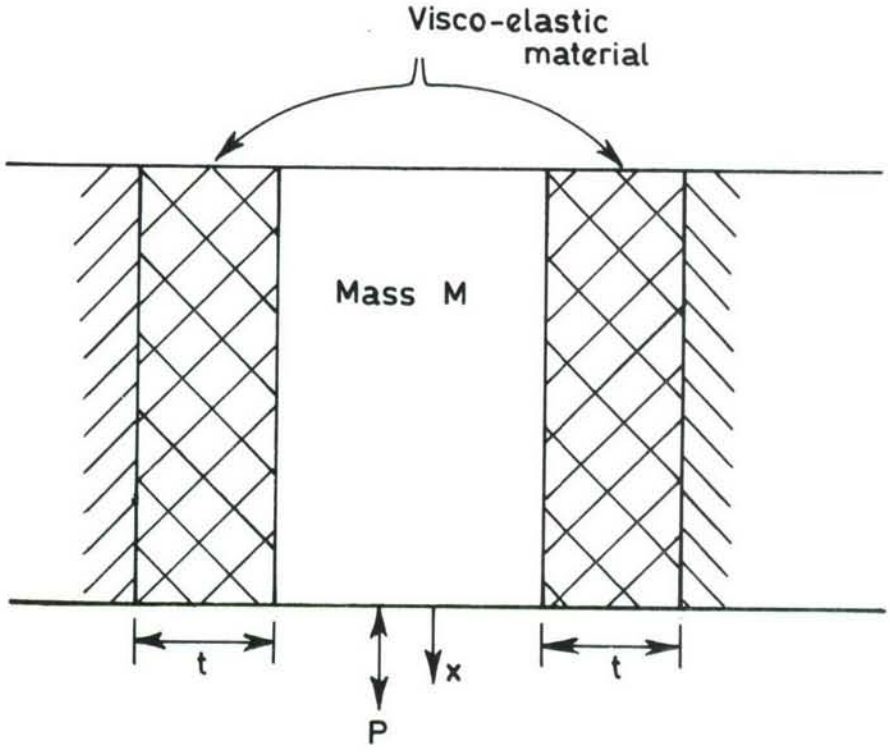

Fig. 5.3 Schematic of the single degree of freedom system used to measure the dynamic properties of Visco-elastic materials.

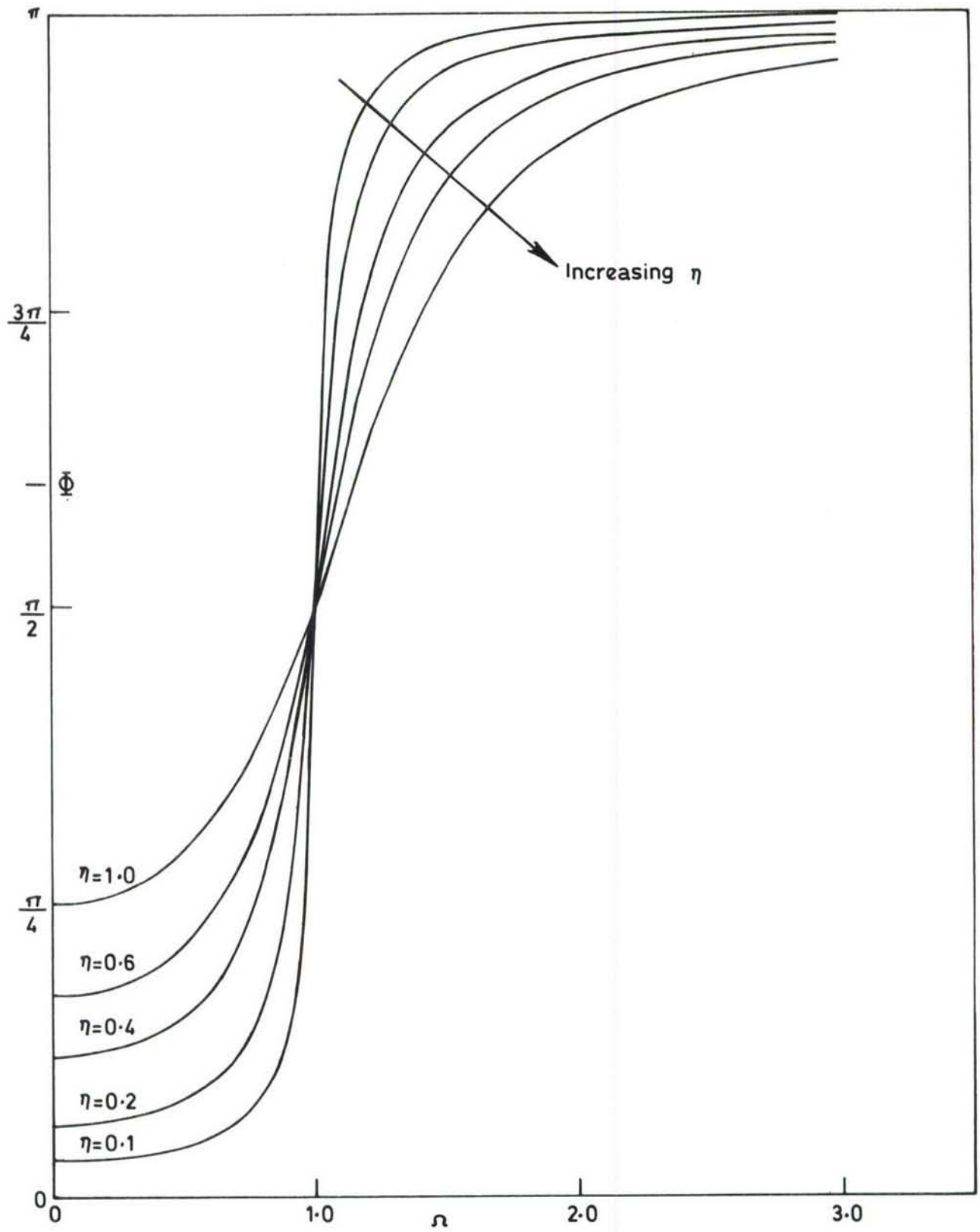

Fig. 5.4 Phase angle between force and displacement for a single degree of freedom system with hysteretic damping

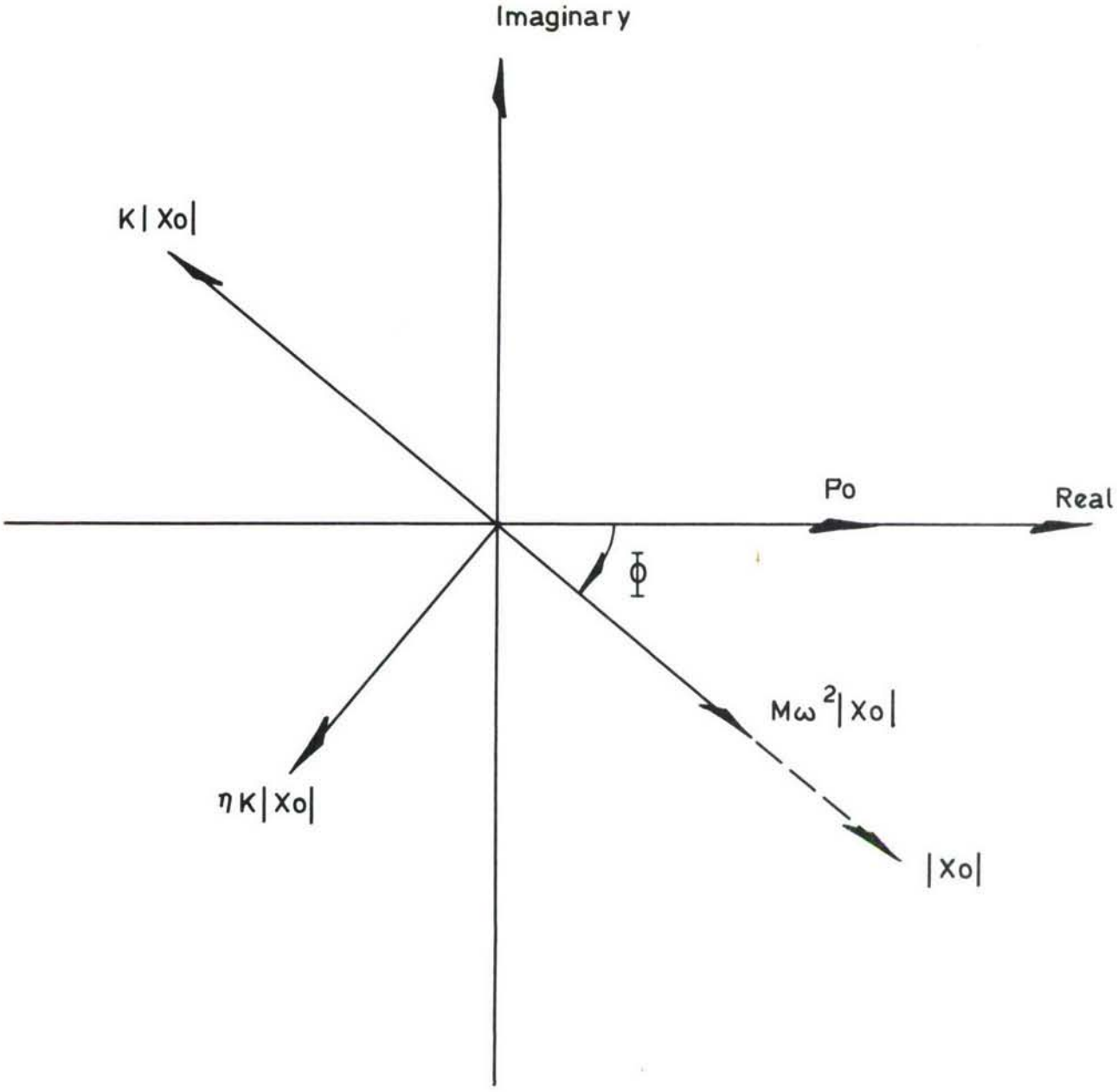

Fig. 5.5 Phase plane representation of the forces in a single degree of freedom system with hysteretic damping.

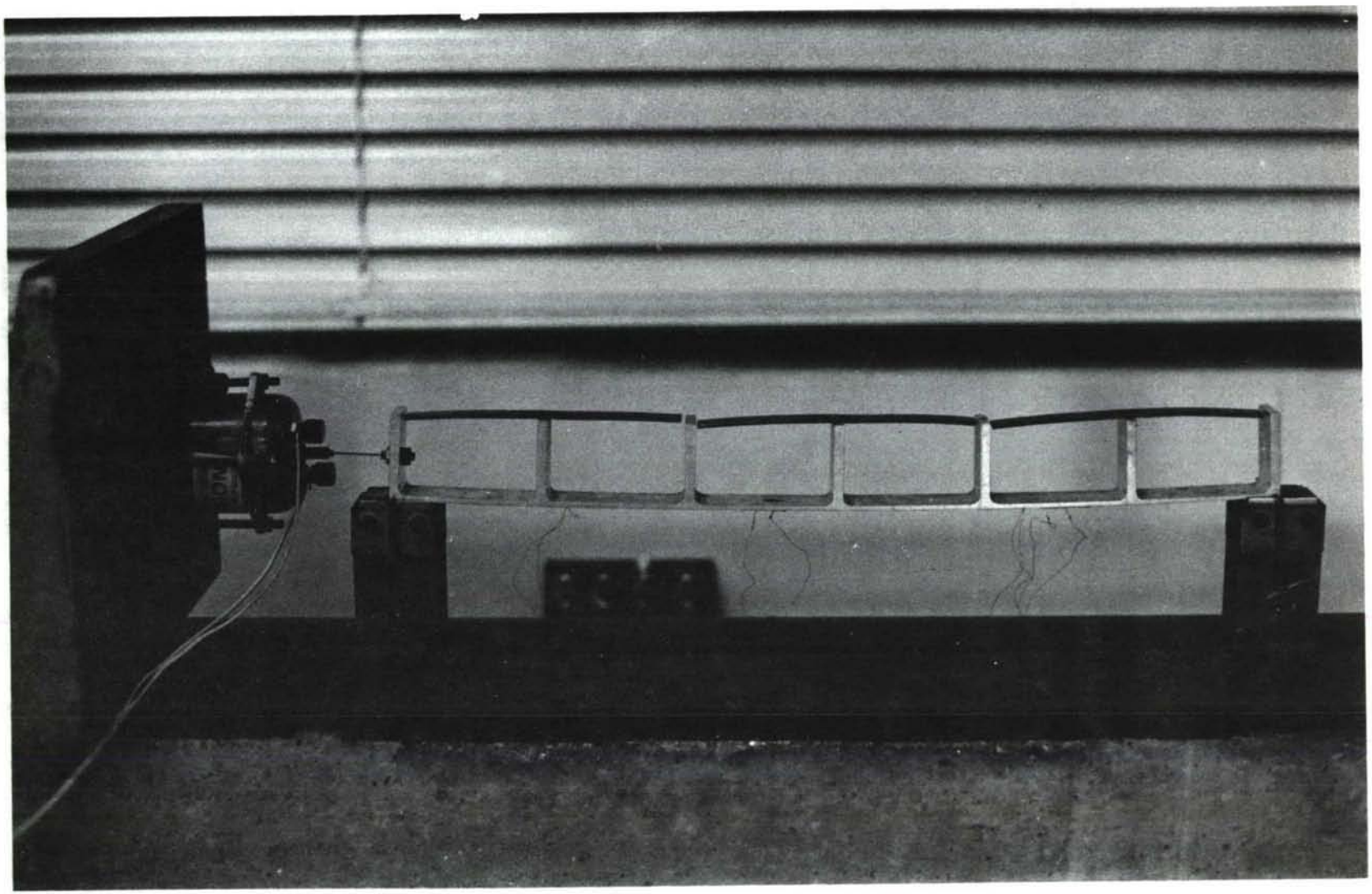

Fig 6.1 Beam specimen with cantilever dampers

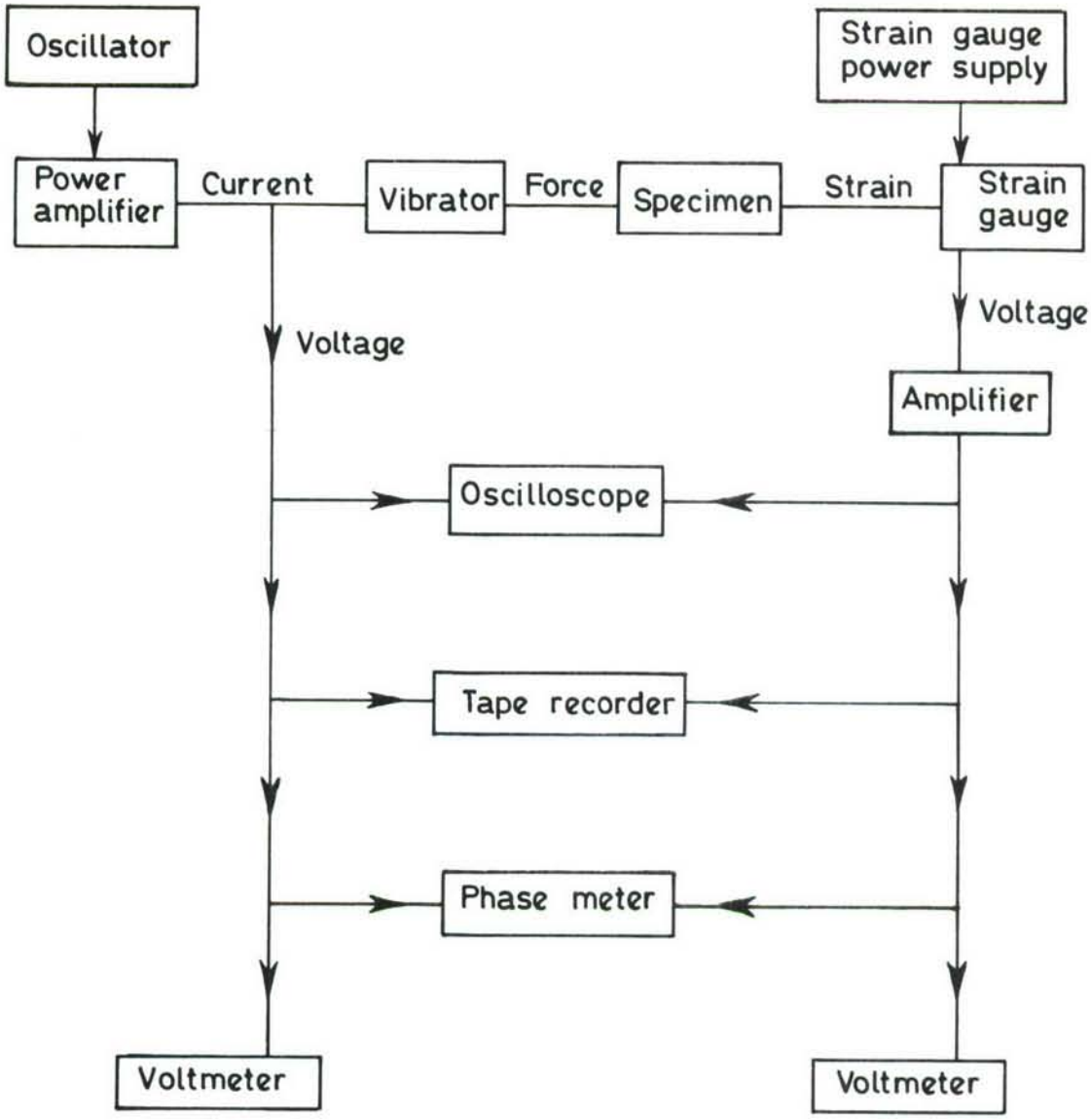

Fig. 6.2 Block diagram of the electronic system for beam response measurements

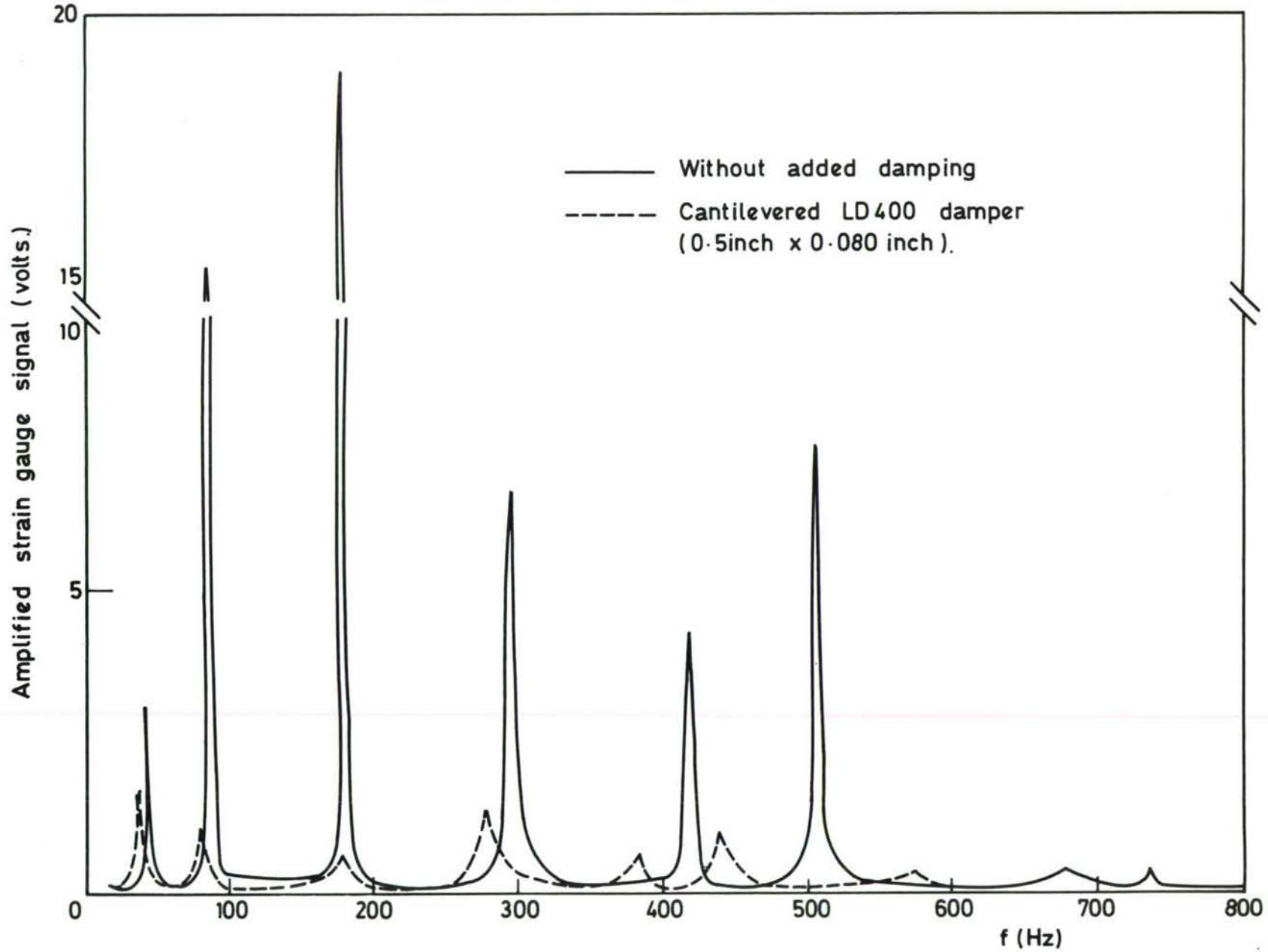

Fig. 6.3 Frequency response of 6 span simply supported beam.

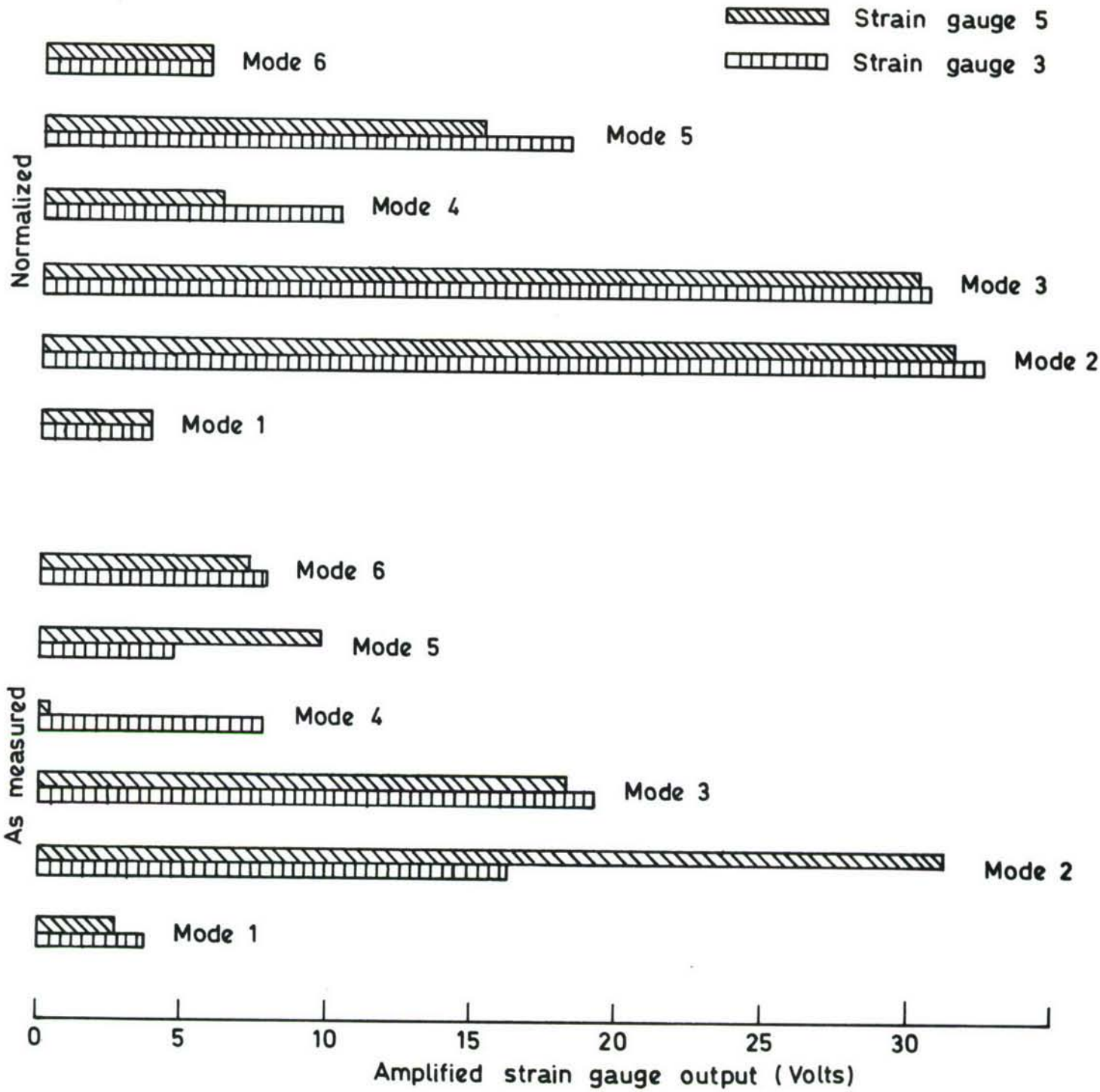

Fig 6·4 Histogram of measured stresses and maximum stresses calculated using the measured values and theoretical mode shapes

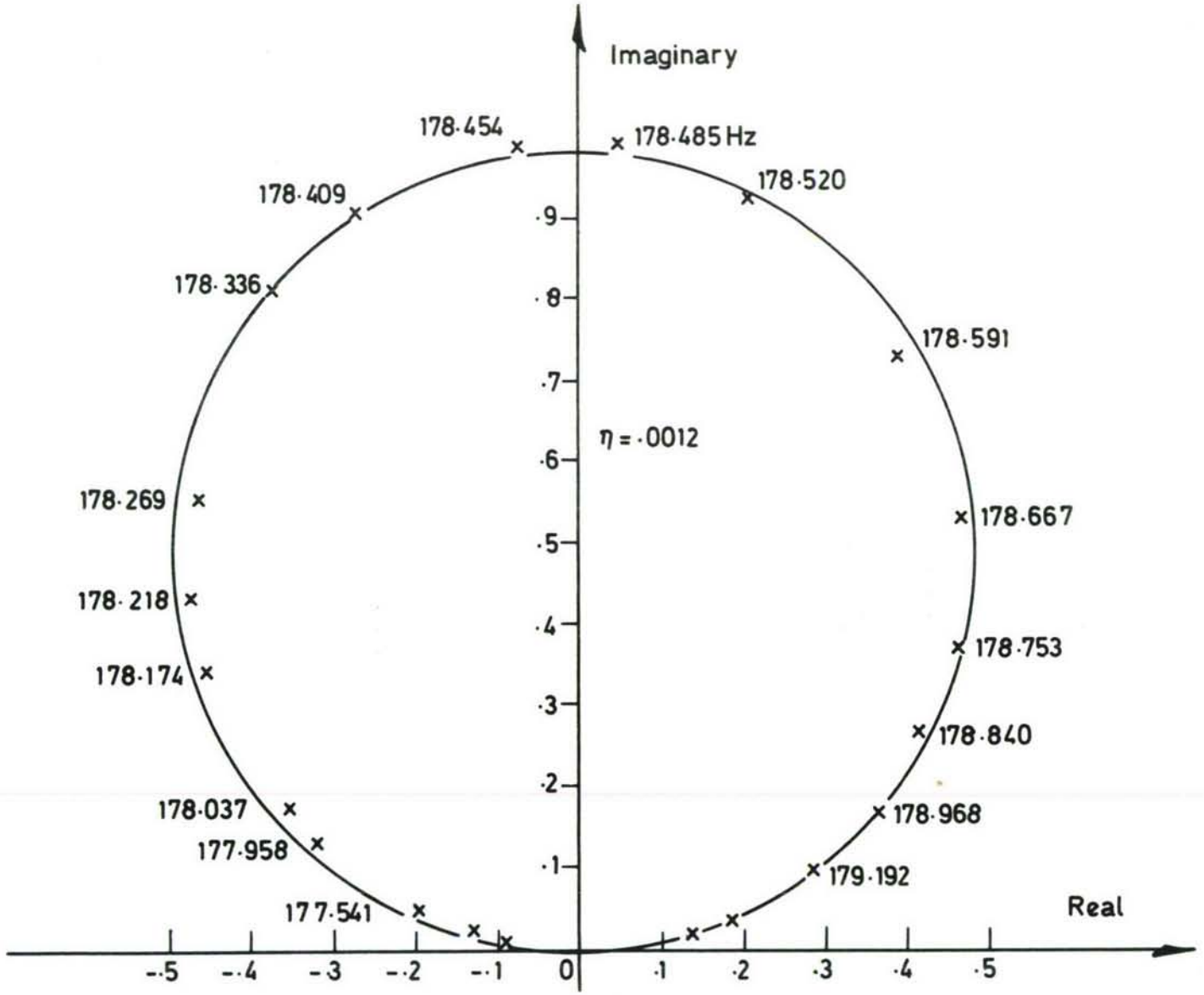

Fig. 6·5 Steady state vector response plot for mode 3 (no added damping) (normalized with respect to maximum response).

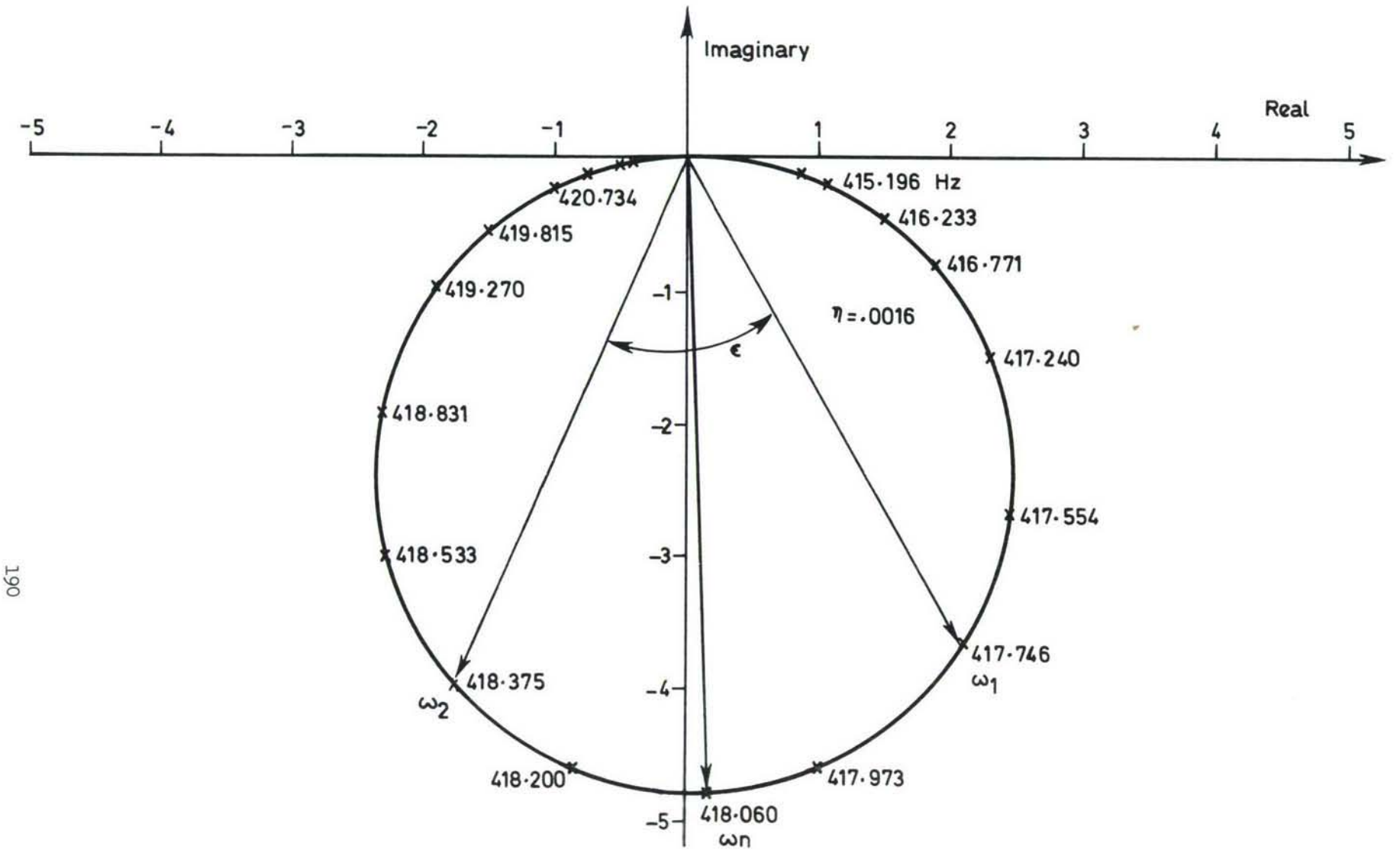

Fig 6·6 Steady state vector response plot for mode 5 (no added damping)

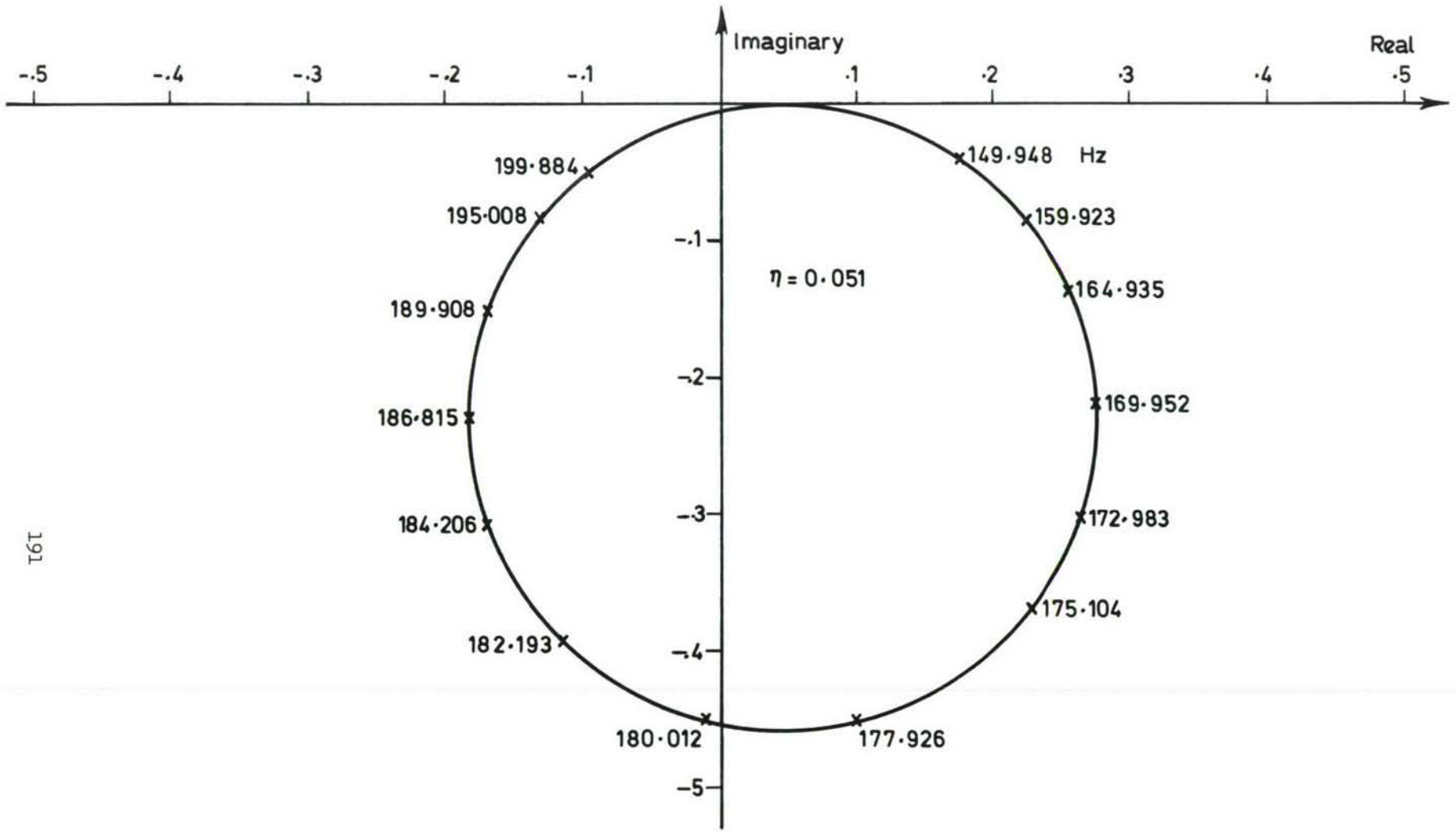

Fig 6.7 Steady state vector response plot for mode 3 (·5″x ·080″ LD 400 cantilever dampers added)

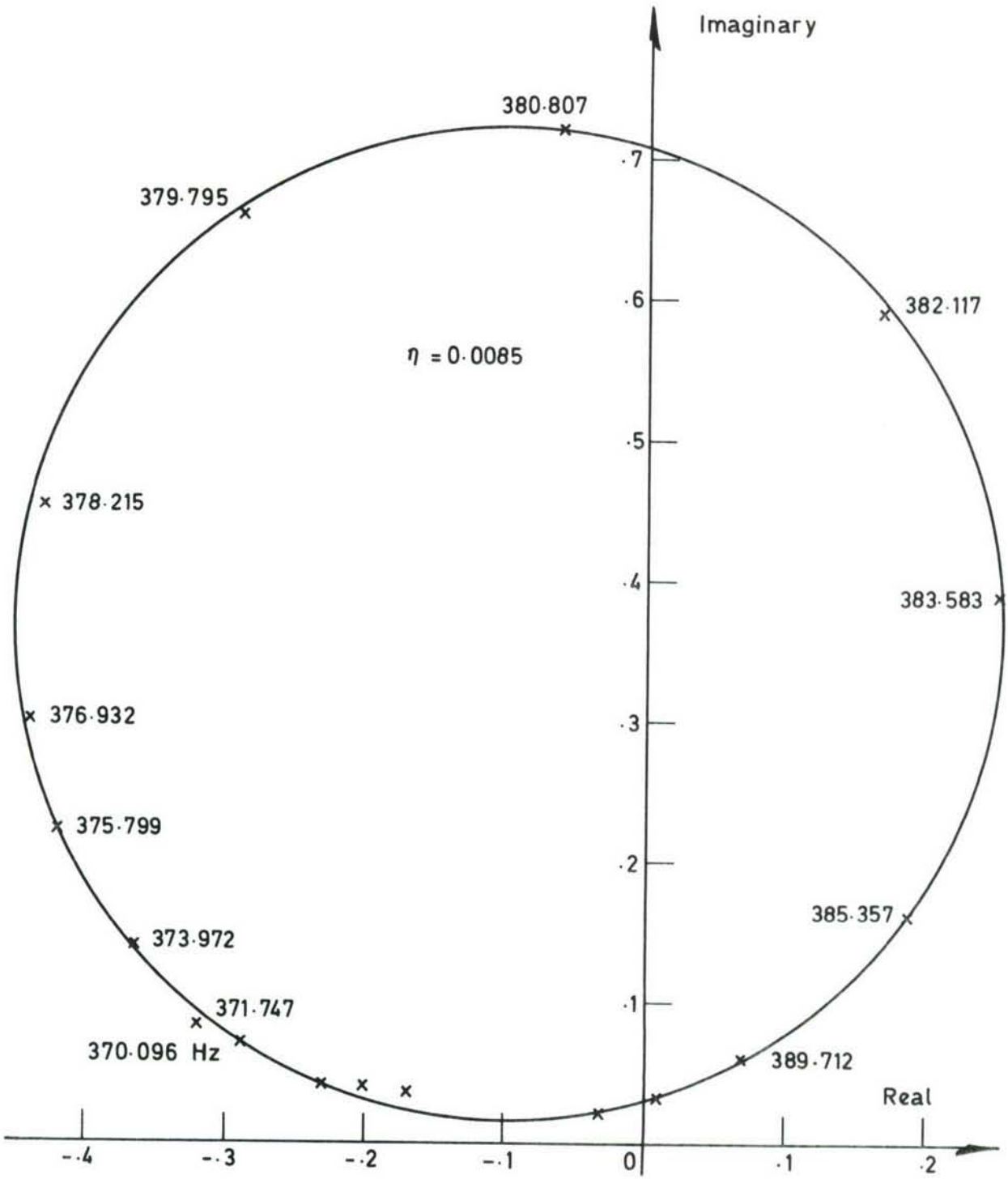

Fig. 6.8 Steady state vector response plot for mode 5 (0.5inch x 0.080inch LD400 cantilever dampers added).

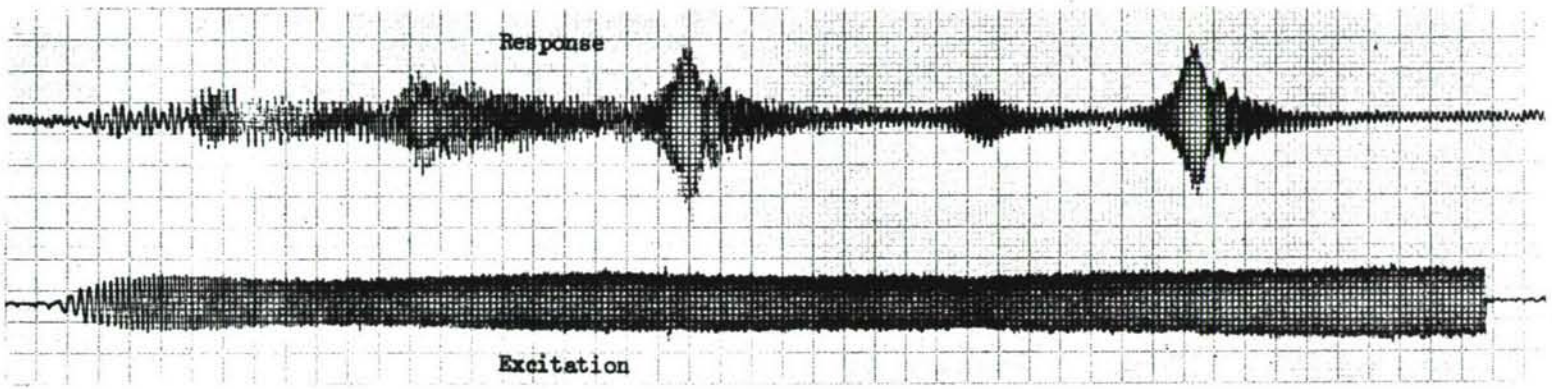

Fig. 6.9(a) No added damping

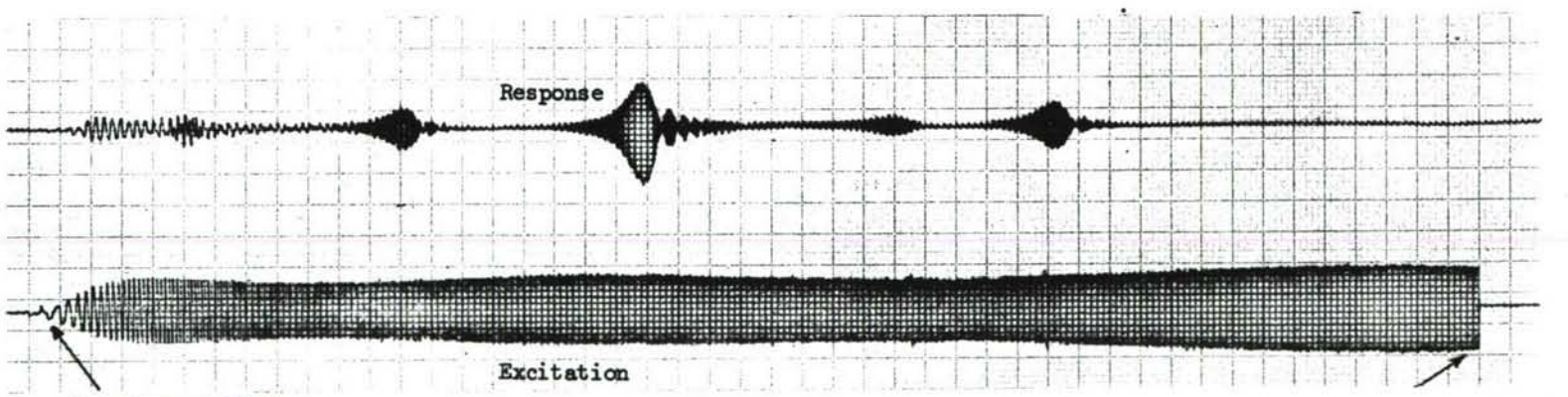

Fig. 6.9(b) .5 inch by .060 inch double cantilevers attached.

Fig. 6.9 Transient response and excitation traces for a 6 span beam.
(Frequency swept from 10 Hz to 600 Hz in 5 sec. Traces recorded at 5 cm/sec.)

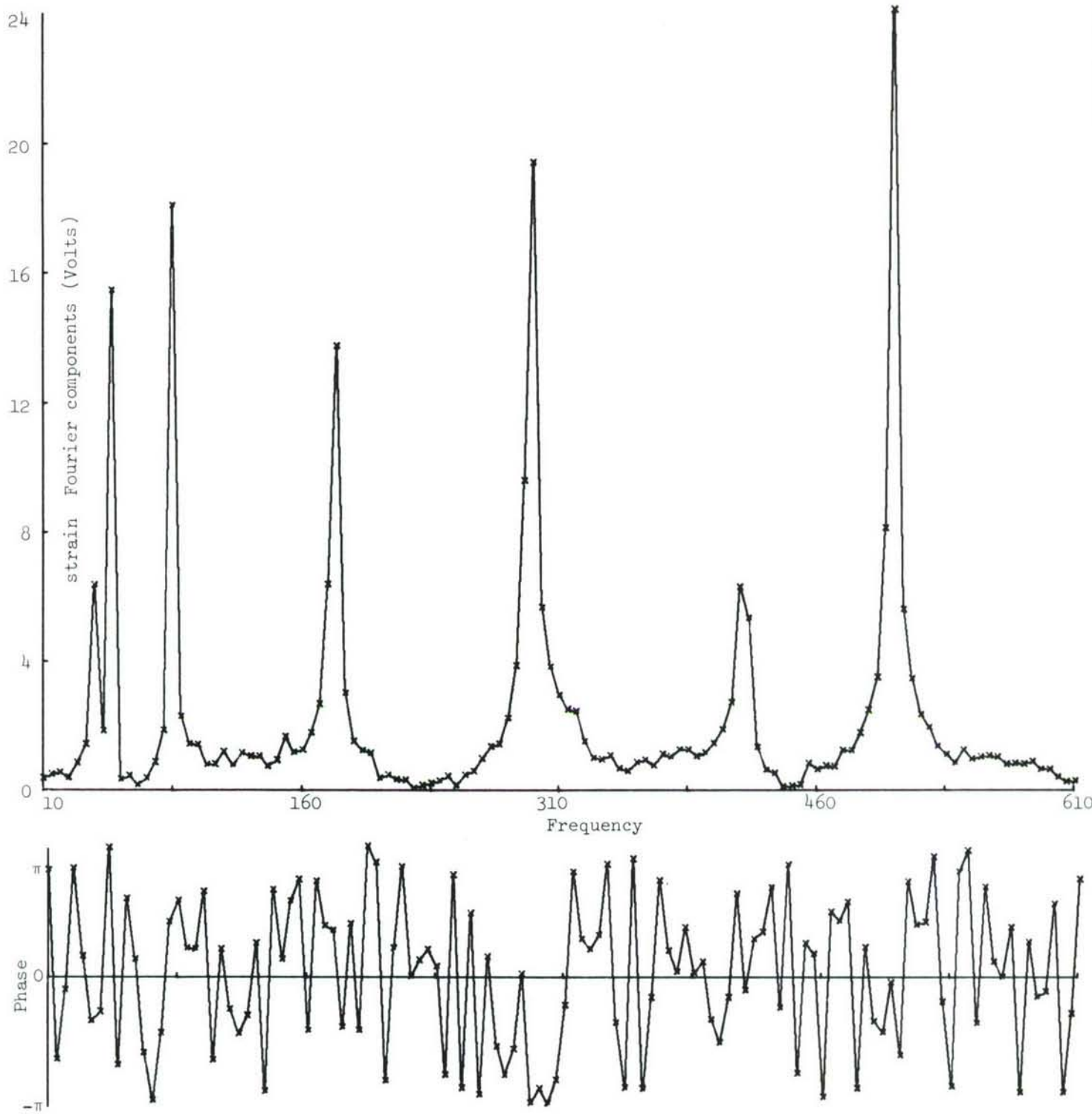

Fig. 6.10(a) Computer evaluated Fourier transform of the response of a six span beam excited by a force swept from 10 Hz to 600 Hz in 5 seconds.

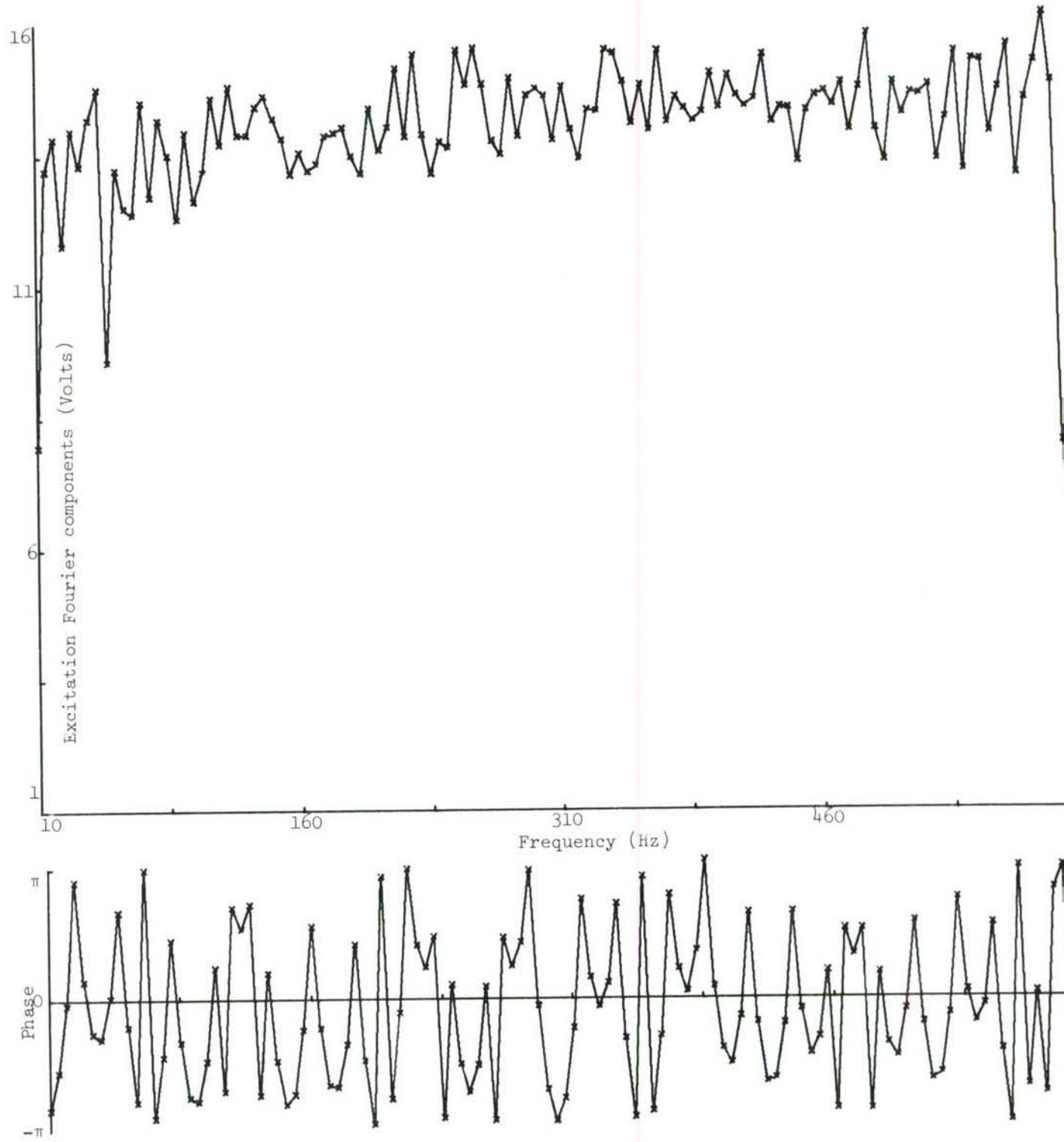

Fig. 6.10(b) Computer evaluated Fourier transform of the transient force swept from 10 Hz to 600 Hz in 5 seconds.

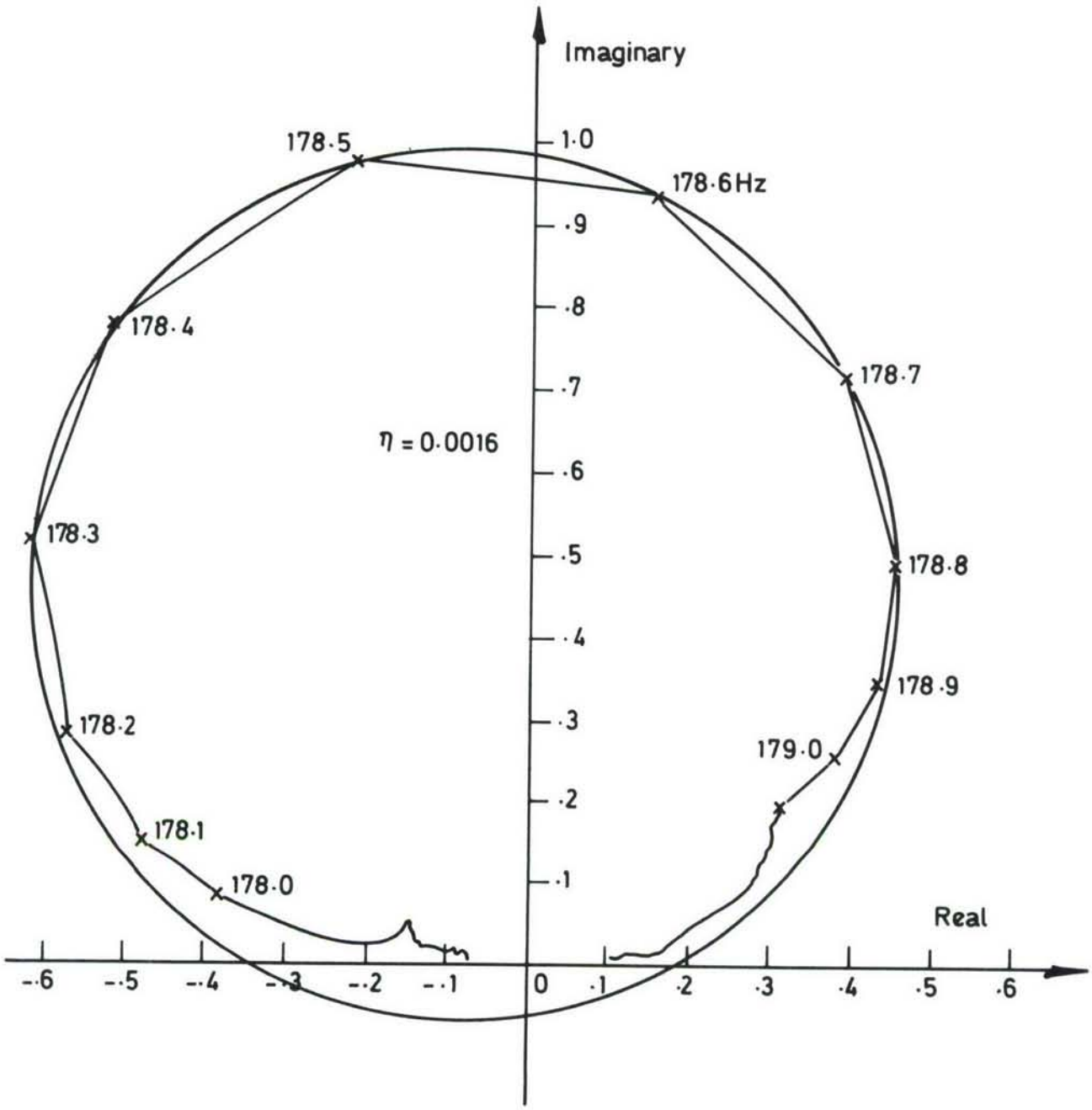

Fig. 6·11 Vector plot for mode 3 obtained by transient analysis technique. (undamped beam).

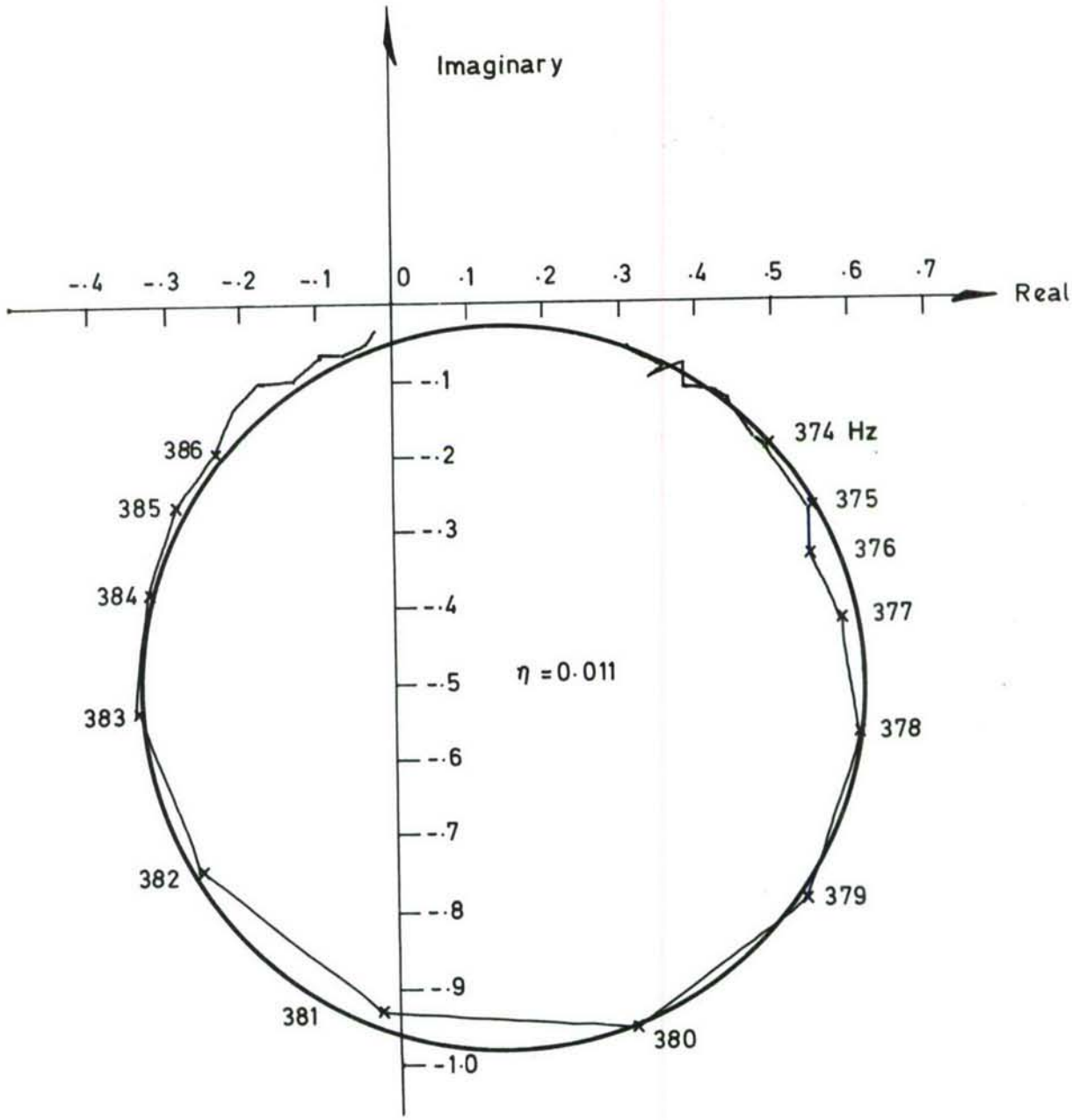

Fig. 6.12 Vector plot for mode 5 obtained by the transient analysis technique. (0.5 inch by 0.080 inch double cantilever dampers).

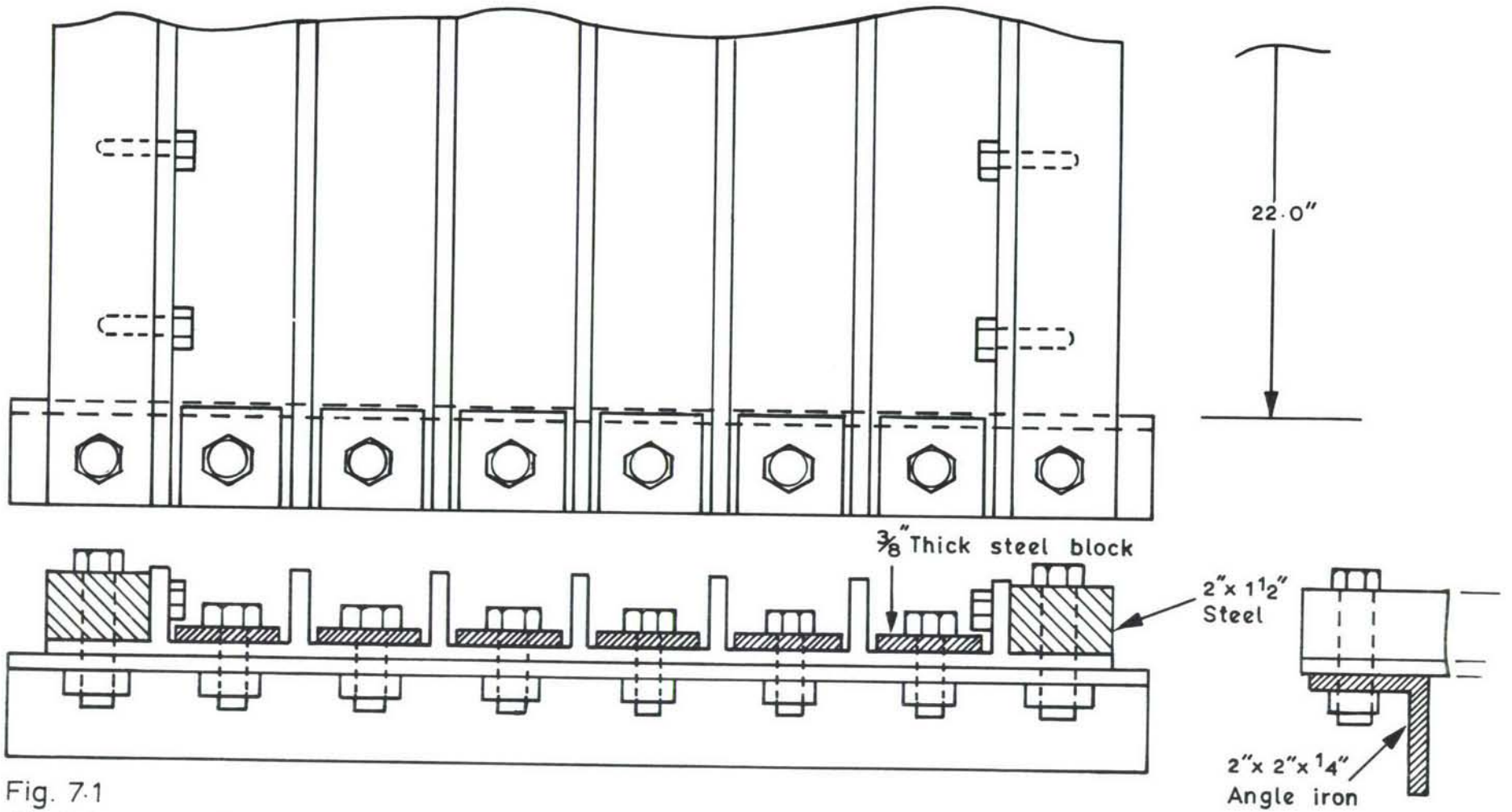

Fig. 7.1
Sketch showing support structure for acoustic tests

A ——— Damping material bonded to skin between stringers over the entire plate area.

B —·—·— 'A' plus 1" wide strip of damping material bonded across the tops of the stringers at panel mid-length.

– – – – As in 'B' but damping material strip 2" wide.

(Damping material 0·060 in thick)

(Panel supported as in Fig. 7·1)

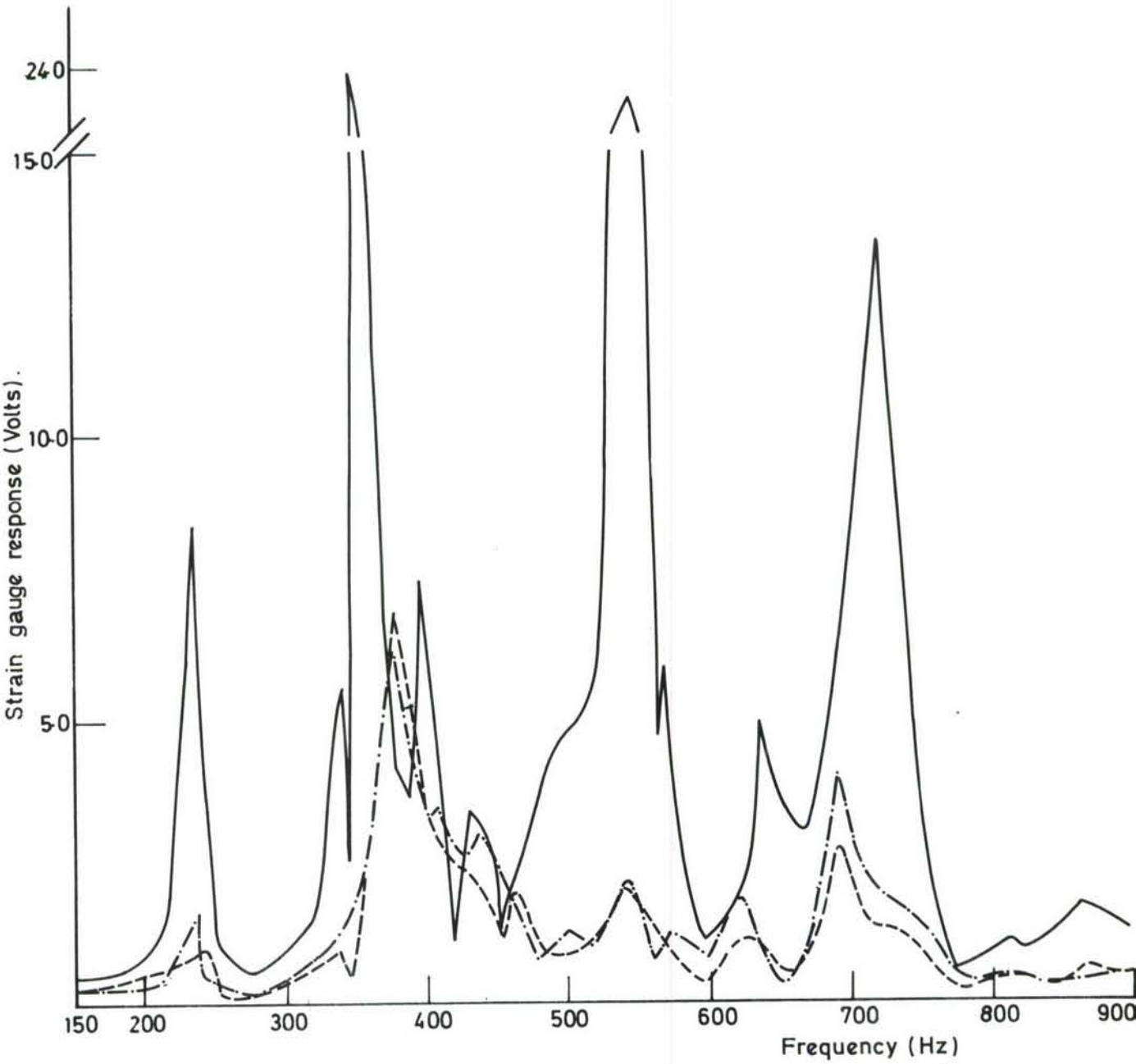

Fig. 7·2 Variation in response of the test panel to harmonic acoustic excitation with the addition of damping material.

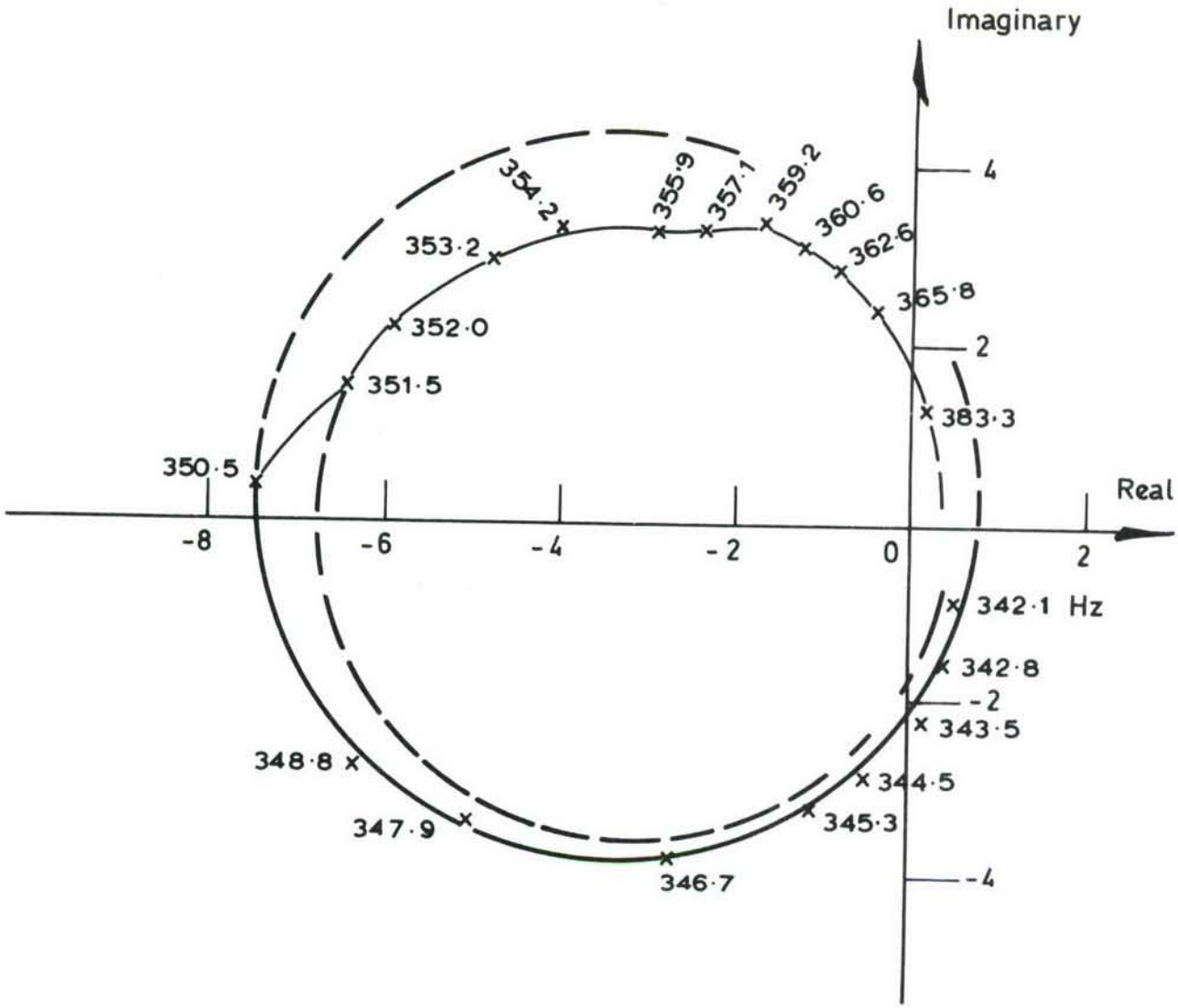

Fig. 7.3 Vector response plot for mode 2 of a 6 span panel excited acoustically.

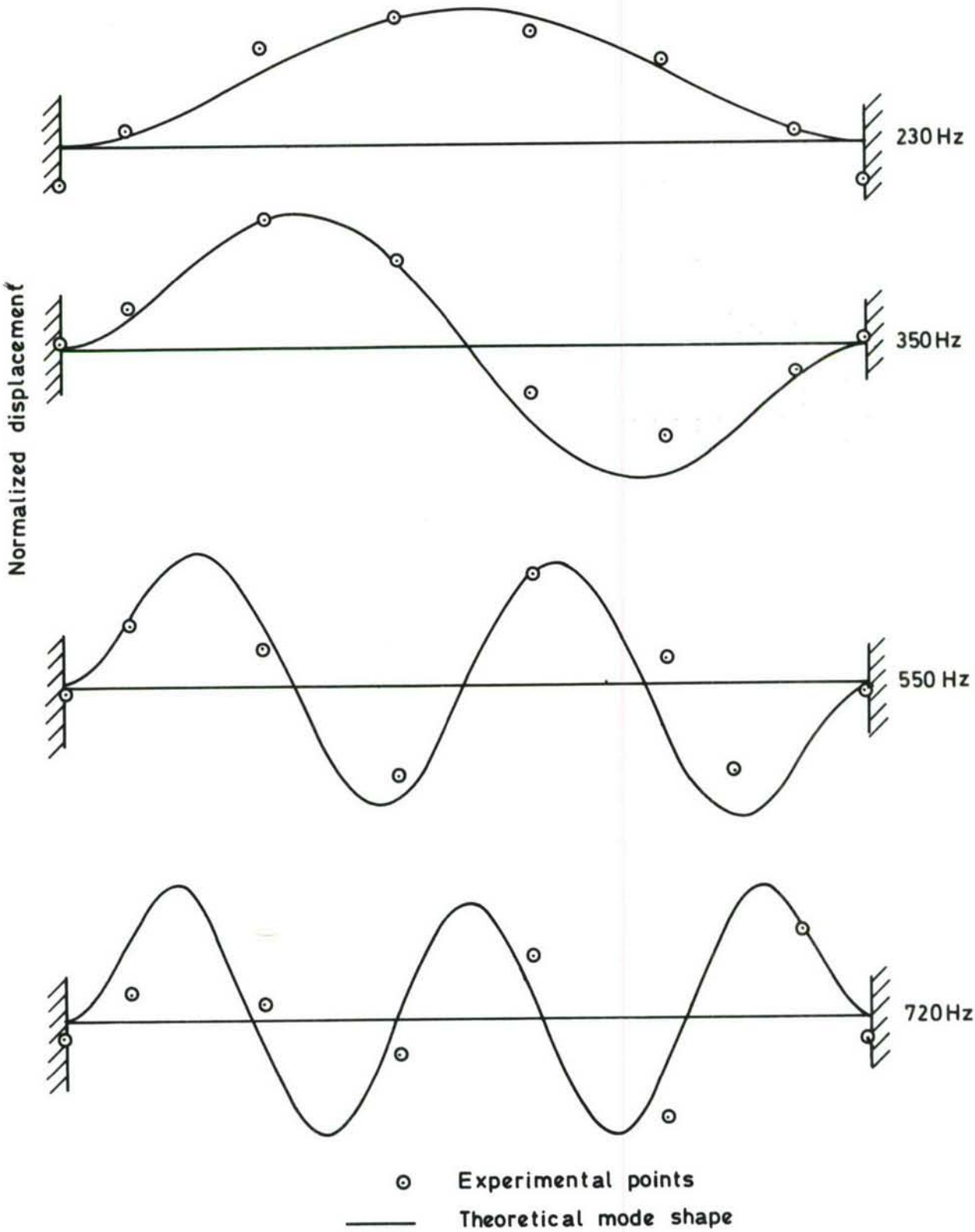

Fig. 7.4. Comparison between theory and measured mode shapes at major peaks in frequency response curve.

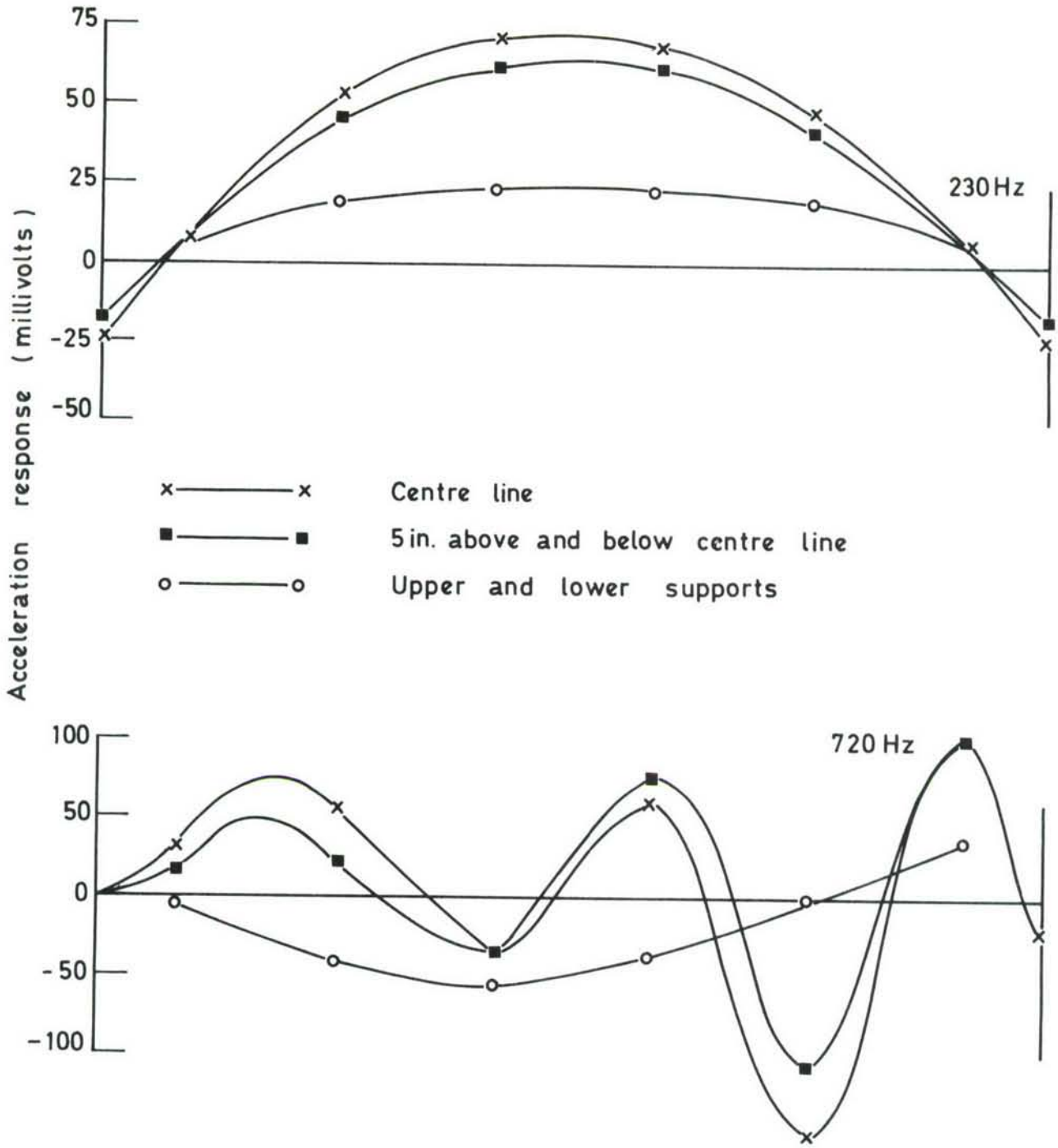

Fig. 7.5 Acceleration response curves at various stations along the panel length for two frequencies.

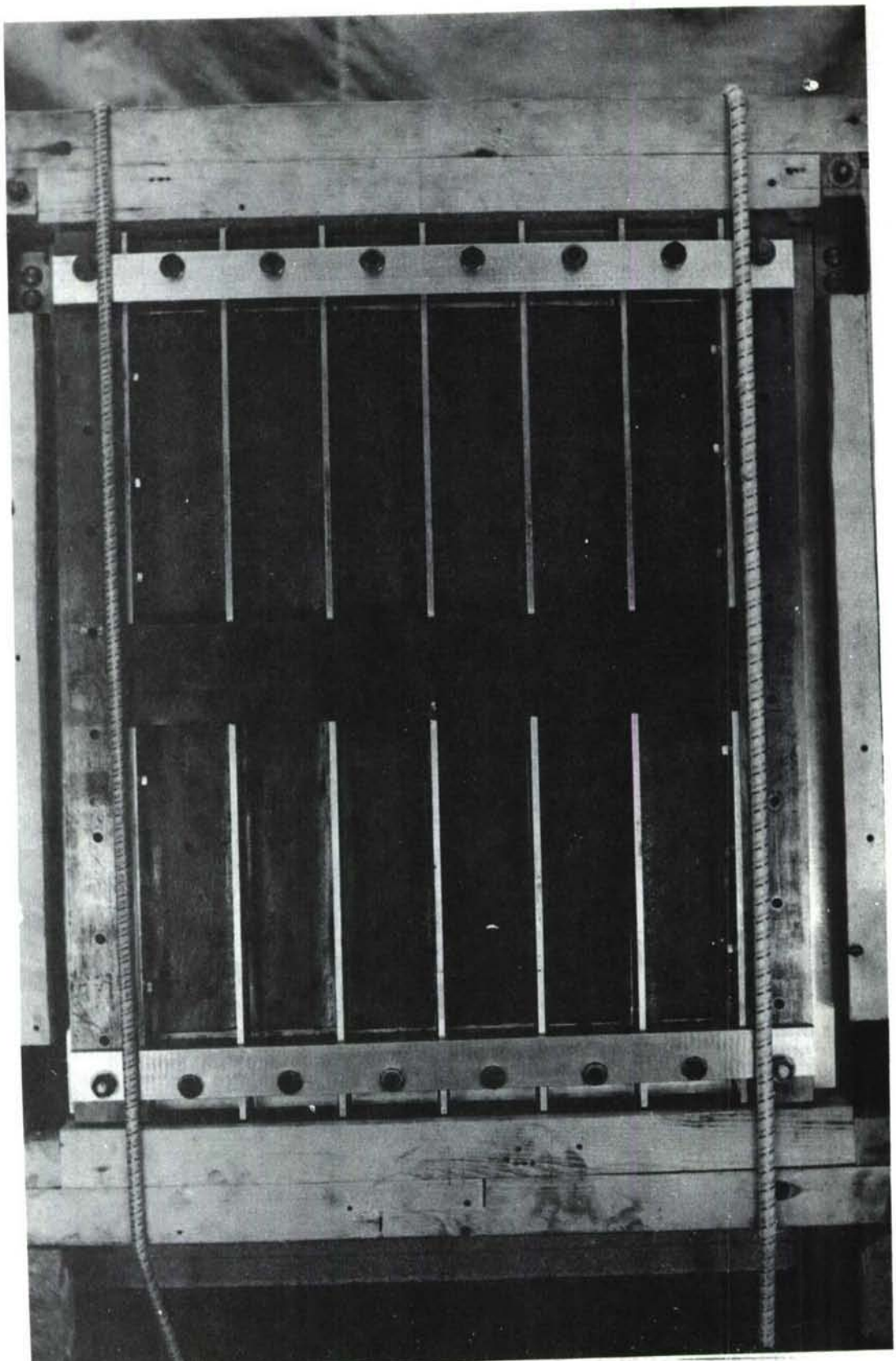

Fig 7.6 Test panel mounted in the acoustic tunnel

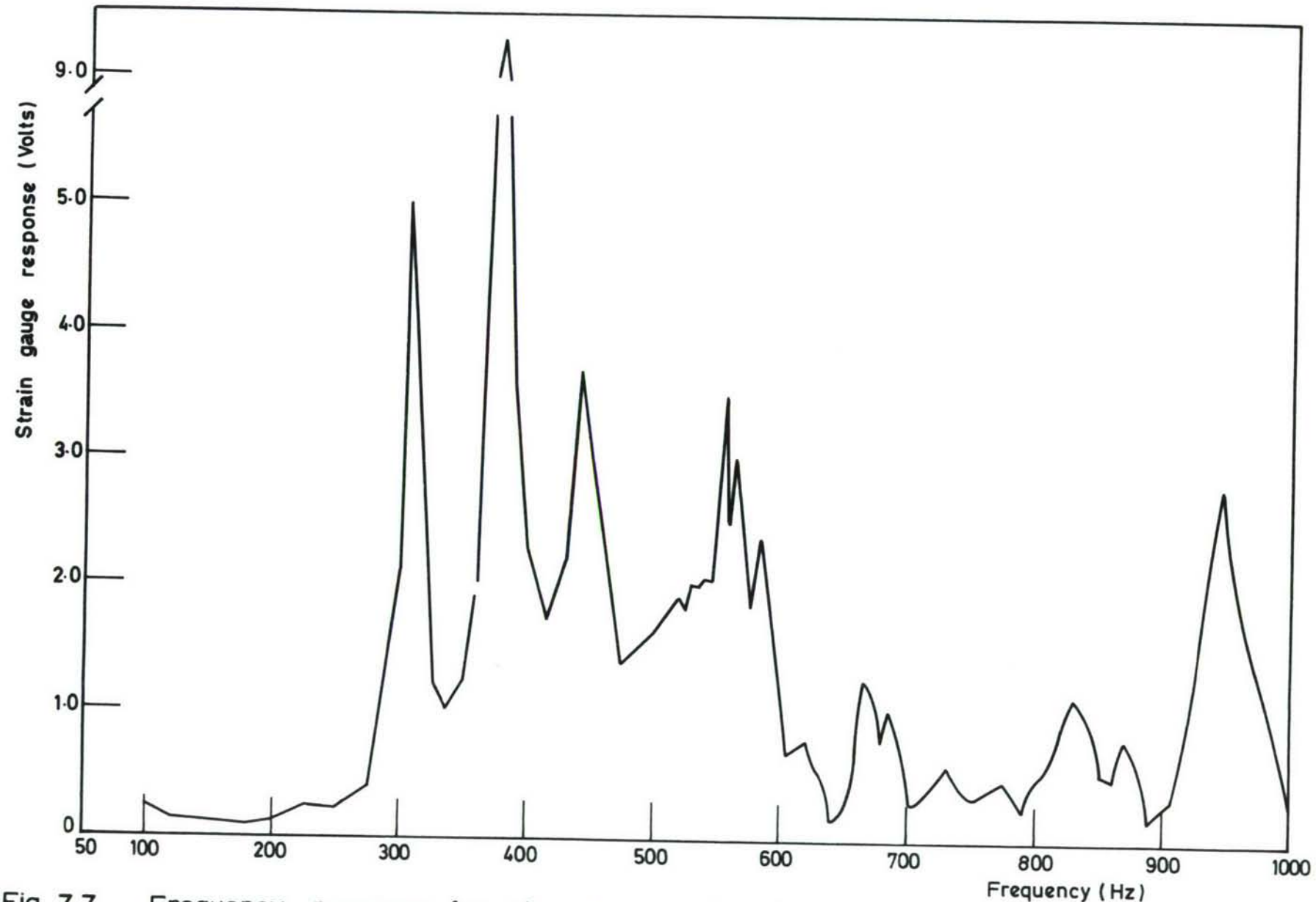

Fig. 7.7 Frequency response for six span panel with added edge support, (unconstrained damping layer only).

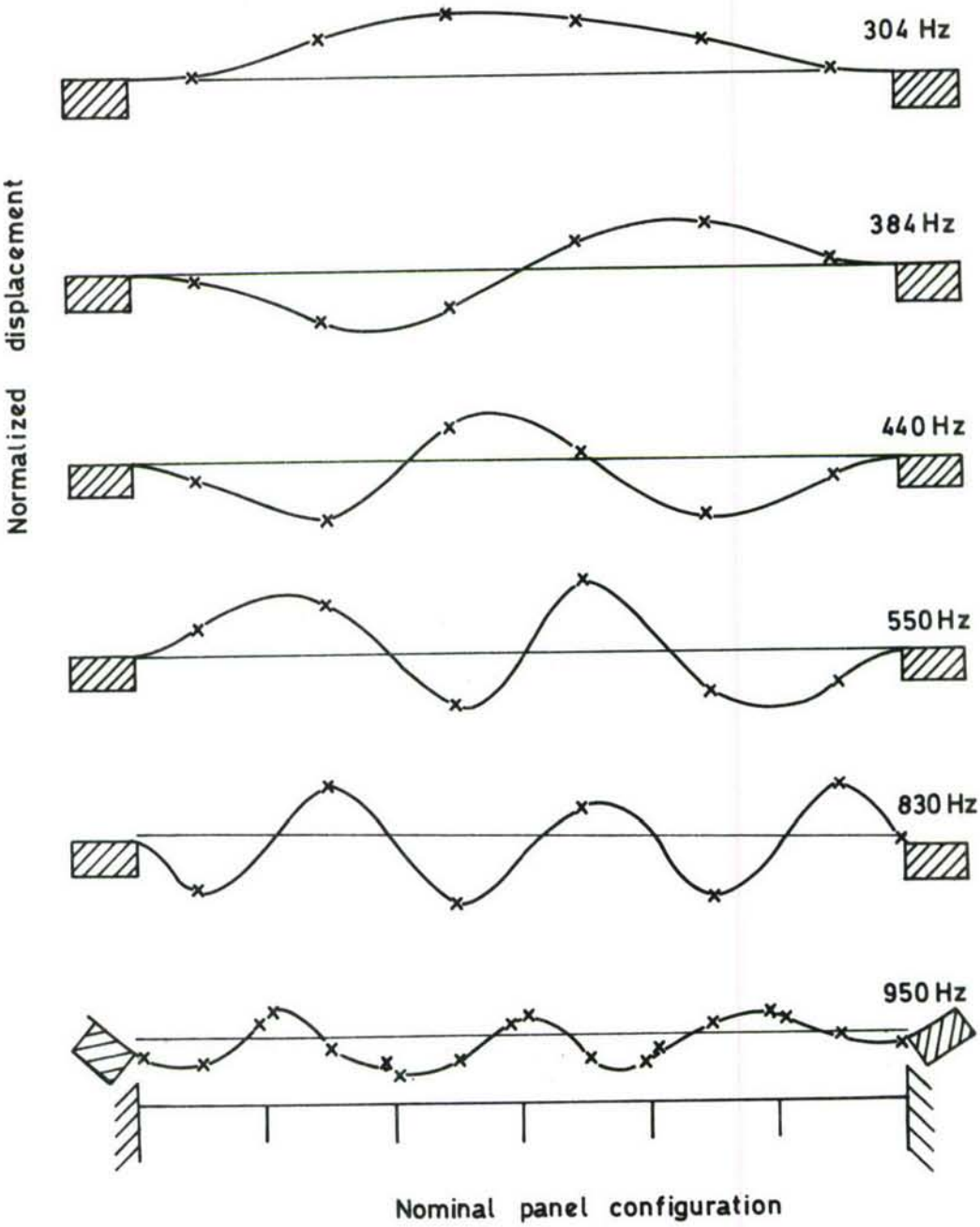

Fig. 7.8 Measured mode shapes at the frequencies of peak response (to acoustic excitation) in the panel frequency response curve.

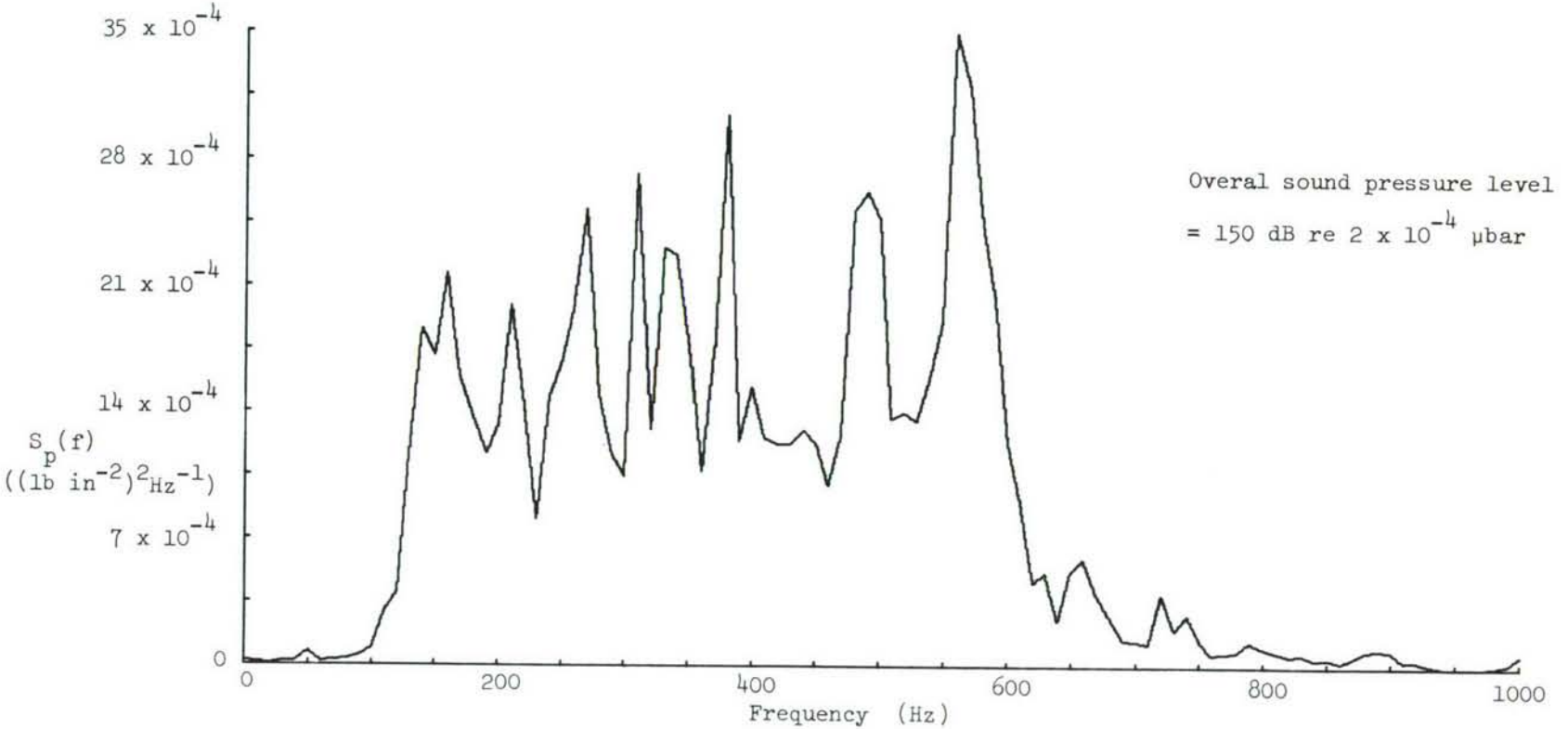

Fig. 7.9 Spectral density of the acoustic tunnel microphone signal.

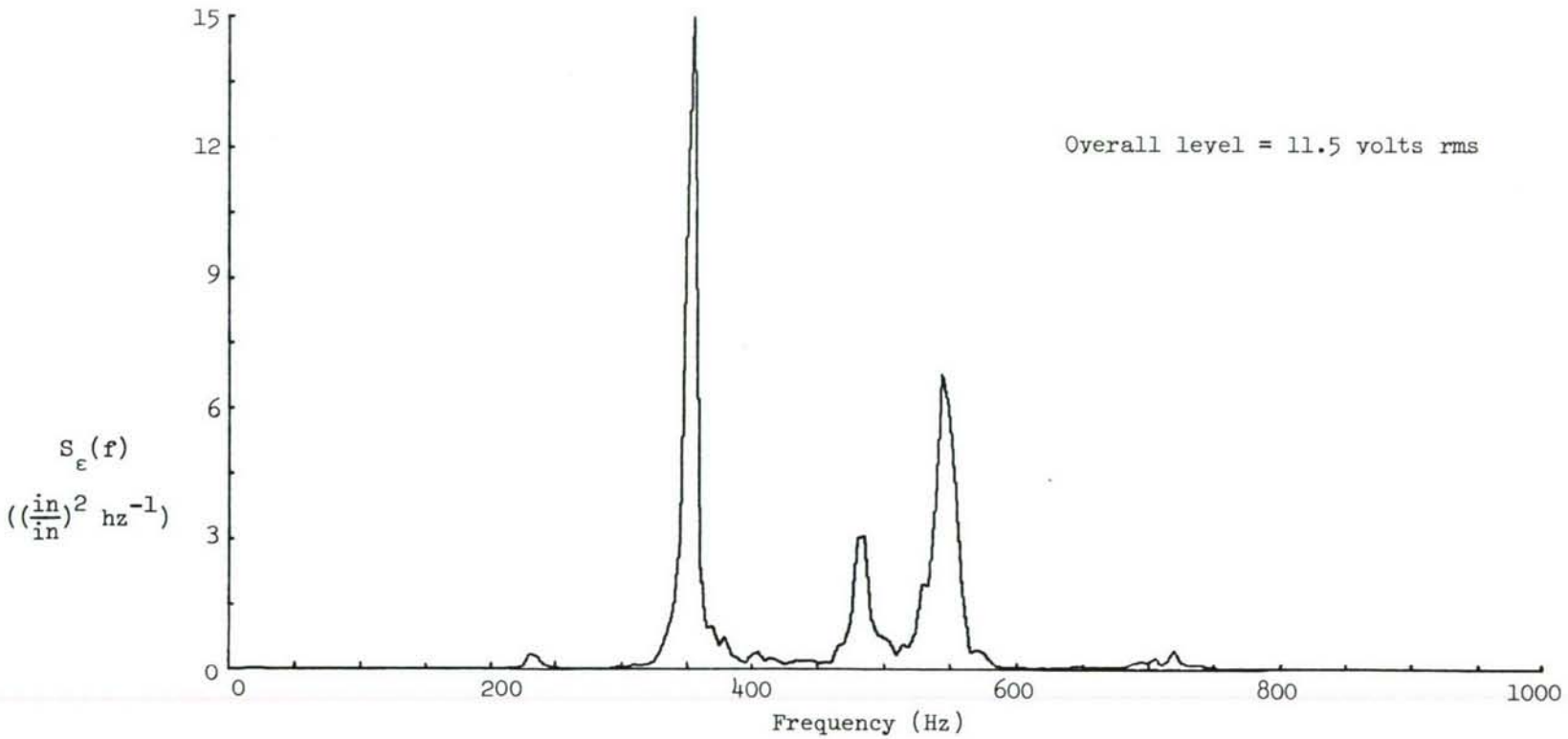

Fig. 7.10 Spectral density of the panel strain response with no damping added to the stringers

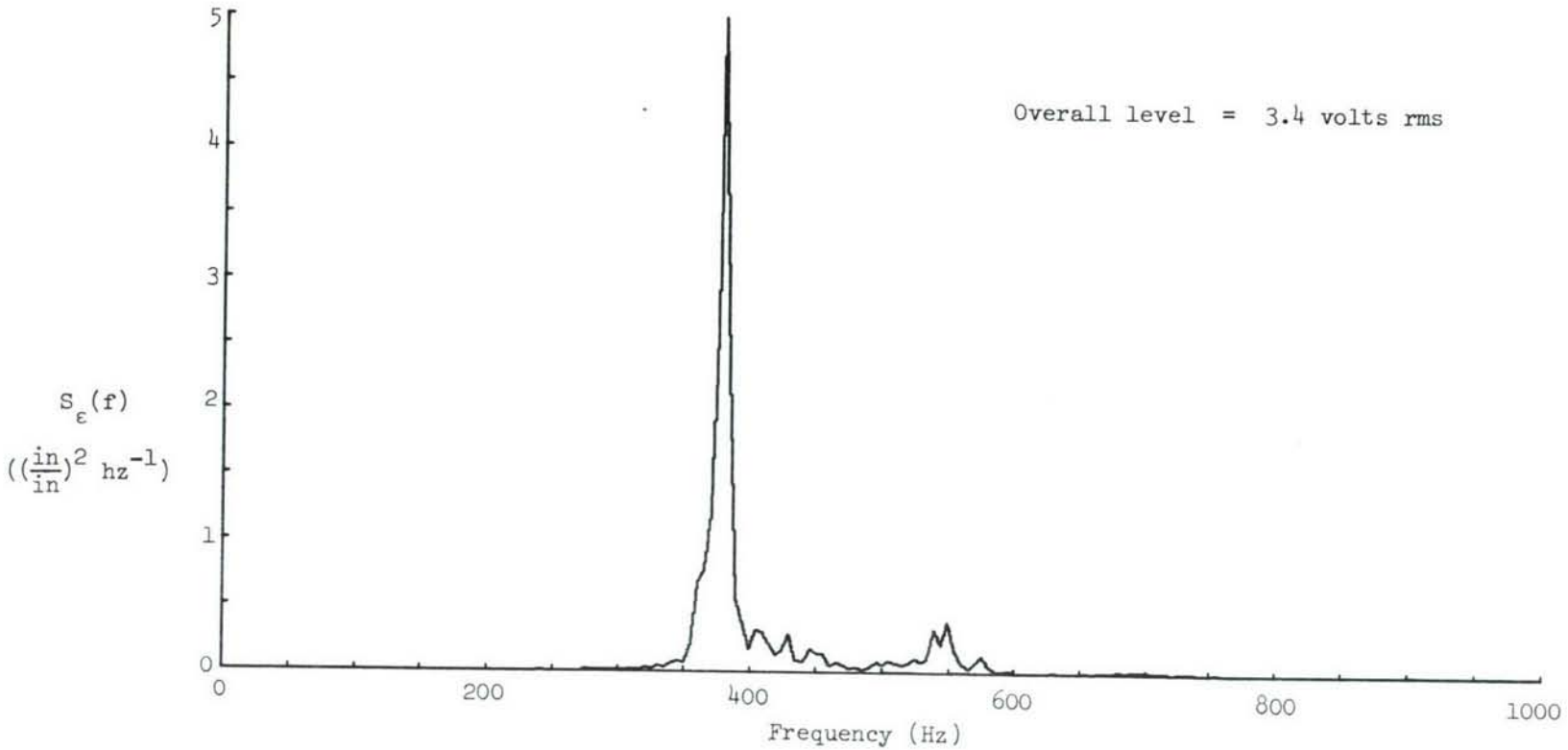

Fig. 7.11 Spectral density of the panel strain response with a strip of damping material 2 inches wide by 0.06 inch thick bonded to the stringers.

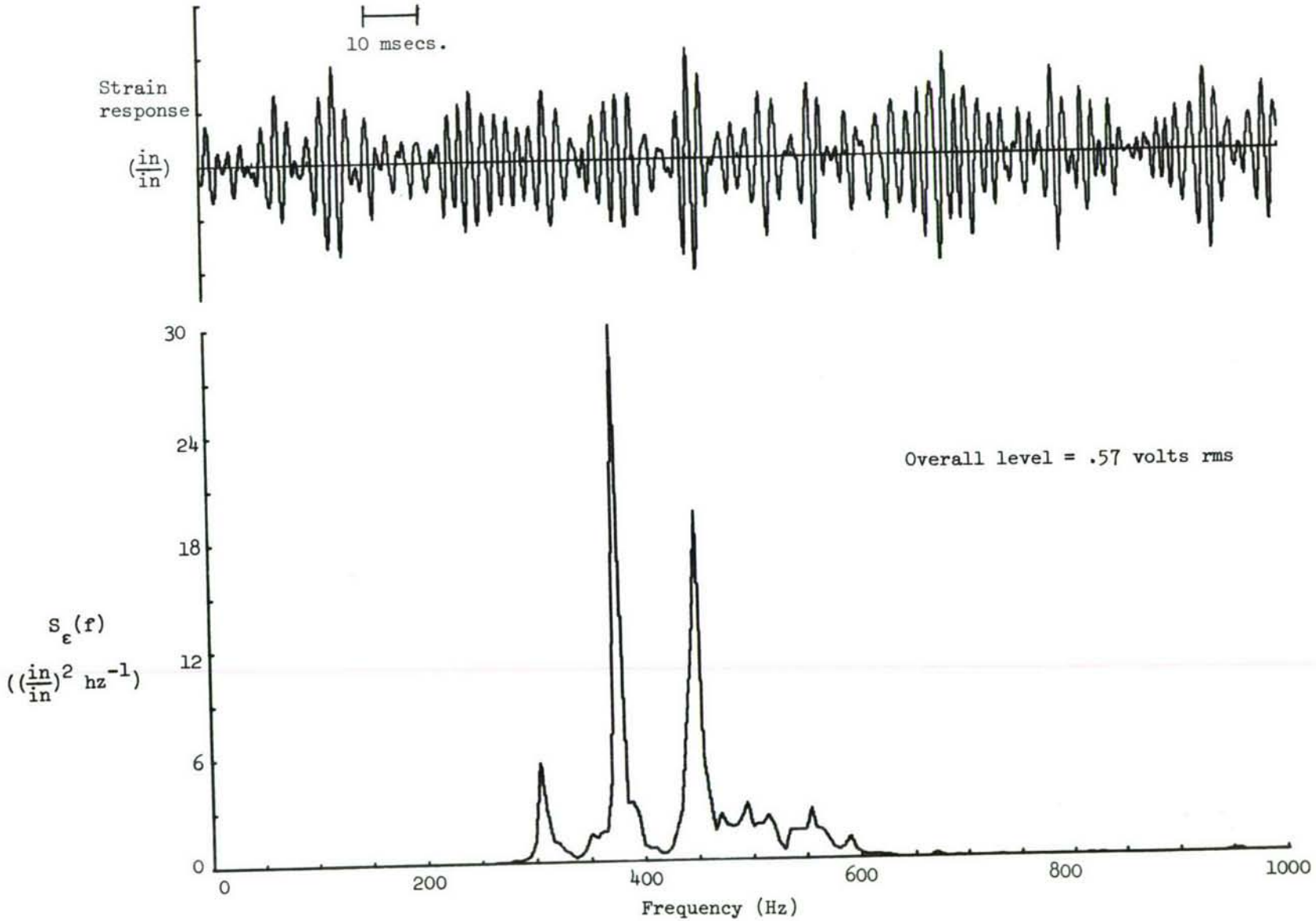

Fig. 7.12 Waveform and spectral density of the panel response with extra edge support and no extra damping.

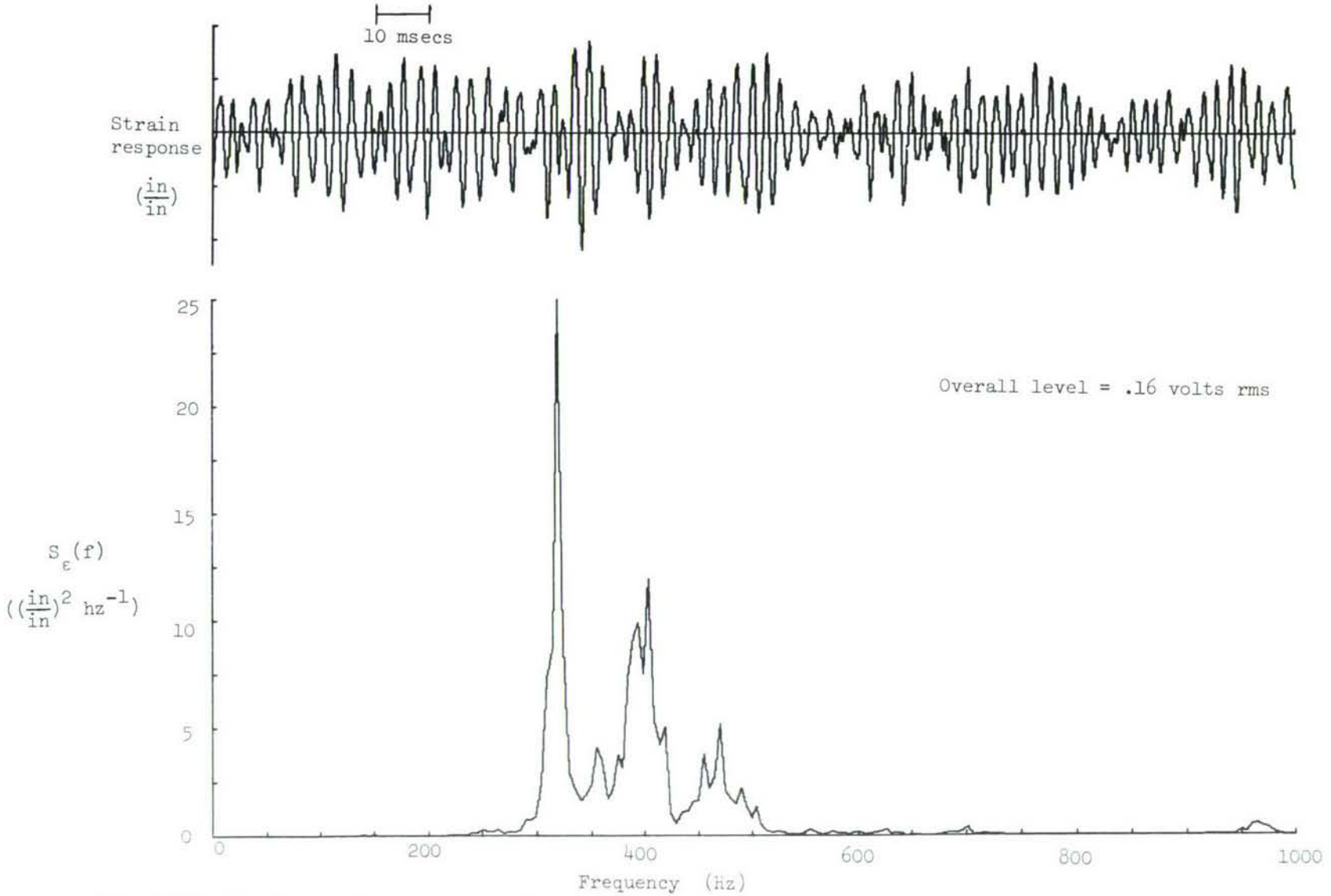

Fig. 7.13 Waveform and spectral density of the panel strain response with extra edge support and a strip of damping material 3 inches wide by .035 inch thick bonded to the stringers.

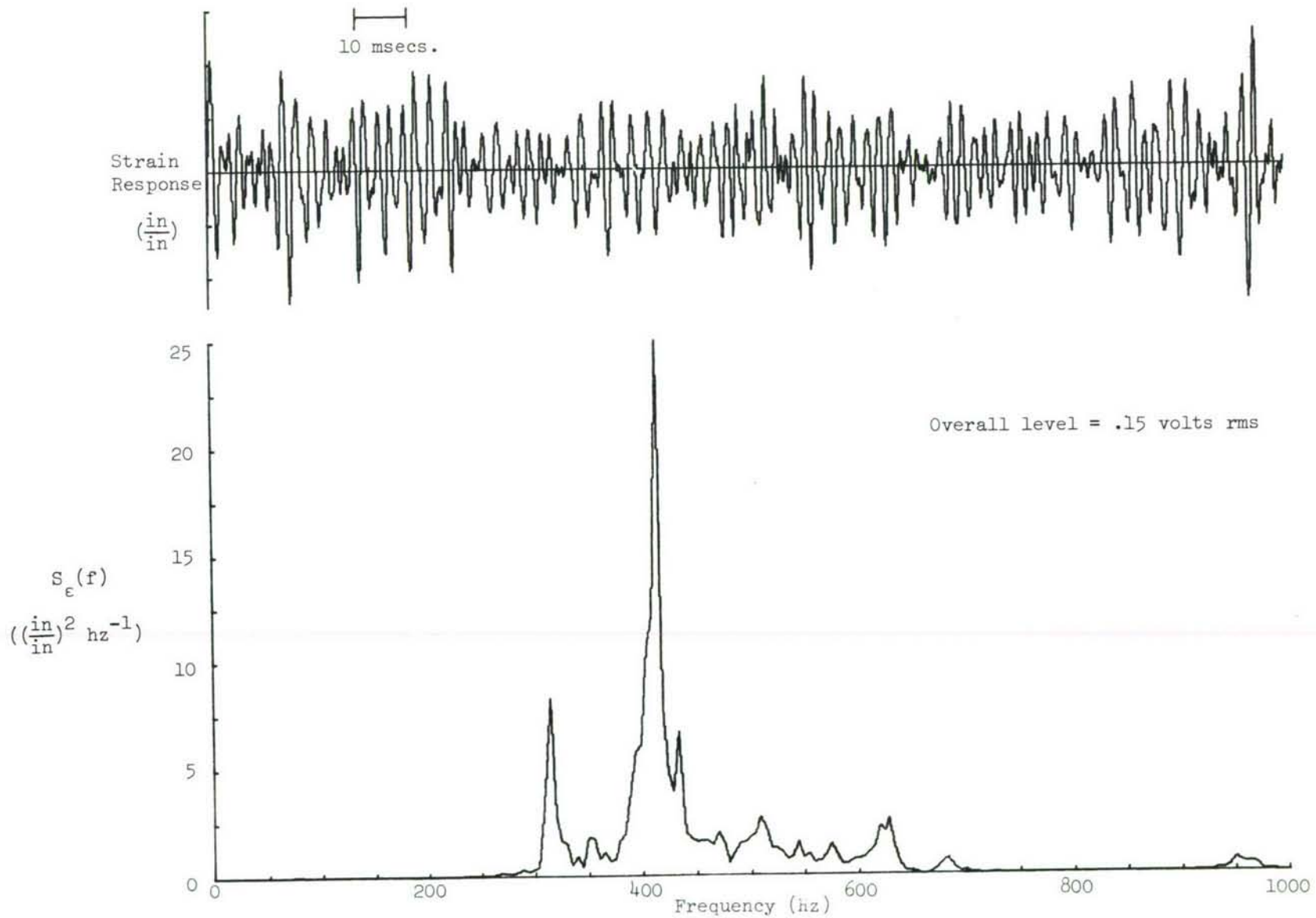

Fig. 7.14 Waveform and spectral density of the panel strain response with extra edge support and a one inch wide shear damper (.018" skins, .020" rubber) bonded to the stringers

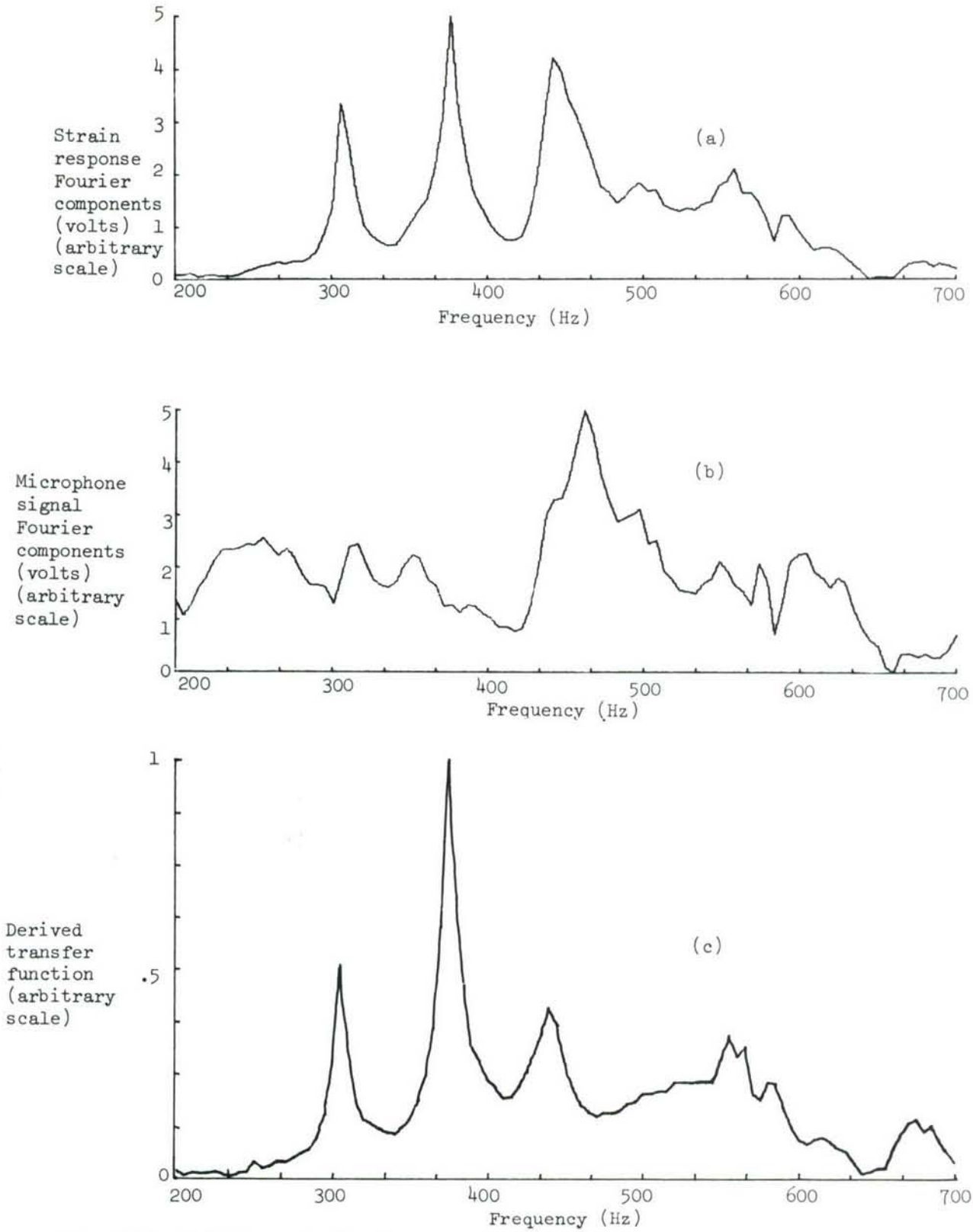

Fig. 7.15 Moduli of the Fourier transforms of the panel transient response and excitation (configuration of Figure 7.12) and the derived transfer function.

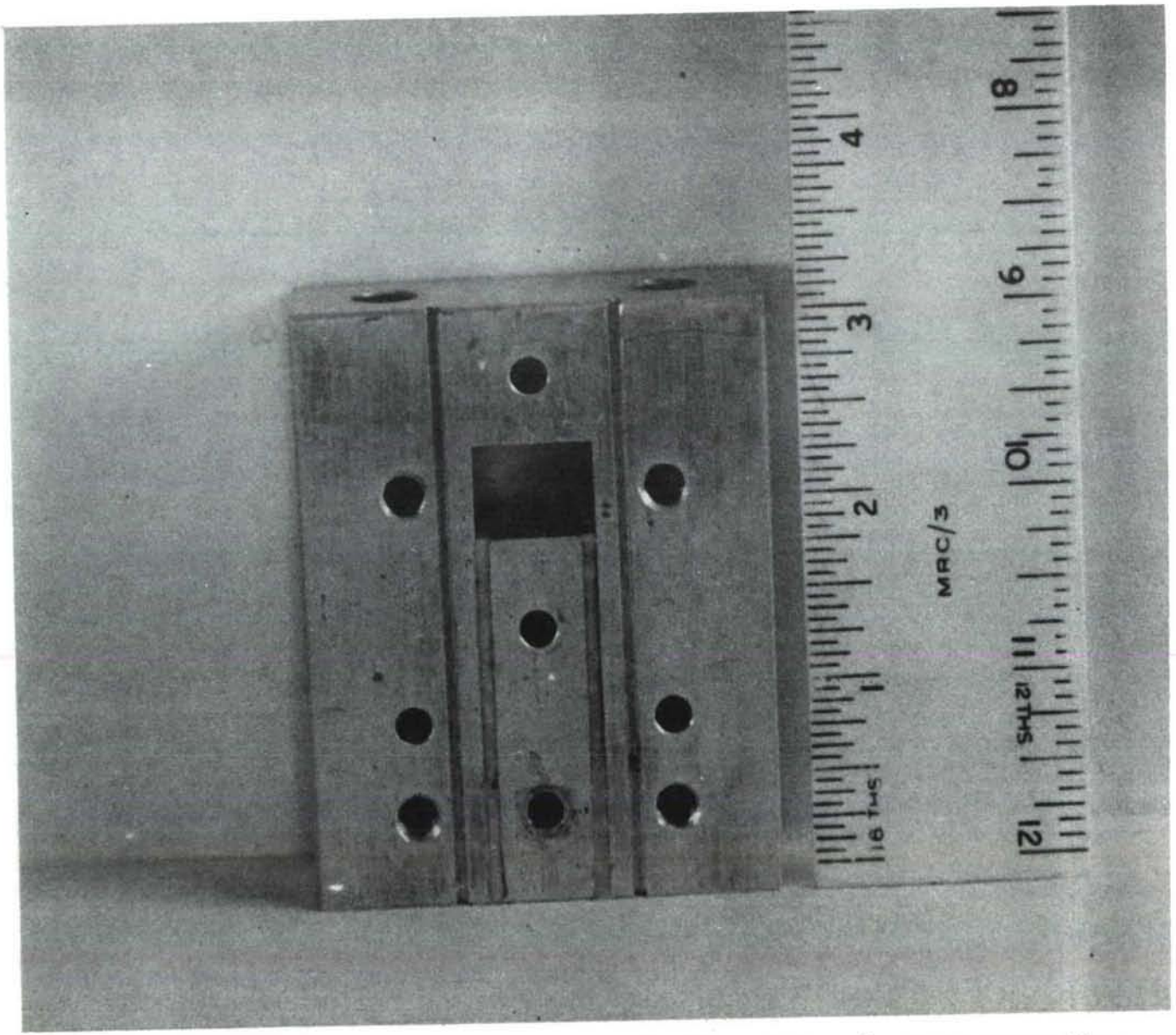

Fig. 8.1 Specimen for the determination of dynamic shear properties

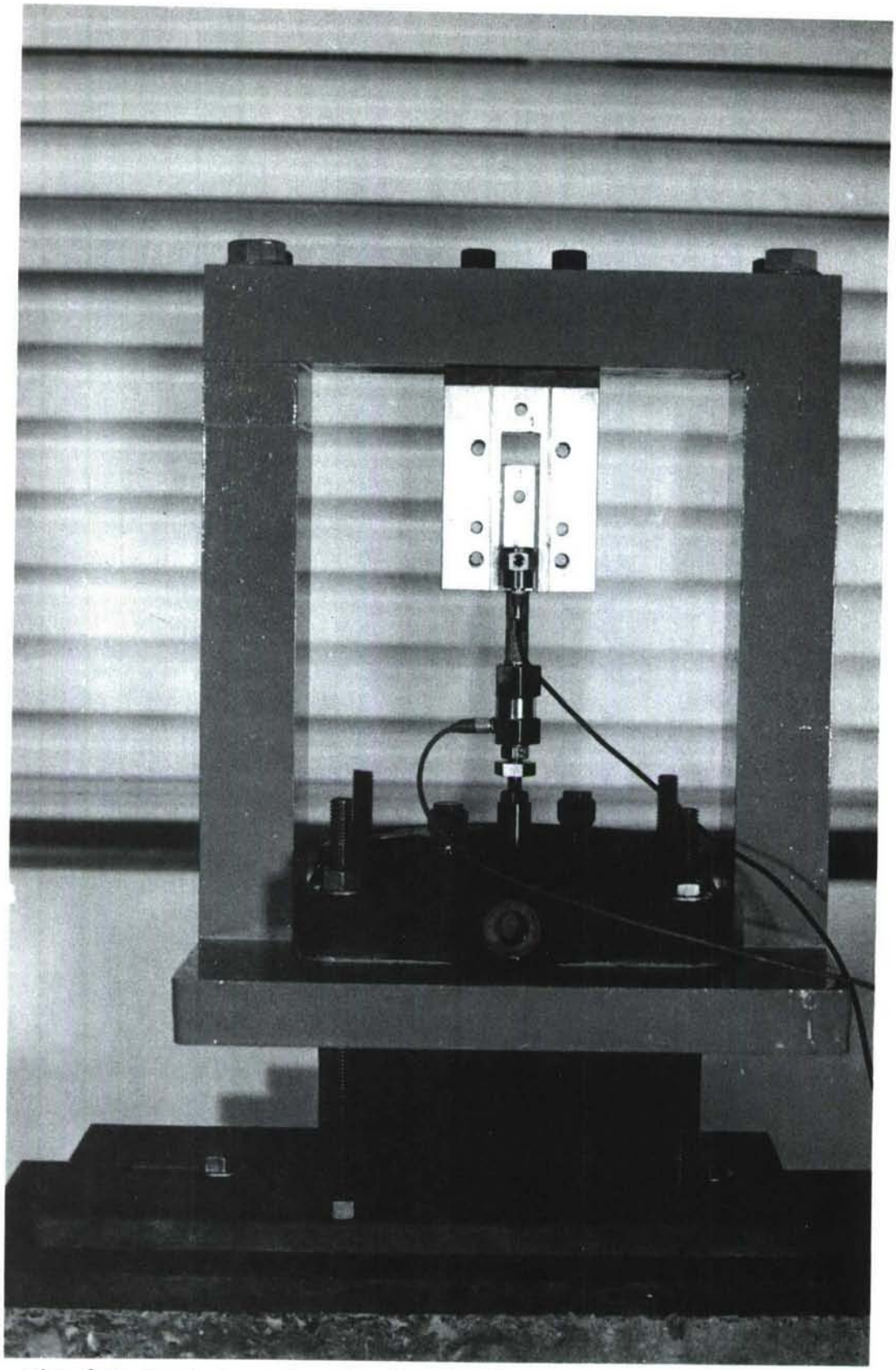

Fig. 8.2 Mounted specimen for dynamic shear property determination

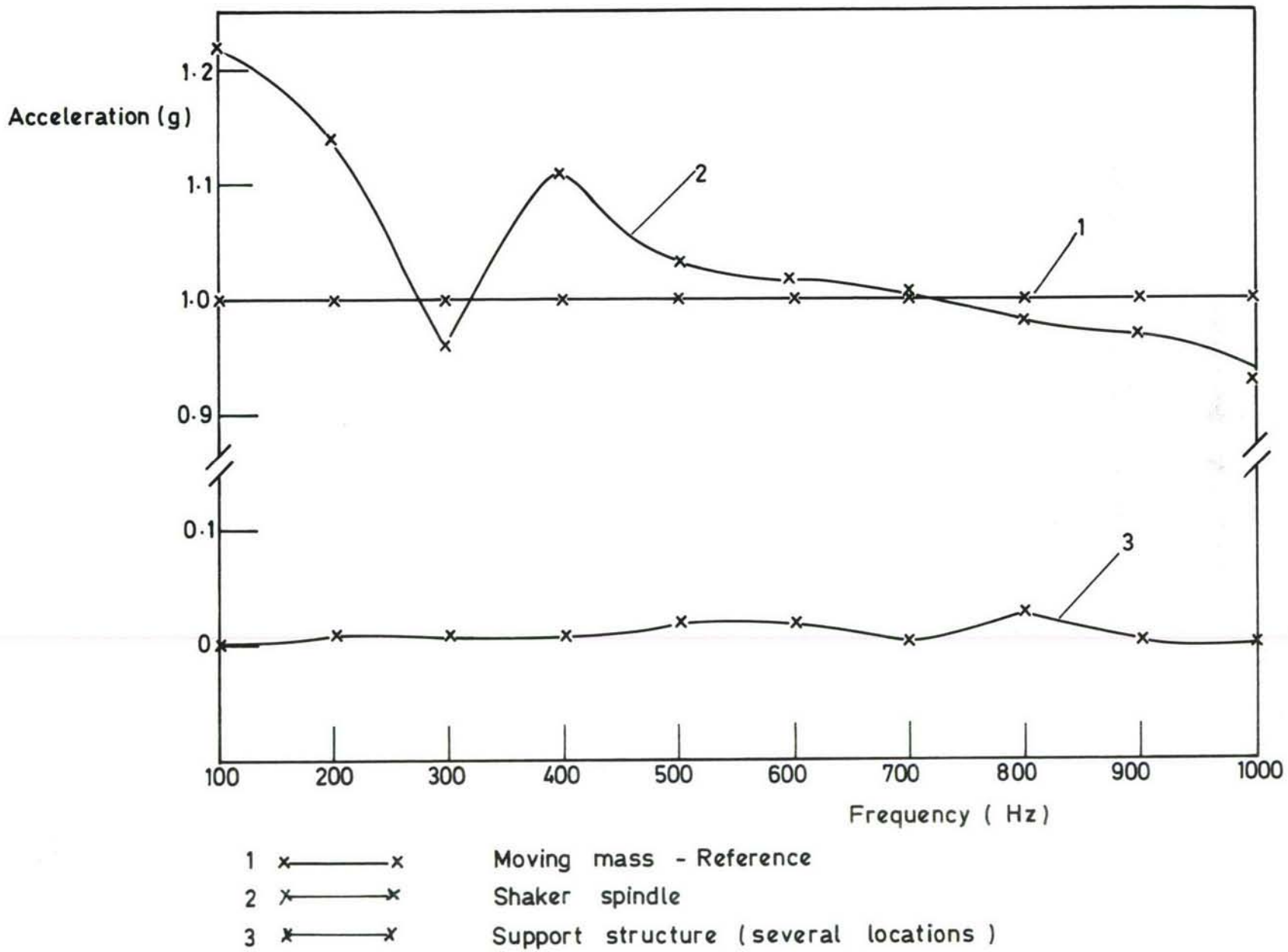

Fig. 8.3 Accelerations measured at various points in the structure of figure 8.2.

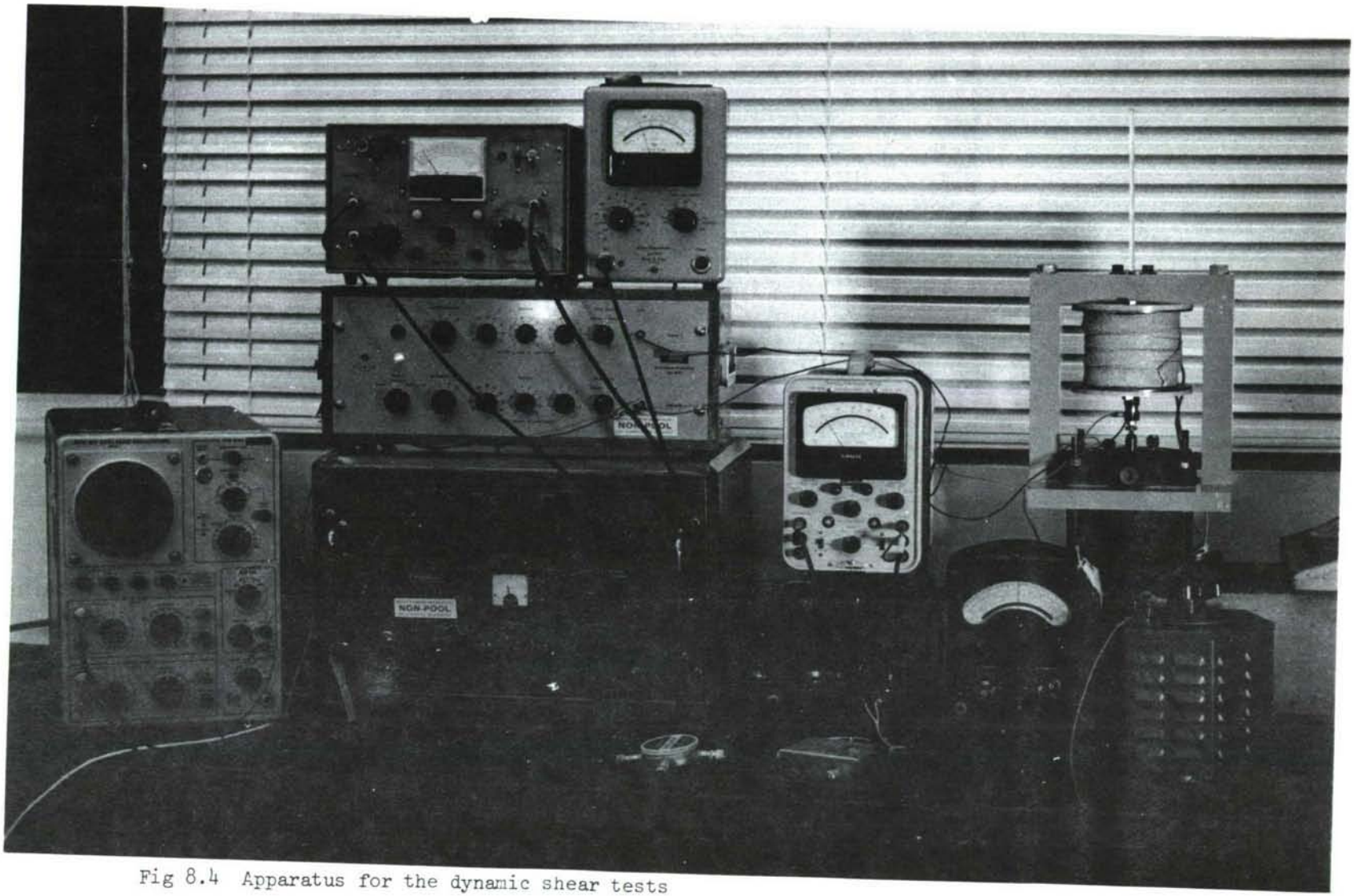

Fig 8.4 Apparatus for the dynamic shear tests

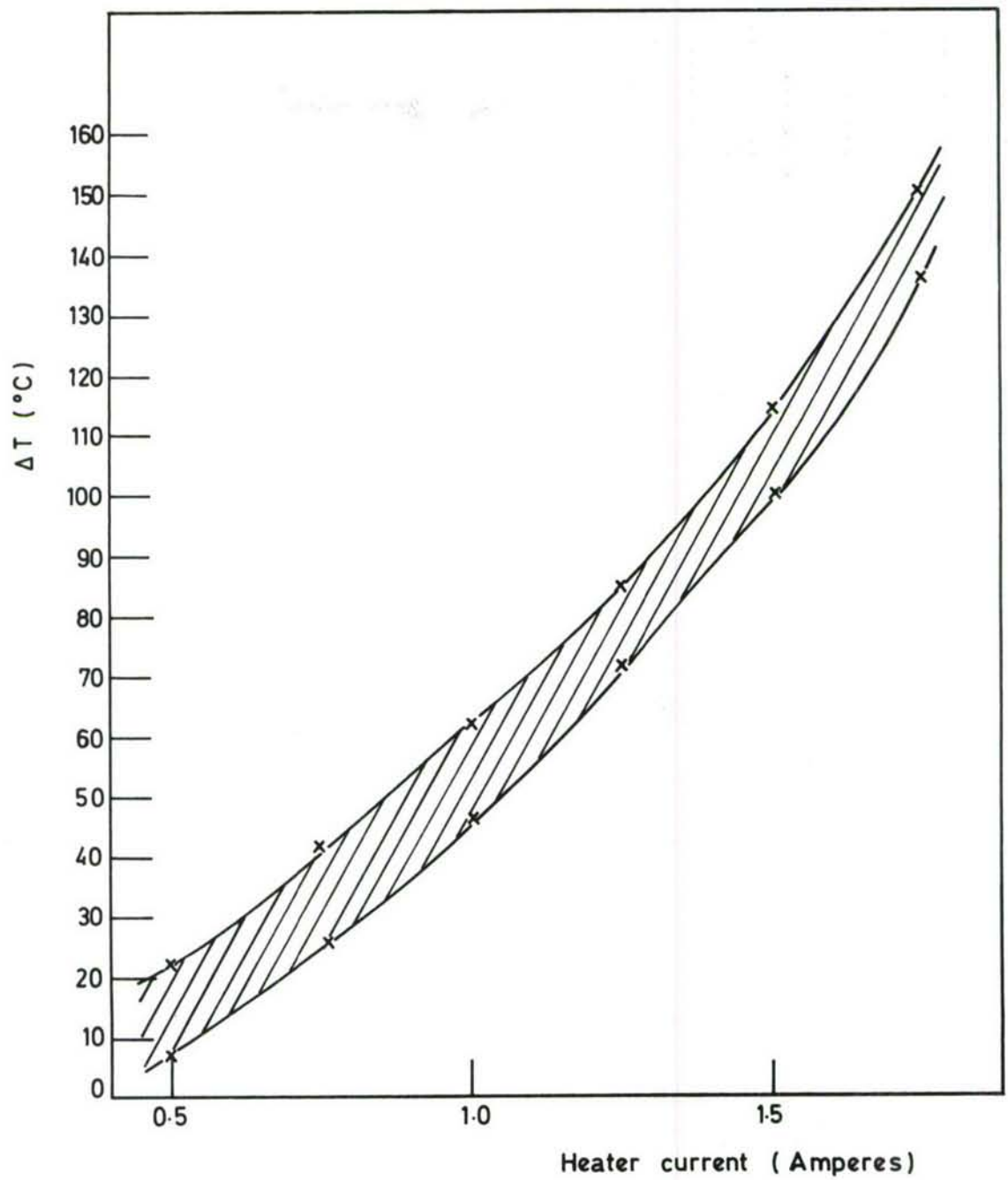

Fig. 8·5 Curve of temperature rise versus heating tape current.

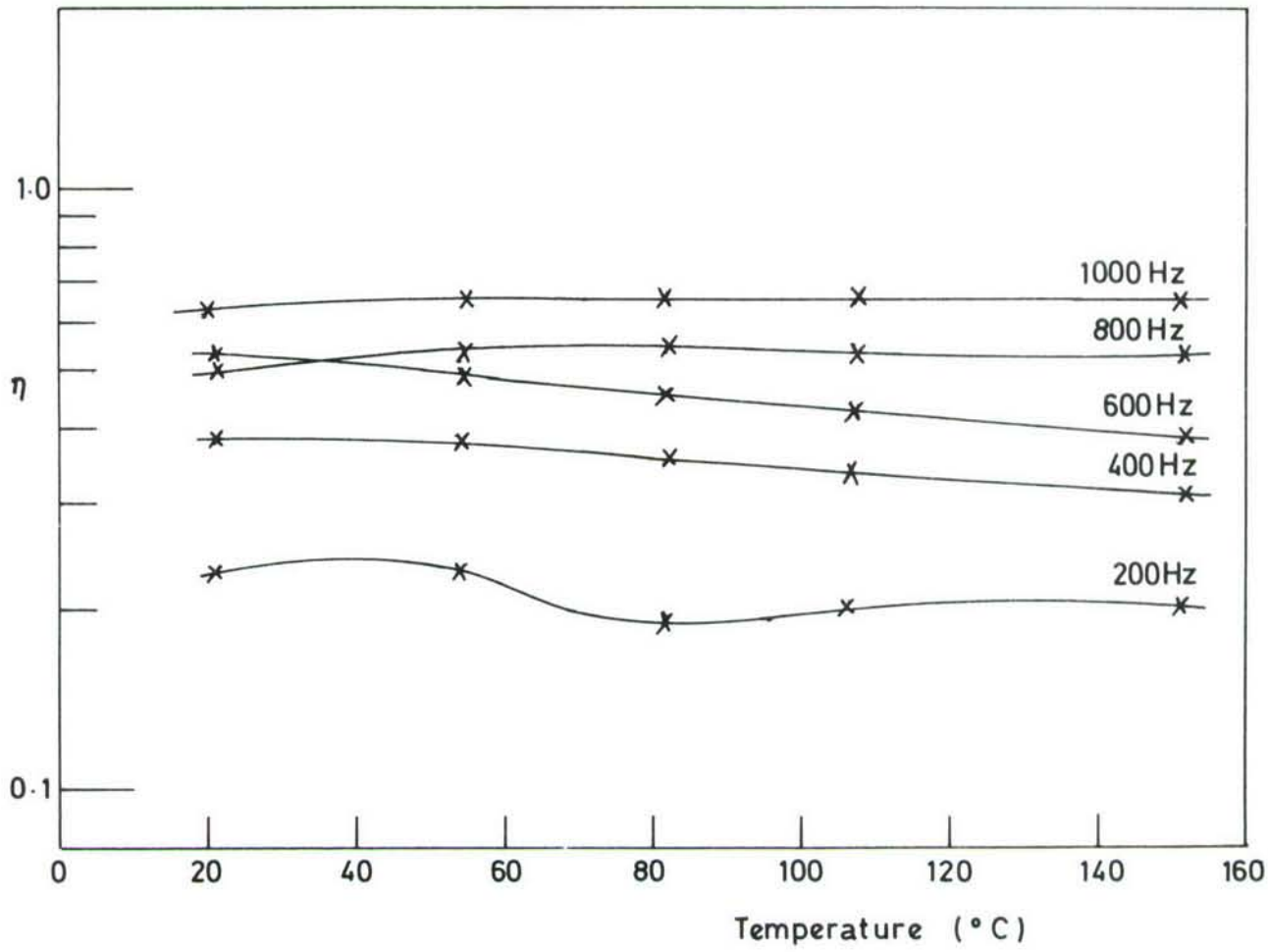

Fig. 8.6 Measured loss factor for material 3

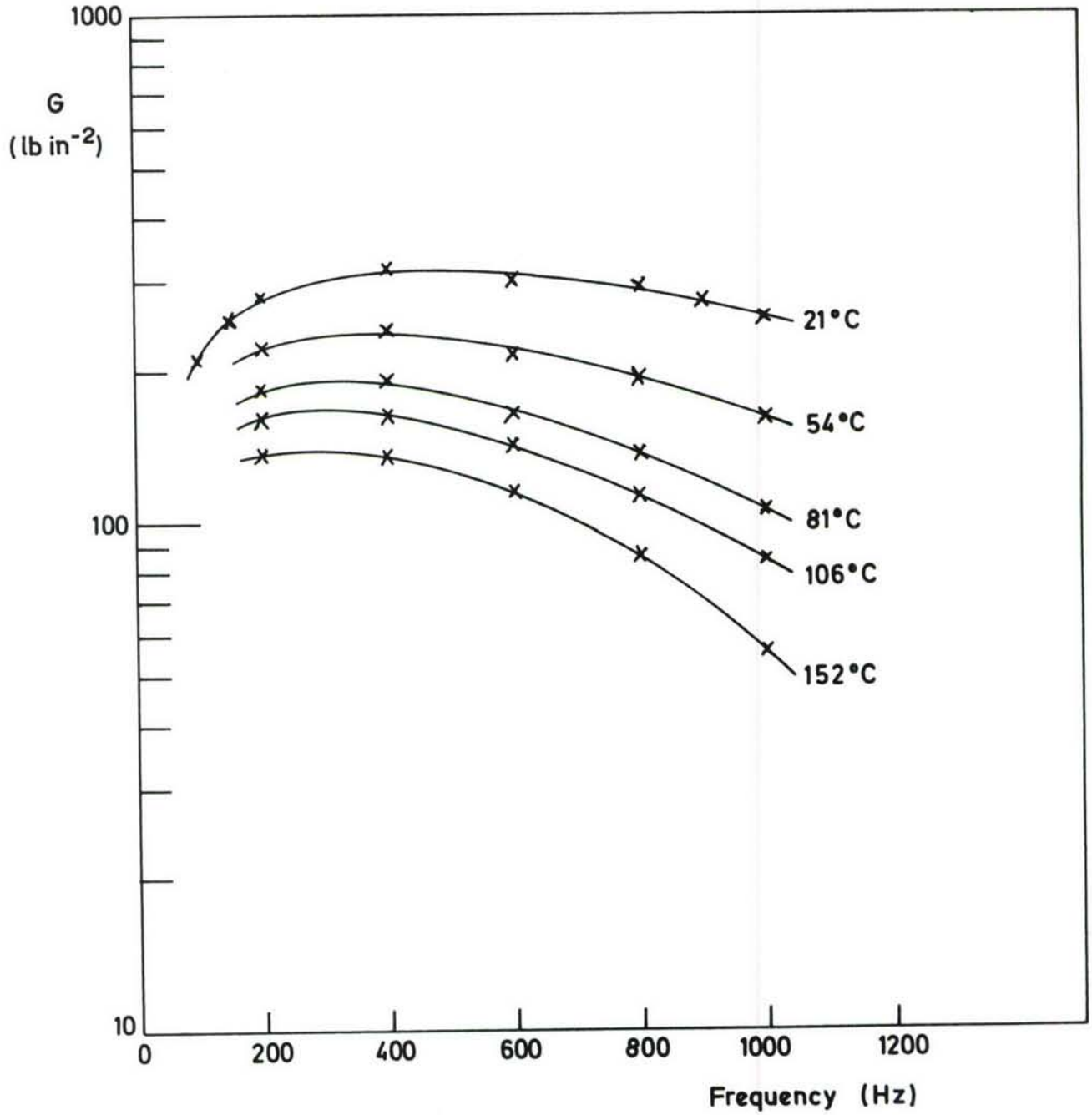

Fig. 8.7 Measured shear modulus for material 3.

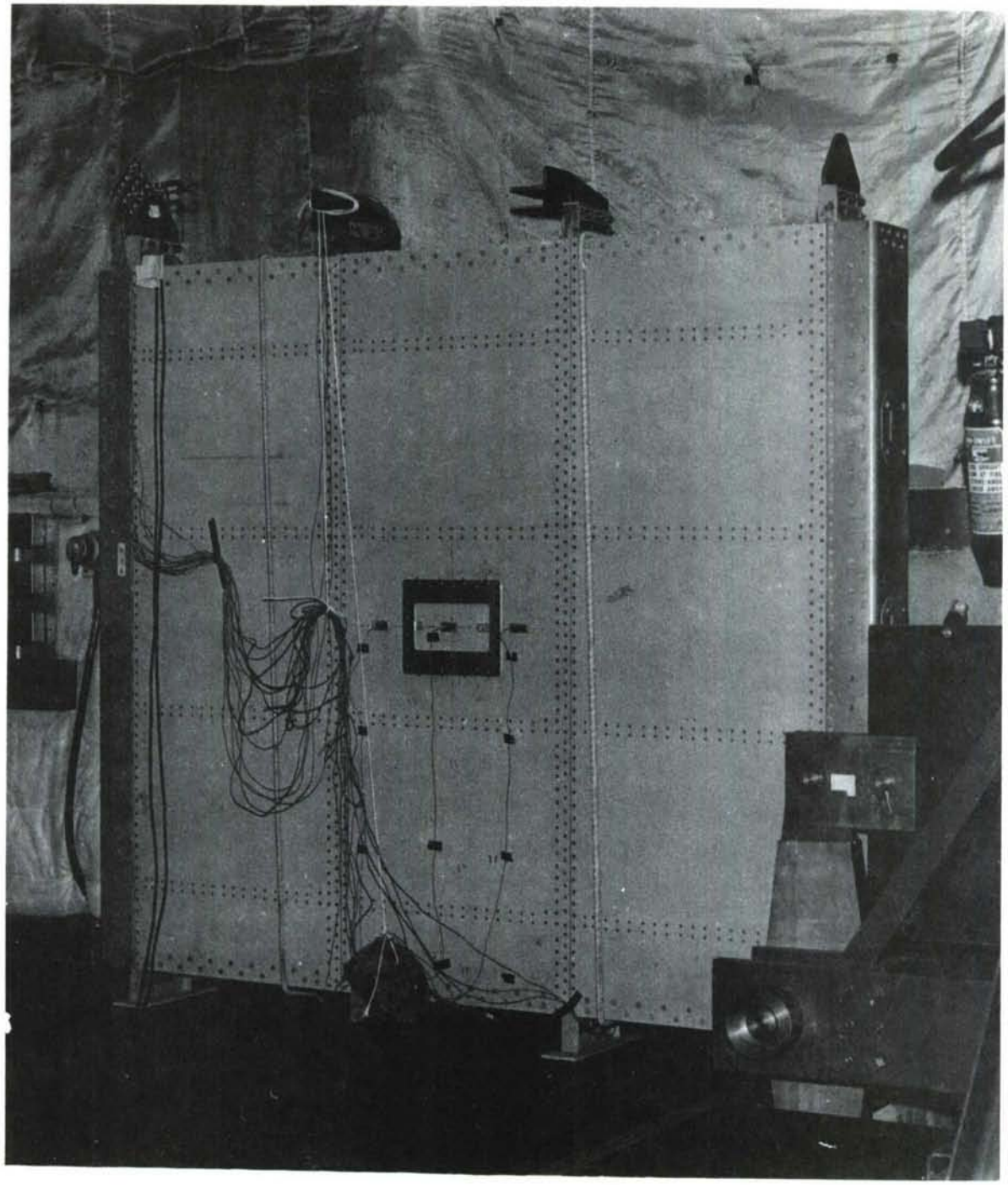

Fig 9.1 Full scale test specimen

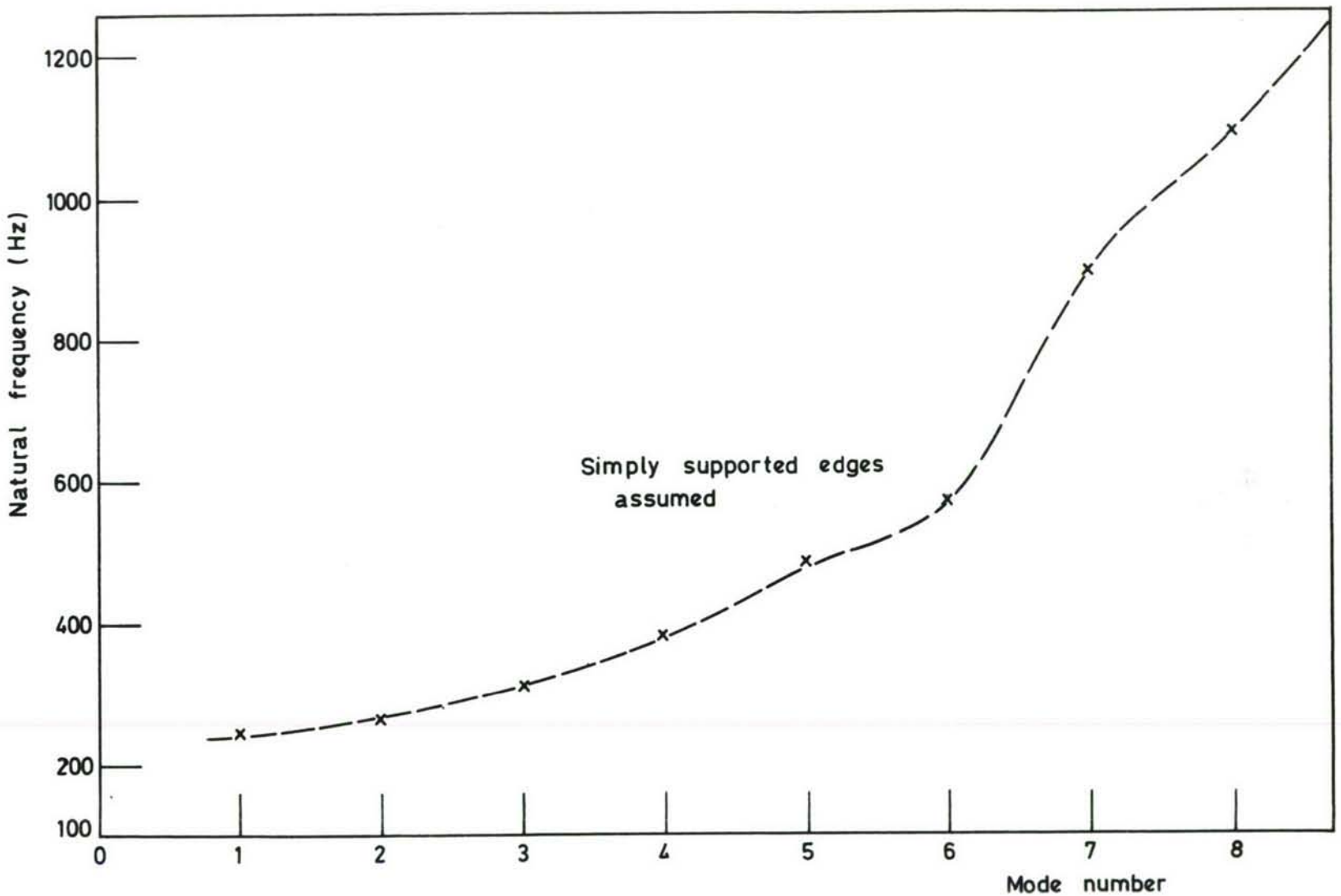

Fig. 9.2 Variation in calculated natural frequency with mode number for the full scale test specimen.

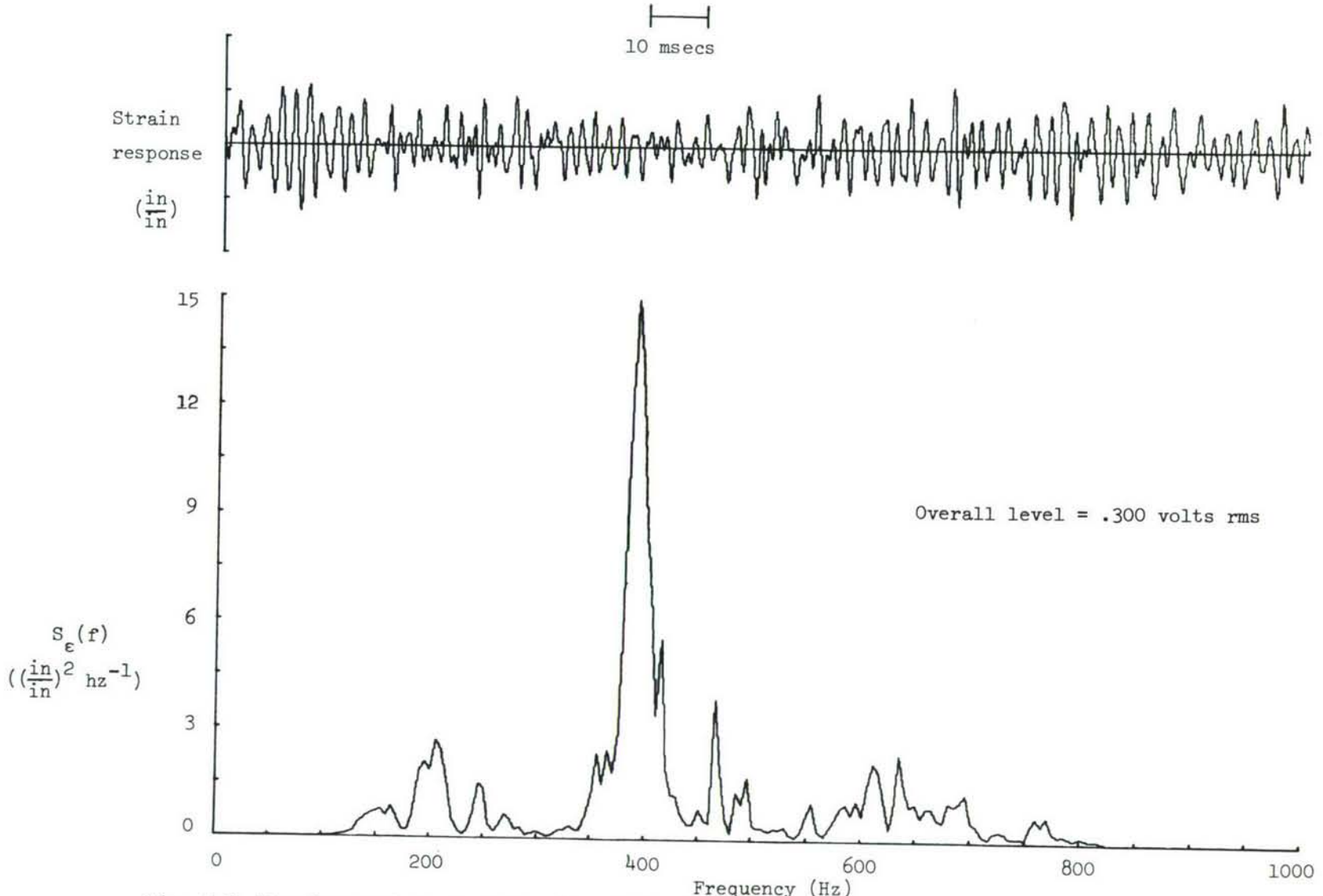

Fig. 9.3 Waveform and spectral density of the full scale structure panel response before the addition of damping treatments.

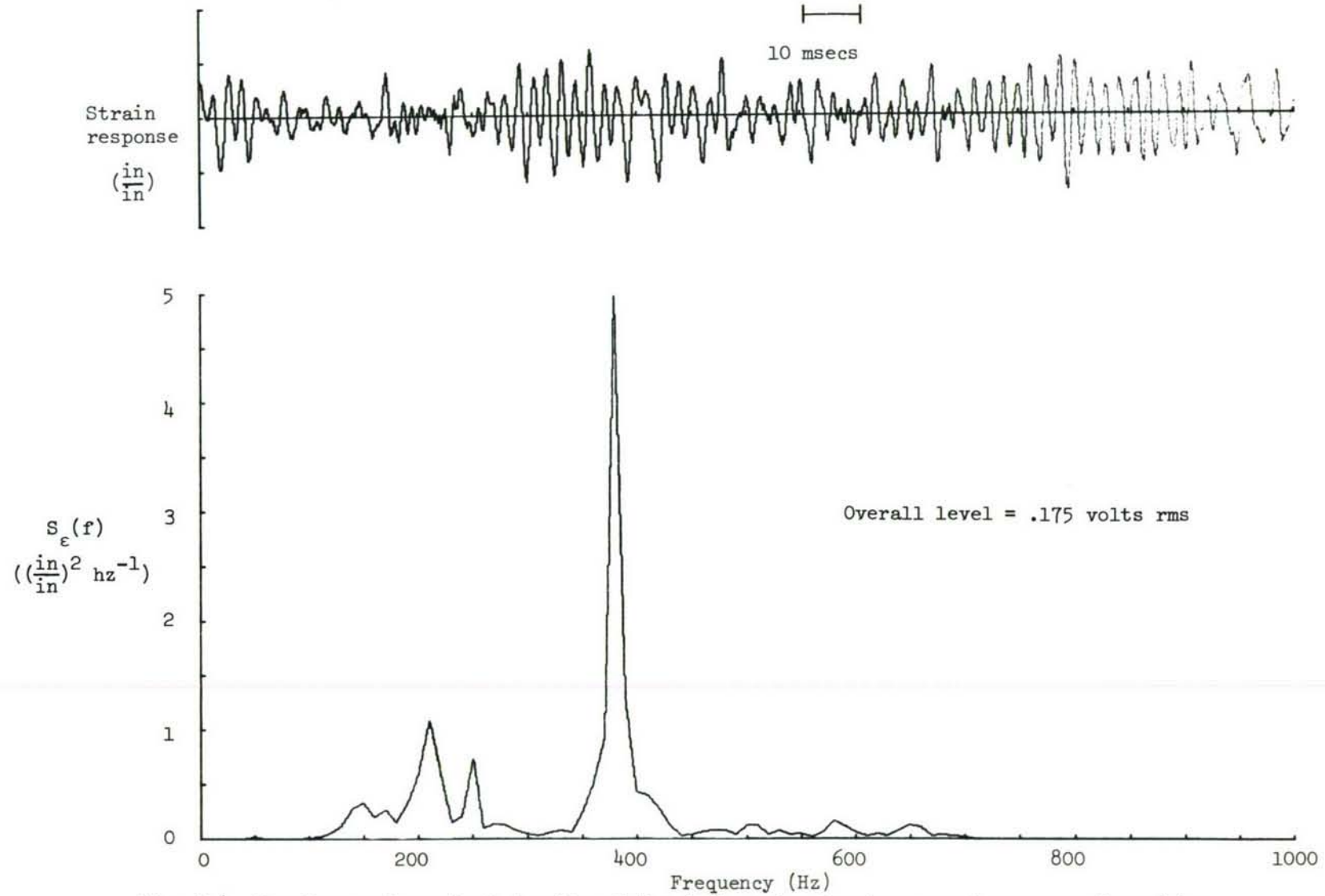

Fig. 9.4 Waveform and spectral density of the full scale structure panel response damped by a single strip of LD 400 3 inches wide by .125 inch thick.

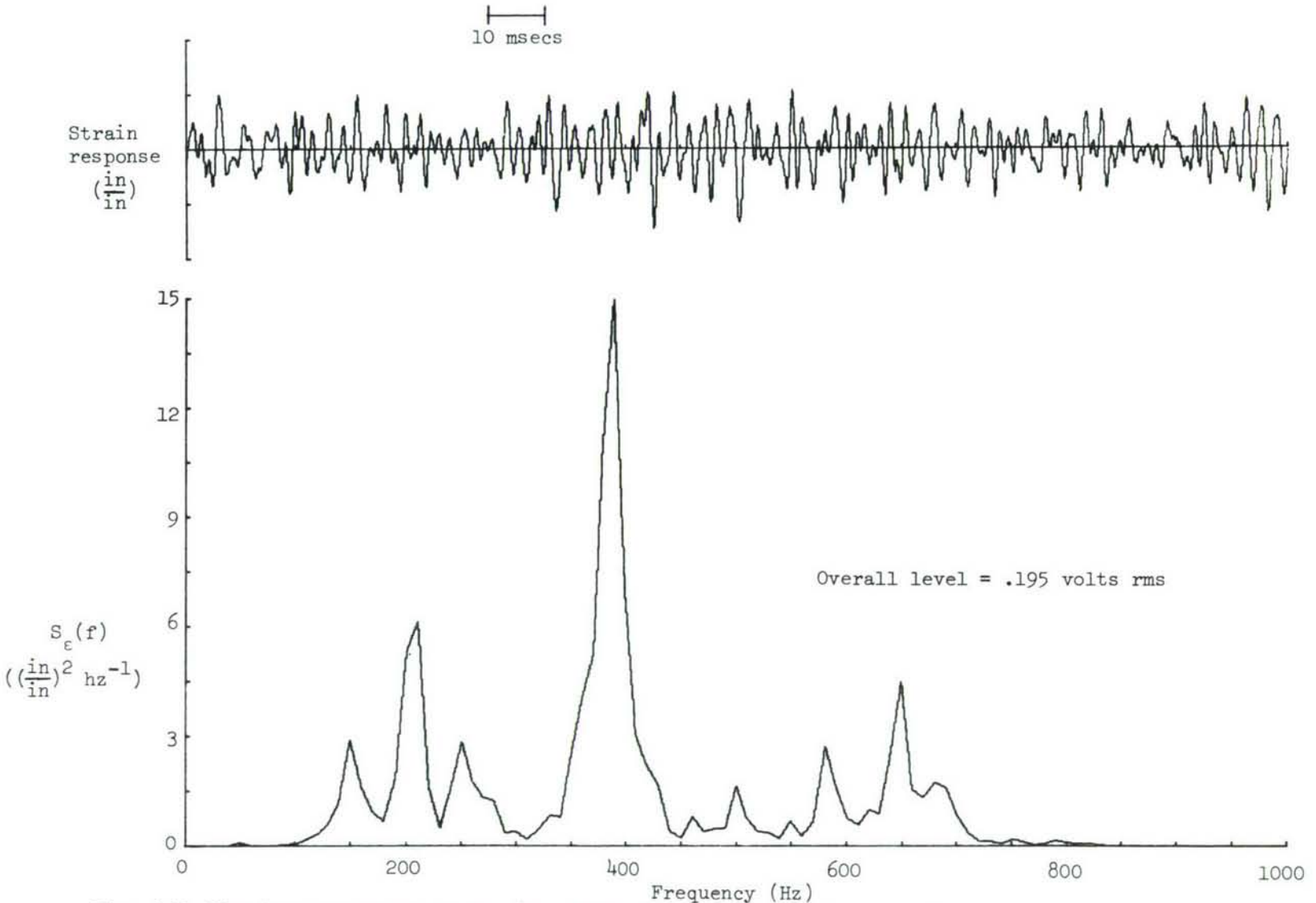

Fig. 9.5 Waveform and spectral density of the full scale structure panel response damped by a single 1 inch wide shear damper. (.018 inch skins and .020 inch rubber)

UNCLASSIFIED

Security Classification

DOCUMENT CONTROL DATA - R & D

(Security classification of title, body of abstract and indexing annotation must be entered when the overall report is classified)

1. ORIGINATING ACTIVITY *(Corporate author)*
Institute of Sound and Vibration Research
University of Southampton
Hampshire, England

2a. REPORT SECURITY CLASSIFICATION
Unclassified

2b. GROUP

3. REPORT TITLE
THE REDUCTION OF RESONANT VIBRATIONS IN INTEGRALLY STIFFENED SKIN-STRINGER PANELS USING VISCOELASTIC MATERIALS

4. DESCRIPTIVE NOTES *(Type of report and inclusive dates)*
Final Report 15 February 1968 to 14 February 1970

5. AUTHOR(S) *(First name, middle initial, last name)*
CICCI, Fernando

6. REPORT DATE	7a. TOTAL NO. OF PAGES	7b. NO. OF REFS
June 1971	239	48

8a. CONTRACT OR GRANT NO. F61052-68-C-0027
b. PROJECT NO. 7351
c. TASK NO. 735106
d.

9a. ORIGINATOR'S REPORT NUMBER(S)

9b. OTHER REPORT NO(S) *(Any other numbers that may be assigned this report)*
AFML-TR-71-100

10. DISTRIBUTION STATEMENT
Approved for public release;
distribution unlimited

11. SUPPLEMENTARY NOTES

12. SPONSORING MILITARY ACTIVITY
Air Force Materials Laboratory (LLD)
Air Force Systems Command
Wright-Patterson AFB, Ohio 45433

13. ABSTRACT

The vibration characteristics of integrally stiffened skin-stringer panels have been investigated theoretically and experimentally. This type of structure was found to have mode shapes similar to those of flat plates due to the relatively low values of stringer bending stiffness. The experimental measurements were made by means of strain gauges and accelerometers, with the typical panel excited acoustically by travelling waves at approximately grazing incidence.

Methods of damping the resonant vibrations were also investigated theoretically and experimentally. Predictions were verified using a beam taken from the cross section of an integrally stiffened panel. It was found that an extremely efficient method was one in which a damper was attached to the free edges of the stringers. This damper could be either a strip of viscoelastic material or a shear system made up of metal skins and a viscoelastic shear layer.

The response of a typical panel to broadband noise (100 to 1000 Hz) was determined experimentally before and after the addition of the damping treatments. A seventy per cent reduction of RMS strain for a weight addition of one and one half per cent was typical. The same tests were carried out on a full scale aircraft box structure with integrally stiffened skin and the addition of negligible weight by adding the damping treatments reduced the panel RMS response by about forty per cent.

DD FORM NOV 65 1473

UNCLASSIFIED

Security Classification

14. KEY WORDS	LINK A		LINK B		LINK C	
	ROLE	WT	ROLE	WT	ROLE	WT
Integrally stiffened skin						
vibration characteristics						
Mode shapes						
Natural frequencies						
Transfer matrix method						
Modal loss factors						
Damping treatments						
Acoustic excitation						
Full scale structure						
Transient tests						
Silicone rubbers						